SELF-ORGANIZED PORPHYRIN NANOMATERIALS FOR SOLAR ENERGY HARVESTING

by

IVANA RADIVOJEVIC

A dissertation submitted to the Graduate Faculty in Chemistry in partial fulfillment of the requirements for the degree of Doctor of Philosophy, The City University of New York

2010

This manuscript has been read and accepted for the
Graduate Faculty in Chemistry in satisfaction of the
dissertation requirement for the degree of Doctor of Philosophy.

04.28.2010.	Dr.Charles M. Drain
Date	Chair of Examining Committee
04.28.2010.	Dr. Mahesh Lakshman
Date	Executive Officer

Dr. Lynn Francesconi

Dr. Hiroshi Matsui

Dr. John R. Lombardi

Dr. Matthew Sfeir
Supervision Committee

THE CITY UNIVERSITY OF NEW YORK

Abstract

SELF-ORGANIZED PORPHYRIN NANOMATERIALS FOR SOLAR ENERGY HARVESTING

by

Ivana Radivojevic

Adviser: Professor Charles Michael Drain

New concepts in the design and function of organic dyes as sensitizers for solar energy harvesting are needed. Commercial viability constrains these designs: (a) cost effective synthesis, (b) long-term stability, and (c) an important goal is to reduce the environmental impact of the product at the end of its life cycle. Simple porphyrinoid dyes meet these constraints, but new modes of incorporation into devices are needed to increase the efficiency of charge separation that drives any photonic device designed to harvest light. In this thesis, we will show how complex material architectures on surfaces need not to be the result of complex molecular structures or strong intermolecular forces that form in solution and deposit intact onto surfaces. Varying environmental conditions we can dictate morphology of self-organized structures on surfaces. These studies provide further insights into the design principles, processing, and extent of electron and energy transfer in supramolecular porphyrin materials.

We are also developing a new strategy to couple porphyrinoid dyes to oxide surfaces using hafnium and zirconium metalloporphyrins and metallophthalocyanines.

The mode of dye attachment to oxide surfaces is a key parameter for the construction of efficient dye sensitized solar cells. Porphyrinoid dyes containing oxophylic group (IV) metal ions that protrude from on face of the macrocycle allow connections directly to oxide surfaces, wherein the metal ion serves as the conduit. Since the charge transport efficiency is mediated by appropriate matching of molecular HOMO-LUMO gaps to semiconductor band gaps, we will show characterized solution phase ground and excited redox potentials of these dyes, and also photophysical properties of dye excited state using transient absorbance spectroscopy.

Dedicated to my family, Mom, Dad, Grandparents and Tamara

Posvećeno mami, Tozi, baki, deki i Tamari

Acknowledgments

Many thanks to all the people who have contributed to the work in this Ph.D Dissertation:

First, I would like to thank my mentor, Professor Charles M. Drain for his guidance, and for being both supportive and inspiring, which made these years of my Ph.D very enjoyable.

Special thanks to all my committee members, Prof. Lynn Francesconi, Prof. Matsui, Prof. Lombardi and Dr. Matt Sfeir for their time and helpful suggestions.

I would like to express thanks to Dr. Chuck Black, Head of the Center for Functional Nanomaterials in Brookhaven National Laboratory, for giving me the opportunity to work in his lab; In particular, Dr. Sfeir and Dr. Nam for their time, patience and contributions to this thesis.

Extended thanks to Professor Grohmann for being more than just a Graduate Advisor to me. I thank Dr. Ben Burton-Pye, post-doc from Prof. Francesconi's Lab for the work we have done together. I thank Kay, my high school student for her help.

Greatest thanks to my lab mates Giorgio, Sebastian, Gabi, Jacopo, Amit, Ale, Sunaina, Matt, Diana, Jennifer, and Donna, for their friendship and for making everyday in Hunter fun.

I thank my family in New York, Jelena and Stevan for making the life in NY so much easier.

Lastly, my family in Serbia, my Mom, Dad, grandparents and my sister for helping me pursue my goals.

Table of Contents

LIST OF FIGURES

Chapter 3 Appendix

Chapter 4

List of tables

CHAPTER 1

Self-Organized Porphyrinoid Nanomaterials for Solar Energy Harvesting

1.1 INTRODUCTION

In this thesis we focus our attention on self-organized porphyrionoid nanoarchitectures that have potential application as materials for solar energy harvesting. This introduction is adapted from our already published review* on self-organized porphyrinic materials and a perspective that is under review on commercially viable dyes for solar cells. We briefly summarize the main concepts and properties of porphyrin and phthalocyanine chromophores. We are inspired by the idea that nanoscale photonic devices exist that harvest light and convert it to electrochemical potential energy with near quantum efficiency, the photosynthetic apparatus; therefore it must be possible to construct nanoscale quantum-efficient photonic devices. At present, no man-made device comes even close to this efficiency.

1.2 PORPHYRINOIDS

Stable organic chromophores that absorb visible light well and/or, luminesce with high efficiency are good candidates as components of photoelectronic materials, such as sensors, electronics, photosensitized solar cells, and organic light emitting devices.

* This chapter is in part adopted with the permission from Charles Michael Drain, Alessandro Varotto and Ivana Radivojevic "Self-Organized Porphyrinic Materials" *Chem. Rev.*, **2009**, 109 (5), 1630–1658.Copyright 2010 American Chemical Society.

Porphyrinoids and their metallo derivatives can be used in such devices due to their unique aromatic structure and excellent photochemical and photophysical properties.[3-5] In addition to the molecular structure, the photonic properties are highly dependent on the architectural arrangement of the chromophores and the environment. The structures of key synthetic porphyrinoids are given in Figure 1.1. The rigid, planar macrocycles are amenable to appending a variety of auxiliary moieties, such as H-bonding motifs and exocyclic ligands, at predefined geometries for the synthesis of designed supramolecular systems.[6] The core porphyrinoid is stable under a wide range of temperatures, pH, and other environmental conditions. The oxidation and reduction potentials, and therefore the chemical and photonic activities, can be tuned by appending a variety of exocyclic organic motifs and by choice of metal ion chelated in the center of anionic porphyrinoid. Axial ligation of the metalated compounds affords an additional means for assembly or organization. Most of the supramolecular chemistry of these macrocycles focuses on porphyrins because of their well-developed chemistry. While liquid crystalline phthalocyanine materials are common, there is a paucity of reported work on discrete self-assembled structures of phthalocyanines, porphyrazines, coroles, and corolazines. In addition to their chemical and photophysical similarities to the hemes and chlorophylls, porphyrins can be considered as ideal molecules for the construction of photonic systems.

Porphyrins are tetrapyrrolic macrocycles that are ubiquitous in nature.[7] In general, porphyrins have very strong absorption bands around 400-430 nm (Soret band) with absorptivities, ε, on the order of 10^5 M^{-1} cm^{-1} and several Q-bands between 500 and 650 nm with ε 10-20 times less. The electronic spectra depend on the exocyclic modifications and coordinated metal ion and are well explained by the Gouterman four-orbital model.[8]

The other porphyrinoids also have strong absorptions, generally to the red of the porphyrins.[4] Phthalocyanines have large extinction coefficients ($\varepsilon=10^5$ $M^{-1}cm^{-1}$), and strong Q bands in the region of 500-600 nm, as well as Soret bands of smaller intensity around 300 nm.[9] The fluorescence quantum yield of typical free base porphyrins and some of their metalloderivatives (e.g., Zn^{2+},Mg^{2+}) range from ca. 1% to 15%, with corresponding lifetimes between ca. 1 and 15 ns. For these systems, a substantial percentage of the molecules in the excited state intersystem cross to the triplet state, such that the phosphorescence quantum yield in matrices can be over 90%, for example, for Pd and Pt derivatives used in oxygen pressure sensing.[10] For many open-shell metal ions such as Ni(II), the excited-state energy is shunted to a metal-centered excited d,d state in a few picoseconds,[11-13] or charge transfer complexes may form.[3] Distortion of the nominally planar porphyrin results in substantial shifts in the electronic spectra and the excited-state properties.[14-15] The highly distorted Ni(II) 5,10,15,20-tetra-tert-butylporphyrin is an excellent example of the interrelated effects of substituents, macrocycle conformation, chelated metal ion, and environmental factors on the ground-state and excited-state energy landscapes. The excited-state lifetime of this metalloporphyrin can be tuned over 6 orders of magnitude, picoseconds to microseconds, by choice of solvent properties, because of the conformational dynamics available to the metal-centered d,d state.[11] Axial ligands to metalloporphyrins can also have a profound effect on excited-state dynamics.[12]

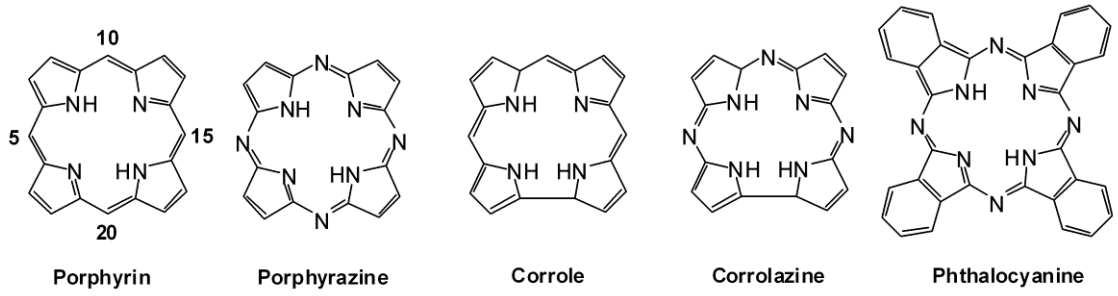

Figure 1.1 Different types of porphyrinoid structures.

1.3 CONCEPTS

Self-Assembly: The nearly exponential growth in the number of publications on self-assembled porphyrinic systems in the last two decade [16-28] was propelled by: (a) the potential to make functional materials from tectons that are significantly easier to synthesize compared to covalently linked arrays, and (b) the large number of potential applications of porphyrinoids including: photonics, sensors, catalysts, electronics, and components of solar energy utilization devices. Self-assembly[22] results in discrete supramolecular systems that are usually topologically closed because the component molecules are carefully designed with complementary recognition groups and geometries to maximize specific intermolecular interactions. This strategy allows the predictable formation of nanoarchitectures with a degree of predictability in their supramolecular properties such as energy or electron transfer and luminescence. The bottom-up design and organization of molecules into materials is conceptually aided by considering four levels of structure: molecular (primary), supramolecular (secondary), the organization of

supramolecular systems into solid state materials such as crystals (tertiary), and materials in devices (quaternary).[22]

Self-organization: generally relies on both specific and non-specific intermolecular interactions to yield non-discrete systems that are less ordered – e.g. liquid crystals, mesogenic materials, and monolayers on surfaces.[9,28-29] As an alternative strategy to the formation of hierarchical functional materials, self-organization offers several advantages and some drawbacks compared to self-assembly. There is usually a defect threshold below which self-organized systems maintain their function. However, a defect in a self-assembled system results in a new supramolecular material that may have diminished or undesired properties. The syntheses of the molecular components of self-organized systems can be easier than those designed for self-assembly because non-specific intermolecular interactions oftentimes means simpler molecular structures can be used (less information has to be programmed into the molecule).

An important advantage afforded by self-assembled/organized materials with potential commercial applications is the high yield syntheses of molecular components.[30-35] Additionally, materials assembled by specific intermolecular interactions such as metal ion coordination, complementary hydrogen bonding, and certain electrostatic constructs are generally more robust than those organized by dispersion forces and hydrophobic/hydrophilic properties.[34] The disadvantages of self-assembled/organized systems largely stem from the complex equilibriums inherent to supramolecular entities (thermodynamic products) that make both characterization and material/device stability keystone issues in real-world applications. On the other hand, these equilibriums also can

be exploited to anneal the material (thereby improving performance and yield) and afford a mechanism of self-repair.[29,36]

Surfaces: Applications of functional materials require interactions with surfaces in devices; however the structure and function of self-assembled/organized materials also depends on interactions with these surfaces. Surface interactions play a complex role in the hierarchical organization of supramolecular systems, and this must be understood as part of the design process.[24,28,37-38] Porphyrinoids can be organized on a variety of surfaces as chemically bound monolayers (SAMs) [37,39-48]or by adsorption.[49-51] The surface deposition of discrete arrays, such as square tetramers pre-assembled by metal ion coordination or H-bonds, is much more difficult.[28,37] This difficulty is due to the intertwined factors affecting the equilibriums of self-assembled systems as they are put on surfaces: e.g. solvent evaporation, fluid dynamics, concentration changes, and surface energetics. Consequently, self-assembled arrays can: (a) fall apart and the components separate into different domains, (b) aggregate, or (c) reorganize into different structures. A detailed understanding of molecular-surface and supramolecular-surface interactions can be exploited both as a design element for the formation hierarchical photonic materials and as a means to couple nanomaterials to the macroscopic world. Discussion of the reliable and predictable control of the structure of supramolecular materials at interfaces is an essential aspect of this work.

Design: The design and implementation of motifs that direct the self-organization of chromophores has facilitated the development of porphyrin-based photonic materials. Materials composed of porphyrins that are difficult or cumbersome to synthesize may have limited commercial potential because of the costs related to the synthesis;

nevertheless these molecules are useful in developing the design principles needed to form complex architectures and understand the physical properties of these materials. The optimization of the chemical and photonic properties of the materials arises from the nanoarchitecture, and these studies have revealed much in terms of both the function and the principles of supramolecular chemistry. The versatility of a building-block approach for the bottom-up fabrication of materials, especially hierarchical organization on surfaces, extends to a plethora of other dyes and functional molecules. These studies have led to a deeper understanding of the chemical, electrochemical, and photochemical properties of supramolecular systems and the multiple roles the recognition motifs play in both structure and function.

Future directions toward practical utilization of self-organized multiporphyrin nanoarchitectures will focus on several areas. The photonic function(s) of many systems will require hierarchical organization on length scales of nanometers (molecule), to tens of nanometers (e.g., film heights), to centimeters (e.g., films), perhaps with different chromophores in analogy to photosynthesis to ensure the directional flow of photonic energy. The assembly of molecules (primary structure) into supramolecular systems (secondary structure) has been well developed, and organization of these into crystalline materials (tertiary structure) is rapidly developing. However the hierarchical organization into materials that interact in predetermined ways with surfaces (quaternary structure) remains a keystone issue.[22]

Intermolecular Interactions: The design and implementation of porphyrin molecules bearing two or more different recognition motifs that can be systematically, either simultaneously or sequentially, used to construct ordered materials is affording the

next generation of supramolecular photonic materials. Controlled use of nonspecific interactions, in addition to H-bonding and different types of coordination chemistry, can result in more complex architectures. Note that the moieties used to assemble or organize the chromophores may bring a function in themselves or modulate the function of the system.[52-53] The role of the recognition motifs in photoinduced energy and electron transfer is not well understood. For example, energy transfer rates from donors to acceptors have been shown to depend on the direction across the intervening H-bonding groups used for self-assembly.[54]

Dynamics: The role of molecular dynamics in covalent electron donor-acceptor systems is well appreciated. There are a few reports on photoinduced conformational changes in systems containing porphyrins, and some are reversible for a limited number of cycles.[55] Considering the substantial vibrational energy imparted to chromophores upon light absorption,[11-13] the intermolecular forces holding supramolecular photonic materials together may weaken or break transiently or result in a reorganization of the nanoarchitecture. For example, in porphyrinic assemblies mediated by axial coordination to chelated metal ions, the axial ligands may transiently deligate in the excited state.[12] There is little work on the precise role of supramolecular dynamics in both the ground state and the excited state in the photonic properties of self-organized systems. A better understanding of these dynamics will afford additional design criteria. Combinations of time-resolved transient optical spectroscopy and time-resolved photoaccoustic analysis[56] of supramolecular porphyrinoid materials can probe the excited-state dynamics.

1.4 SELF-ORGANIZATION BY HYDROGEN BONDS

H-bonding can be a remarkably diverse driving force for the self-assembly and self-organization of materials. The exact nature of H-bonds, for example, the degree of electrostatic character, remains a topic of considerable interest.[57-58] H-bonds are commonly used for the fabrication of supramolecular assemblies because they are directional and have a wide range of interaction energies that are tunable by adjusting the number of H-bonds, their relative orientation, and their position in the overall structure.[58-60] H-bonds in the center of protein helices can be ca. 20 kcal mol^{-1} due to cooperative dipolar interactions.[59,61]

1.4.1 Intermolecular H-Bonding

Porphyrins bearing multiple H-bonding donor and acceptor groups are being investigated as components of new materials for a diverse array of applications [62] and to study the fundamental photophysics of these systems.[63] Because the porphyrin macrocycle is rigid, the placement of rigid H-bonding moieties and their relative orientation allows the design of a variety of specific architectures. For example, H-bond groups directed along the plane of the macrocycle and on the 5,10-meso positions afford a molecule with a rigid right angle topology,[1,64] whereas when these groups are on opposite sides, the 5 and 15 positions, a linear topology results. Alternatively, the H-bond groups can be directed above or below the plane of the macrocycle to organize structures vertically.[64] The variety of supramolecular structures using H-bonds as a primary driver of nanoarchitecture range from open to closed topologies, films on surfaces, tubes, wires, rods, and more complex 3D architectures. As with other supramolecular systems, the structure of solid state materials is also mediated by other nonspecific or designed

intermolecular interactions. The synergistic combination of different intermolecular interactions such as metal ion coordination and π-stacking with H-bonding allows formation of more robust materials and diversifies the possible structural orientation of the chromophores.[62,65-66] These self-assembled structures can be used in sensors, molecular sieves, photonics, and catalysis.[25]

1.4.2 Energy Transfer in Systems Organized by Hydrogen Bonds

Arrays of porphyrins assembled by covalent[67] and noncovalent[68] interactions are used as model systems to mimic natural photosynthesis. Supramolecular systems are used to understand the mechanism of electron transfer through intermolecular interactions. Nearly isoenergetic covalent porphyrin multimers on surfaces have electron transfer kinetics complicated by reverse reactions,[69] thus systems with different porphyrins or combinations of porphyrinoids arranged from greatest to least HOMO-LUMO energy gaps may afford better vectoral electron transfer. Beyond donor-acceptor dyads, it is difficult to design and precisely assemble in high yields multiple component structures with different dyes that possess energetic gradients (HOMO-LUMO gaps). Good yields with high structural fidelity are needed to examine the kinetics of electron or energy transfer down the energy gradient. However, recent work done using H-bonds and coordination chemistry to assemble arrays of porphyrins shows that efficient energy transfer may occur across the intermolecular bonds.[54,70]

H-bonding moieties directly attached to the meso positions result in rigid topologies that favor formation of organized structures. Similar to the coordination arrays, the use of heterocomplementary H-bond recognition units, such as 2,6-diacetamidopyridyl and uracyl, at specified geometries allows assembly of porphyrin

dimers, tapes, tetrameric squares, and two-dimensional sheets with various yields.[1,25,71-72] The right angle disposition of 5,15-(3,5-diacetamido-4-pyridyl) groups results in self-complementary interactions between porphyrins to form a square structure in solution, but in crystals of this array, one of the porphyrins cants at an angle to form a square helical structure that allows denser packing (Figure 1.2).[1,72] This illustrates the differences that can be found between solution and solid-state structures. Steady-state fluorescence of some of these square arrays indicates energy transfer across the H-bonding groups,[64,72] but not reported are lifetime and electron transfer measurements analogous to those on the recent square array assembled by coordination chemistry.[73]

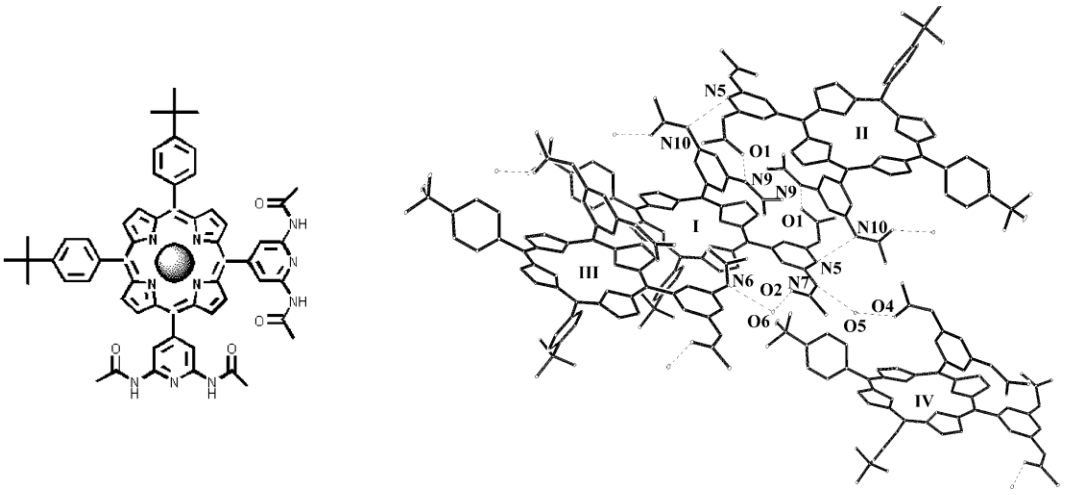

Figure 1.2 Self-assembly of square helix by self-complementary hydrogen bonding motifs. The recognition groups are attached directly to the meso positions of the porphyrins. Thus, the optimal positioning minimizes the dynamics that would decrease the structural fidelity of the assembled systems (from reference[1]).

1.5 PORPHYRIN-METAL-POLYOXOMETALATE COMPLEXES

Discrete, ternary porphyrin-metal-polyoxometalate (Por-MPOM) complexes, where M is a Hf(IV) or Zr(IV) metal ion bound both to the porphyrin core and to the lacunary site of a Keggin POM, $PW_{11}O_{39}^{-7}$, can be nearly quantitatively prepared.[74]The seven to eight coordination and large size of the metal ions forces them to reside outside the plane of the porphyrin macrocycle and protrude from the Keggin POM, thus enabling the simultaneous coordination to both. The physical properties of the $(TPP)Hf(PW_{11}O_{39})[TBA]_5$, $(TPyP)Hf(PW_{11}O_{39})[TBA]_5$, and $(TPP)Zr(PW_{11}O_{39})[TBA]_5$ complexes are similar. The crystal structure of $(TPyP)Hf(PW_{11}O_{39})[TBA]_5$ (Figure 1.3) is organized by H-bonding of water to the pyridyl moieties. This architecture couples the photonic properties of the porphyrin to the POM because the metal ion is incorporated into both frameworks. Thus the ternary complexes can serve as a basis for the characterization of Hf(IV) and Zr(IV) porphyrins bound to oxide surfaces via these metal ions. The Hf(Por) and Zr(Por) were found to bind strongly to TiO_2 nanoparticles and indium tin oxide (ITO) surfaces but significantly less bind to crystalline SiO_2 or TiO_2. The strong binding of the metalloporphyrins to the POM, TiO_2 nanoparticles, and ITO surfaces, together with the paucity of binding to crystalline surfaces, suggests that the three to four open coordination sites on the Hf(Por) and Zr(Por) are predominantly bound at surface defect sites. Whether this is a good means to bind porphyrins to sensitize the TiO_2 remains to be seen.

Hafnium(IV) metalloporphyrins have also been assembled into dimers with a variety of other multitopic oxygen containing ligands, such as sulfate and phosphate, which bind to the open coordination sites of the metal ion.[2] Using metal ions that reside

outside the plane of the macrocycle with multitopic counterions represents a new strategy for porphyrinoid assembly, and new photonic properties may emerge from these constructs and materials.

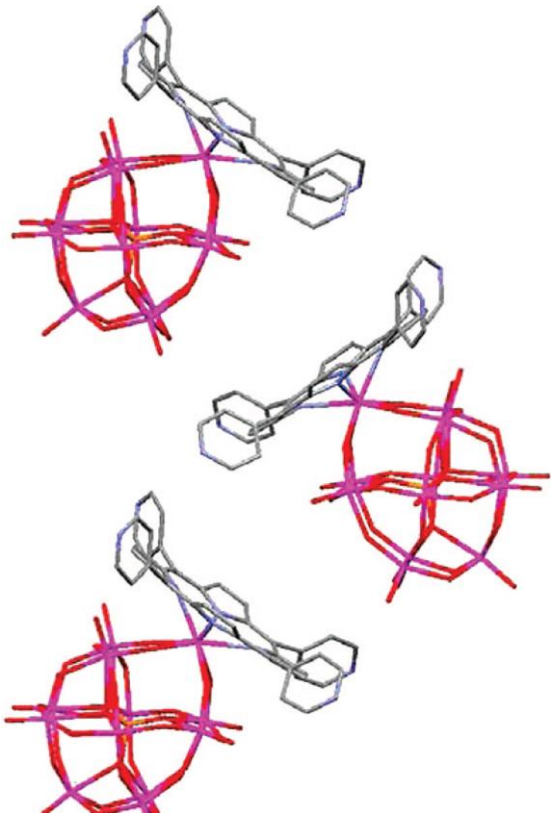

Figure 1.3 Crystal packing of the $[(TPyP)Hf(PW_{11}O_{39})]^{-5}$ complex shows formation of the zigzag pattern along the *a*-axis, solvent omitted, where the top surface of one porphyrin approaches the side of the POM of an adjacent complex. The structure is reinforced by H-bonds between water and the pyridyl moeieties.[2]

1.6 COMBINATIONS OF DIFFERENT CHROMOPHORES

There remains a paucity of self-assembled systems containing different chromophores, such as porphyrins and phthalocyanines, in precise architectures that can serve as efficient light-harvesting materials wherein energy flows in a predictable direction. Therefore new design algorithms are needed to assemble and organize two or more different types of dye into specific architectures before functional evaluation of these systems can lead to the design of new materials. In addition to added stability relative to the porphyrins, the extended π-systems in phthalocyanine and naphthalocyanines bring new photonic properties to the design palette, but it can be difficult to synthesize specific molecules. The formation of hybrid materials, such as porphyrins with fullerenes or with polyoxometalates, is developing rapidly as well. The supramolecular approaches to forming these hybrid systems aim to synergistically exploit the useful properties of each. These burgeoning efforts have yielded catalysts, but the detailed photonic properties are not well studied. Porphyrins adsorbed or organized onto conducting or semiconducting surfaces, either crystalline or nanoparticle, are yielding information on the transport properties in terms of molecular photonic and molecular electronic materials.[75] The majority of the well-characterized materials are self-assembled monolayers or crystals. The organized deposition of discrete self-assembled arrays onto surfaces remains a challenge, and as a result, the transport properties between these structures and conducting or semiconducting materials are poorly understood. Therefore, many exciting challenges remain in understanding the fundamental chemistry and physics of supramolecular photonic materials composed of porphyrins and other chromophores on surfaces.

1.7 APPLICATIONS FOR SOLAR ENERGY

Materials composed of porphyrinoids can be very robust to real-world conditions such as elevated temperatures, the presence of dioxygen and/or water. [21,45,76-78] Since the photonic and chemical properties of Pc are complementary to the Por (e.g. the UV-visible spectra, luminescence, stability, metal ion binding are different), supramolecular materials composed of combinations of chromophores will enable devices that are unobtainable using only one dye. As expected, additional fused benzenes on the Pc core, e.g. to yield naphthocyanine, shifts the absorption spectra to the red, but the additional fused benzene rings makes the ligands more vulnerable to oxidative degradation.[79]

Simple Pc derivatives are commodity chemicals used as dyes, toners, and photonics. Simple tetra aryl Por can be made in greater than 60% yield and can have similar applications.[80] For both Pc and Por, mixtures of positional isomers or even mixtures of compounds may be used as the material.[81] Core Por and Pc platforms that can serve as test-bed for new molecular design concepts have been reported (Figures 1.4 and 1.5).[82-84]

Dyes in solar cells. The advantages, disadvantages, and architectural considerations of organic and dye-based solar cell devices are well reviewed.[85-95] These generally fall into two groups: (a) dye-sensitized solar cells wherein a dye resides on an inorganic semiconductor surface such as TiO_2, SnO_2, and ZnO;[88] (b) organic solar cells that use conducting or semiconducting polymers. The main concerns with dye systems are charge separation and transport versus recombination kinetics. Recombination kinetics should be much slower than electron injection/collection. These depend on the component dyes, the substrate and the presence of intervening electron acceptors in the organic devices.

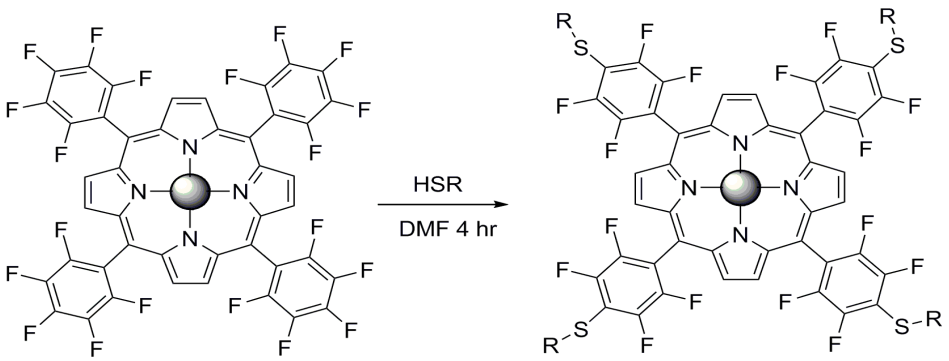

Figure 1.4 Facile modification of a core porphyrin platform, $TPPF_{20}$ enables investigate new molecular design concepts. For example, R = $(CH_2)_{11}CH_3$, or $CH_2CH_2(CF_2)_9CF_3$ Using a core Por platform affords chemically compatible systems. ● = $2H^+$ or metal ion.

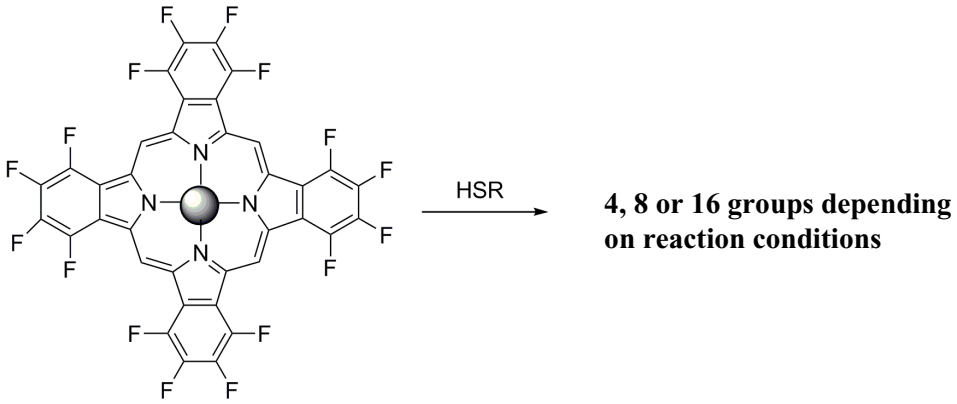

Figure 1.5 Facile modification of a core phthalocyanine platform, PcF_{16} enables investigation of new molecular design concepts. For example, Pc735 has eight $S(CH_2)_{11}CH_3$ mostly on the outside positions and Pc787 substitutes all of the F for the thioalkane. $SCH_2CH_2(CF_2)_9CF_3$ can also be used to form highly fluorous derivatives. Using a core Pc platform affords chemically compatible systems. ● = $2H^+$ or metal ion.

Since a good solar cell should have a 20+ year lifetime, the dye will need to undergo more than 10^8 turnover cycles without significant decomposition.[96] The goal of this work is to describe porphyrinoids that can be readily synthesized in large scales, and the chelates of earth-abundant metal ions. We focus herein on the dye systems that can be incorporated into devices that are designed for photovoltaics, photocatalysts for water splitting, or to derive the overpotential for water splitting catalysts.

Matching the excited state energies to the device design, such as substrate band gaps, is critical to performance. Charge injection or separation from the singlet state yields the most potential energy, but the triplet state may be sufficient in some device designs. Cyclic voltammetry and optical spectra allow the energies of the HOMO and LUMO to be evaluated.[97-98] Also, the photophysical properties of the dye need to be determined, e.g.: singlet state lifetimes, yield of inter-system-crossing to the triplet state, and triplet state lifetimes.

Surface Deposition. There are many means to deposit porphyrinoids onto surfaces ranging from chemical vapor deposition using elevated temperatures and high vacuum, to solution casting. The latter approach can be accomplished by spin casting, aerosol spraying, dipping, layer-by-layer methods, and electrodeposition. Each fabrication method has associated energy consumption and results in different surface morphologies. With judicious choice of substituents, it is possible to use self-organization via solution deposition to achieve highly ordered structures similar to those observed in materials made by CVD. Layer-by-layer methods for Por[99] and Pc[100] are more recent and afford opportunities to incorporate other active materials within the active layer in a sequential manor. There is also considerable work on examining the electrochemical[37,39-40,42,44-

[48,69,101] and transport[75] properties of Por and Pc covalently bound to surfaces, but for the most part these dyes are not commercially viable on the scales needed to deploy them for common usage. Though there are many papers describing porphyrins on surfaces, we concentrate here on active devices with simple dyes.

As opposed to covalently linked donor-bridge-acceptor and related molecules,[102] axial coordination of acceptors to metalloporphyrinoids can be a simpler means to constructing dye systems where the initial charge separation remains efficient, e.g. with SiPc-C_{60},[103] but significantly reduces the synthetic efforts. These donor-acceptor systems facilitate charge dislocation in active layers of several types of photovoltaic device. These constructs have been incorporated into a variety of active layer architectures, vide infra.

1.8 CONCLUSIONS

Self-assembly and self-organization may allow formation of active layers with several spectrally complementary chromophores in pre-specified geometries to more effectively harvest solar energy and convert it into electrochemical potential energy. Robust but reversible intermolecular interactions, such as metal ion coordination,[21,27,104-106] can realize complex supramolecular architectures by self-assembly such that the chromophores are in a specified order so that the direction of electron or energy transfer is correspondingly predictable, albeit in much less predictable quantum yields. Conversely, self-organized nanoparticles (aggregates) of dyes such as Por[26,76,107] and Pc[108-109] with much less structural order, or colloidal crystals[110] can display significantly enhanced or modulated photonic properties because of quantum mechanical effects at this scale.[109,111] A considerable advantage of the organic NP systems is that the dyes can be

simple commercial molecules and the exocyclic motif used to enhance materials and photonic properties rather than potentiate intermolecular interactions. Thus, in conjunction with advances in device design, the deployment of commercially viable dyes in the active layers, including chelates of earth-abundant metal ion, will require supramolecular design concepts.

Part of this discussion are adopted from a perspective " Commercially Viable Porphyrinoid Dyes for Solar Cells" , Ivana Radivojevic, Alessandro Varotto , Charles M. Drain submitted to J. Energy. Environ. Sci.

References

(1) Shi, X.; Barkigia, K. M.; Fajer, J.; Drain, C. M. J. Org. Chem. 2001, 66, 6513-6522.

(2) Falber, A.; Todaro, L.; Goldberg, I.; Favilla, M. V.; Drain, C. M. Inor. Chem. 2008, 47, 454-467.

(3) Dolphin, D. The Porphyrins. Physical Chemistry, Part A; Academic Press: New York, 1978; Vol 3.

(4) Smith, K. M. Porphyrins and Metaloporphyrins; Elsevier Amsterdam, 1972.

(5) Suslick, K. S. In The Porphyrin Handbook; Kadish, K. M., Smith, K. M., Guilard, R., Eds.; Academic Press: New York, 2000; Vol. 6

(6) Drain, C. M.; Chen., X. In Encyclopedia of Nanoscience & Nanotechnology; Nalwa, H. S., Ed.; American Scientific Press: New York, 2004; Vol. 9, pp 593-616

(7) Mauzerall, D. C. Clin. Dermatol. 1998, 6, 195–201.

(8) Gouterman, M. In The Porphyrins; Dolphin, D., Ed.; Academic Press: New York, 1978; Vol. 3, p 1-153

(9) Lehn, J.-M. Science 2002, 2400-2403.

(10) Khalil, G. E.; Chang, A.; Gouterman, M.; Callis, J. B.; Dalton, L. R.; Turro, N. J.; Jockusch, S. Rev.Sci. Instrum. 2005, 76, 54101-54101 -54101-54108.

(11) Drain, C. M.; Gentemann, S.; Roberts, J. A.; Nora Y. Nelson; Medforth, C. J.; Jia, S.; Simpson, M. C.; Smith, K. M.; Fajer, J.; Shelnutt, J. A.; Holten, D. J. Am. Chem. Soc. 1998, 120, 3781-3791.

(12) Retsek, J. L.; Drain, C. M.; Kirmaier, C.; Nurco, D. J.; Medforth, C. J.; Smith, K. M.; Sazanovich, I. V.; Chirvony, V. S.; Fajer, J.; Holten., D. J. Am. Chem. Soc. 2003, 125, 9787-9800.

(13) Drain, C. M.; Kirmaier, C.; Medforth, C. J.; Nurco, D. J.; Smith, K. M.; Holten, D. J. Phys. Chem. 1996, 100, 11984-11993.

(14) Retsek, J. L.; Gentemann, S.; Medforth, C. J.; Smith, K. M.; Chirvony, V. S.; Fajer, J.; Holten, D. J. Phys. Chem. B 2000, 104, 6690-6693.

(15) Retsek, J. L.; Medforth, C. J.; Nurco, D. J.; Gentemann, S.; Chirvony, V. S.; Smith, K. M.; Holten, D. J. Phys. Chem. B 2001, 105, 6396-6411.

(16) Drain, C. M.; Christensen, B.; Mauzerall, D. C. Proc. Natl. Acad. Sci. USA 1989, 86, 6959-6962.

(17) Drain, C. M.; Mauzerall, D. Bioelectrochem. Bioenerg. 1990, 24, 263-268.

(18) Drain, C. M.; Mauzerall, D. C. Biophys. J. 1992, 63, 1556-1563.

(19) Drain, C. M.; Lehn, J.-M. Chem. Commun. 1994, 2313-2315 (correction 1995, p2503).

(20) Drain, C. M.; Russel, K. C.; Lehn, J.-M. Chem. Commun. 1996, 337-338.

(21) Drain, C. M.; Nifiatis, F.; Vasenko, A.; Batteas, J. D. Angew. Chem. Int. Ed. 1998, 37, 2344-2347.

(22) Drain, C. M. Proc. Natl. Acad. Sci. USA 2002, 99, 5178-5182.

(23) Drain, C. M.; Batteas, J. D.; Flynn, G. W.; Milic, T.; Chi, N.; Yablon, D. G.; Sommers, H. Proc. Natl. Acad. Sci., USA 2002, 99, 6498-6502.

(24) Drain, C. M.; Smeureanu, G.; Batteas, J.; Patel, S. In Dekker Encyclopedia of Nanoscience and Nanotechnology; Schwartz, J. A., Contescu, C. I., Putyera, K., Eds.; Marcel Dekker, Inc.: New York, 2004; p 3481-3502

(25) Drain, C. M.; Bazzan, G.; Milic, T.; Vinodu, M.; Goeltz, J. C. Isr. J. Chem. 2005, 45, 255–269.

(26) Drain, C. M.; Smeureanu, G.; Patel, S.; Gong, X.; Garno, J.; Arijeloye, J. New J. Chem. 2006, 30, 1834-1843.

(27) Drain, C. M.; Varotto, A.; Radivojevic, I. Chem. Rev. 2009, 109, 1630-1658.

(28) Milic, T. N.; Chi, N.; Yablon, D. G.; Flynn, G. W.; Batteas, J. D.; Drain, C. M. Angew. Chem., Int. Ed. 2002, 41, 2117-2119.

(29) Lehn, J.-M. Supramolecular Chemistry: Concepts and Perspectives; Wiley VCH: Weinheim, 1995.

(30) de Silva, A. P.; Uchiyama, S.; Vance, T. P.; Wannalerse, B. Coord. Chem. Rev. 2007, 251, 1623-1632.

(31) Loeb, S. J. Chem. Soc. Rev. 2007, 36, 226-235.

(32) Hoeben, F. J. M.; Jonkheijm, P.; Meijer, E. W.; Schenning, A. P. H. J. Chem. Rev. 2005, 105, 1491-1546.

(33) Papaefstathiou, G. S.; MacGillivray, L. R. Coord. Chem. Rev. 2003, 246, 169-184.

(34) Alivisatos, A. P.; Barbara, P. F.; Castleman, A. W.; Chang, J.; Dixon, D. A.; Klein, M. L.; McLendon, G. L.; Miller, J. S.; Ratner, M. A.; Rossky, P. J.; Stupp, S. I.; Thompson, M. E. Adv. Mater. 1998, 10, 1297-1336.

(35) Basabe-Desmonts, L.; Reinhoudt, D. N.; Crego-Calama, M. Chem. Soc. Rev. 2007, 36, 993-1017.

(36) Schmittel, M.; Kalsani, V.; Bats, J. W. Inor. Chem. 2005, 44, 4115-4117.

(37) Milic, T.; Garno, J. C.; Batteas, J. D.; Smeureanu, G.; Drain, C. M. Langmuir 2004, 20, 3974-3983.

(38) Drain, C. M.; Milic, T.; Garno, J. C.; Smeureanu, G.; Batteas, J. D. ACS Polymer Reprints 2004, 45, 346-347.

(39) Padmaja, K.; Youngblood, W. J.; Lingyun, W.; Bocian, D. F.; Lindsey, J. S. Inor. Chem. 2006, 45, 5479-5492.

(40) Padmaja, K.; Lingyun, W.; Lindsey, J. S.; Bocian, D. F. J. Org. Chem. 2005, 70, 7972-7978.

(41) Wang, Z.; Zhiyong, L.; Medforth, C. J.; Shelnutt, J. A. J. Am. Chem. Soc. 2007, 129, 2440-2441.

(42) Zhiming, L.; Yasseri, A. A.; Loewe, R. S.; Lysenko, A. B.; Malinovskii, V. L.; Qian, Z.; Surthi, S.; Qiliang, L.; Misra, V.; Lindsey, J. S.; Bocian, D. F. J. Org. Chem. 2004, 69, 5568-5577.

(43) Yasseri, A. A.; Syomin, D.; Loewe, R. S.; Lindsey, J. S.; Zaera, F.; Bocian, D. F. J. Am. Chem. Soc. 2004, 126, 15603-15612.

(44) Qiliang, L.; Surthi, S.; Mathur, G.; Gowda, S.; Qian, Z.; Sorenson, T. A.; Tenent, R. C.; Muthukumaran, K.; Lindsey, J. S.; Misra, V. Appl. Phys. Lett. 2004, 85, 1829-1831.

(45) Muthukumaran, K.; Loewe, R. S.; Ambroise, A.; Tamaru, S. i.; Li, Q.; Mathur, G.; Bocian, D. F.; Misra, V.; Lindsey, J. S. J. Org. Chem. 2004, 69, 1444-1452.

(46) Liu, Z.; Yasseri, A. A.; Loewe, R. S.; Lysenko, A. B.; Malinovskii, V. L.; Zhao, Q.; Surthi, S.; Li, Q.; Misra, V.; Lindsey, J. S.; Bocian, D. F. J. Org. Chem. 2004, 69, 5568-5577.

(47) Patchanita, T.; Lianhe, Y.; Padmaja, K.; Jieying, J.; Bocian, D. F.; Lindsey, J. S. J. Org. Chem. 2006, 71, 1156-1171.

(48) Balakumar, A.; Lysenko, A. B.; Carcel, C.; Malinovskii, V. L.; Gryko, D. T.; Schweikart, K. H.; Loewe, R. S.; Yasseri, A. A.; Liu, Z.; Bocian, D. F.; Lindsey, J. S. J. Org. Chem. 2004, 69, 1435-1443.

(49) Scudiero, L.; Hipps, K. W.; Barlow, D. E. The J.Phys.Chem. B 2003, 107, 2903-2909.

(50) Barlow, D. E.; Scudiero, L.; Hipps, K. W. Langmuir 2004, 20, 4413-4421.

(51) Ogunrinde, A.; Hipps, K. W.; Scudiero, L. Langmuir 2006, 22, 5697-5701.

(52) Wasielewski, M. R. J. Org. Chem. 2006, 71, 5051-5066.

(53) Ahrens, M. J.; R.F.Kelley; Z.E.Dance; M.R.Wasielewski Phys. Chem. Chem. Phys. 2007, 9, 1469-1478.

(54) Balaban, T. S.; Berova, N.; Drain, C. M.; Hauschild, R.; Huan, X.; Kalt, H.; Lebedkin, S.; Lehn, J.-M.; Nifaitis, F.; Pescitelli, G.; Prokhorenko, V. I.; Riedel, G.; Smeureanu, G.; Zeller, J. Chem. Eur. J. 2007, 13, 8411 – 8427.

(55) Kinbara, K.; Aida, T. Chem. Rev.2005, 105, 1377-1400.

(56) Mauzerall, D.; Liu, Y.; Edens, G. J.; Grzymski, J. Photochem. Photobiol. Sci. 2003, 2, 788 - 790.

(57) Salvador, P.; Dannenberg, J. J. J. Phys. Chem. B 2004, 108, 15370-15375.

(58) Wieczorek, R.; Haskamp, L.; Dannenberg, J. J. J. Phys. Chem. A 2004, 108, 6713-6723.

(59) Dannenberg, J. J.; Haskamp, L.; Masunov, A. J. Phys. Chem. A 1999, 103, 7083-7086.

(60) Masunov, A.; Dannenberg, J. J. J. Phys. Chem. B 2000, 104, 806-810.

(61) Asensio, A.; Kobko, N.; Dannenberg, J. J. J. Phys. Chem. A 2003, 107, 6441-6443.

(62) George, S.; Goldberg, I. Cryst. Growth Des. 2006, 6, 755-762.

(63) Fujimoto, K.; Toyoshi, T.; Doi, Y.; Inouye, M. Mater. Sci. Eng. C. 2007, 27, 142.

(64) Drain, C. M.; Fischer, R.; Nolen, E. G.; Lehn, J.-M. Chem. Commun. 1993, 243 - 245.

(65) Lipstman, S.; Muniappan, S.; George, S.; Goldberg, I. CrystEngComm 2006, 8, 601-607.

(66) Shmilovits, M.; Vinodu, M.; Goldberg, I. New J. Chem. 2004, 28, 223-227.

(67) Holten, D.; Bocian, D. F.; Lindsey, J. S. Acc. Chem. Res. 2002, 35, 57-69.

(68) Balaban, T. S.; Linke-Schaetzel, M.; Bhise, A. D.; Vanthuyne, N.; Roussel, C.; Anson, C. E.; Buth, G.; Eichh fer, A.; Foster, K.; Garab, G.; Gliemann, H.; Goddard, R.; Javorfi, T.; Powell, A. K.; R sner, H.; Schimmel, T. Chem. Eur. J. 2005, 11, 2267-2275.

(69) Wei, L.; Syomin, D.; Loewe, R. S.; Lindsey, J. S.; Zaera, F.; Bocian, D. F. J. Phys. Chem. B 2005, 109, 6323-6330.

(70) Koepf, M.; Trabolsi, A.; Elhabiri, M.; Wytko, J. A.; Paul, D.; Albrecht-Gary, A. M.; Weiss, J. Org. Lett. 2005, 7, 1279-1282.

(71) Drain, C. M.; Goldberg, I.; Sylvain, I.; Falber, A. Top.Curr. Chem. 2005, 245, 55-88.

(72) Drain, C. M.; Shi, X.; Milic, T.; Nifiatis, F. Chem. Commun. 2001, 287–288.

(73) Jensen, R. A.; Kelley, R. F.; Lee, S. J.; Wasielewski, M. R.; Hupp, J. T.; Tiede, D. M. Chem. Commun. 2008, 16, 1886–1888.

(74) Falber, A.; Burton-Pye, B. P.; Radivojevic, I.; Todaro, L.; Saleh, R.; Francesconi, L.; Drain, C. M. Eur.J.Inorg.Chem. 2009, 2459-2466.

(75) Chan, Y. H.; Schuckman, A. E.; Perez, L. M.; Vinodu, M.; Drain, C. M.; Batteas, J. D. J. Phys. Chem. C 2008, 112, 6110-6118.

(76) Gong, X.; Milic, T.; Xu, C.; Batteas, J. D.; Drain, C. M. J. Am. Chem. Soc. 2002, 124, 14290-14291.

(77) Liu, Z.; Yasseri, A. A.; Lindsey, J. S.; Bocian, D. F. Science 2003, 302, 1543-1546.

(78) Pasetto, P.; Chen, X.; Drain, C. M.; Franck, R. W. Chem. Commun. 2001, 81–82 (erratum 507).

(79) Kobayashi, N. D. P.; Nakajima, S.-i. D.; Ogata, H. D.; Fukuda, T. D. Chem -A Eur. J. 2004, 10, 6294 - 6312.

(80) Kadish, K.; Smith, K. M.; Guiard, R. The Porphyrin Handbook; Academic Press: New York, 2000,2003.

(81) Varotto, A.; Nam, C.-Y.; Radivojevic, I.; Tom , J. P. C.; Cavaleiro, J. A. S.; Black, C. T.; Drain, C. M. J. Am. Chem. Soc. 2010, 132, 2552-2554.

(82) Leznoff, C. C.; Sosa-Sanchez, J. L. Chem. Commun. 2004, 338 - 339.

(83) Samaroo, D.; Soll, C. E.; Todaro, L. J.; Drain, C. M. Org. Lett. 2006, 8, 4985 - 4988.

(84) Samaroo, D.; Vinodu, M.; Chen, X.; Drain, C. M. J. Combi. Chem 2007, 9, 998-1011.

(85) Campbell, W. M.; Burrell, A. K.; Officer, D. L.; Jolley, K. W. Coor.Chem.Rev. 2004, 248, 1363–1379.

(86) Heremans, P.; Cheyns, D.; Rand, B. P. Acc.Chem. Res. 2009, 42, 1740-1747.

(87) Grätzel, M. Acc.Chem. Res. 2009, 42, 1788-1798.

(88) Yu, K.; Chen, J. Nanoscale. Res. Lett. 2009, 1-10.

(89) Kippelen, B.; Br das, J.-L. Energy Environ. Sci. 2009, 2, 251 - 261.

(90) Mishra, A.; Fischer, M. K. R.; Buerle, P. Angew. Chem. Int. Ed. 2009, 48, 2474 – 2499.

(91) Peet, J.; Heeger, A. J.; Bazan, G. C. Acc.Chem. Res. 2009, 42, 1700-1708.

(92) Potscavage, W. J.; Sharma, A.; Kippelen, B. Acc.Chem.Res. 2009, 42, 1758-1767.

(93) Roncali, J. Acc.Chem.Res. 2009, 42, 1719-1730.

(94) Perez, M. D.; Borek, C.; Forrest, S. R.; Thompson, M. E. J. Am. Chem. Soc. 2009, 131, 9281-9286.

(95) Yang, F.; Forrest, S. R. ACS Nano 2008, 2, 1022-1032.

(96) Grätzel, M. J.Photochem.Photobiol. C: Photochem.Rev. 2003, 4, 145–153.

(97) Kim, S.; Lee, J. K.; Kang, S. O.; Ko, J.; Yum, J. H.; Fantacci, S.; De Angelis, F.; Di Censo, D.; Nazeeruddin, M. K.; Grätzel, M. J. Am. Chem. Soc. 2006, 128, 16701-16707.

(98) J rgen, H. Angew. Chem. Int. Ed. 1984, 23, 831-847.

(99) Bazzan, G.; Smith, W.; Francesconi, L.; Drain, C. M. Langmuir 2007, 24, 3244 - 3249.

(100) Doherty, W. J.; Friedlein, R.; Salaneck, W. R. J. Phys. Chem. C, 2007 2007, 111, 2724–2729.

(101) Wei, L.; Tiznado, H.; Liu, G.; Padmaja, K.; Lindsey, J. S.; Zaera, F.; Bocian, D. F. J. Phys. Chem. B 2005, 109, 23963-23971.

(102) Albinsson, B.; Mårtensson, J. J.Photochem.Photobiol. C: Photochem. Rev. 2008, 9, 138-155.

(103) Honda, S.; Nogami, T.; Ohkita, H.; Benten, H.; Ito, S. ACS Appl. Mater. Interfaces 2009, 1, 804-810.

(104) Drain, C. M.; Hupp, J. T.; Suslick, K. S.; Wasielewski, M. R.; Chen, X. J. Porph. Phthal. 2002, 6, 241-256.

(105) Cheng, K. F.; Thai, N. A.; Teague, L. C.; Grohmann, K.; Drain, C. M. Chem. Commun. 2005, 4678-4680.

(106) Lee, S. J.; Hupp, J. T. Coord. Chem. Rev. 2006, 250, 1710-1723.

(107) Smeureanu, G.; Aggarwal, A.; Soll, C. E.; Arijeloye, J.; Malave, E.; Drain, C. M. Chem. Eur. J. 2009, 15, 12133 - 12140.

(108) Keuren, E. V.; Bone, A.; Ma, C. Langmuir 2008, 24, 6079-6084.

(109) Nitschke, C.; O'Flaherty, S. M.; Kroll, M.; Doyle, J. J.; Blau, W. J. Chem. Phys. Lett. 2004, 383, 555-560.

(110) Berhanu, S.; McLachlan, M. A.; McComb, D. W.; Jones, T. S., San Diego, CA, USA, 2008; p 70521H-70510.

(111) Rangel-Rojo, R.; Matsuda, H.; Kasai, H.; Nakanishi, H. J. Opt. Soc. Am. B 2000, 17, 1376-1382.

CHAPTER 2

Self-Organized Nanofibers and Nanorods of Porphyrins Bearing Hydrogen Bonding Motifs

2.1 INTRODUCTION [*]

Self-assembled and self-organized nanoarchitectures of porphyrinoids are of great interest for diverse applications, such as sensors, molecular sieves, catalysts, photonic and electronic materials such as photosensitized solar cells.[1] Since porphyrins have tunable photophysical and chemical properties, the functionalities of their materials can be designed. Photosynthetic antenna complexes contain self-assembled arrays of pigments in precise architectures, thus supramolecular porphyrin arrays also are studied as model systems for light harvesting. Assemblies of chromophores formed via non-covalent interactions such as electrostatics, H-bonding, metal ion coordination, π-stacking, dispersion forces, and combinations of these, can yield robust supramolecular photonic materials.[1] The organization of supramolecular systems in solution can be different than on surfaces since both the deposition process, e.g. fluid dynamics, and surface structure/energetics can play pivitol rols.[2]

[*] This work is reproduced by permission of the Royal Society of Chemistry website and adopted from Ivana Radivojevic, Ija Likhtina, Xinxu Shi, Sunaina Singh, Charles Michael Drain "Self-organized Nanofibres and Nanorods of Porhyrins Bearing Hydrogen Bonding Motiefs" *Chem. Commun.*, **2010**, 46, 1643–1645.

There are numerous reports on the fabrication of nanostructured porphyrinic materials on surfaces.[2,3] Complex multiporphyrin monomers[3b] and porphyrins with motifs on the 5,15-positions,[3c] can form nanofibers and nanocrystals, respectively. Nanorods [4,] nanotubes,[5] nanowires,[6] rings,[7]and micelles[8] are reported. The work of Shelnutt [5a,b,9] shows that appropriate conditions can be found to form nanotubes from simple Sn(IV) porphyrins driven by electrostatic interactions combined with axial coordination. The diverse supramolecular structures of Kobuke[10] and Balaban[3] are driven by self-complementary coordination and H-bond interactions. Long alkyl chains can also organize porphyrins into nanorods or fibers.[11] Since these assemblies rely on strong interporphyrin interactions and/or complex molecular topologies, the formation of robust nanofibers primarily mediated by weak H-bonds and π-π interactions between simple porphyrins is unexpected (Figure 2.1). This study provides further insights into the design principles, processing, and extent of electron and energy transfer in supramolecular porphyrin materials.

Thermodynamic equilibriums between different supramolecular structures or aggregates in weakly self-organized systems change throughout the deposition process because of the changing of environmental conditions. Concentration, temperature, moisture, solvent, evaporation rate, fluid dynamics, and surface energetics combine to dictate the solid state structure of these materials on surfaces.[2,3] Here, we illustrate these concepts by the self-organization of 5,10,15,20-tetrakis(1-butyl-6-uracyl) porphyrinato zinc(II) (ZnTUrP)[12] wherein the uracyl moieties serve as homo-complementary H-bonding donor acceptor motifs, and by the free base 5,10,15,20-tetrakis-(1-pyrenyl)porphyrin (TPyrP)[13] wherein organization is effected by the π-stacking of the

pyrenyl moieties (Figure 2.1). The morphology of self-organized ZnTUrP on glass and mica surfaces ranges from thin films to nanorods and nanofibers depending on deposition conditions, while the TPyrP forms nanoparticles only.

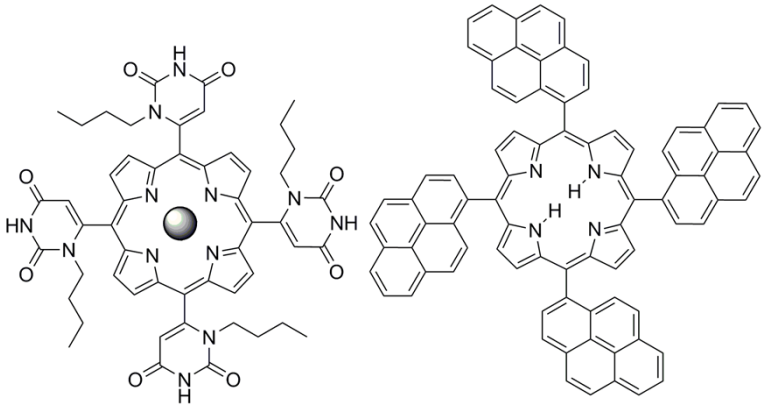

Figure 2.1 Left: 5,10,15,20-tetrakis(1-butyl-6-uracyl)porphyrin; the sphere represents Zn(II) (ZnTUrP) or free base (TUrP). Right: 5,10,15,20-tetrakis(1-pyrenyl)porphyrin (TPyrP). The uracyl and the pyrenyl groups are orthogonal to the porphyrin plane and the mixture of the four atropisomers (αααα, αααβ, ααββ, αβαβ, as synthesized) were used.

2.2 DISCUSSION AND RESULTS

2.2.1. H-bonding interactions

The uracyl moieties at the four meso porphyrin positions present motifs that can form self-complementary double H-bonds (ca. 15-21 KJ mol^{-1}, Fig. 2.2).[12] Though zinc metalloporphyrins have a propensity to aggregate by π-stacking with about the same energy,[14] the orthogonal uracyl moieties project the N-butyl group above/below the

porphyrin plane to diminish π-stacking interactions. The atropisomers do not significantly influence the H-bond energetics and kinetics of self-assembly in solution. [12]

The morphology of the deposited materials found by casting solutions of ZnTUrP onto surfaces depends on a variety of environmental conditions. Tetrahydrofuran (THF) is a good solvent for these porphyrins and weakly hydrogen bonds with the uracyl N-H.

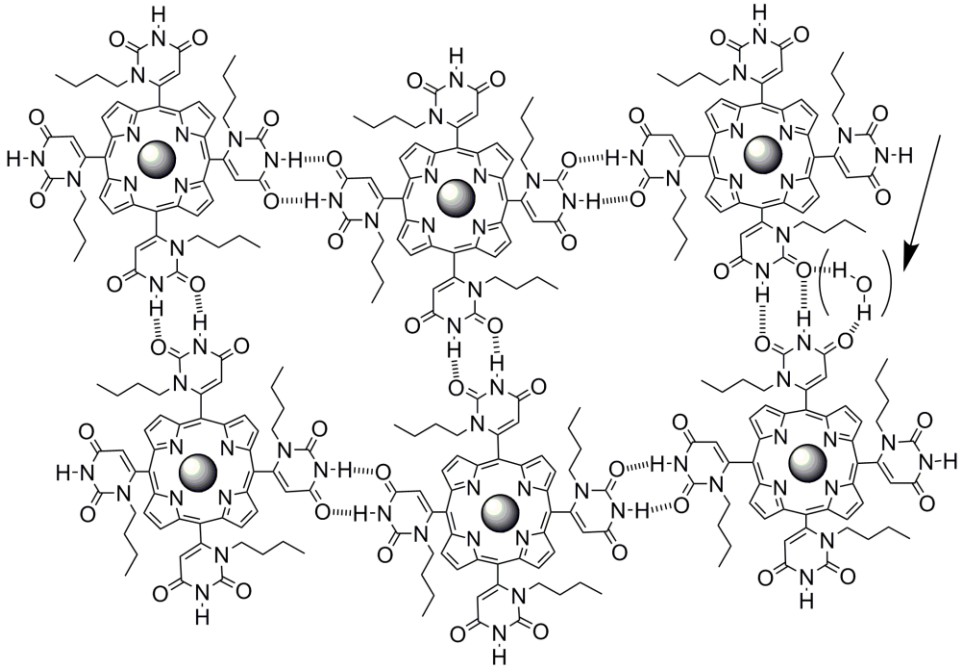

Figure 2.2 Possible arrangement of porphyrins in the materials mediated by H-bonds. The arrow indicates possible participation of water in the self-organization**.** The uracyls moieties remain orthogonal to the porphyrin.

Atomic force microscopy (AFM) studies reveal that the porphyrin materials cast from wet THF (ca. 5% water) onto mica and glass consistently results in 5-20 nm thin films with varying degrees of surface coverage, whereas when deposited from dry THF,

ZnTUrP forms nanofibers and nanorods (Figure 2.3). Deposition from 10 μM solutions yields similar structures but with less surface coverage than from 100 μM solutions.

Since the porphyrin with the substituents is ca. 0.5 nm thick, and most adsorbed porphyrins lay flat on surface,[1c,2] the films likely represent 10 to 40 layers. The formation of the thin films is driven primarily by equatorial H-bond interactions. The water in the solvent competes with the H-bond sites, likely participates in the organization of the films (Figure 2.2),[12] and slows the evaporation rates to allow film formation. Thus, films represent an equilibrium architecture. The water in the solvent also interacts with the substrates to modulate the adsorption of the porphyrinic materials.

Cast from dry THF solutions, ZnTUrP self-organizes into nanofibers and rods with somewhat more surface density on mica compared to glass. The results suggest that 3-D structures are due to both H-bonds along the porphyrin plane and π-stacking interactions in the axial direction. The 1-butyl groups can modulate the π-π interactions differently depending on their conformations in the different solvents arising from hydrophobic effects. On mica nanorods and nanofibers are formed from both 10 μM and 100 μM solutions of ZnTUrP, independent of solvent evaporation rate (Figure 2.3). On mica, the nanorods are measured to be 6-25 nm high by 200-600 nm long, (Figure 2.4,2.5 ,2.6) while the fiber heights range from 2-50 nm and can be many μm long. On glass substrates, no fibers or rods were observed from the 100 μm solution (Figure 2.7). Deposition of the 10 μm ZnTUrP solution yields many bundels of fibers with heights ranging form 2-45 nm, again independent of solvent evaporation rate (Figure 2.8). Examination of many samples indicates that many fibers possess substructures, but there is no clear indication of a fundamental structural unit in the height histograms (Figure

2.9, 2.10, 2.11, 2.12). From uracyl NH to uracyl NH, the porphyrin is ca. 1.8 nm wide and this is the minimum height measured. Alternatively this height can represent ca. three porphyrins stacked.

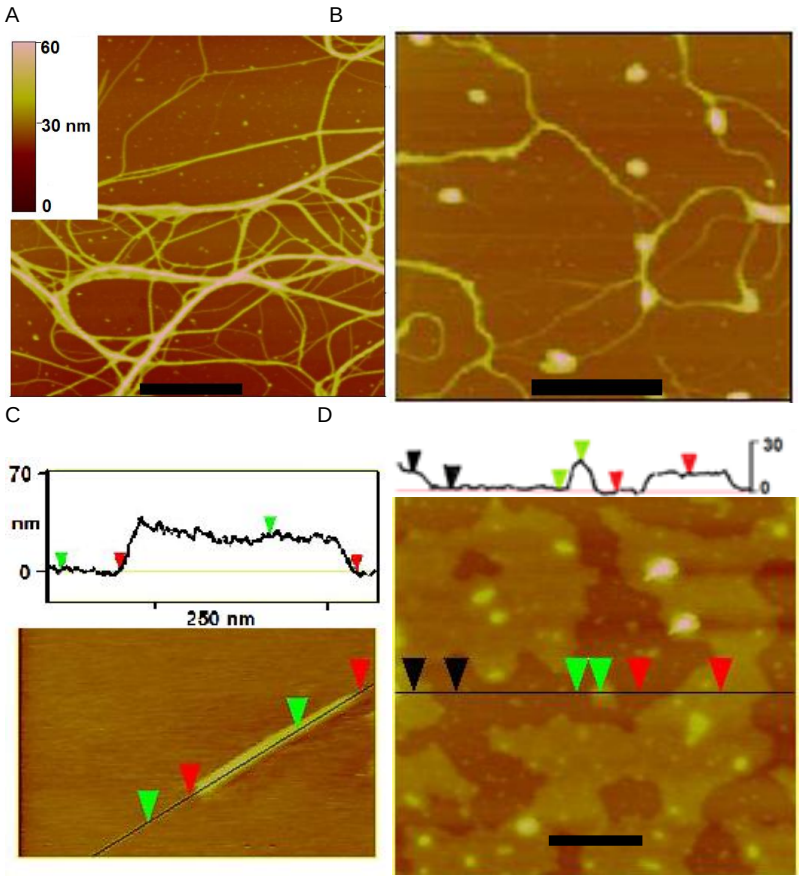

Figure 2.3 ZnTUrP nanostructures: (A) nanofibers on mica from 100 µM in dry THF; (B) nanofibers on mica from 10 µM in dry THF; (C) a nanorod on glass from 10 µM in dry THF; (D) a film cast on mica from a 10 µM solution of 5% water in THF; scale bars = 200 nm. Supporting information shows films cast on glass from a 100 µM solution of 5% water in THF are 14-20 nm, other AFM studies and histograms.

These results indicate that the fibers and rods are kinetically trapped products wherein π-π and H-bond interactions cooperate to dictate growth rate. The rigid attachment of the H-bond moieties to the macrocycle limits the molecular and supramolecular dynamics, thereby allowing the formation of rods and fibers. When similar H-bonding groups are attached via flexible alkane linkers, neither rods nor fibers are observed under a variety of conditions.[3]

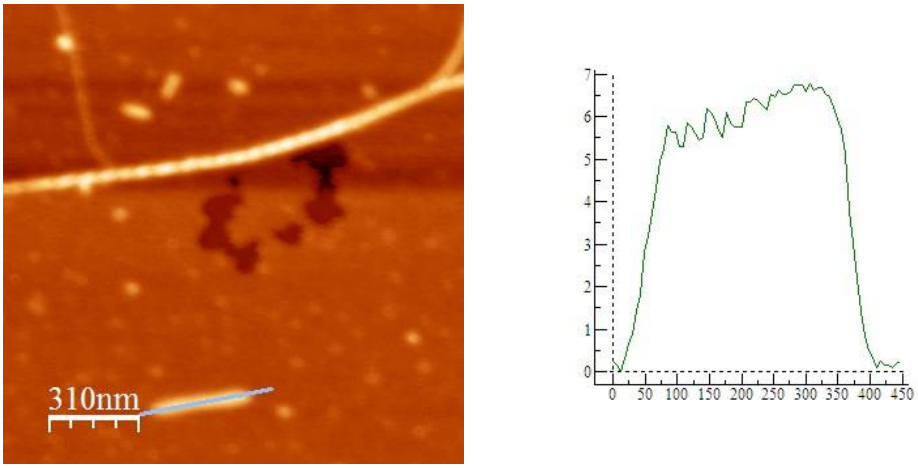

Figure 2.4. Vertical and horizontal distance of a nanorod formed from a 100 μM ZnTUrP solution in dry THF cast on mica using a slow evaporation rate.

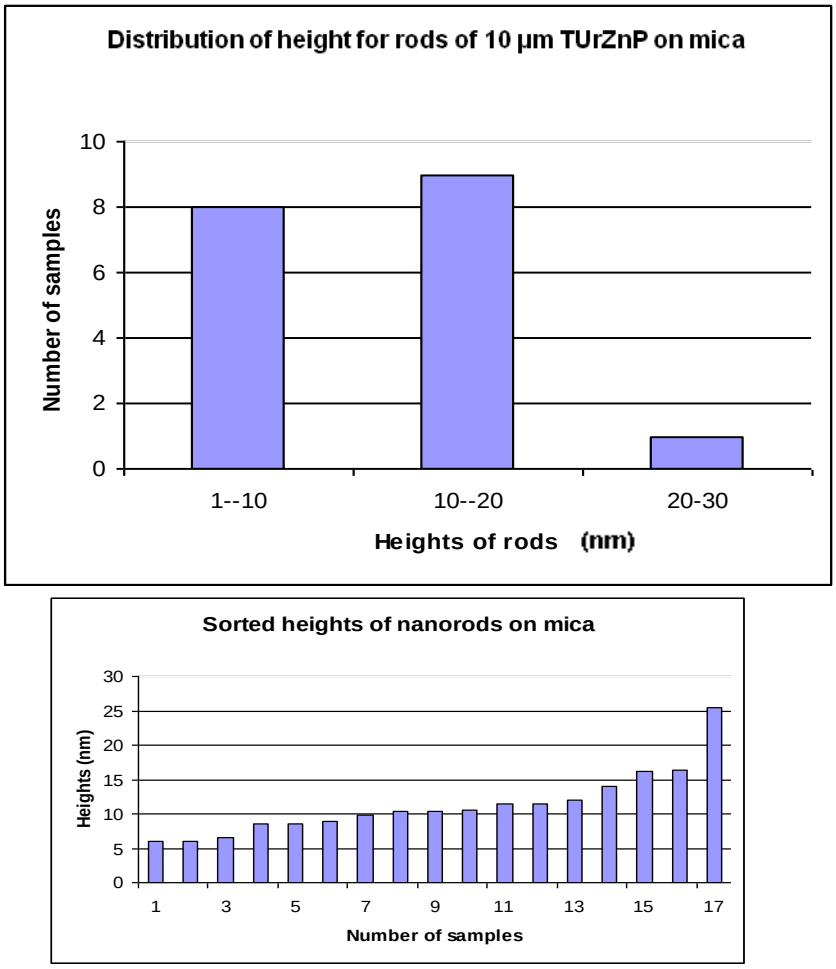

Figure 2.5. Distribution of vertical distances for nanorods deposited out of a 10 µM THF solution on mica. The lower plot shows the sorted values of heights of individual nanorods ranging from 6.0 nm to 25.4 nm for slow rates of evaporation.

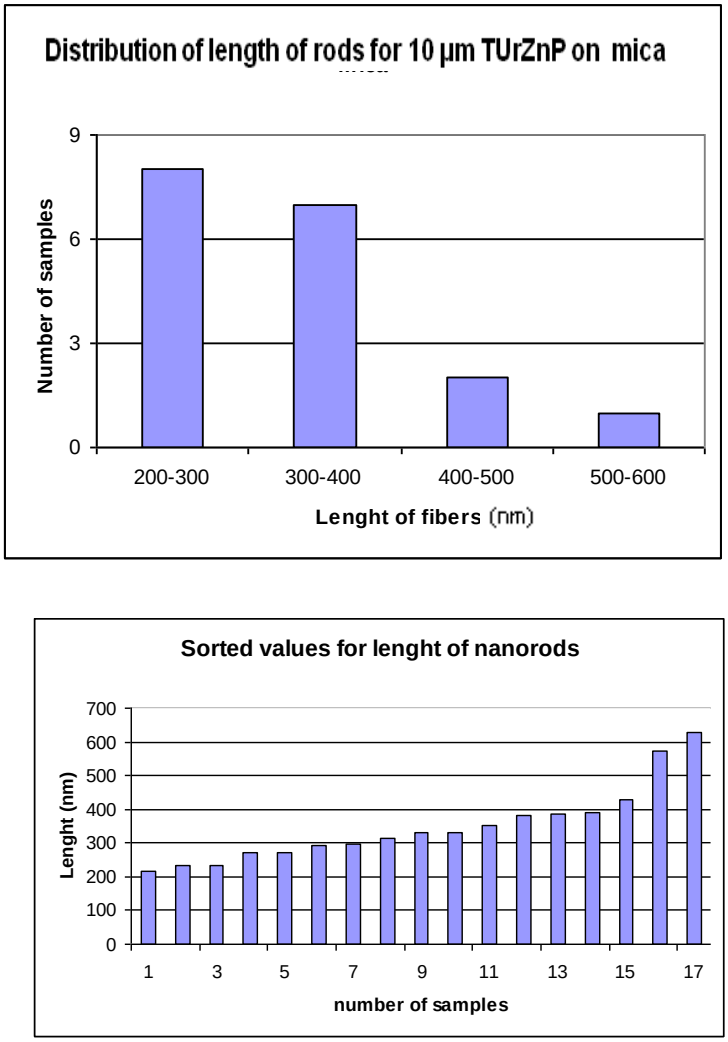

Figure 2.6. Distribution of horizontal distances for nanorods deposited out of 10 µM THF solutions on mica using a slow rate of evaporation. The lower plot shows the sorted values of length of individual nanorods ranging from 215 nm to 629 nm.

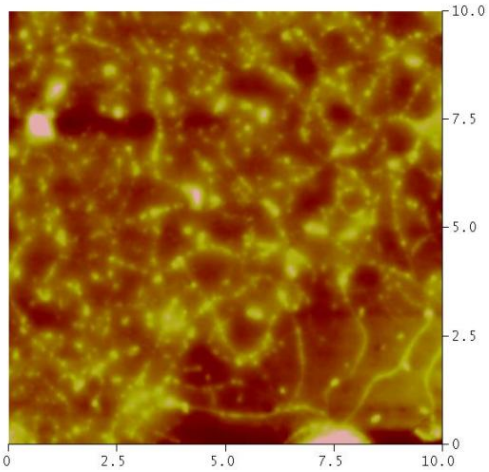

Figure 2.7. A 100 μM ZnTUrP solution drop cast from dry THF on a glass substrate with a slow evaporation rate results in a few fibrous nanostructures and a preponderance of island. No fibers or rods are observed using faster evaporation rates.

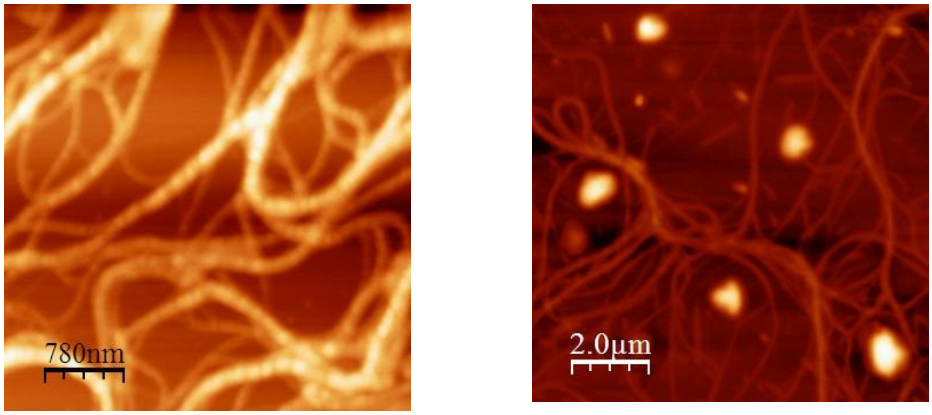

Figure 2.8. Images indicating that different surface energetic do not influence formation of very dense bundles of nanofibers from a 10 μM ZnTUrP solution drop cast from dry THF on mica (left) and glass slides (right) with a faster rate of evaporation. The smallest heights in these figures correspond to one ZnTUrP unit of 2 nm (see Figure 2.11).

A

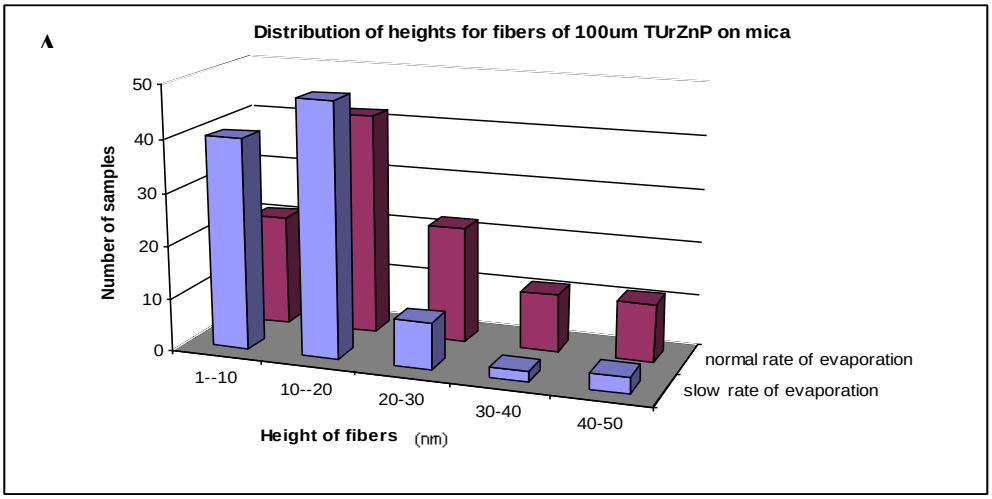

B

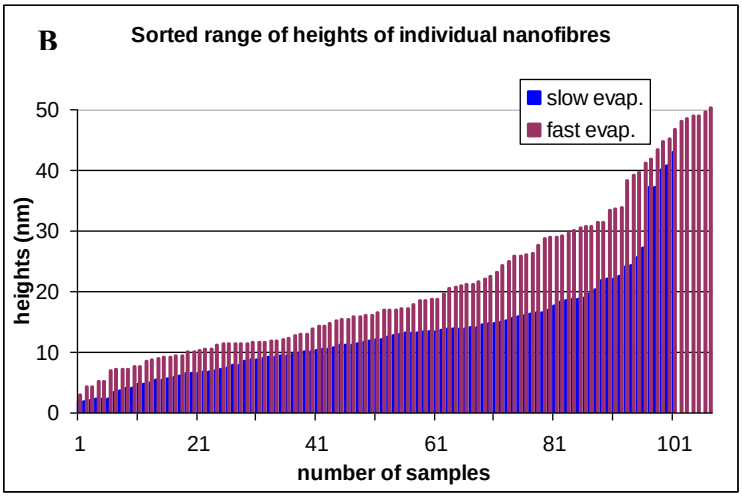

Figure 2.9 A. Distribution of vertical distances for nanofibers deposited from a 100 μM dry THF solution on mica substrates. **B.** Diagrams of the sorted values of heights of individual nanofibers ranging from 1.75 nm to 43 nm for a slow rate of evaporation, and 2.97 nm to 50.21 nm for fast evaporation rates. Slightly greater heights are observed for fast rate of evaporation. The minimum unit seems to be a single porphyrin for the fibers formed from slow evaporation and two porphyrin molecules for the faster rates of evaporation.

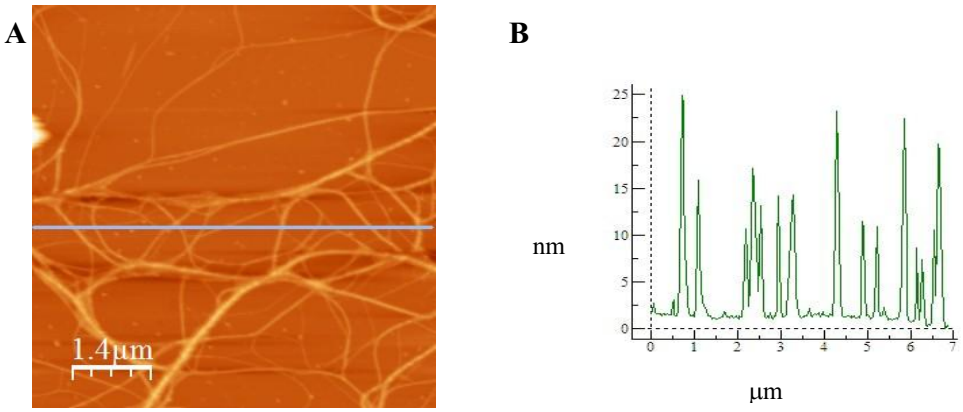

Figure 2.10 A. AFM height image and **B.** distribution (nm) of the vertical distances for materials deposited from 100 µM solutions of ZnTUrP on mica substrates, deposited from freshly distilled, dry THF with slow evaporation rates.

A

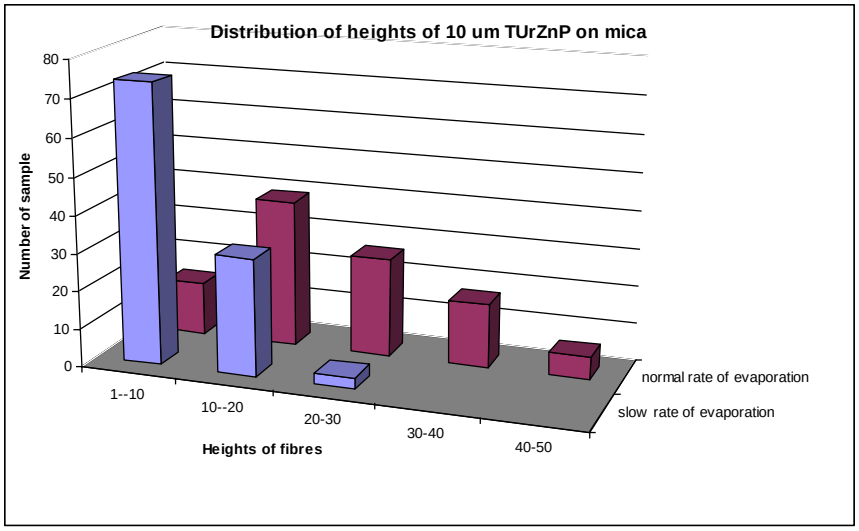

B

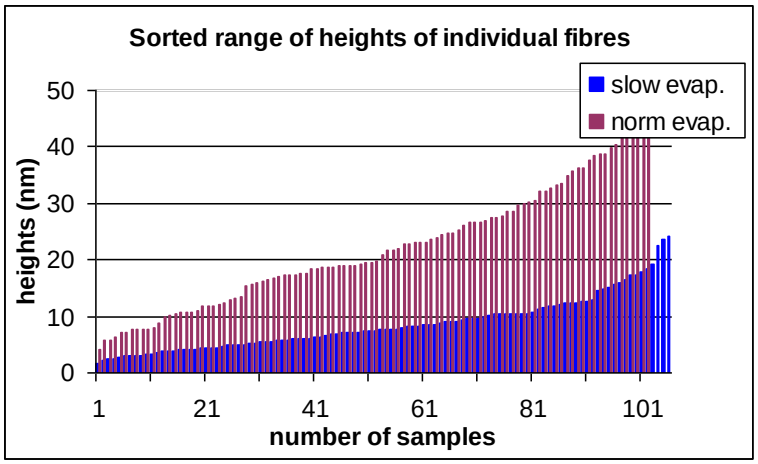

Figure 2.11 A. Distribution of vertical distances for nanofibers deposited from a 10 μM solution on mica substrates. Fibers are formed no matter the evaporation rate. **B.** Sorted values of the heights of individual nanofibers ranging from 1.8 nm to 24.1 nm for slow rates of evaporation, and 4.2 nm to 51.6 nm for faster evaporation rates. Slightly greater heights are observed for fast rate of evaporation. In this case the 1.8 nm height is consistent with a single porphyrin laying flat on the surface.

A

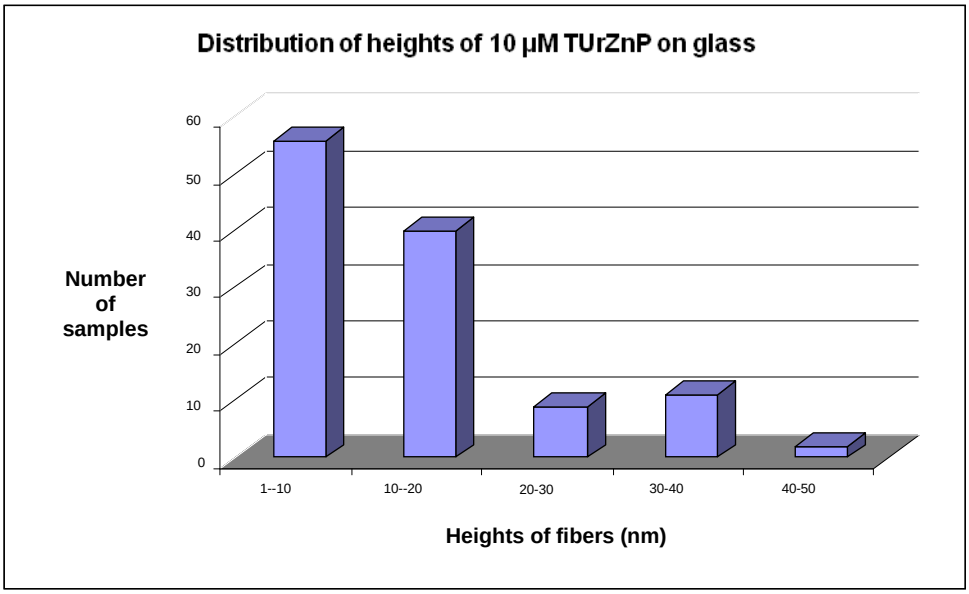

B

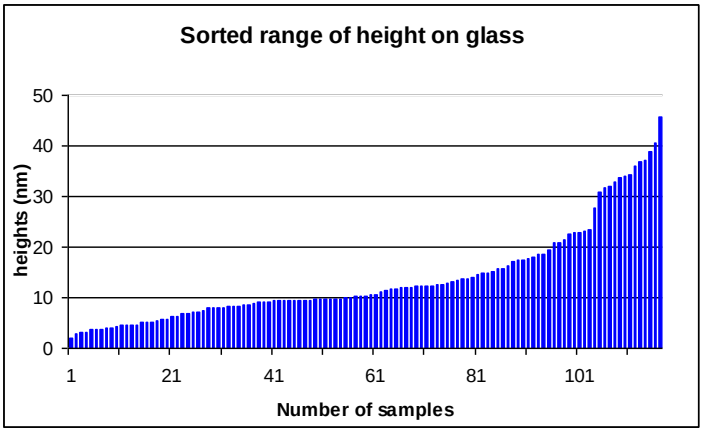

Figure 2.12 A. Distribution of vertical distances for nanofibers deposited from a 10 µM solution on glass substrates with slower evaporation rate. **B.** The lower plots the sorted heights values of individual nanofibers ranging from 2.04 nm to 45.58 nm. Slightly greater heights are observed for fast rate of evaporation. No obvious subunit or minimal structure is observed.

UV-visible absorption and emission spectra of ZnTUrP (solution phase and on the surface)

As expected for aggregates of porphyrin materials on surfaces,[1-2] the films, nanofibers, and nanorods exhibit ca. 5 nm red shifts and broadening in the electronic absorption and emission spectra compared to the starting solutions (Figure 2.13, 2.14). Energy transfer from the ZnTUrP antenna to <10% free base doped into these materials is observed in fluorescence experiments. No detectable change in the optical properties or morphologies after months of storage under ambient conditions indicates robustness of these materials.

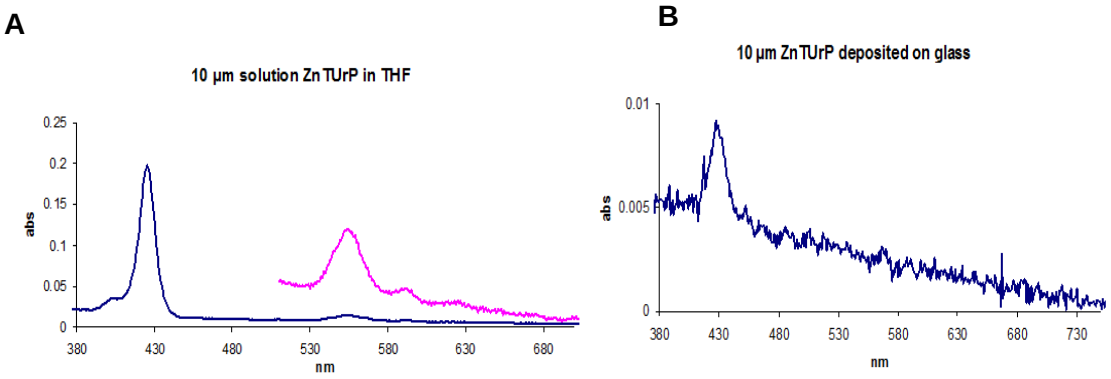

Figure 2.13 A. Absorption spectra of 10 µM solution ZnTUrP in THF in a 1.0 mm glass cuvette (blue); Soret band 424 nm, Q bands 555 nm and 591 nm (expanded 10 times in pink). **B.** Deposition of a 10 µM ZnTUrP solution in THF on ozone cleaned glass. The Soret band is shifted by 5 nm (429 nm), while Q bands are hard to observe due to the low concentration.

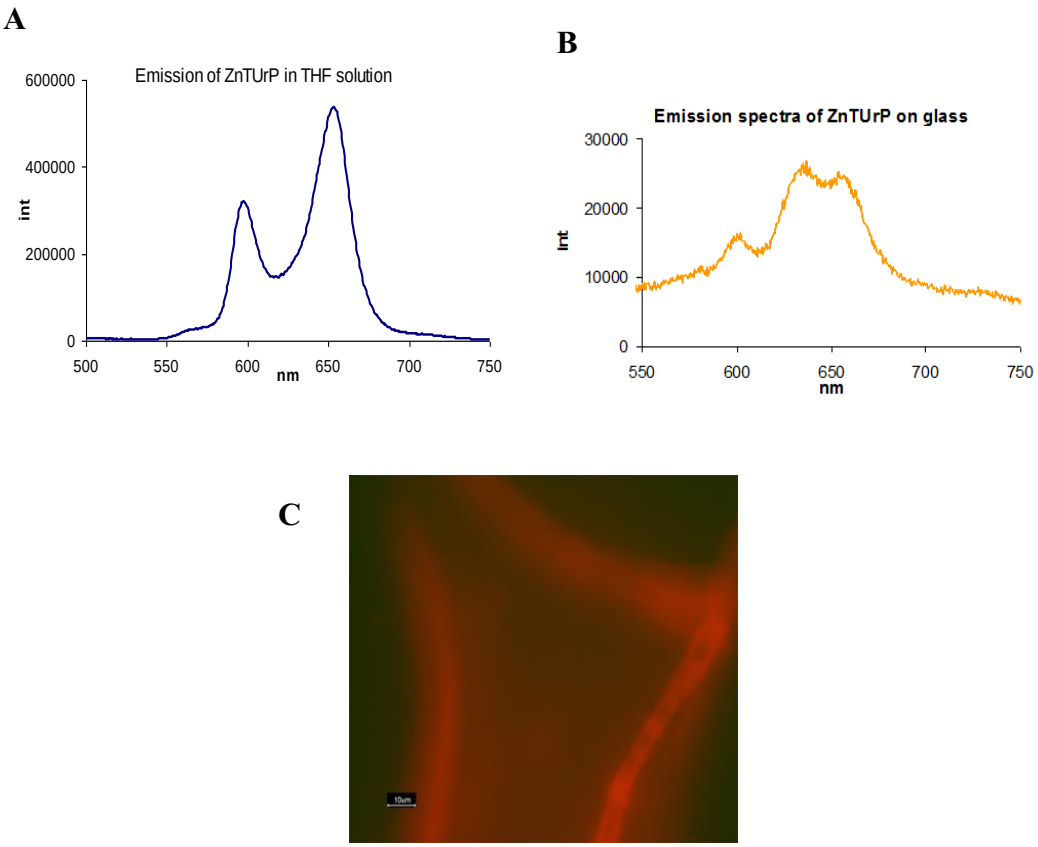

Figure 2.14 A. Emission spectra of a 10 μM solution ZnTUrP in THF, excited in the Soret band at 425 nm, exhibits characteristic bands at 600 nm and at 656 nm. A small broadening of the 656 nm band (shoulder at 636 nm) and the band at ca. 700 nm shows presence of < 10% of free base porphyrin. **B**. Front face emission spectra of ZnTUrP on a glass surface; bands at 600 nm and 658 nm correspond to the solution. The 636 nm free base peak is observed though the ZnTUrP is excited preferentially (ca. 2-fold); this shows some energy transfer to the < 10% free base in this sample because the emission band at 600 nm is diminished and the bands at 631 nm and 656 nm are enhanced. **C**. Fluorescence microscopy image of ZnTUrP fibers formed by drop casting on glass slide, 20 x. The slide was also scanned with AFM and showed formation of bundles of nanofibers (see AFM images below). Image C is taken six months after fiber formation and indicates that the structures are robust and remain fluorescent.

AFM images of free base TUrP as a control molecule for ZnTUrP

Under identical conditions free base TUrP self-organizes into rods and fibers on mica substrate but to a much smaller extent that ZnTUrP (Figure 2.15, 2.16). Since Zn(II) coordination increases electronic density on para pyridyl moieties[2] we suspect that ZnTUrP may be forming stronger H-bonds compared to TUrP. Although in other metalloporphyrin nanostructures the coordinated metal ion plays an important role in molecule organization[5] there is no UV-visible or NMR evidence for the coordnation of the uracyl moieties into the axial position on the Zn center. Thus, axial coordination is not required for formation of the nanostructured assemblies.

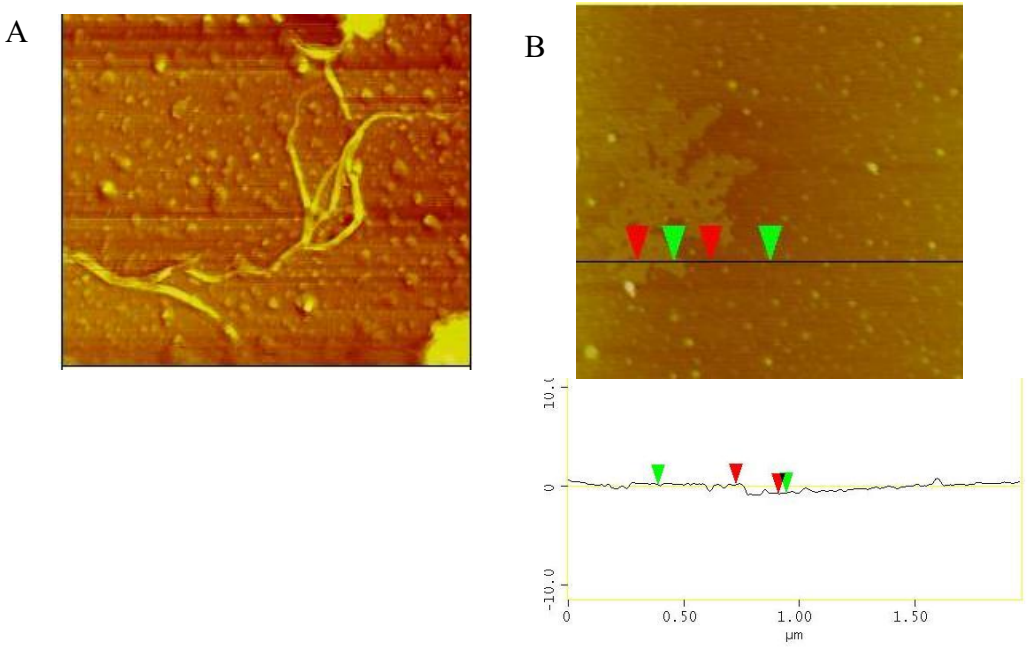

Figure 2.15 A. Phase image (2.75 µm x 2.75 µm) of free base TUrP deposited on mica surface from a 10 µM solution in THF with slow evaporation rate yield some fibers that are ca. 5 nm high, and **B.** Thin films of no more that 2 nm in height.

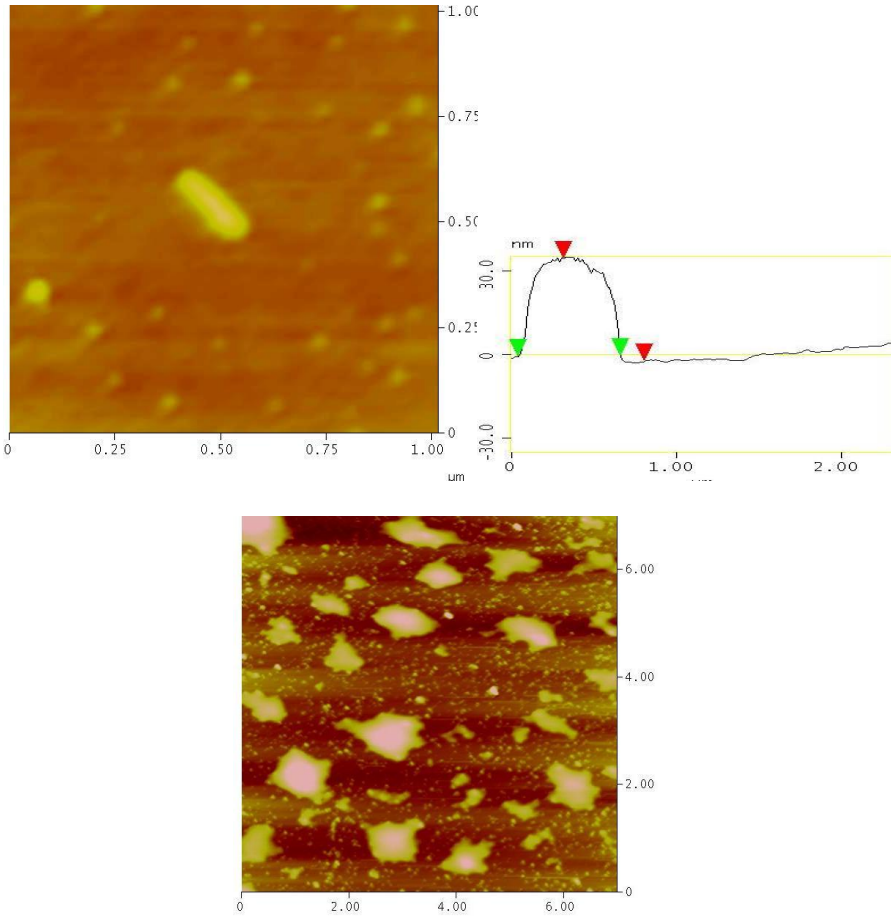

Figure 2.16 Top: A nanorod from a 10 μM solution of free bas TUrP has a horizontal distance of 620 nm and a height of 37 nm; **bottom:** on glass surfaces only aggregates and flat islands form.

2.2.2. π-π interactions

In contrast to the H-bond motifs, self-organization of TPyrP is mediated only by π-π interactions between the orthogonal meso pyrene subunits and the atropisomers inhibit porphyrin π-stacking. TPyrP is of interest because of the coupling of the two different chromophores into one molecule, e.g. porphyrins bearing fluorenyl moieties[15] or 2-pyrene[13] imparts new photonic properties. As expected for hydrophobic TPyrP, the presence of water in toluene has no observable effect on the morphology of the deposited materials. A variety of deposition methods show that the surface structure on glass, mica, and HOPG substrates is dictated by the four pyrene units and that films or nanoparticles form depending solely on solvent evaporation rate. Meso tetraphenylporphyrin (TPP) results in amorphous aggregates using the same deposition conditions. Therefore, the known propensity of pyrene to form aggregates can be exploited to drive the formation of nanostructured materials on surfaces.

On mica, deposition from both 5 μM and 20 μM toluene solutions result in small nanoparticles independent of evaporation rate or solvent (Figure 2.17). Conversely, on glass, slow evaporation of 5 μM solutions of TPyrP results in 2-9 nm thick films, and faster evaporation results in 65 nm tall by 400-600 nm wide islands (Figure 2.18, 2.19). Since TPyrP is ca. 0.8 nm wide, the films are a minimum of three molecules. Under slower evaporation conditions, the domain size increases to greater than 100 nm in height and by several microns in length. We found no organization of TPyrP on HOPG (Figure 2.20). The atropisomers inhibit TPyrP organization driven by surface energetics and structure unlike what is observed for flat porphyrins.[1c]

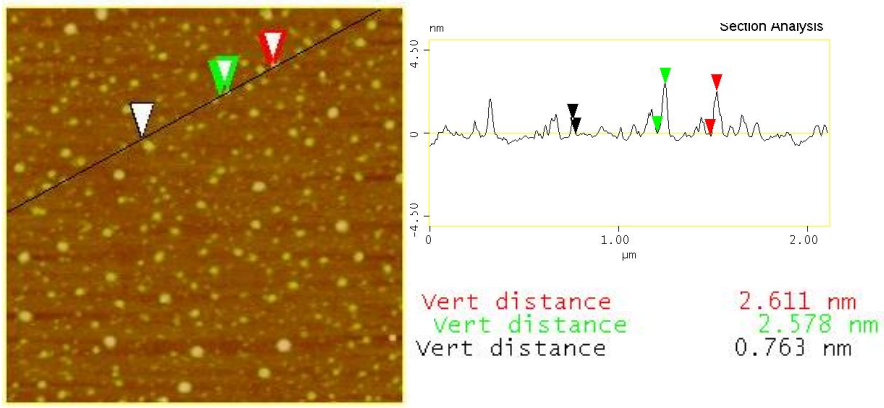

Figure 2.17 Small particles formed from 20 µM solution of TPyrP in toluene deposited on a mica substrate. The particles have heights of < 5nm.

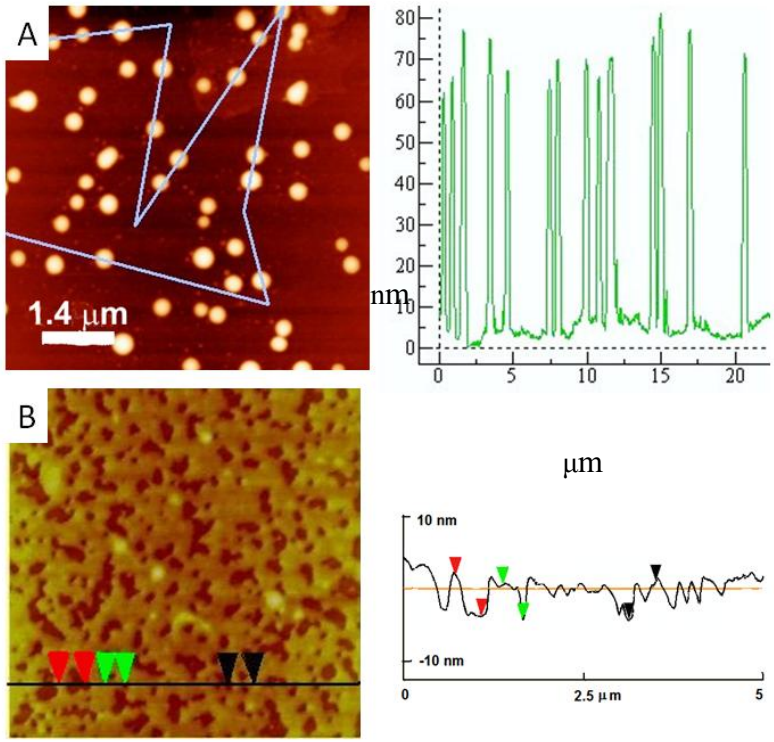

Figure 2.18 TPyrP drop cast on glass: **A**. nanoparticles from a 20 µM solution with evaporation under ambient conditions, **B.** films from a 5 µM solution with slow evaporation. Heights of line traces on the right.

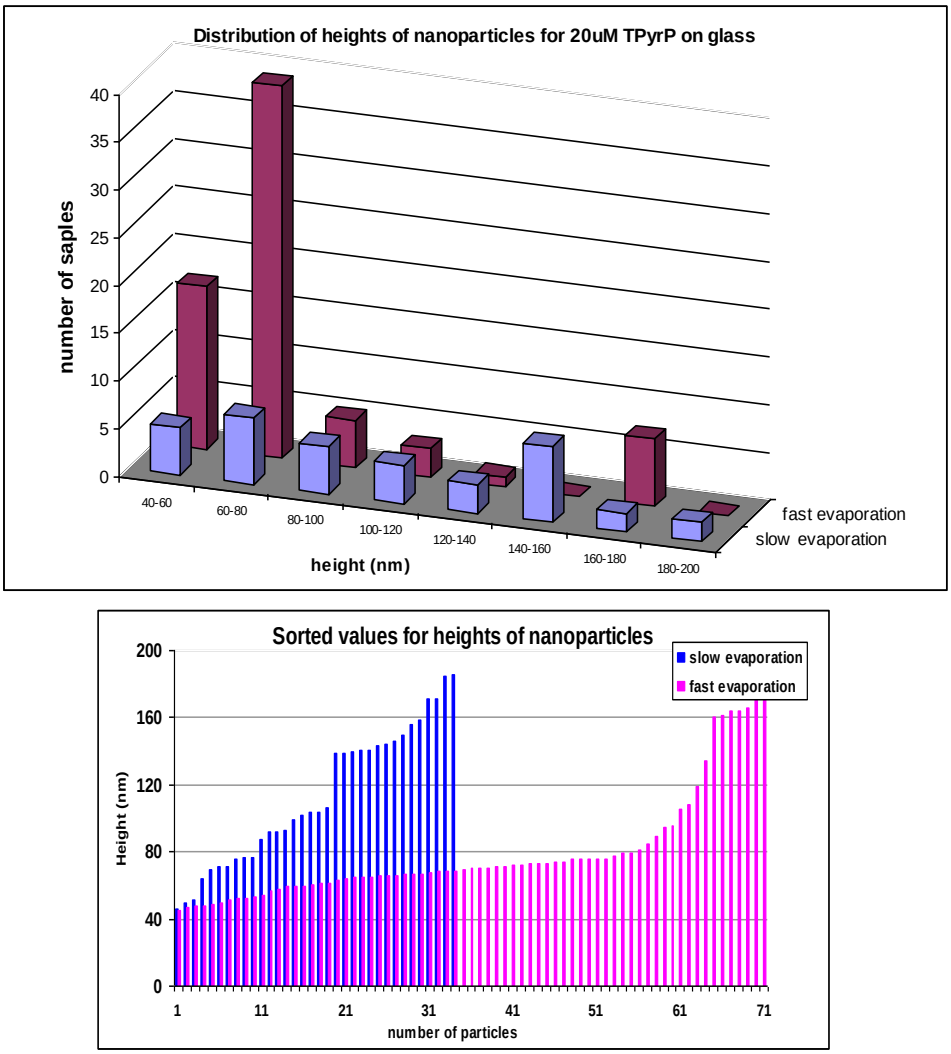

Figure 2.19 Top: AFM measured distribution of vertical distances for TPyrP nanoparticles deposited from a 20 μM solutions on glass with fast and slow evaporation rates. Bottom: plot of the sorted heights values of particles ranging from 42.7 nm to 185 nm for slow and 35.3 nm to 177.6 nm for fast evaporation.

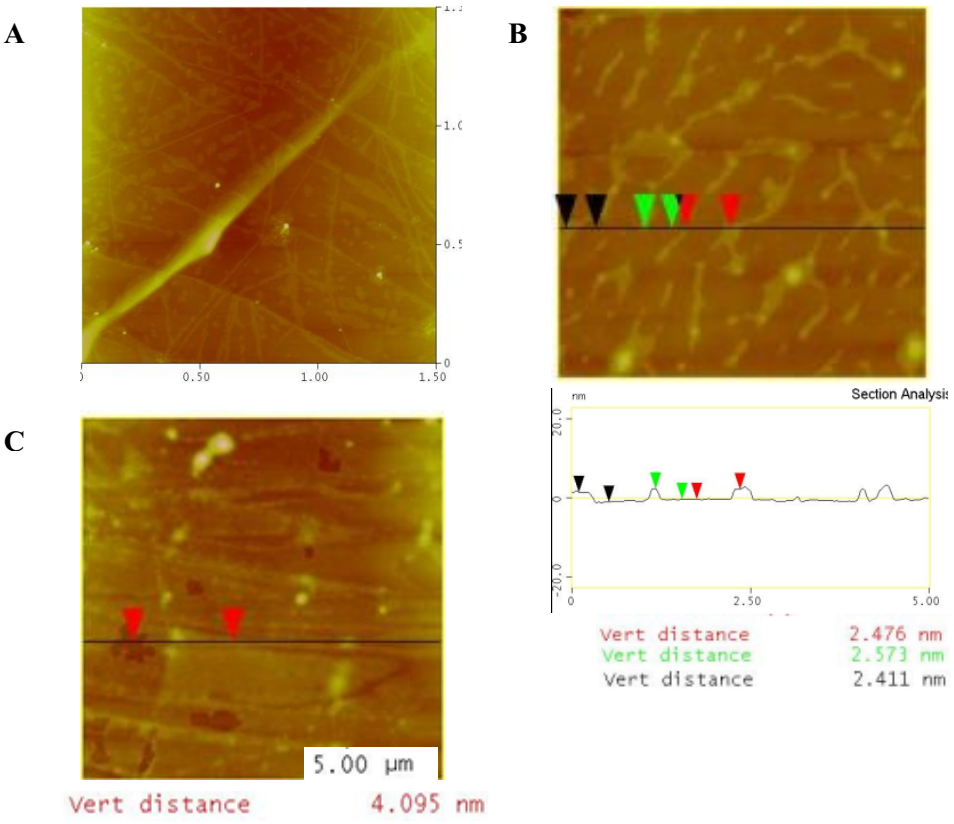

Figure 2.20 A. AFM of a 5 µM solution of TPyrP in toluene cast on HOPG forms < 5 nm thick films (image size 1.5 x 1.5 µm) and **B.** islands (image size 5x5 µm) with fast and slow evaporation rate, respectively. **C.** TPP 5 µM solution in toluene drop cast on HOPG with fast evaporation. Neither TPP nor TPyrP show significant organization on HOPG surfaces under these conditions.

2.3 CONCLUSIONS

The algorithms to control supramolecular structure in solution and in crystals are reasonably well established. However, the inherently non-equilibrium processes for self-assembly and self-organization on surfaces require additional considerations in terms of the varying concentrations, fluid dynamics, surface interactions, and supramolecular dynamics. Complex material architectures on surfaces need not to be the result of complex molecular structures or strong intermolecular forces that form in solution and deposit intact onto surfaces. Simple porphyrins can be used to form hierarchical structures on surfaces by control of the kinetics and thermodynamics of intermolecular interactions.

2.4 EXPERIMENTAL PROCEDURE

Instrumentation and Reagents.

Tetraphenylporphyrin, tetrahydrofuran (THF) and toluene were purchased from Sigma Aldrich. Solvents were distilled using standard procedures. 200 proof ethyl alcohol was from Pharmaco Products, Inc. Glass slides and cover slips were purchased from Fisher Scientific. Mica substrate was from SPI Supplies. A Cary 3-Bio UV-visible spectrophotometer, a Spex Tau-3 fluorescence spectrophotometer, and a Leica fluorescence microscope were used. The atomic force microscope used was a Veeco Multimode SPM. A home-built ozone cleaner was used.

Synthesis of compounds.

The porphyrins were prepared as previously described. ZnTUrP:[12]; TUrP: by demetalation on the zinc complex,[16] ; TPyrP:[13]

Preparation of glass and mica substrates.

The glass substrate was ozone cleaned for 20 min in a home-made ozone cleaner, and then rinsed with water and 200 proof ethanol. The slides were finally dried with a nitrogen stream at RT. Mica and HOPG substrates were cleaved just prior to use without any further preparation. The concentrations of the porphyrin solutions in THF were calculated to be 10 μM and 100 μM from UV-visible absorption data (absorption values ~ 2.0 and 0.2) using a 1 mm glass cuvette and an approx. extinction coefficient of $2x10^5$ $M^{-1}cm^{-1}$ at the maximum Soret absorbance. The concentration of solutions of TPyrP in toluene were calculated to be 5 μM and 20 μM from UV-visible absorption data (absorption values ~ 2.0) using 1 cm and 1 mm glass cuvettes and an approx. extinction coefficient of $4.1 x10^5$ $M^{-1}cm^{-1}$ at the Soret band maximum[13]

Preparation of AFM, UV-vis and fluorescence samples.

A drop of solution was cast on the substrates and let dry overnight at RT in a closed glass cell culture dish. To slow the rate of evaporation of the solvent and give the porphyrins more time to self-organize on the substrate, a few drops of THF were placed in the closed dish next to the sample. The low boiling point of THF enables the samples to dry in ca. 3 minutes and 30 minutes, respectively. When completely dried, samples were rinsed with THF to remove amorphous aggregates at the edge of deposited area. After drying them again at RT in a cell culture dish, samples were ready for AFM

measurements. The same samples were used for fluorescence microscopy studies. The same conditions for preparation of samples for UV-visible and fluorescent measurements were used for the glass slides. The same sample preparation was used for TPyrP in toluene, but the samples were not rinsed after deposition because of the weak interactions between these molecules and glass and mica surfaces. The same experimental conditions were used for the free base TUrP in THF as well as for TPP in toluene as control molecules. In the text we refer to "dry" THF as freshly distilled THF, and "wet" with approx. 5% of water. Because of the difficulties in obtaining accurate UV-visible spectra on mica, those on glass are shown.[17]

References

(1) (a) Drain, C. M.; Bazzan, G.; Milic, T.; Vinodu, M.; Goeltz, J. C. Israel J. Chem. 2005, 45, 255–269(b) Doan, S. C.; Shanmugham, S.; Aston, E.; McHale, J. L. J. Am. Chem. Soc. 2005, 127, 5885-5892(c) Drain, C. M.; Batteas, J. D.; Smeureanu, G.; Patel, S. Encyclopedia of Nanoscience and Nanotechnology, ed.J.A.Schwartz, C.I.Contescu and K.Putyera, Marcel Dekker, Inc., New York 2004, 3481-3502.

(2) Milic, T.; Garno, J. C.; Batteas, J. D.; Smeureanu, G.; Drain, C. M. Langmuir 2004, 20, 3974-3983.

(3) (a) Balaban, T. S.; Linke-Schaetzel, M.; Bhise, A. D.; Vanthuyne, N.; Roussel, C.; Anson, C. E.; Buth, G.; Eichh fer, A.; Foster, K.; Garab, G.; Gliemann, H.; Goddard, R.; Javorfi, T.; Powell, A. K.; R sner, H.; Schimmel, T. Chem. Eur. J.

2005, 11, 2267-2275(b) Hameren, R. v.; Sch¨on, P.; Buul, A. M. v.; Hoogboom, J.; Lazarenko, S. V.; Gerritsen, J. W.; Engelkamp, H.; Christianen, P. C. M.; Heus, H. A.; Maan, J. C.; Rasing, T.; Speller, S.; Rowan, A. E.; Elemans, J. A. A. W.; Nolte, R. J. M. Science 2006, 314, 1433-1436(c) Lee, S. J.; Hupp, J. T.; Nguyen, S. T. J. Am. Chem. Soc. 2008, 130, 9632-9633(d) Balaban, Teodor S.; Berova, N.; Drain, Charles M.; Hauschild, R.; Huang, X.; Kalt, H.; Lebedkin, S.; Lehn, J.-M.; Nifiatis, F.; Pescitelli, G.; Prokhorenko, Valentyn I.; Riedel, G.; Smeureanu, G.; Zeller, J. Chem. - A Eur. J. 2007, 13, 8411-8427.

(4) (a) Schwab, A. D.; Smith, D. E.; Bond-Watts, B.; Johnston, D. E.; Hone, J.; Johnson, A. T.; Paula, J. C. d.; Smith, W. F. Nano Lett. 2004, 4, 1261-1265(b) Schwab, A. D.; Smith, D. E.; Rich, C. S.; Young, E. R.; Smith, W. F.; Paula, J. C. d. J. Phys. Chem. B 2003, 107, 11339-11345.

(5) (a) Wang, Z.; Medforth, C. J.; Shelnutt, J. A. J. Am. Chem. Soc. 2004, 126, 15954-15955(b) Wang, Z.; Medforth, C. J.; Shelnutt, J. A. J. Am. Chem. Soc. 2004, 126, 16720-16721(c) Kojima, T.; Harada, R.; Nakanishi, T.; Kaneko, K.; Fukuzumi, S. Chem. Mater. 2007, 19, 51-58.

(6) Li, C.; Ly, J.; Lei, B.; Fan, W.; Zhang, D.; Han, J.; Meyyappan, M.; Thompson, M.; Zhou, C. J. Phys. Chem. B 2004, 108, 9646-9649.

(7) Jeukens, C. c. R. L. P. N.; Lensen, M. C.; Wijnen, F. J. P.; Elemans, J. A. A. W.; Christianen, P. C. M.; Rowan, A. E.; Gerritsen, J. W.; Nolte, R. J. M.; Maan, J. C. Nano Lett. 2004, 4, 1401-1406.

(8) Yuasa, M.; Oyaizu, K.; Yamaguchi, A.; Kuwakado, M. J. Am. Chem. Soc. 2004, 126, 11128-11129.

(9) Medforth, C. J.; Wang, Z.; Martin, K. E.; Song, Y.; Jacobsen, J. L.; Shelnutt, J. A. Chem.Commun. 2009, 7261-7277.

(10) (a) Kobuke, Y. Structure and Bonding 2006, 121, 49-104(b) Kobuke, Y. Eur. J. Inorg. Chem. 2006, 12, 2333-2351.

(11) (a) Jintoku, H.; Sagawa, T.; Takafuji, M.; Ihara, H. Org. Biomol. Chem. 2009, 7, 2430-2434(b) Iavicoli, P.; Simon-Sorbed, M.; Amabilino, D. B. New J. Chem. 2009, 33, 358-365.

(12) Shi, X.; Barkigia, K. M.; Fajer, J.; Drain, C. M. J. Org. Chem. 2001, 66, 6513-6522.

(13) Knor, G. Inorg. Chem. Com. 2001, 4, 160-163.

(14) Hunter, C. A.; Sanders, J. K. M. J. Am. Chem. Soc. 1990, 112, 5525.

(15) Drouet, S.; Paul-Roth, C. O.; Simonneaux, G. Tetrahedron 2009, 65, 2975-2981.

(16) Shi, X. Ph.D. Thesis, City University of New York 2002.

(17) Bazzan, G.; Smith, W.; Francesconi, L. C.; Drain, C. M. Langmuir 2008, 24, 3244-3249.

CHAPTER 3

Synthesis and Characterization of Hafnium(IV) and Zirconium(IV) Phthalocyaninato diacetate complexes and Ternary Phthalocyaninato Hf(IV) and Zr(IV) - Polyoxometalate Complexes

3.1 ABSTRACT

We report here a simple synthesis and characterization of discrete, ternary phthalocyaninato-metal-polyoxometalate (Pc-M-POM) complexes and metallophthalocyaninato diacetate (Pc)M(OAc)$_2$ complexes where a group (IV) transition metal ion is bound both to the phthalocyanine core and to the lacunary site of a Keggin POM, $PW_{11}O_{39}^{7-}$. These remarkably robust complexes exploit the fact that Hf(IV) and Zr(IV) are 7-8 coordinate and reside outside the plane of the phthalocyanine macrocycle, thus enabling the simultaneous coordination to Pc core and to the defect site in the Keggin framework. The physical properties of the (Pc)Hf($PW_{11}O_{39}$)[TBA]$_5$, and (Pc)Zr($PW_{11}O_{39}$)[TBA]$_5$ complexes are similar because the metal ions exhibit similar oxidation states, and coordination chemistry. This architecture couples the photonic properties of the phthalocyanine to the POM because the metal ion is incorporated into both frameworks. Thus, the ternary complexes can serve as a basis for the characterization of Hf(IV) and Zr(IV) porphyrins bound to oxide surfaces via the group (IV) metal ions. The discussion in Chapter 4 highlights the strong binding between TiO_2 nanoparticles and the HfPc and ZrPc complexes. Together, the strong binding of the

phthalocyanine to the POM and nanoparticles suggests that the 3-4 open coordination sites on the Hf(Pc) and Zr(Pc) are predominantly bound at surface defect sites.

3.2 INTRODUCTION

Previous work done in Dr. Drain's Lab *

Polyoxometalates (POMs) and porphyrins (Por) are widely studied as components of functional materials, such as catalysts and photonics, because each possesses enormous potential for structural variation and tuning of their electronic properties. Porphyrins[2-8] and POMs [9-14] have been investigated for applications such as photovoltaics and supramolecular materials. There are numerous reports on the adsorption or attachment of porphyrins to a variety of surfaces using exocyclic motifs with a moiety designed to bond to the surface and a linker intervening between the macrocycle and the surface.[15-22] There are numerous supramolecular constructs of porphyrins and electron acceptor species such as C_{60}.[23-28] In addition to POMs being good electron acceptors, in many ways the diverse photochemical, and coordination chemistry of porphyrins and POMs are complementary; therefore, robust complexes that photonically couple porphyrins and POMs should have unique properties. There are reports of films and other materials wherein cationic porphyrins and POMs are mixed[29] e.g. for catalysis,[30] an axially bound POM counterion on Mo(V)Por,[31] two metalloporphyrins bridged by a POM bearing two nicotinamide moieties coordinated to the metal centre,[32] and other porphyrin – POM structures,[33-35] but here we describe discrete ternary systems wherein a central metal ion is coordinated to both the Por and a defect site in the lacunary POM. Previously, Keggin structures have been functionalized with cyclopentadienyl ligands at

the lacunary site through Ti(IV), Zr(IV), and/or Hf(IV) metal ions.[8,36-37] The recent report on the formation of Hf(Por) dimers bridged by oxo ligands such as sulfate, phosphate, and peroxo indicates that multitopic counter ions may serve as tectons to construct arrays of group four metalloporphyrins.[38]

The three complexes reported herein are made in high yields from previously reported Zr(IV) and Hf(IV) porphyrinates[39] and the lacunary POM[13], $H_3PW_{11}O_{39}^{4-}$ (Figure 3.1): (TPP)Hf($PW_{11}O_{39}$)$[TBA]_5$, 1, (TPyP)Hf($PW_{11}O_{39}$)$[TBA]_5$, 2, and (TPP)Zr($PW_{11}O_{39}$)$[TBA]_5$ 3. In contrast to the aforementioned systems, this nanoarchitecture enables photonic coupling of the two chelates mediated by the central metal ion. Since the chemistry of Zr(IV) is generally similar to Hf(IV), the significantly greater natural abundance of Zr may make Zr(Por) materials more cost effective if the functional properties are competitive.

Since POMs are often regarded as good models for defect sites in oxide surfaces,[13] the crystal structure and physical properties of these ternary complexes suggested to us that one way to self-organize porphyrins onto oxide surfaces such that the photonic properties of the macrocycles are strongly coupled to the semiconductor is to use porphyrins coordinated to oxophilic group IV metals such as Hf, Zr. Indeed, when a variety of oxide particles, such as silica gel,[38] ITO or TiO_2, are exposed to a solution containing the (Por)Hf$(L)_2$ or (Por)Zr$(L)_2$, where L = acetate or chloride, the spectroscopic signatures are observed to be similar to those of compounds 1-3. While these group (IV) metalloporphyrins are strongly bound to the nanostructured surfaces, both scanning probe and reflectance data find a paucity of the complexes bound to crystalline TiO_2 and SiO_2 surfaces. Together, this data suggests that the 3-4 open metal

ion coordination sites of the $Hf(Por)^{2+}$ and $Zr(Por)^{2+}$ are bound primarily to surface defect sites by displacement of the auxiliary acetate or chloride ligands. Further data analysis will be discussed in chapter 4 .

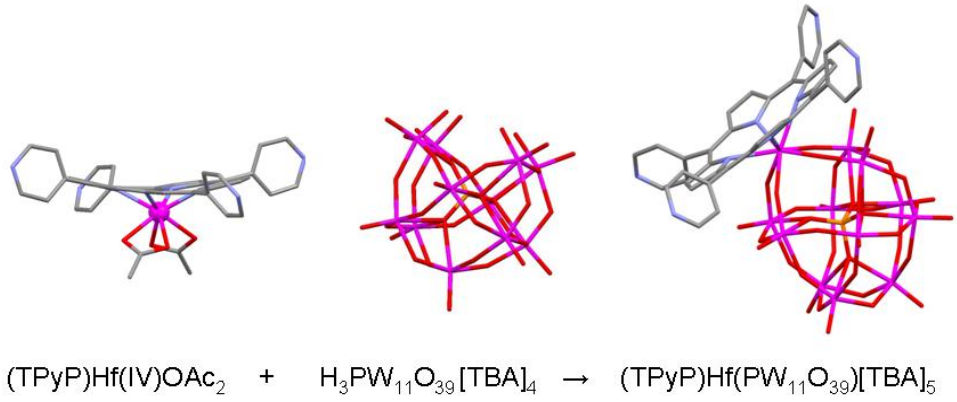

Figure 3.1 Crystal structures of the starting $(TPyP)Hf(OAc)_2$ and the ternary complex **2**, counter ions left out for clarity. (i) to $(TPyP)Hf(OAc)_2$ in 1:1: CH_2Cl_2:CH_3OH is added one equivalent of $H_3PW_{11}O_{39}[TBA]_4$ in CH_3CN with an excess [TBA]Br and 1 %TEA.

* Adopted from Alexander Falber, Benjamin P. Burton-Pye, Ivana Radivojevic, Louis Todaro, Raihan Saleh, Lynn Francesconi, Charles Michael Drain, "Ternary Porphyrinato Hf(IV) and Zr(IV) Polyoxometalate Complexes", Eur. J. Inorg. Chem. 2009, 2459-2466.

3.3 DISCUSSION AND RESULTS

Synthesis of $(Pc)Hf(OAc)_2$ and $(Pc)Zr(OAc)_2$

The very simple apparatus used in this synthesis was adopted from similar porphyrin synthesis and is shown in Figure 3.2.[1] The starting materials dichloro(phthalocyaninato) hafnium(IV) $[(Pc)Hf(Cl)_2]$ and dichloro(phthalocyaninato) zirconium(IV) $[(Pc)Zr(Cl)_2]$ were synthesized according to the methods provided by the literature in which the phthalocyanine ring is built around a central metal (Figure 3.3).[40]

Tomachynski et al. have reported many new phthalocyanine compounds in which two chloride atoms can be easily exchanged for other ligands. There are also reports of axially substituted hafnium and zirconium metal (IV) phthalocyanines with gallic, oxalic acids,[41] with various carbonic acids,[42] β-diketonates,[40] etc. We used similar methods to exchange chlorides for OAc- as has already been observed in a porphyrin synthesis where chloride ions are interchanged on silica columns and mixtures of solvents with acetic acid are used to remove acetates from the column (Figure 3.4).[38]

The chloride forms of metallophthalocyanines have low solubility in many solvents. This necessitated that we dissolve $(Pc)Hf(Cl)_2$ in minimum amount of DMSO. The solution was then placed on the silica column and the first fraction was washed with methanol until it was colorless. The second fraction was eluted with a 3:1:1 mixture (CH_2Cl_2: methanol: acetic acid). The solution was then evaporated, re-dissolved in small amount of CH_2Cl_2 and filtered.[38] No material remained on the filter paper. Finally, it was precipitated with hexane overnight. A dry solid, sample of dark blue $(Pc)Hf(OAc)_2$ was isolated.

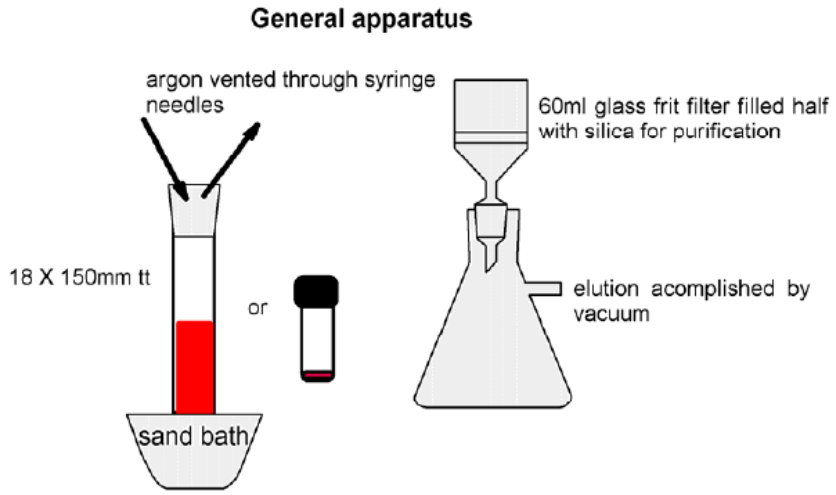

Figure 3.2 Apparatus for the synthesis of $(Pc)Hf(OAc)_2$ and $(Pc)Zr(OAc)_2$. Adopted from Falber thesis.[1]

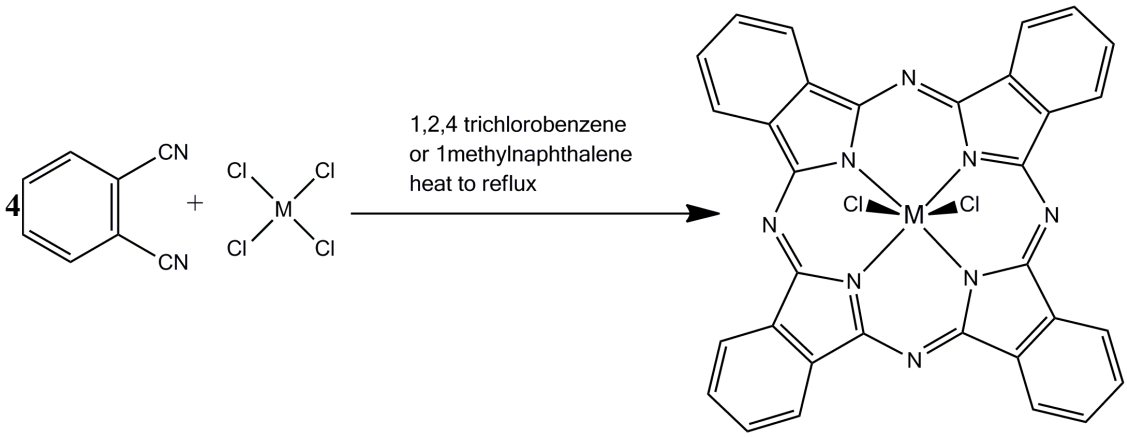

Figure 3.3 Synthesis of $(Pc)M(Cl)_2$ from dicyanobenzene, $Hf/ZrCl_4$, 1-methylnaphthalene in 1,2,4-trichlorobenzene.

In the case of $(Pc)Zr(Cl)_2$ we experienced trouble when trying to isolate $(Pc)Zr(Cl)_2$ as a solid product. According to the reported procedure, the filtration was done with benzene and methanol.[40] Our material was soluble in methanol and could not be purified from the column. When washing with methanol the 1st fraction was a dark/green mixture and the 2nd was green/blue solution that was used for further synthesis. The reaction mixture was directly loaded onto silica. After elution with a solvent mixture of 3:1:1 CH_2Cl_2: methanol:acetic acid, the product was collected in one fraction, the solution was evaporated and then re-dissolved in CH_2Cl_2. To make sure that there was no unreacted starting material remaining we filtered the product with CH_2Cl_2. Black solids were observed on the filter paper. Only the green clear solution was collected and used for further purification with hexane. The precipitate formed was a bright green color.

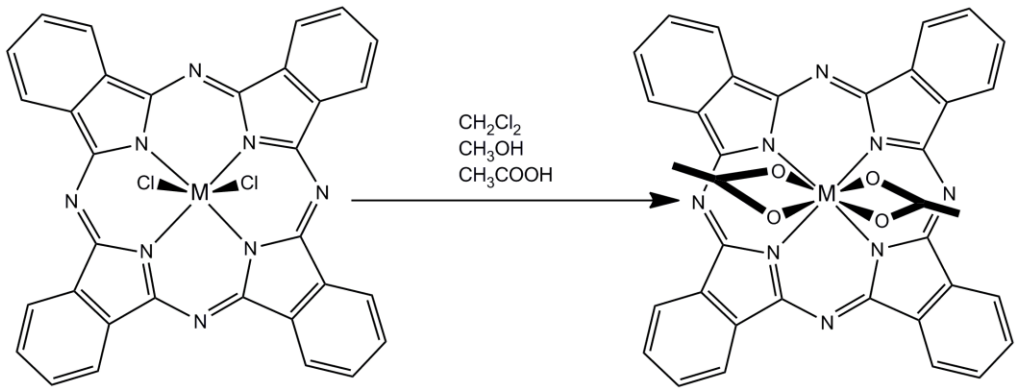

Figure 3.4 Illustration of procedure for the synthesis of $(Pc)M(OAc)_2$ from $(Pc)M(Cl)_2$. M= Zr/Hf.

Synthesis of (Pc)HfPW$_{11}$O$_{39}$[TBA]$_5$ and (Pc)ZrPW$_{11}$O$_{39}$[TBA]$_5$

The synthesis of (Pc)-M-PW$_{11}$O$_{39}$[TBA]$_5$ ternary complex is simple and similar to the already described synthesis of (Por)-M-PW$_{11}$O$_{39}$[TBA]$_5$ complexes by our lab.[43] By slowly adding a stoichiometric amount of the POM to solutions of the (Pc)Hf(OAc)$_2$ or (Pc)Zr(OAc)$_2$ yields Pc-M-POM complexes by displacement of the acetate ligands by the lacunary oxygens of the H$_3$PW$_{11}$O$_{39}$[TBA]$_4$. The formal charge of the ternary complex is -5 requiring one additional equivalent of [TBA]Br to be added to the mixture to yield the neutral (Pc)Hf(PW$_{11}$O$_{39}$)[TBA]$_5$ or (Pc)Zr(PW$_{11}$O$_{39}$)[TBA]$_5$ complexes. The porphyrin-POM reaction was buffered by a base triethylamine since the acidic protons from the POM can cause some demetalation of the starting material. The chelating effect of the four oxygens on the POM to the oxophilic Hf(IV) or Zr(IV) centers is known to be strong enough to lead to porphyrin demetalation of the Hf-Por complexes, and the addition of just one excess equivalent of POM led to formation of the Hf(PW$_{11}$O$_{39}$)$^{3-}$ or the corresponding dimer Hf(PW$_{11}$O$_{39}$)$_2^{10-}$ complexes.[43] The characterization of the compounds are described below and the spectra are found in the appendix (Figures A3.1-A3.23). Interestingly, (Pc)Hf(PW$_{11}$O$_{39}$)$^{5-}$ and (Pc)Zr(PW$_{11}$O$_{39}$)$^{5-}$complexes are more stable and even addition of two equivalents of POM does not result in demetalation of the phthalocyanine molecules (Figure A3.9 and A3.11). The reason for this could be stronger bonds between Hf or Zr metal ion to the phthalocyanine core, which are much less distorted than porphyrin macrocycle, as evidenced by the small red shift in the UV-vis absorption spectra (Figure A3.6 and A3.17). In the Por-M-POM complex, the POM pushes up against the phenyl groups enough to distort the porphyrin microcycle.

Previous work with (Por)M$(OAc)_2$ and (Pc)M$(OAc)_2$ has demonstrated that acetate ligands are easily exchanged. We also tried synthesis using (Pc)$HfCl_2$ as the starting material because we assumed that Cl^- would be even easier to remove and should therefore decrease the reaction time (Figure A3.11). However, no significant change was observed in the kinetics of the reaction and the fact that (Pc)$HfCl_2$ is soluble only in DMSO made it unreasonably difficult for us to remove the solvent from the final product.

The progress of all reactions was monitored with UV-vis spectra and no change nor significant shift in absorption spectra was observed. The reaction mixture was stirred overnight, and the final product was isolated in the supernatant while some darker blue color precipitate was formed. After centrifugation of the mixture, the precipitate formed a pellet at the base of the tube well separated from the original solution. Slightly more ppt was formed with Zr complex. The precipitate had a low solubility in CH_2Cl_2 and exhibits very broad UV- spectra with small peaks from the stronger Q-band of the starting material. The ^{31}P NMR spectra of the precipitate showed no peaks were observed for both ternary complexes confirming that there is no POM in the ppt. The precipitate can be a mixture of the bis Pc sandwich complex with some of the starting material. The supernatant was evaporated, and the dried material was re-dissolved in CH_2Cl_2 and filtered to remove all the impurities (salts of POM, seen as a green-whitish solid that remains on the filter paper). Finally, the product was precipitated with hexane and the blue-green solid (Pc)Hf$(PW_{11}O_{39})^{5-}$ was isolated. (Pc)Zr$(PW_{11}O_{39})^{5-}$ had a greener color.

Characterization

Uv-visible spectroscopy Pc-POM

All phthalocyanines exhibit strong absorption in Q-band region from 500-600 nm and Soret band of smaller intensity around 300 nm. The UV-visible spectra for the hafnium (IV) and zirconium (IV) phthalocyaninato diacetate complexes is almost identical: Soret band at 334nm and 336 nm respectively, and Q-bands at 614 nm and 684 nm for the hafnium complex and at 615 nm and 685 nm for the zirconium complex (Figure A3.1 and A3.5).

The formation of ternary complexes was monitored by UV-visible absorption spectra of the phthalocyanine portion of the complex. The Q-band regions of the spectra display minimum red shifts as the reaction progresses. The Q bands are located at 616 nm and 685 nm for the Hf ternary complex, and for Zr complexes shift to 617 nm and 687 nm (Figure A3.6 and A3.17). The small red-shifts of 2 nm indicates minimal or no structural distortion in the phthalocyanine macrocycle since the core is quite rigid. Generally, changing the ligands bound to the metal (IV) phthalocyanines does not significantly influence absorption spectra and a very small shift of Q-bands was observed. The reported values are in accordance with our data.[40]

Fluorescence

Both starting material and ternary complexes, excited at the wavelength of the phthalocyanine Q- band at 615 nm exhibit similarly shaped emission spectra with one large peak close to 700 nm and one weak band near 730 nm (Figure A3.2, A3.6, A3.10 and A3.18). It is worth noting that the heavy atom effect is more pronounced with

(Pc)Hf$(OAc)_2$ as compared to (Pc)Zr$(OAc)_2$. This is observed as greater fluorescence intensity in emission spectra for the latter compound. The intensity of fluorescence is ca. 100 times less for Pc-M-POM complex vs. acetate compounds. We hypothesize that electron transfer from the Pc to POM is likely major cause for the fluorescence quenching. The same behavior was observed with Por-M-POM compounds. Alternatively, the heavy metals in the POM can contribute to fluorescence quenching.

^{1}H NMR

^{1}H NMR for (Pc)Hf$(OAc)_2$ and (Pc)Zr$(OAc)_2$ in $CDCl_3$ shows two broad singlets in the aromatic region that integrate to 8 H^{α} and 8 H^{β} atoms. H^{α} atoms are closer to the Pc ring and are shifted more downfield and the broad singlet peaks are centered at 9.48 ppm and 9.43 ppm , while H^{β} atoms are further away from the Pc macrocycle and shifted more upfield to 8.23 ppm and 8.20 ppm for Hf and Zr complex. There is also a broad singlet at 0.42 ppm indicating -CH_3 groups which integrates to a total of 6H (Figure A3.4 and A3.8).

The NMR spectra for (Pc)Hf$(PW_{11}O_{39})[TBA]_5$ complexes is better resolved than the spectra of (Pc)Zr$(PW_{11}O_{39})[TBA]_5$. Since Hf has a greater ionic radius than Zr, Hf it does not sit as deep into the vacant position of the POM molecule, so the steric interactions between Pc and the POM are less. Since the POM is tilted more to one side of the phthalocyanine (Figure 3.5) an asymmetry arises which creates two different planes of the molecule. Thus, the chemical shift of the H^{α} and H^{β} atoms will be depending on their proximity to the POM. This effect is however very difficult to resolve, because the rotation of the Pc is fast. We found three multiplets centered at 9.53 ppm

integrated one to one with two multiplets centered at 8.21 ppm (Figure A3.13, A3.14).The spectra shows presence of excess TBA but NMR integration verifies 40H for -CH_2- groups and 60H for -CH_3 group for all 5 TBA groups attached to the ternary complex (Figure A3.15). The same behavior was seen for (Pc)Zr($PW_{11}O_{39}$)[TBA]$_5$, where broad multiplet peaks were centered at 9.49 ppm and 8.11 ppm (Figure A3.21 and A3.22).

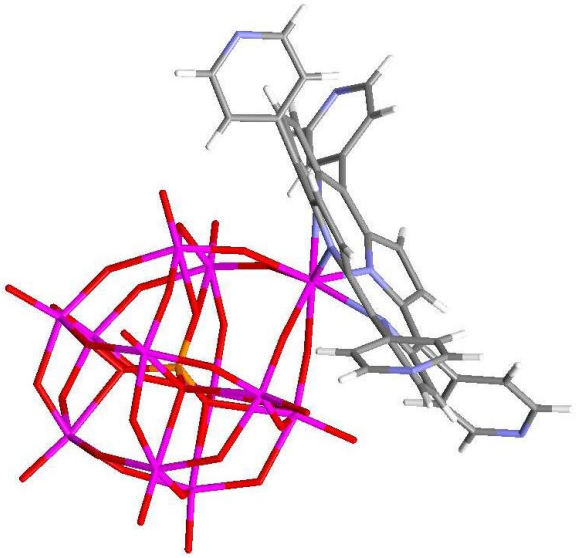

Figure 3.5 Crystal structure of (TPyP)HfPOM showing asymmetry in the molecule due to POM being tilted more to one side of the porphyrin.

^{31}P NMR

^{31}P NMR for both (Pc)HF($PW_{11}O_{39}$)[TBA]$_5$ and (Pc)Zr($PW_{11}O_{39}$)[TBA]$_5$ complexes display a singlet peak at -15.68 ppm and -15.46 ppm, respectively (Figure A3.16 and A3.23). Note that for (Pc)Zr($PW_{11}O_{39}$)[TBA]$_5$ a smaller peak at -15.77 ppm is observed that may arise from exchange of TBA cations (consistent with our earlier observations in Falber et al.). The phosphorus peaks have similar chemical shifts to those reported in the literature. For example, the cyclopentadienyl analogue,

(cp)Hf($PW_{11}O_{39}$)[TBA]$_4$ displays a peak at -12.3 ppm[36], the porphyrin-free $HfPW_{11}O_{39}^{-3}$ complex has a peak at -14.67 ppm. Also TPP and TPyrP hafnium complexes show sharp peaks at -16.20 ppm and -16.25 ppm.[43]

Mass spectroscopy

MALDI MS for (Pc)Hf($OAc)_2$, formula ($C_{36}H_{16}N_8$)Hf($C_2H_3O_2$) found m/z= 807.17 while calculated m/z= 807.2. For (Pc)Z($OAc)_2$, formula ($C_{36}H_{16}N_8$)Zr ($C_2H_3O_2$) found m/z= 720.17 while calculated m/z= 661.2 (Figure A3.3 and A3.7 respectively).

MALDI MS for (Pc)Hf(POM), formula ($C_{36}H_{16}N_8$)Hf($PW_{11}O_{39}$)[$C_{16}H_{36}N$]$_5$ calculated m/z= 4578.27 found m/z= 4579.00. For (Pc)Zr(POM) formula ($C_{36}H_{16}N_8$)Zr($PW_{11}O_{39}$)[$C_{16}H_{36}N$]$_5$ found m/z= 4492.72 while calculated m/z= 4492.1 (Figure A3.12 and A3.20 respectively).

3.4 EXPERIMENTAL PROCEDURE

Instrumentation and Reagents

All UV-Visible spectra were taken in 1 cm quartz or glass cuvettes in CH_2Cl_2 on a Carey Bio 3 spectrophotometer. Mass spectrometry was done as a service by the University of Illinois, using Applied Biosystem Voyager System 4178. A Bruker Avance 500 MHz NMR instrument was used. A Joel 400 MHz NMR instrument was used for ^{31}P spectra. Fluorescence spectra were taken on a Spex Tau-3 fluorometer in 1 cm quartz cuvettes in right angle mode. Gasses, reagents, and solvents were used as received. Zirconium tetrachloride, hafnium tetrachloride, 1,2-dicyanobenzene, 1-methylnaphthalene, 1-chloronaphthalene, were purchased from Sigma Aldrich. All

solvents were from Sigma Aldrich. Disposable vials and test tubes were used once. The free base lacunary Keggin polyoxometalate, $H_3PW_{11}O_{39}[TBA]_4$ was provided from Prof. Francesconi's Lab.

Synthesis of compounds

Hafnium (IV) phthalocyaninato diacetate $(Pc)Hf(OAc)_2$

200 mg of $(Pc)Hf(Cl)_2$ (763.94 g/mol) was dissolved in a minimum amount of DMSO in a 18 x150 mm test tube with stir bar at room temperature and loaded onto silica gel in a glass frit filter, then placed on a filtering flask under vacuum. The first fraction was eluted with methanol. The second fraction $(Pc)Hf(OAc)_2$, was eluted with 3:1:1 mixture (CH_2Cl_2: methanol: acetic acid). The solvent was evaporated by rotary evaporation and the dried solid was re-dissolved in CH_2Cl_2 , filtered with CH_2Cl_2 and finally precipitated with hexane. The dark blue dry solid was weight to yield 166mg (83%). $(C_{36}H_{16}N_8)Hf(C_2H_3O_2)$: ^{1}H NMR (500 MHz, CD_2Cl_2) δ ppm: 9.48 (br s, 8H, H^{α}), 8.23 (br s, 8H,H^{β}), 0.41 (br s, 6H, OAc). UV-Vis CH_2Cl_2 λmax nm (log ε) 334 (6.04), 614 (5.73), 652 (5.67), 684 (6.49). MALDI-MS m/z= 807.17 calcd., found 807.2

Zirconium (IV) phthalocyaninato diacetate $(Pc)Zr(OAc)_2$

This complex is prepared through the similar procedure as the hafnium complex except using starting material $(Pc)Zr(Cl)_2$ (676.67 g/mol) which was not accessible as an isolated solid product. 2 mL of trichlorobenzene in 18 x150 mm test tube with stir bar was heated in sand bath to a temperature > 100 ^{0}C. 0.517 mg (0.004 mol) dicyanobenzene and 0.165 mL (0.0011 mol) 2-methylnaphthalene were added and heated >200^{0}C. When reaction mixture appeared clear 276 mg (0.002 mol) of $ZrCl_2$ was added to the solution.

The reaction mixture turned dark yellow, was refluxed for 1 h, and finally turned a dark color. When cooled down to 50 ^{0}C, the solution was filtered with methanol and dark/green fraction was separated from 2nd blue/green fraction. No solid product was isolated on the filter paper. The reaction mixture was loaded onto 30 g of silica and eluted with 3:1:1 mixture (CH_2Cl_2: methanol: acetic acid). The solvent was evaporated by rotary evaporation. The dry solid was re-dissolved in CH_2Cl_2, filtered with CH_2Cl_2 and finally precipitated with hexane. The green dry solid was weight to yield 230mg (~84%). $(C_{36}H_{16}N_8)Zr(C_2H_3O_2)$: ^{1}H NMR (500 MHz, CD_2Cl_2) δ ppm: 9.43 (br s, 8H, H^{α}), 8.20 (br s, 8H,H^{β}), 0.42 (br s, 6H, OAc). UV-Vis CH_2Cl_2 λmax nm (log ε) 336 (6.01), 616(5.64), 652 (5.58), 685 (6.35) MALDI-MS m/z=723.0. calcd., found 720.17

Phthalocyanine Hafnium(IV)$PW_{11}O_{39}$ tetra-butylammonium salt
$(Pc)Hf(PW_{11}O_{39})[TBA]_5$

18 mg of $(Pc)Hf(OAc)_2$ (811.11 g/mol, 0.022 mmol) was dissolved in 10 mL of a 1:1 mixture of CH_2Cl_2:CH_3OH in a 18 x150 mm test tube with a magnetic stir bar at room temperature. 76 mg of $H_3PW_{11}O_{39}[TBA]_4$ (3650 g/mol, 0.021 mmol) and 5 mg of [TBA]Br was dissolved separately in 5 mL of acetonitrile containing 1% v/v triethylamine. The resulting clear POM solution was added drop-wise over the course of 5 minutes to a stirring hafnium porphyrinate solution. The reaction was left to run overnight. A small amount of precipitate was formed at the bottom of the test tube. The reaction was monitored by UV-Visible spectroscopy where the presence of the ternary complex is signified by a small red shift of ~ 2 nm in the Q- bands. The precipitate and supernatant were separated by centrifugation. The solvent from the supernatant was removed under vacuum and the residue was dissolved in a minimal volume of CH_2Cl_2,

ca. 4 mL, and filtered off a small amount of insoluble salts. The product was precipitated with 25 mL of hexanes and collected on a glass filter. The product was allowed to air dry and with the yield of 57mg, 58% yield of (Pc)Hf($PW_{11}O_{39}$)[TBA]$_5$. ^{1}H NMR (500 MHz, CD_2Cl_2) δ= 9.53 (m, 8H$^{\alpha}$), 8.21(m, 8H$^{\beta}$), 3.18(m, 40H, N-CH_2-), 1.59(m, 40H, -CH_2-), 1.41(m,40H, -CH_2-), 0.99(t, 60H, -CH_3). ^{31}H NMR (CD_2Cl_2): δ= -15.68 ppm. UV-Vis CH_2Cl_2 λmax nm (log ε) 334 (5.76), 616 (5.48), 652 (5.45), 685(6.25) MALDI-MS: m/z= 4578.6 calcd., found 4579.00

Phthalocyaninato Zirconium(IV)$PW_{11}O_{39}$ tetra-butyl ammonium salt
(Pc)Zr($PW_{11}O_{39}$)[TBA]$_5$

This is prepared by the same procedure as the hafnium ternary complex except using (Pc)Zr(OAc)$_2$ (16mg, 723.84 g/mol, 0.021 mmol).Yield: 50% ^{1}H NMR (500 MHz, CD_2Cl_2) δ= 9.49 (m, 8H$^{\alpha}$), 8.11(m, 8H$^{\beta}$), 3.08(m, 40H, N-CH_2-), 1.51(m, 40H, -CH_2-), 1.34(m, 40H, -CH_2-), 0.95(t,60H, -CH_3). ^{31}P NMR (CD_2Cl_2) δ= -15.46 ppm. UV-Vis CH_2Cl_2 λmax nm (log ε) 336 (5.63), 618 (5.37), 652 (5.33), 687 (6.03).MALDI-MS m/z= 4492.1 calcd., found 4492.72

3.5 CONCLUSIONS

These ternary (Por)M(POM) and (Pc)M(POM) complexes are capable of binding to surfaces by direct metal association, and represent new organic-inorganic, hybrid materials that can be synthesized in high yields. These complexes exhibit excellent light absorbing and photonic properties derived from their porphyrinoid core as well as photonic and structural properties derived from their simultaneous multidentate

coordination of a single metal ion. In general, the efficiency of charge transport from molecules to semiconductors is a critical factor for a variety of hybrid (molecular-semiconductor) device architectures. Charge transport efficiency is mediated by appropriate matching of molecular HOMO-LUMO gaps to semiconductor band gaps, the nature of the linker, and the proximity of the molecule to the surface.[4,19-20,22,44]. These ternary structures can serve as models for direct binding of porphyrinoids to oxide surface via Hf and Zr metals. There are also other metals that axially bind oxygen, e.g. Ti, Sn, and Mo, and may also promote direct attachment to surfaces. In the majority of meso tetraarylporphyrins these metal ions reside near the porphyrin plane and the orthogonal aromatic moieties inhibit direct metal-surface interactions so tethers are needed to enable the attachment. Therefore, ternary (Por)M(POM) and (Pc)M(POM) materials will yield a better understanding of the fundamental properties of porphyrinoids attached to oxide surfaces.[18,45]

Appendix

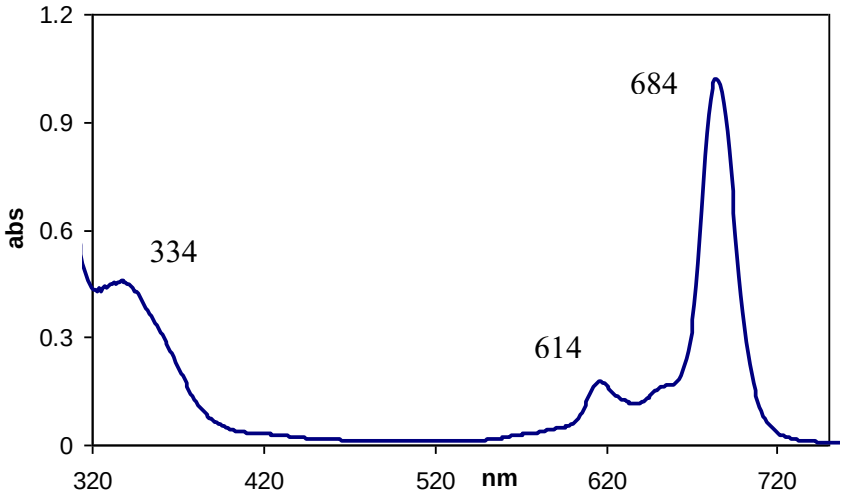

Figure A3.1 Absorption spectra of (Pc)Hf(OAc)$_2$ in CH_2Cl_2 solution.

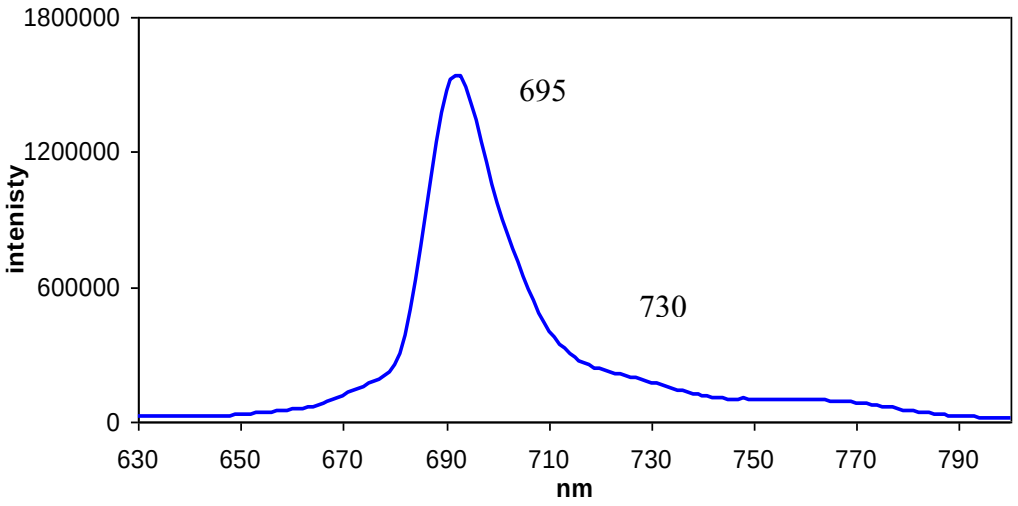

Figure A3.2 Emission spectra of (Pc)Hf(OAc)$_2$ in CH_2Cl_2 solution excited at 615 nm Q band.

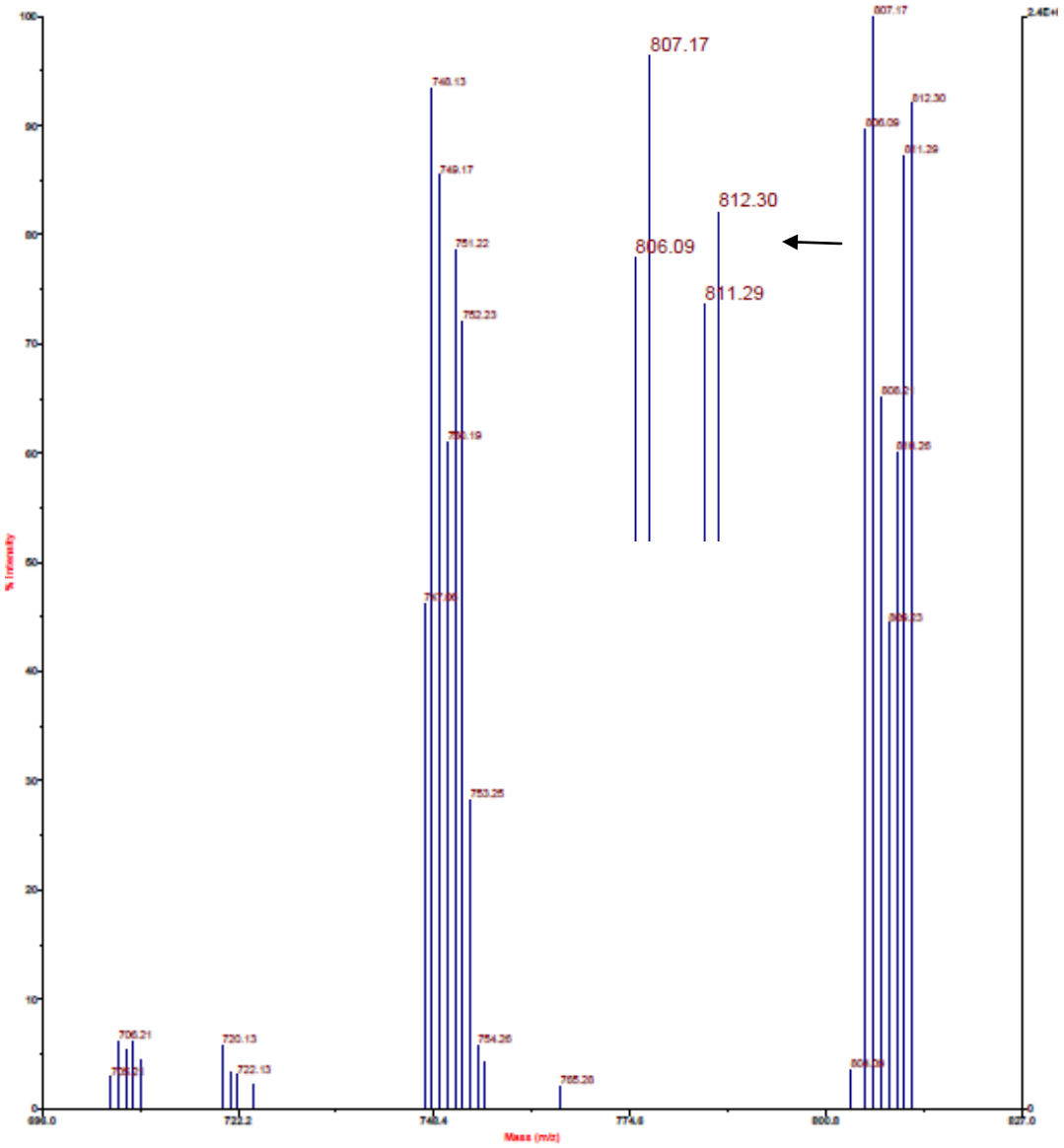

Figure A3.3 MALDI MS (Pc)Hf(OAc)$_2$ m/z= 807.2 calcd., found 807.17. No matrix used.

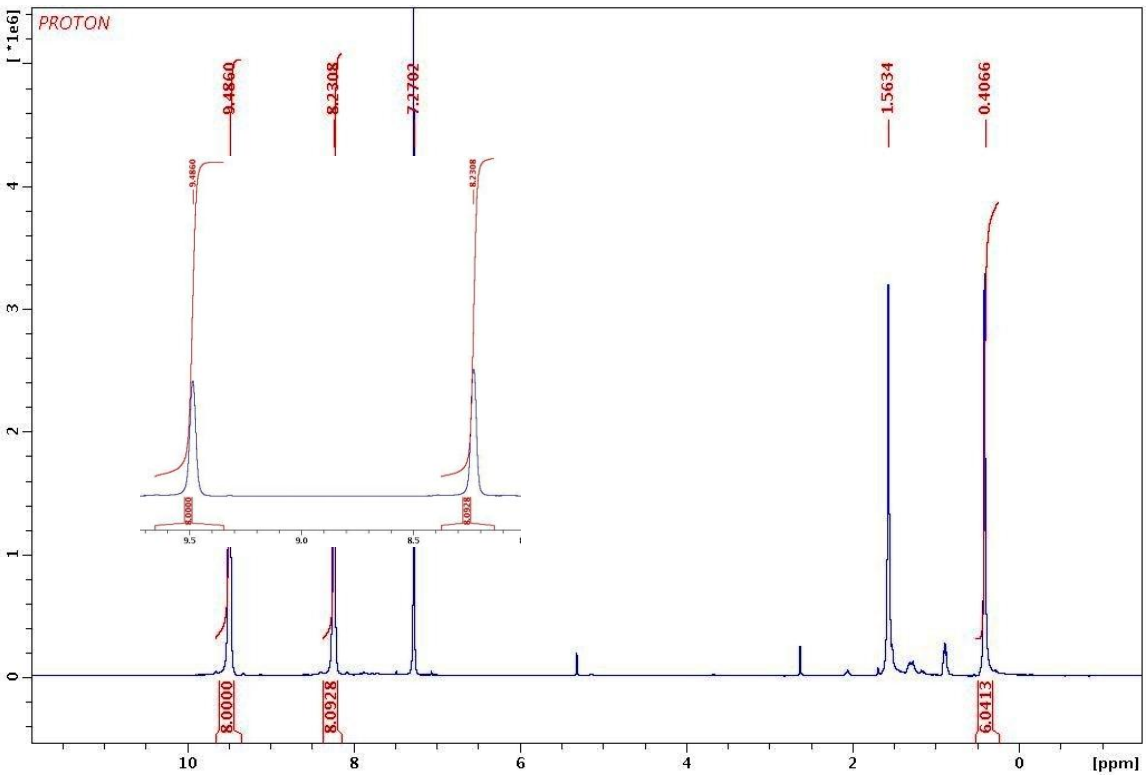

Figure A3.4 (Pc)Hf(OAc)$_2$ ^{1}H- NMR full spectrum in $CDCl_3$. 7.27 ppm $CDCl_3$ and 1.56 ppm H_2O. Inset shows the aromatic region.

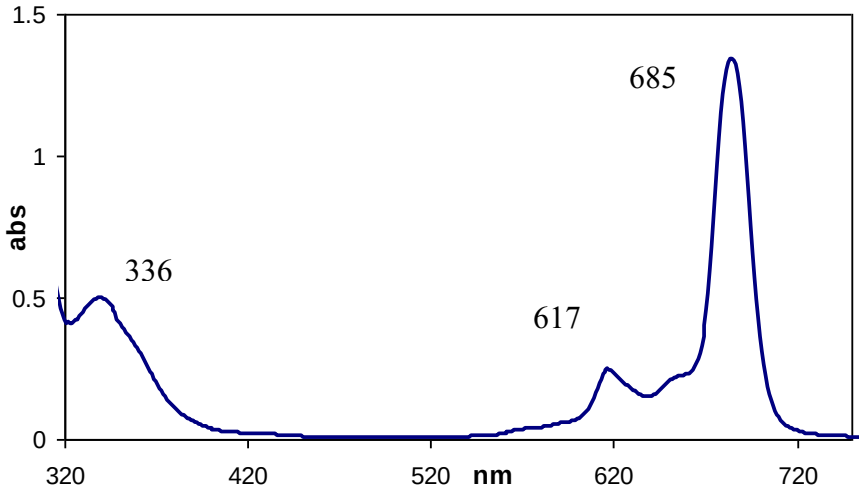

Figure A3.5 Absorption spectra of $(Pc)Zr(OAc)_2$ in CH_2Cl_2 solution.

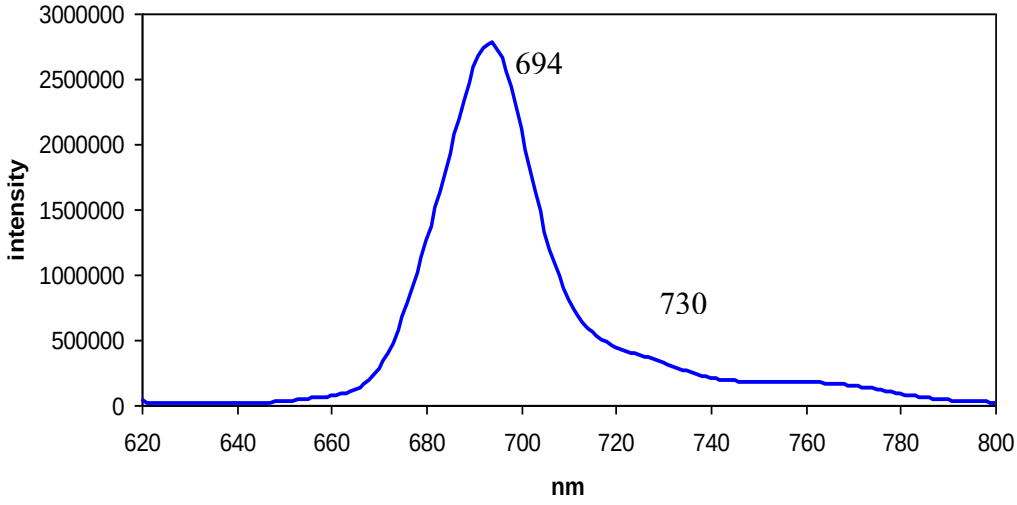

Figure A3.6 Emission spectra of $(Pc)Zr(OAc)_2$ in CH_2Cl_2 solution excited at 615 nm Q band.

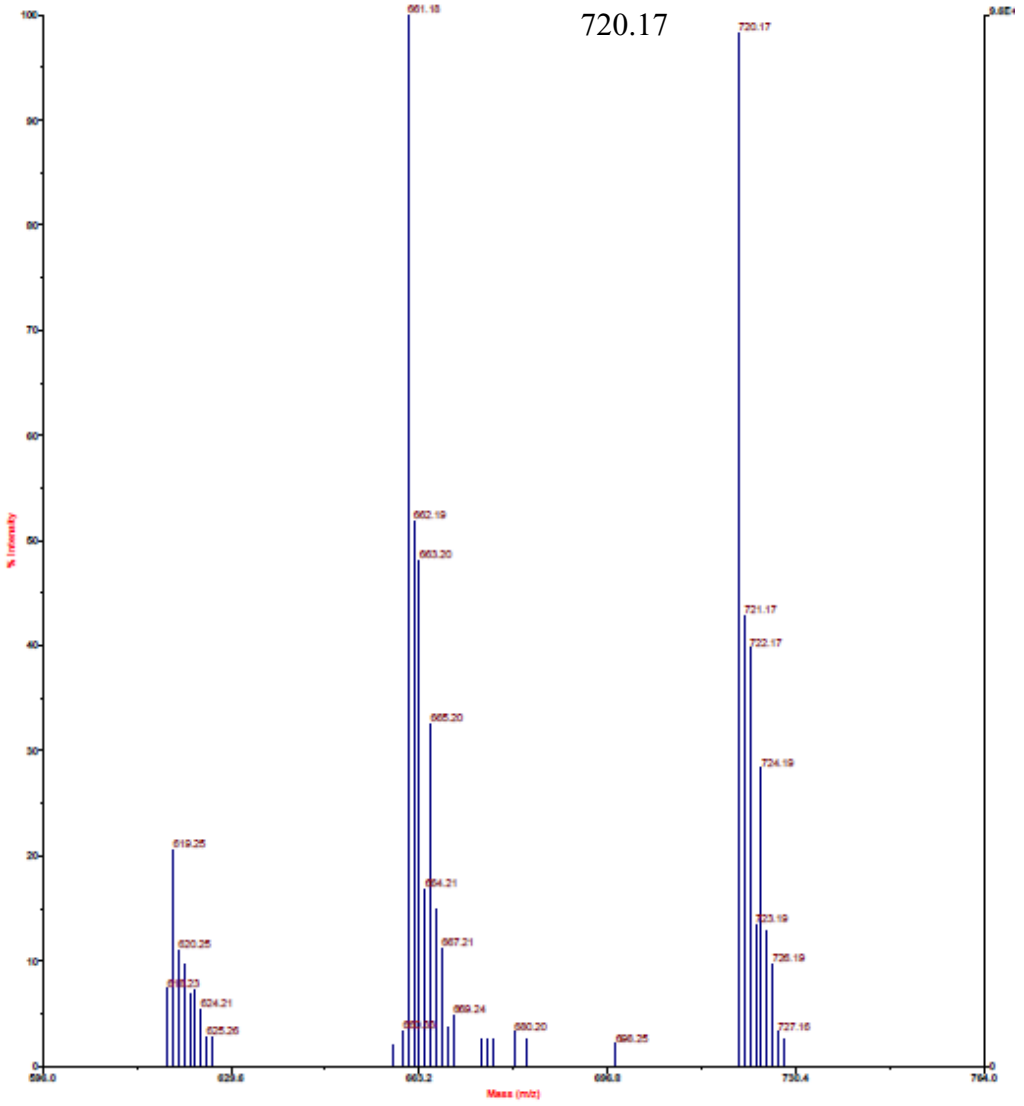

Figure A3.7 MALDI MS (Pc)Zr $(OAc)_2$ m/z= 723.0 calcd., found 720.17. No matrix used.

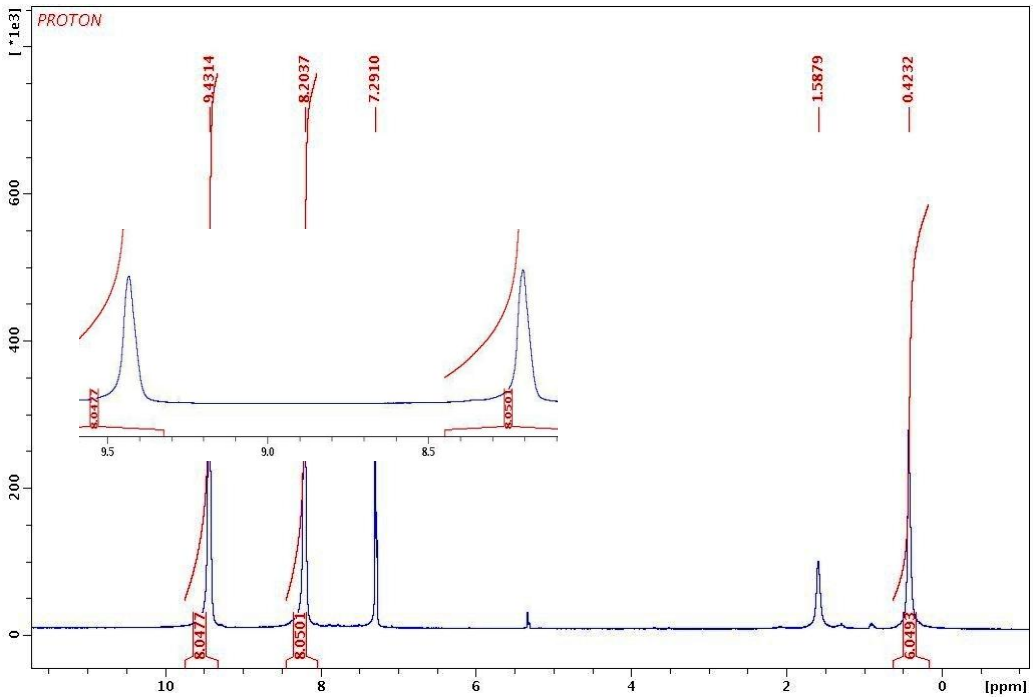

Figure A3.8 (Pc)Zr(OAc)$_2$ ^{1}H- NMR full spectrum in $CDCl_3$. 7.29 ppm $CDCl_3$ and 1.58 ppm H_2O. Inset shows the aromatic region.

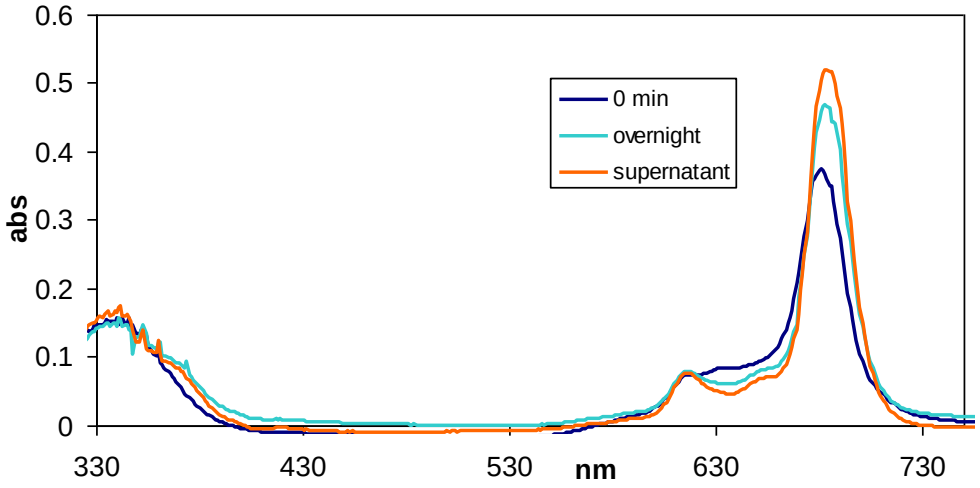

Figure A3.9 Absorption spectra of (Pc)Hf (POM) at the beginning of reaction, after the reaction and after filtration of supernatant with CH_2Cl_2 and precipitation with hexane solution. The Q-band red shift is about 2 nm.

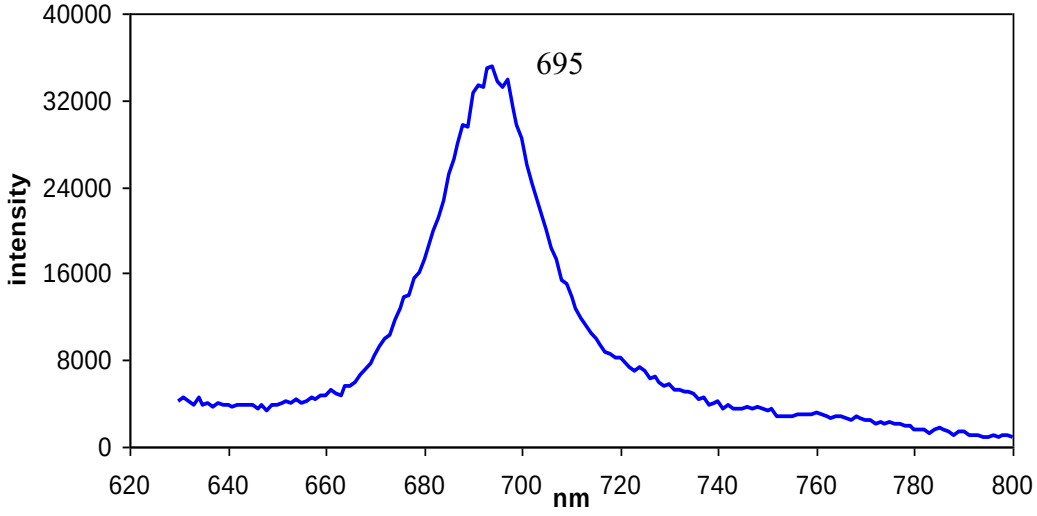

Figure A3.10 Emission spectra of (Pc)Hf(POM) in CH_2Cl_2 solution excited at 618 nm Q band.

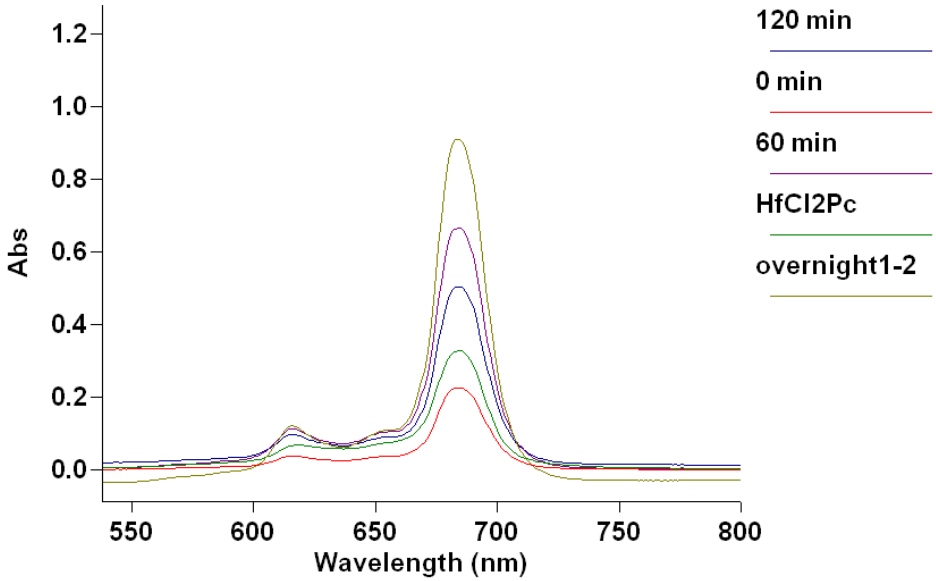

Figure A3.11 Absorption spectra of the progress of the (Pc)Hf(POM) reaction. (Pc)Hf(POM) synthesized from (Pc)Hf(Cl)$_2$ starting material and addition of 2 equivalents of POM.

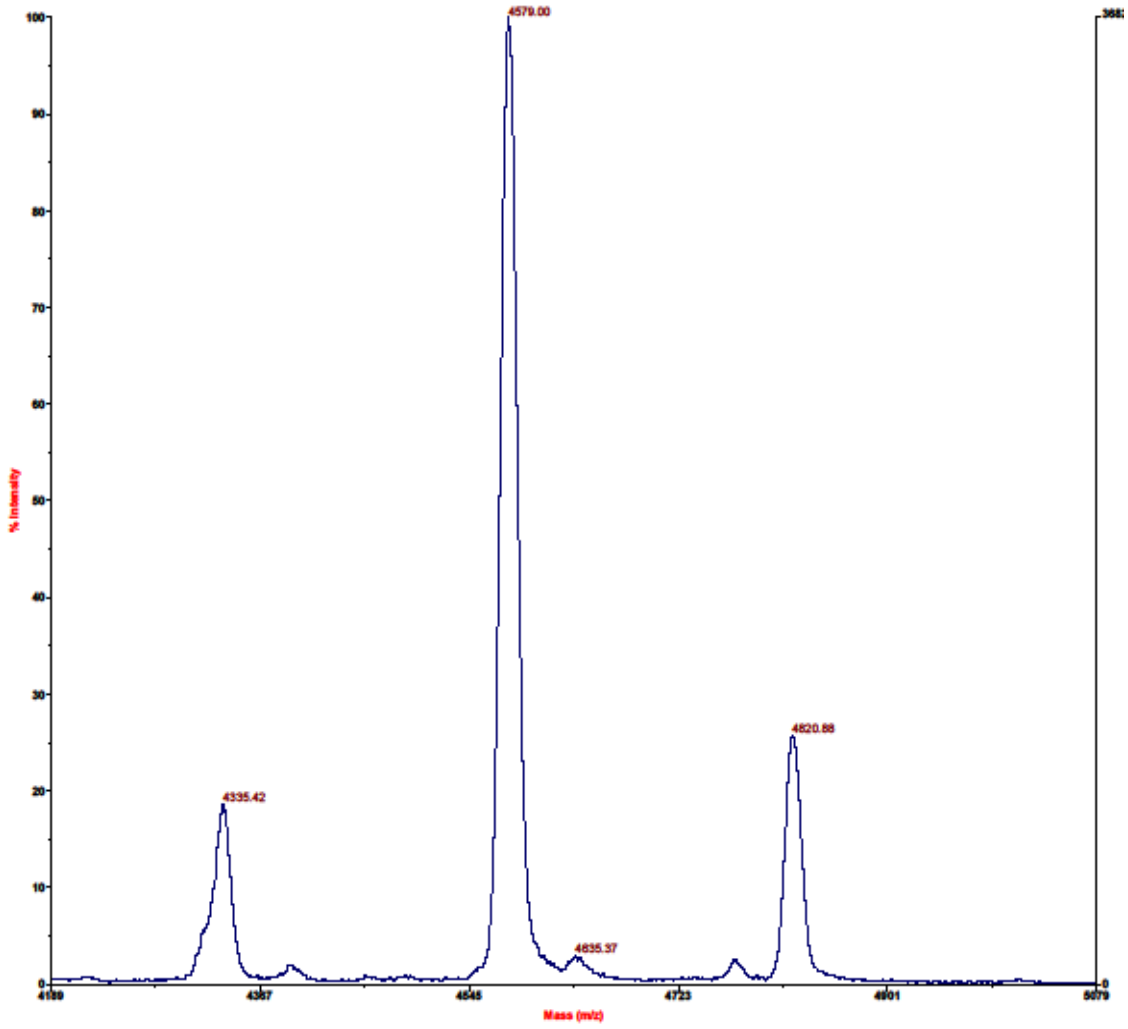

Figure A3.12 MALDI MS of (Pc)Hf(POM) m/z= 4578.27 calcd., found 4579.00. The peak on 4820 has an additional TBA and that at 4355 has one less TBA.

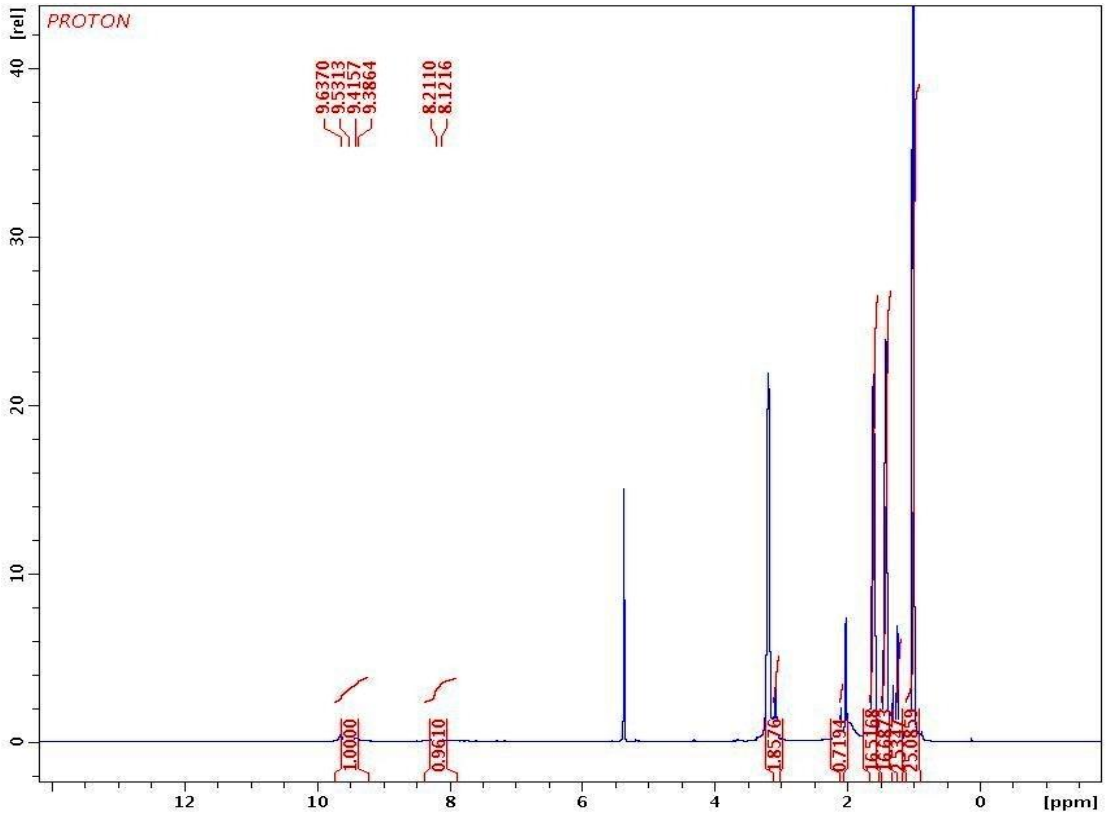

Figure A3.13 500MHz ^{1}H- NMR full spectrum of the supernatant from the synthesis of (Pc)Hf (POM) in CD_2Cl_2.

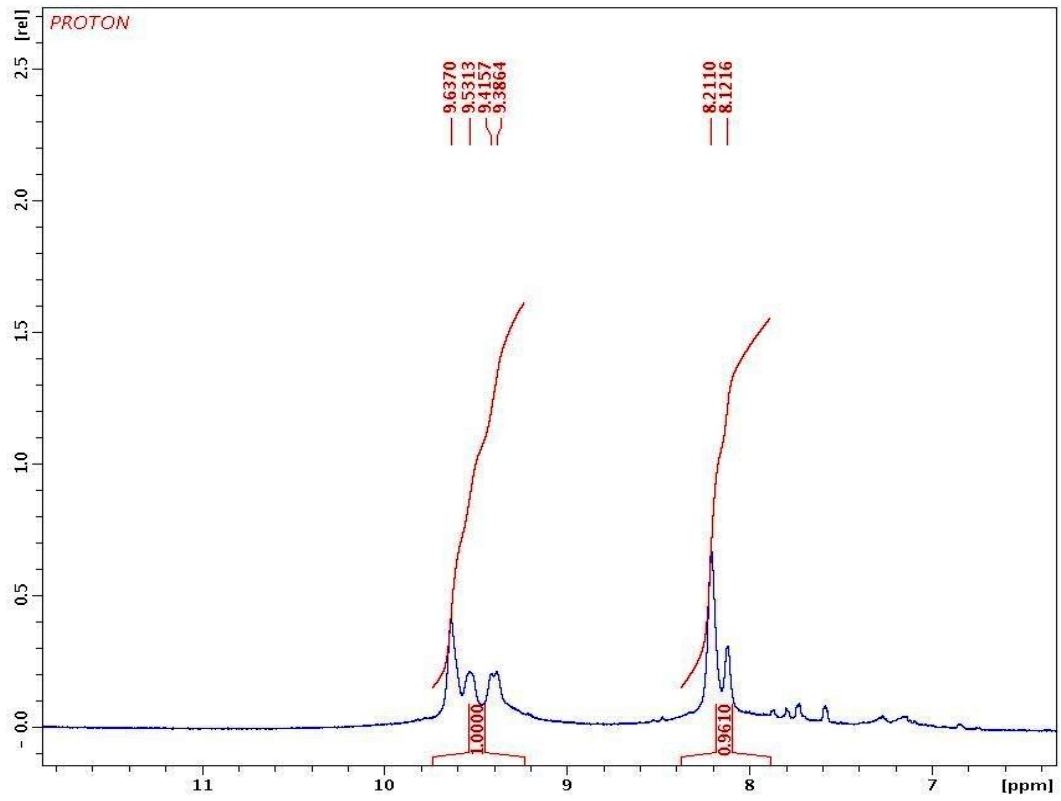

Figure A3.14 (Pc)Hf (POM) ^{1}H- NMR full spectrum in CH_2Cl_2 supernatant, aromatic region.

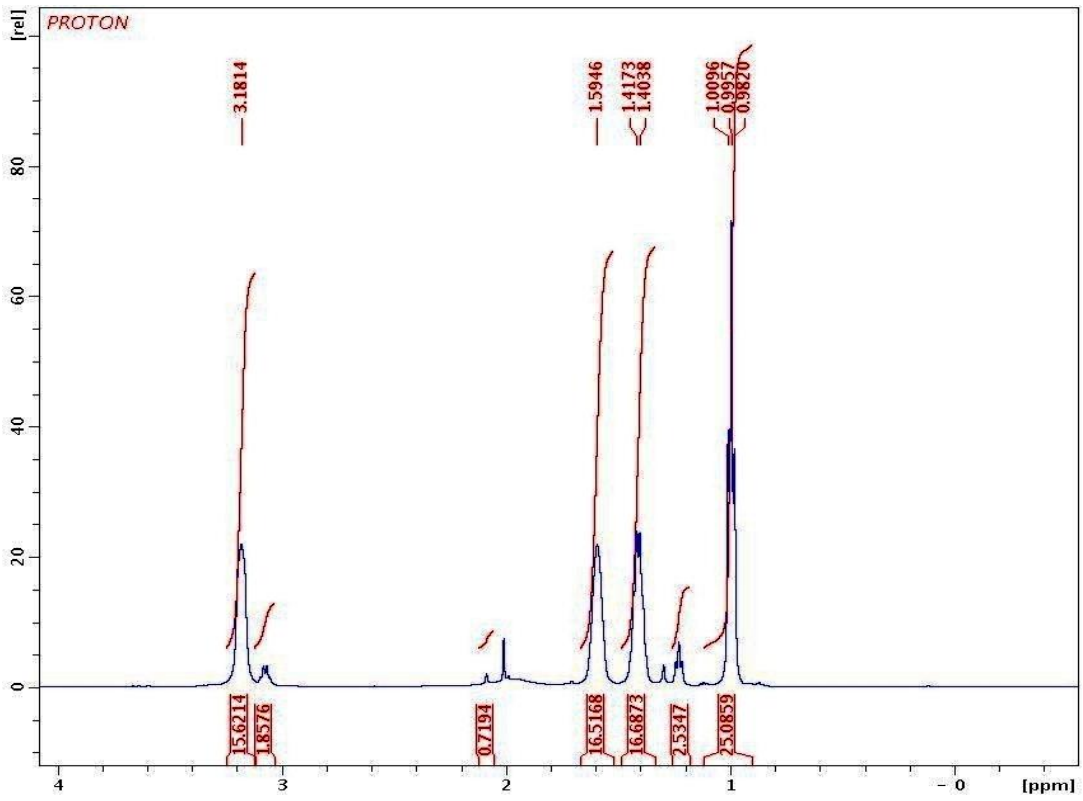

Figure A3.15 (Pc)Hf (POM) ^{1}H- NMR full spectrum in CH_2Cl_2 supernatant, TBA region.

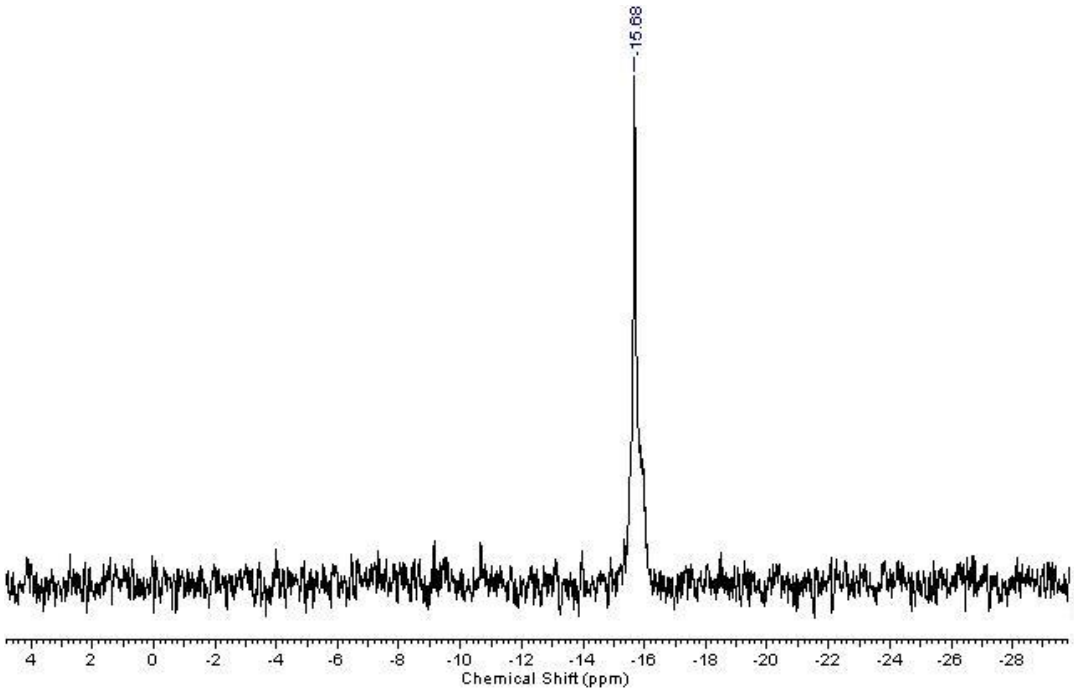

Figure A3.16 ^{31}P NMR of (Pc)Hf (POM) in CD_2Cl_2.

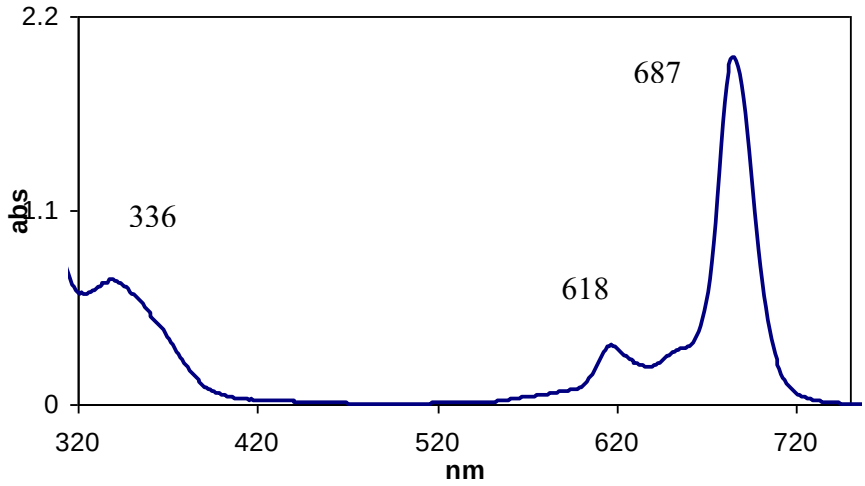

Figure A3.17 Absorption spectra of (Pc)Zr(POM) in CH_2Cl_2 solution.

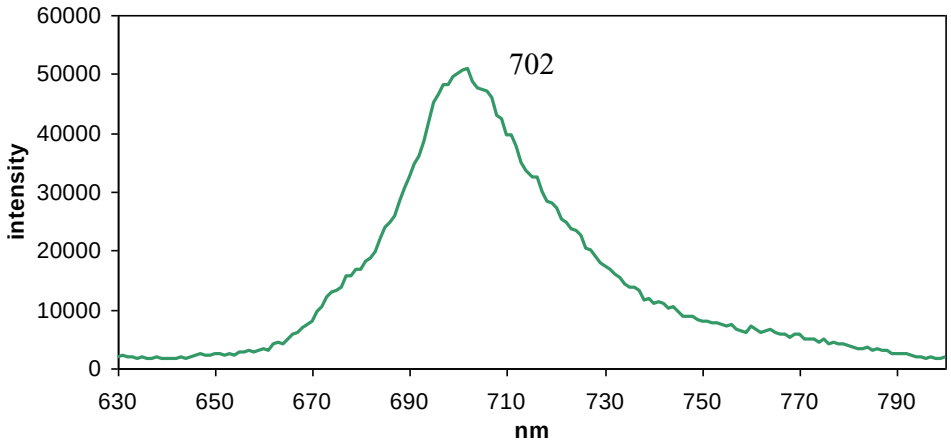

Figure A3.18 Emission spectra of (Pc)Zr POM in CH_2Cl_2 solution excited at 618 nm Q band.

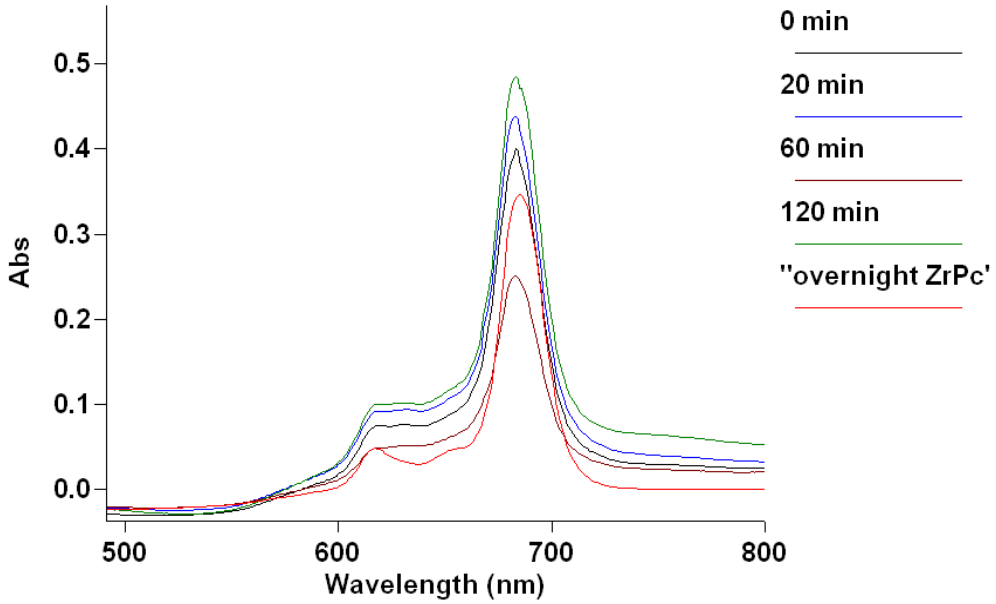

Figure A3.19 Absorption spectra of the progress of (Pc)Zr POM the reaction. The Q-band shift for about 2 nm from starting material.

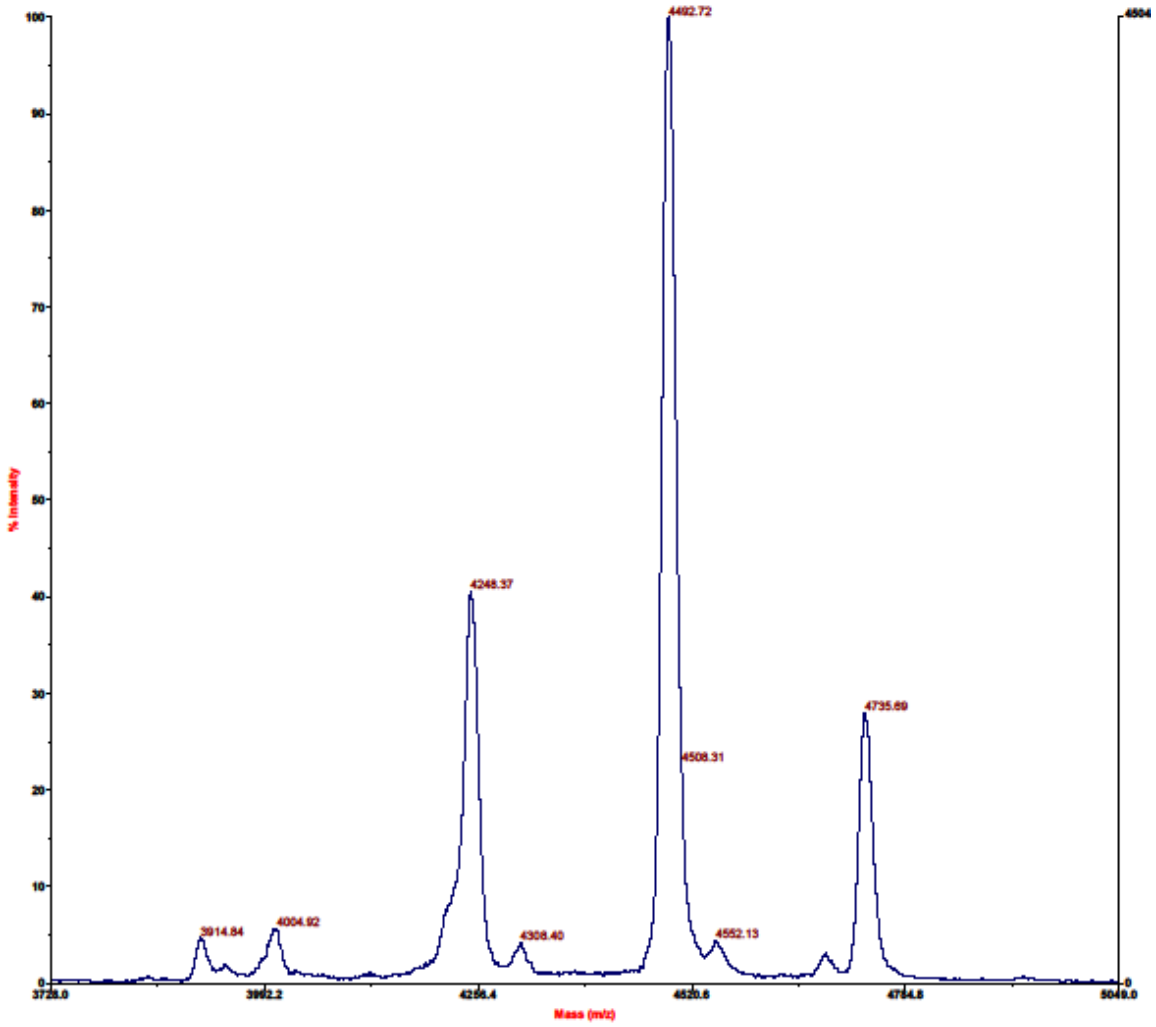

Figure A3.20 MALDI MS of (Pc)Zr(POM) m/z= 4492.10 calcd., found 4492.72.The peak at 4735 has an additional TBA, and peak at 4248 has one TBA less.

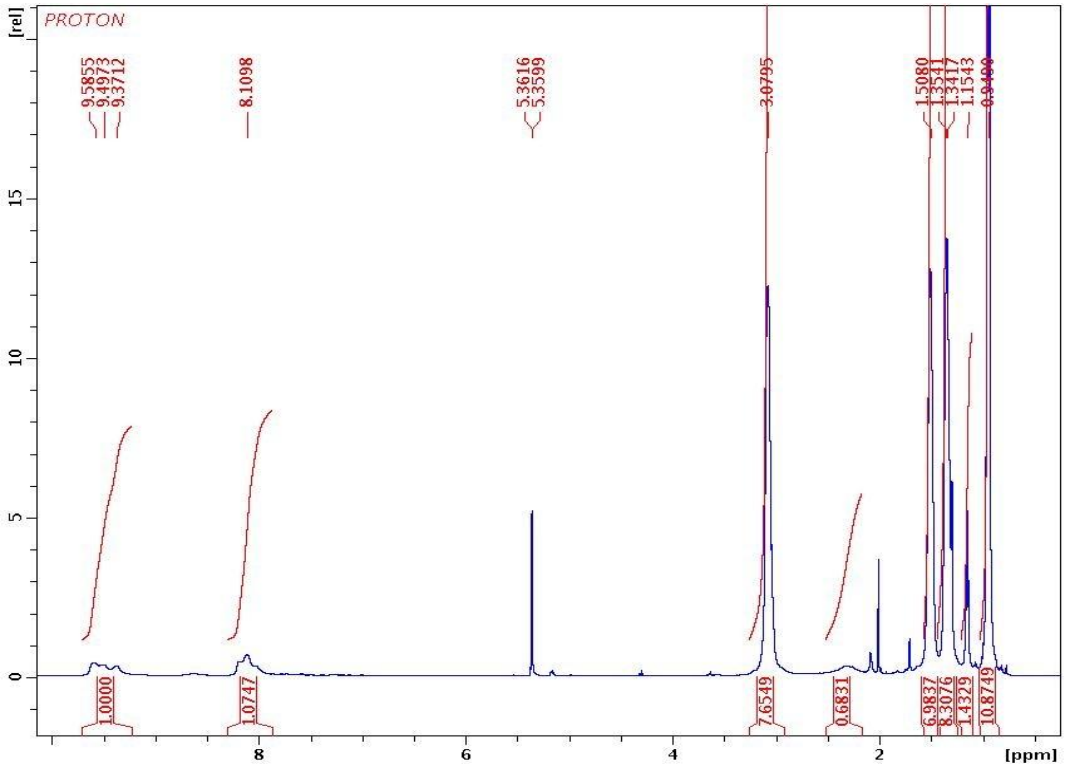

Figure A3.21 500 MHz ^{1}H- NMR full spectrum of (Pc)Zr(POM) in CD_2Cl_2.

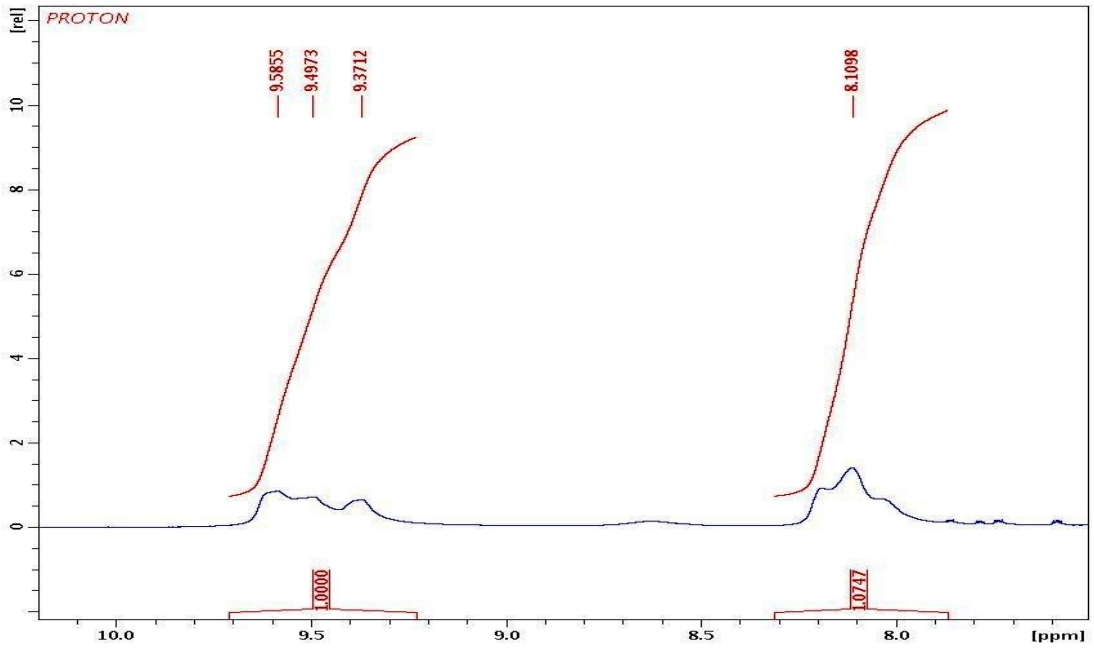

Figure A3.22 [1] H- NMR spectrum of (Pc)Zr(POM) in CH_2Cl_2 supernatant, aromatic region.

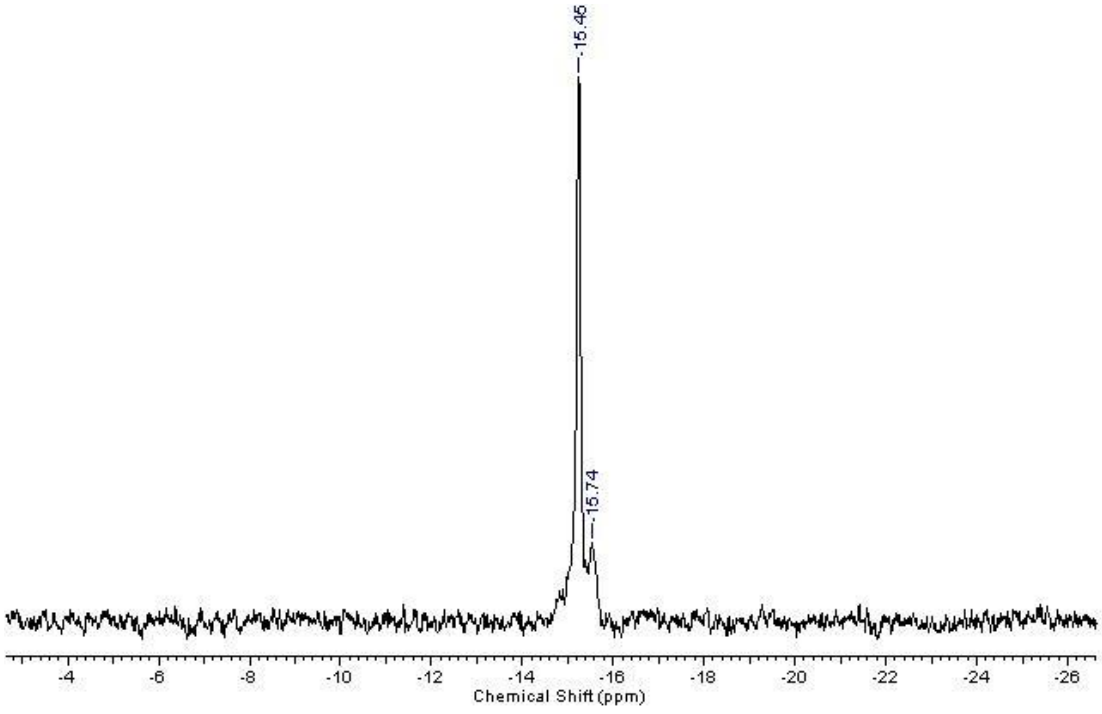

Figure A3.23 ^{31}P NMR of (Pc)Zr (POM) in CD_2Cl_2.

References

(1) Falber, A. Synthesis and Crystallography of Cerium(IV) Bis Porphyrinates and Hafnium(IV) mono Porphyrinates; a Tool Box for Supramolecular Chemistry, Ph.D. Thesis,; City University of New York: New York, 2007.

(2) Hao, J.; Giraudeau, A.; Ping, Z.; Ruhlmann, L. Langmuir 2008, 24, 1600-1603.

(3) Cherian, S.; Wamser, C. C. J. Phys. Chem. B 2000, 104, 3624-3629.

(4) Tachibana, Y.; Haque, S. A.; Mercer, I. P.; Durrant, J. R.; Klug, D. R. J. Phys. Chem. B 2000, 104, 1198-1205.

(5) Drain, C. M.; Bazzan, G.; Milic, T.; Vinodu, M.; Goeltz, J. C. Israel J. Chem. 2005, 45, 255-269.

(6) Drain, C. M.; Chen., X. In Encyclopedia of Nanoscience & Nanotechnology; Nalwa, H. S., Ed.; American Scientific Press: New York, 2004; Vol. 9.

(7) Milic, T. N.; Chi, N.; Yablon, D. G.; Flynn, G. W.; Batteas, J. D.; Drain, C. M. Angew. Chem., Int. Ed. 2002, 41, 2117-2119.

(8) Drain, C. M.; Nifiatis, F.; Vasenko, A.; Batteas, J. D. Angew. Chem. Int. Ed. 1998, 37, 2344-2347.

(9) Dmitrenko, O.; Huang, W.; Polenova, T. E.; Francesconi, L. C.; Wingrave, J. A.; Teplyakov, A. V. J. Phys. Chem. B 2003, 107, 7747-7752.

(10) Toth, J. E.; Anson, F. C. J. Am. Chem. Soc. 1989, 111, 2444-2451.

(11) Keana, J. F. W.; Ogan, M. D. J. Am. Chem. Soc. 1986, 108, 7951-7957.

(12) Keana, J. F. W.; Ogan, M. D.; LU, Y.; Beer, M.; Varkey, J. J. Am. Chem. Soc. 1986, 108, 7957-7963.

(13) Katsoulis, D. E. Chem. Rev. 1998, 98, 359-388.

(14) Long, D. L.; Burkholder, E.; Cronin, L. Chem. Soc. Rev. 2007, 36, 105-121.

(15) Drain, C. M.; Smeureanu, G.; Batteas, J.; Patel, S. In Dekker Encyclopedia of Nanoscience and Nanotechnology; Schwartz, J. A., Contescu, C. I., Putyera, K., Eds.; Marcel Dekker, Inc.: New York, 2004; Vol. 5.

(16) Barlow, D. E.; Scudiero, L.; Hipps, K. W. Langmuir 2004, 20, 4413-4421.

(17) Otsuki, J.; Kawaguchi, S.; Yamakawa, T.; Asakawa, M.; Miyake, K. Langmuir 2006, 22, 5708-5715.

(18) Nazeeruddin, M. K.; Hunphry-Baker, R.; Officer, D. L.; Campbell, W. M.; Burrell, A. K.; Graetzel, M. Langmuir 2004, 20, 6514-6517.

(19) Stromberg, J. R.; Marton, A.; Kee, H. L.; Kirmaier, C.; Diers, J. R.; Muthiah, C.; Taniguchi, M.; Lindsey, J. S.; Bocian, D. F.; Meyer, G. J.; Holten, D. J. Phys. Chem. C 2007, 111, 15464-15478.

(20) Chan, Y.-H.; Schuckman, A. E.; Perez, L. M.; Vinodu, M.; Drain, C. M.; Batteas, J. D. J. Phys. Chem. C 2008, 112, 6110-6118.

(21) Tanaka, M.; Hayashi, S.; Eu, S.; Umeyama, T.; Matano, Y.; Imahori, H. Chem. Commun. 2007, 2069-2071.

(22) Rochford, J.; Chu, D.; Hagfeldt, A.; Galoppini, E. J. Am. Chem. Soc. 2007, 129, 4655-4665.

(23) Varotto, A.; Todaro, L.; Vinodu, M.; Koehne, J.; Liu, G.-y.; Drain, C. M. Chem. Comm. 2008, 4921–4923.

(24) Tong, Lok H.; Wietor, J.-L.; Clegg, W.; Raithby, Paul R.; Pascu, Sofia I.; Sanders, Jeremy K. M. Chem. Eur. J. 2008, 14, 3035-3044.

(25) Marorri, F.; Bonifazi, D.; Gehrig, R.; Gallani, J.-L.; Diederich, F. Israel J. Chem. 2005, 45, 303-319.

(26) Tashiro, K.; Aida, T. Chem. Soc. Rev. 2007, 36, 189-197.

(27) Hasobe, T.; Saito, K.; Kamat, P. V.; Troiani, V.; Qiu, H.; Solladie, N.; Kim, K. S.; Park, J. K.; Kim, D.; D'Souza, F.; Fukuzumi, S. J. Mater. Chem. 2007, 17, 4160–4170.

(28) D'Souza, F.; El-Khouly, M. E.; McCarty, A. L.; Gadde, S.; Karr, P. A.; Zandler, M. E.; Araki, Y.; Ito, O. J. Phys. Chem. B 2005, 109, 10107-10114.

(29) Bazzan, G.; Smith, W.; Francesconi, L. C.; Drain, C. M. Langmuir 2008, 24, 3244-3249.

(30) Santos, I. C. M. S.; Rebelo, S. L. H.; Balula, M. S. S.; Martins, R. R. L.; Pereira, M. M. M. S.; Simoes, M. M. Q.; Neves, M. G. P. M. S.; Cavaleiro, J. A. S.; Cavaleiro, A. M. V. J. Mol. Catal. A: Chem. 2005, 231, 35-45.

(31) Yokoyama, A.; Kojima, T.; Ohkubo, K.; Fukuzumi, S. Chem. Comm. 2007, 3997 – 3999.

(32) Allain, C.; Favette, S.; Chamoreau, L.-M.; Vaissermann, J.; Ruhlmann, L.; Hasenknopf, B. Eur. J. Inorg. Chem. 2008, 2008, 3433-3441.

(33) Hagrman, D.; Hagrman, P. J.; Zubieta, J. Angew. Chem. Int. Ed. 1999, 38, 3165-3168.

(34) Tsuda, A.; Hirahara, E.; Yeong-Sang Kim; Tanaka, H.; Kawai, T.; Aida, T. Angew. Chem. Int. Ed. 2004, 43, 6327 - 6331.

(35) Drain, C. M.; Varotto, A.; Radivojevic, I. Chem. Rev. 2009, 109, 1630-1658.

(36) Babcock, L. M., University of Illinois, 1988.

(37) Kim, H. J.; Jung, S.; Jeon, Y. M.; Whang, D.; Kim, K. Chem. Comm. 1997, 2201-2202.

(38) Falber, A.; Todaro, L.; Goldberg, I.; Favilla, M. V.; Drain, C. M. Inorg. Chem. 2008, 47, 454-467.

(39) Kim, H. J.; Whang, D.; Kim, K.; Do, Y. Inorg. Chem. 1993, 32, 360-362.

(40) Tomachynski, L. A.; Tretyakova, I. N.; Chernii, V. Y.; Volkov, S. V.; Kowalska, M.; Legendziewicz, J.; Gerasymchuk, Y. S.; Radzki, S. Inor.Chim.Acta 2008, 361, 2569-2581

(41) Gerasymchuk, Y. S.; Volkov, S. V.; Chernii, V. Y.; Tomachynski, L. A.; Radzki, S. J. Alloys Compd. 2004, 380, 186–190.

(42) Tretyakova, I. N.; Chernii, V. Y.; Tomachynski, L. A.; Volkov, S. V. Dyes and Pigments 2007, 75, 67-72.

(43) Falber, A.; Burton-Pye, B. P.; Radivojevic, I.; Todaro, L.; Saleh, R.; Francesconi, L.; Drain, C. M. Eur.J.Inorg.Chem. 2009, 2459-2466.

(44) Hagfeldt, A.; Grätzel, M. Acc. Chem. Res. 2000, 33, 269-277.

(45) Nazeeruddin, M. K.; Klein, C.; Liska, P.; Grätzel, M. Coord. Chem. Rev. 2005, 249, 1460-1467.

CHAPTER 4

Group (IV) Metalloporphyrins and Metallophthalocyanines as New Dyes for Solar Cell Devices

4.1 ABSTRACT

New dyes as sensitizers for photovoltaic devices, such as 5,10,15,20-tetraphenylporphyrin (TPP) and phthalocyanine (Pc) complexes of Zr(IV) and Hf(IV) were investigated. (TPP)$Hf(OAc)_2$, (TPP)$Zr(OAc)_2$, (Pc)$Hf(OAc)_2$, and (Pc)$Zr(OAc)_2$ contain oxophilic metals that also will bind tightly to oxide band gap materials via the ligated metal ion. The hypothesis is that the new mode of binding to the surface will improve the efficiency of the charge separations in solar cells because of enhancing the trapping and injecting electrons in the conduction band of the oxide surface. The efficiency of solar cell devices can be improved using different dyes to broaden absorption of the solar energy spectra. In this chapter, the deposition of the dyes on indium-tin-oxide (ITO) surfaces and TiO_2 nanoparticles will be evaluated, as well as their electrochemical properties and finally incorporation into proof-of-principle devices.

4.2 INTRODUCTION

As described in chapter 3, polyoxometalates (POMs) are often regarded as good models for defect sites in the oxide surface.[5] Thus, our synthesis and characterization of ternary complexes of porphyrin and/or phthalocyanine with Keggin POM, $PW_{11}O_{39}^{7-}$ suggested that one way to self-organize porphyrinoids onto oxide surfaces is to use porphyrinoids coordinated to oxophilic group IV metals such as Hf and Zr. The POM

studies indicate that the 3-4 open metal ion coordination sites of the $Hf(Por)^{2+}$, $Zr(Por)^{2+}$, $Hf(Pc)^{2+}$, and $Zr(Pc)^{2+}$ are bound primarily to TiO_2 and ITO via surface defect sites upon displacement of the auxiliary acetate or chloride ligands.[6]

Furthermore, the hypothesis is that such dyes bound tightly to the oxide band gap materials via the ligated metal ion will improve the efficiency of charge separation (electron or hole injection depending on the specific redox potentials). This proposed new mode of binding to oxides surfaces is in stark contrast to other adsorption or binding modes to these surfaces. Porphyrinoids are most commonly substituted with carboxylic or sulfonic groups for better attachment to oxide surfaces. To test this hypothesis, the goal is to make photovoltaic solar cells fabricated from TiO_2 as the semiconductor sensitized by dyes such as $Hf(TPP)^{2+}$, $Zr(TPP)^{2+}$ and $Hf(Pc)^{2+}$, $Zr(Pc)^{2+}$. These will be compared to similarly constructed devices using conventional dye systems.

4.3 DISCUSSION AND RESULTS

4. 3.1 Surface binding to glass, ITO and TiO_2

Hf(TPP) and Zr(TPP) on oxide surfaces *

Since the POM is a good model of oxide surfaces[5] and the exchange of the acetate ligands on the $(Por)M(OAc)_2$ complexes for the lacunary site on the POM is facile, the protruding Hf(IV) and Zr(IV) ions may be a good way to attach tetraarylporphyrins to oxide surfaces such as ITO, SiO_2, SnO_2, and TiO_2. Using metal ions that protrude from the macrocycle as a mode of chromophores attachment to oxide surfaces is in contrast to the many organic moieties used to tether porphyrins to metals.[7-15] The significant changes

in the optical spectra between the (Por)M$(OAc)_2$ and the ternary complex indicate good electronic coupling between the porphyrin and the POM.[16] To evaluate surface binding, drop casting, or dipping a glass substrate or glass with an ITO coating, with a root mean square (rms) roughness of < 1 nm, results in robust binding of $Zr(TPP)^{2+}$ and $Hf(TPP)^{2+}$ to the surface. The metalloporphyrin does not wash off with vigorous rinsing with toluene or other solvents, but can be removed with alcohols or organic acids, which further indicates binding via the oxophilic metal ions. UV-visible absorption spectra reveal that more of the $Zr(TPP)^{2+}$ and $Hf(TPP)^{2+}$ complexes bind piranha cleaned glass than ozone cleaned glass, because the former leaves more hydroxyl groups on the surface than the latter,[17] and note the UV- visible spectra are similar to the ternary complexes (Figure 4.1).

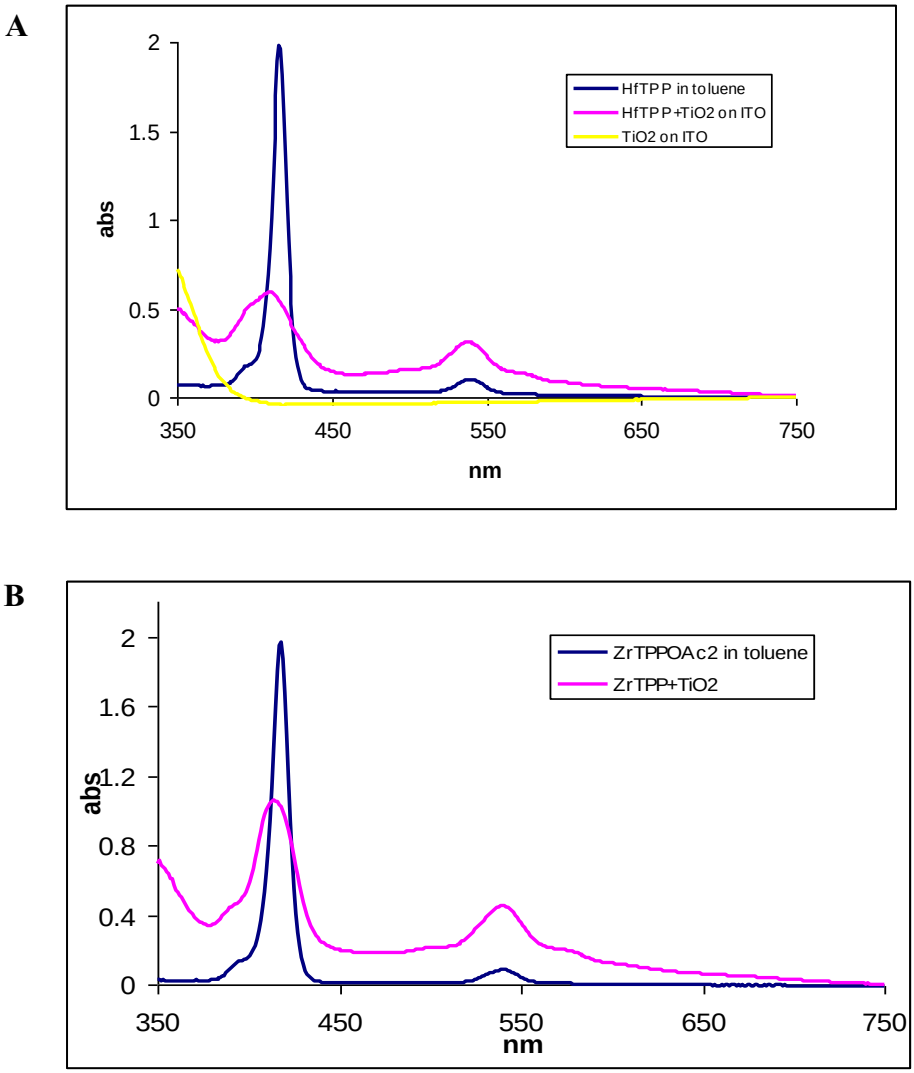

Figure 4.1 (A) UV-visible spectra of the starting (TPP)Hf(OAc)$_{2.}$ in toluene (blue), reflectance spectrum of a ca. 1 mm film of TiO_2 nanoparticles coated with (TPP)Hf(OAc)$_2$ (pink) and an untreated TiO_2 film (yellow); **(B)** UV-visible spectra of the starting (TPP)ZrHf(OAc)$_{2.}$ in toluene (blue), reflectance spectrum of a ca. 1 mm film of TiO_2 nanoparticles coated with (TPP)Zr(OAc)$_2$ (pink). The dynamic range of the reflectance integrating sphere is ca. 1 absorbance units.

A

B

Figure 4.2 (A) Slurries of TiO_2 nanoparticles with left to right: TPP, (TPP)Zr(OAc)$_2$, Zn(TPP) and (TPP)Hf(OAc)$_2$. 30 mg of TiO_2 nanoparticles were treated with 2 ml of 0.5 mM porphyrin solution by mixing slurry overnight, removing the solvent, and rinsing 2-3 times with toluene. **(B)** Powders on upper row from left: TPP, Zn(TPP) and (TPP)Zr(OAc)$_2$; lower row from left: TCPP (THF used as solvent and for rinse) and (TPP)Hf(OAc)$_2$.

Stirring a slurry of ca. 5 nm particles of TiO_2 in a 0.5 mM solution of (TPP)M(OAc)$_2$, where M= Hf or Zr, or other metalloporphyrin complexes with other anionic ligands such as Cl^- in dry toluene for a minimum of 2 h effectively binds the chromophore to this material (Figure 4.2). The rate of binding to the surface is proportional to the lability of the auxiliary anionic ligands (Cl^->HPO_4^{2-}>OAc^-). The metalloporphyrin is not removed from the TiO_2 by washing with toluene and the slurries are readily cast onto glass or ITO for analysis. The charge balance can be accommodated

by either deprotonation of hydroxyl groups on the surface or the presence of the anionic ligands in the vicinity. After similar incubation of crystalline SiO_2 and TiO_2 surfaces with the $Hf(TPP)^{2+}$ complex and rinsing, very little metalloporphyrin is observed using AFM and UV-visible reflectance. The (TPP)M(POM) ternary complex, the tight binding of the Hf and Zr TPP complexes to nanopowders of silica and TiO_2, the minimal binding to crystalline SiO_2 surfaces, and the results on glass are all indications that Hf(Por) and Zr(Por) prefer to bind to defect sites and those with a greater surface density of hydroxyl groups (Figure 4.3). The diffuse reflectance UV-visible spectra of all surface-bound systems are similar to the ternary complexes in solution, but the red shifts in the Soret bands near 410 nm are somewhat less (Figure 4.1, A4.1, A4.2, A4.3, A4.4, A4.5). The slight red shift likely indicates that the group IV metal ion is not pulled out of the macrocycle to the same extent when bound to the surface compared to the POM. This is expected because the lacunary site of the POM is in an optimal geometry for Hf or Zr binding. The broadened optical spectra are typical of surface bound dyes. While the fluorescence intensity of the $(Por)Hf(OAc)_2$ and $(Por)Zr(OAc)_2$ is diminished due to the heavy atom effect, it is further quenched both in the ternary complexes and when the $Zr(TPP)^{2+}$ and $Hf(TPP)^{2+}$ are bound to the ITO surfaces. The fluorescence is not similarly quenched when the (Por)M complexes are strongly adsorbed to glass. After similar binding and rinsing of the particles, UV-visible reflectance spectra show that free base and Zn(II) TPP adsorb onto these substrate to a much smaller extent but exhibit much greater fluorescence intensities.[18] The widely studied tetracarboxyphenylporphyrin TCPP also remains on the TiO_2. AFM studies of the compound on the ITO do not reveal large aggregates of the metalloporphyrin and a somewhat decreased rms roughness. Since the

$Zr(TPP)^{2+}$ and $Hf(TPP)^{2+}$complexes robustly bind surfaces, likely at defect sites and we remove unbound materials, the surface coverages are much less than coating of porphyrins such as tetracarboxyphenyl derivatives on ITO or TiO_2 surfaces by chemisorption.[10-11,19-20] Relative to the surface, the horizontal orientation of the Zr and Hf complexes of TPP also diminishes the maximum potential coverage compared to the vertical orientation of the TCPP.[20] Thus, the optical cross sections in the visible region for the materials with Hf and Zr porphryins on TiO_2 and on ITO are smaller compared to the absorbed coatings.

* Adapted from Alexander Falber, Benjamin P. Burton-Pye, Ivana Radivojevic, Louis Todaro, Raihan Saleh, Lynn Francesconi, Charles Michael Drain , "Ternary Porphyrinato Hf(IV) and Zr(IV) Polyoxometalate Complexes", Eur. J. Inorg. Chem. 2009,2459-2466.

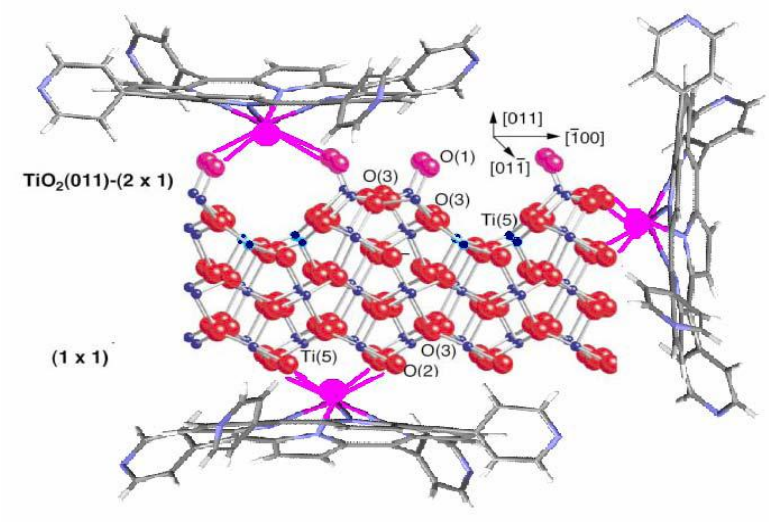

Figure 4.3 Possible binding of Hf(IV)(Por) and Zr(IV)(Por) to anatase TiO_2 surfaces; red balls = O, black =Ti, grey = C, blue = N, and pink =Hf or Zr. Surface binding studies and the crystal structure suggest that the Hf(IV)(Por) and Zr(IV)(Por) bind to step edges and defect sites as shown top left rather than the planar surfaces. The metalloporphyrins are from crystal structures and the TiO_2 matrix was adapted from: Beck, T. J.; Klust, A.; Batzill, M.; Diebold, U.; DiValentin, C.; Selloni, A., Surface Structure of TiO_2 (011)-(2x1). *Phys. Rev.Let.* **2004,** 93, (3), 036104-1-4.

Hf(Pc) and Zr(Pc) on oxide surfaces

Phthalocyanines are widely studied in solar cell research since they are robust and stable molecules, cheap and easy to synthesis, and they absorb in red part of the solar spectra at wavelengths between 500-700 nm with high extinction coefficients [21] on the order of ~ 10^5 $cm^{-1}M^{-1}$. Pc can be synthesized in high yields and are currently used, e.g. as dyes and colorants in the textile industry, as inks, and for recordable CDs. Simple Pc tend to aggregate on TiO_2 surfaces to a greater extent than Por, which is observed as a broadening of absorption spectra compared to the solution phase. The aggregation generally results in deactivation of the excited state resulting in

reduced electron injection. We have preformed analogues experiments as mention in the previous section to test the attachment of (Pc)Hf$(OAc)_2$ and (Pc)Zr$(OAc)_2$ to TiO_2 surfaces (Figure 4.4 and 4.5). After similar procedures to bind the particles, UV-visible reflectance spectra show that free base Pc and ZnPc adsorb onto these substrates to a much smaller extent than the (Pc)Hf and the (Pc)Zr complexes. Rinsing of the particles with solvent removes almost all the free base or ZnPc materials (Figure A4.6).

A

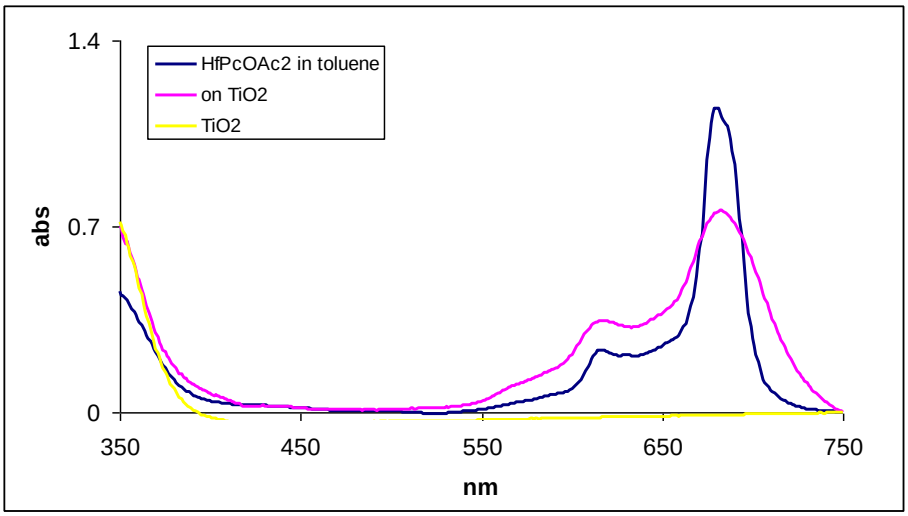

B

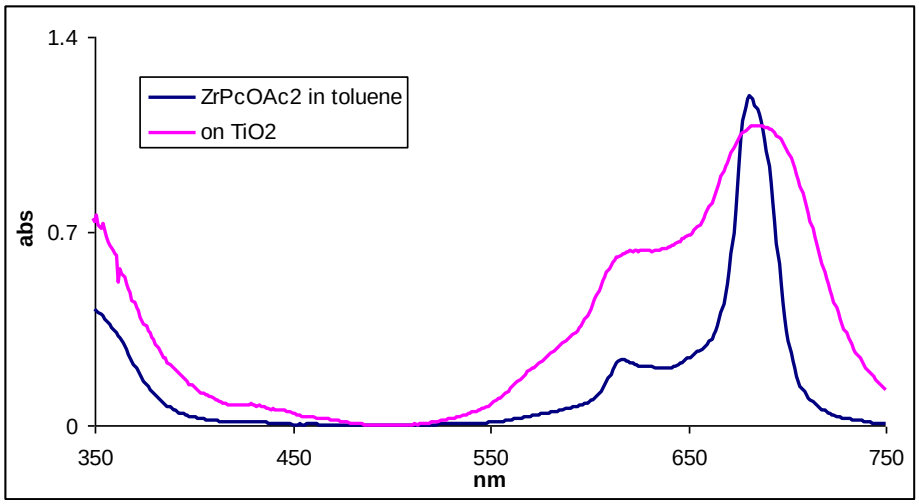

Figure 4.4 (A) UV-visible spectra of the starting (Pc)Hf(OAc)$_2$. in toluene (blue), reflectance spectrum of a ca. 1 mm film of TiO_2 nanoparticles coated with (Pc)Hf(OAc)$_2$ (pink) and an untreated TiO_2 film (yellow); **(B)** UV-visible spectra of the starting (Pc)Zr(OAc)$_2$. in toluene (blue), reflectance spectrum of a ca. 1 mm film of TiO_2 nanoparticles coated with (Pc)Zr(OAc)$_2$ (pink). The dynamic range of the reflectance integrating sphere is ca. 1 absorbance units.

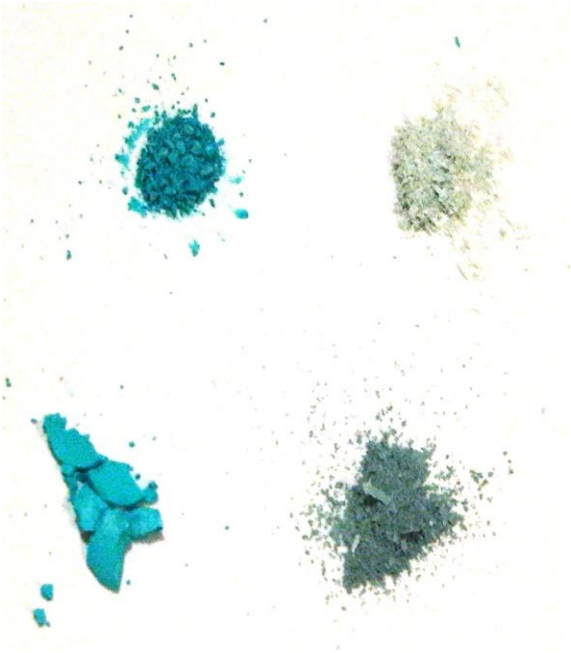

Figure 4.5 30 mg of TiO_2 nanoparticles treated with 2 ml of 0.5 mM phthalocyanine solution by mixing a slurry overnight, removing the solvent, and rinsing 2-3 times with solvent. Powders on upper row from left : (Pc)Hf$(OAc)_2$ and ZnPc; lower row from left : (TPP)Zr$(OAc)_2$ and H_2Pc.

Mixing of porphyrin and phthalocyanine dyes to cover a broader range of solar spectra

Since a single organic dye cannot cover the entire solar energy spectrum well, our second hypothesis is that using several chromophores that absorb at different wavelengths will increase the efficiency by absorbing a broader spectrum of light. Thus, combining the above mentioned metalloporphyrins and metallophthalocyanices can be tested in dye sensitized solar cell in future studies. This can be accomplished by mixing two or more of the dye coated TiO_2 nanoparticles (NP) before incorporation into the device, or by mixing the dyes in solution before adsorbing them to yield TiO_2 NP with both dyes randomly distributed on the NP (Figure 4.6).

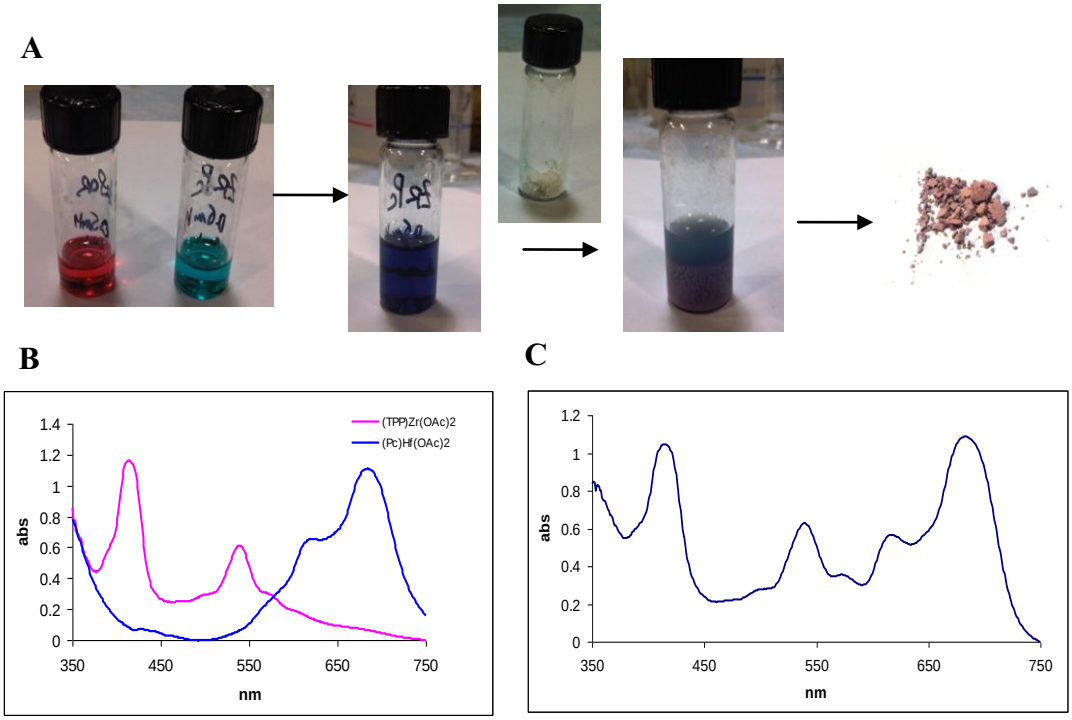

Figure 4.6 (A) The 0.5 mM solution of ZrTPP, ZrPc, the mixture of two, the slurry of mixture with TiO_2 nanoparticles and the resulting powder of coated TiO_2 NP. **(B)** The overlap of reflectance absorption spectra of TiO_2 NP coated with $(TPP)M(OAc)_2$ or with $(Pc)M(OAc)_2$ indicating broader coverage of solar spectra is possible using two dyes, in this case the Zr complexes are used. **(C)** The reflectance absorption spectra of a film of TiO_2, when a 1 mM mixture of ZrPor and ZrPc in toluene is used for coating. The spectrum shows attachment of both dyes on metal oxide surface.

4.3.2 Electrochemistry

Electrochemical properties

Cyclic voltammetry is used for determination of electrochemical characteristics of redox active compounds. We will briefly summarize some important parameters used when presenting electrochemical data. In a simple CV plot shown below (Figure 4.7), the cathodic, positive current is produced when the scan goes into negative potential and represents a reduction process, while the anodic current is associated with oxidation process. If the process is reversible the oxidation and reduction peaks will have slightly different potential (ΔE_p), (eq.4.1) and will be close to Nernstian potential ~ 59mV.

$$\Delta E_p = E_{pa} - E_{pc} \quad , \text{ electrochemical reversibility} \quad \text{(eq. 4.1)}$$

In practice, solutions tend to have high resistance particularly in non-aqueous solvents so the electron transfer gets slower, resulting in greater peak separations, and the systems are said to be quasi-reversible. Irreversible systems show only one wave indicating that the species has undergone a chemical transformation. The scan rate throughout the measurements can vary, but it is usually 100 mV/s. Higher rates can help system become more reversible by competing with the rate of chemical reaction/transformation.

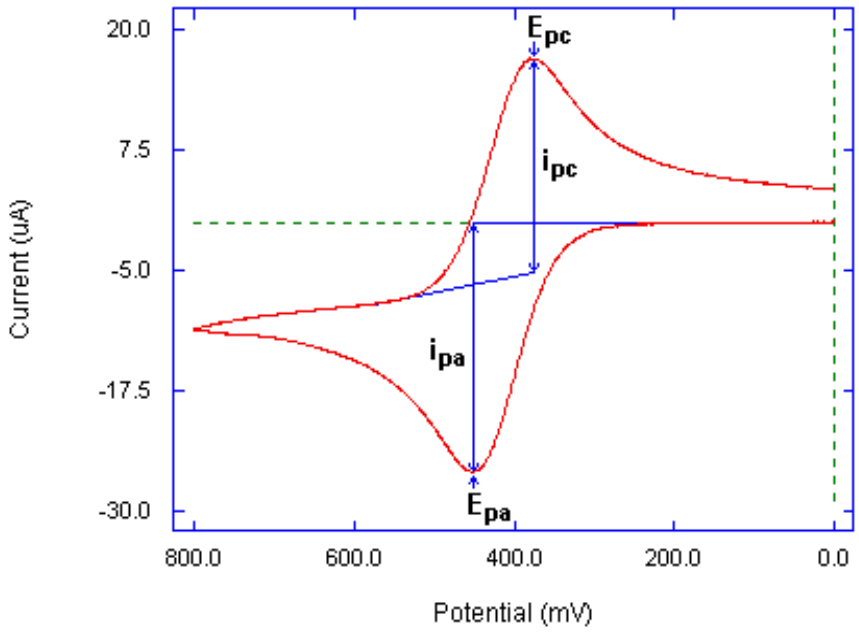

Figure 4.7 A typical cyclic voltammogram showing the important peak parameters. E_{pc} – the cathodic peak potential; E_{pa} – the anodic peak potential; i_{pc}- the cathodic peak current and i_{pa}- the anodic peak current.

The half-wave potential is calculated according to eq. 4.2:

$$E_{1/2}=(E_{pc}+E_{pa})/2 \qquad \text{(eq. 4.2)}$$

In our experiments in non-aqueous solvents, all potentials are referenced to the ferrocene, Fc/Fc^{+} redox couple, as an internal standard, which is very stable and reversible in all solutions. Ferrocene is known to have a potential of 0.400 V vs the normal hydrogen electrode (NHE) scale.[22-23]

Transferred electrons in an electrochemical process depends on the nature of the macrocycle, substituents on the macrocycle, nature of the metal ion, ligands bound to the metal, etc. The appropriate solvent system, electrolyte, and carefully chosen experimental conditions also can influence the reversibility of electro-oxidation and reduction. For example, ZnTPP has an inactive, closed shell central metal ion and undergoes two oxidation and two reduction process in nonaqueous media, that occur at the π conjugated porphyrin ring, to yield the π-dication and π-dianion. Electrochemical properties of many porphyrins and phthalocyanines are reported in the literature.[24] However, for Zr and Hf metalloporphyrins the electrochemistry of sandwich type complexes $Zr(Por)_2$ and $Hf(Por)_2$ have been reported, but not the diacetates and dichlorides.[24]

The electrochemical properties of our compounds were studied in dichloromethane with 0.1 M Bu_4NPF_6 as the supporting electrolyte. We referenced all potentials to the NHE so that we could compare them to TiO_2 conduction band potential that is - 0.5 V.[25] We measured potentials at different scan rates from 50 mV/s, 100 mV/s, 200 mV/s and 500 mV/s and showed that the oxidation and reduction waves are independent of the scan rate. Throughout all experiments of all four compounds, the values for the first oxidation potentials at 200 mV/s scan rate were used for further HOMO-LUMO and energy level calculations because the wave peaks were the best defined. Since similar behavior was observed from our results on both metal complexes, we will use only $(TPP)Zr(OAc)_2$ to show characteristic electrochemical properties (Table 4.1, Figure A4.7).

Table 4.1 Oxidation potentials (eV) of (TPP)Zr(OAc)$_2$ in CH_2Cl_2 solution vs Fc^+/Fc standard at different scan rates (mV/s); half-wave redox potentials for 1st oxidation used for further calculations (in red).

V vs Fc^+/Fc	Scan rate (mV/s)	Epc_1(mV)	Epa_1(mV)	Epa_2(mV)	$E_{1/2}^{o'}$ (mV)
1st oxidation	50	860	988	1436	924
	100	821	1007	1473	938
	200	788	1056	1528	922
	500	784	1102	1728	943

Both (TPP)Hf(OAc)$_2$ and (TPP)Zr(OAc)$_2$ show one quasi-reversible reduction process at negative potential range, and one reversible and irreversible oxidation process at positive potential range (Figure 4.8(A), 4.9(A)). The quasi-reversible reduction represents formation of porphyrin radical anion in the negative potential range of –1.31 V and -1.28 V vs NHE for ZrTPP and HfTPP, respectively, using a 200 mV/s scan rate. The reversible oxidation is due to formation of radical cation in the positive range 1.02 V and 1.01 V vs NHE, respectively. Scanning the solution for nine cycles at a constant scan rate of 100 mV/s, indicates that the porphyrin molecules are stable and do not undergo any chemical change throughout the entire experiment (Figure 4.8(B), 4.9(B)).

Electrochemically measured HOMO-LUMO gap is represented as absolute value between reversible half-wave potentials for oxidation and reduction process.[24] We have referenced this energy gap (Eg) vs ferrocene and expressed results in units of eV (the value of 4.8 eV for ferrocene with respect to the vacuum level, that serves as zero). Thus, the data we have collected from cyclic voltammetry experiments are in good agreement with literature for metalloporphyrins.[14,26] The data are recalculated and summarized in table 4.2.

Table 4.2 Electrochemically calculated (eV) HOMO, LUMO levels and energy gap Eg (eV); used later for plotting energy diagrams in Figure 4.17(C)

vs Fc/Fc^+ (eV) 200mV/s	HOMO (eV)	LUMO (eV)	Eg (eV)
$(TPP)Hf(OAc)_2$	5.41	-3.12	2.29
$(TPP)Zr(OAc)_2$	5.43	-3.09	2.32
$(Pc)Hf(OAc)_2$	5.17	-3.50	1.66
$(Pc)Zr(OAc)_2$	5.19	-3.51	1.68

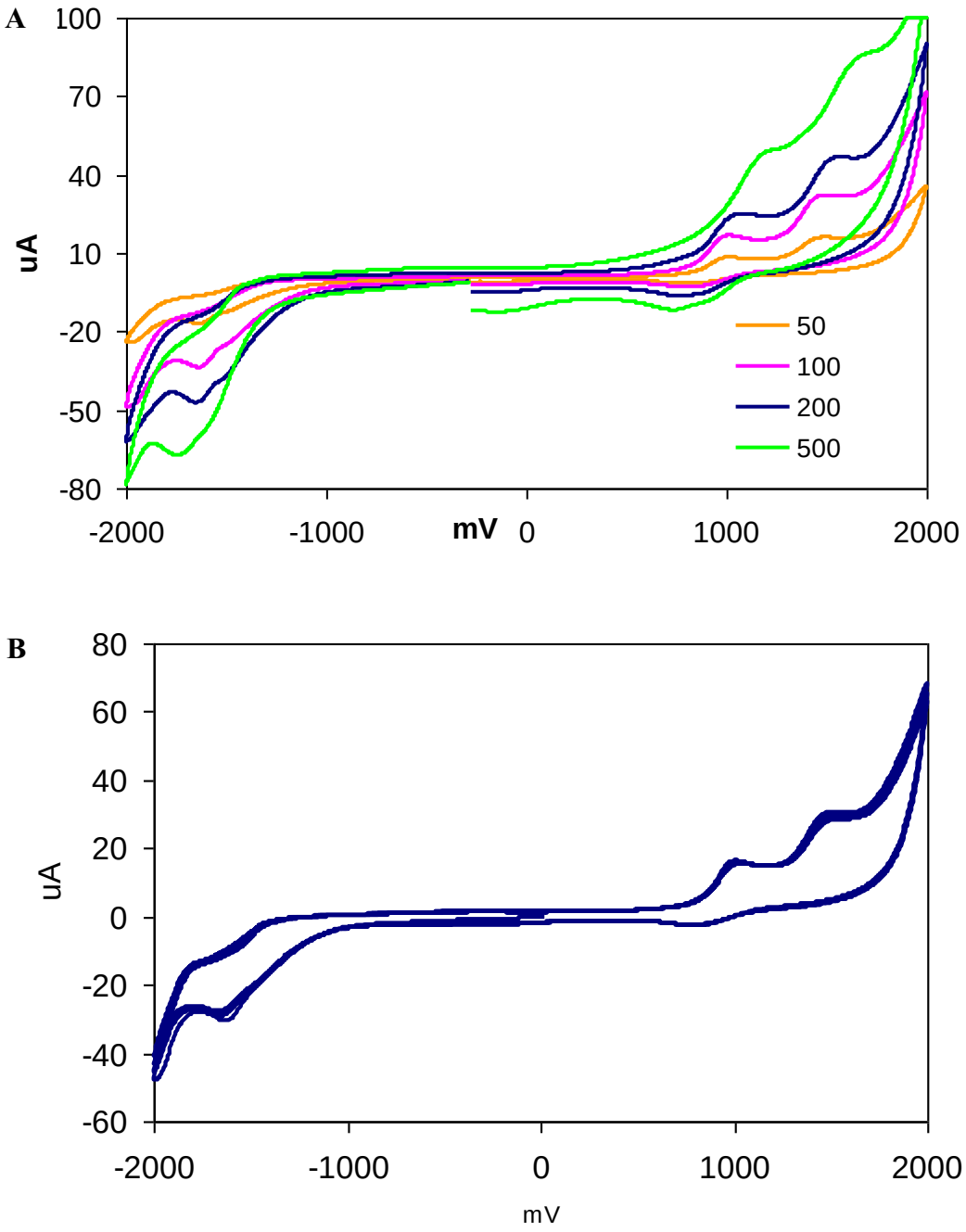

Figure 4.8 Cyclic voltammetry of **(A)** 1 mM (TPP)Hf(OAc)$_2$ solution in dichloromethane containing 0.1 M Bu_4NPF_6 as the supporting electrolyte at different scan rates ranging from 50-500 mV/s. **(B)** After 9 cycles scanned at 100 mV/s compound remains unchange.

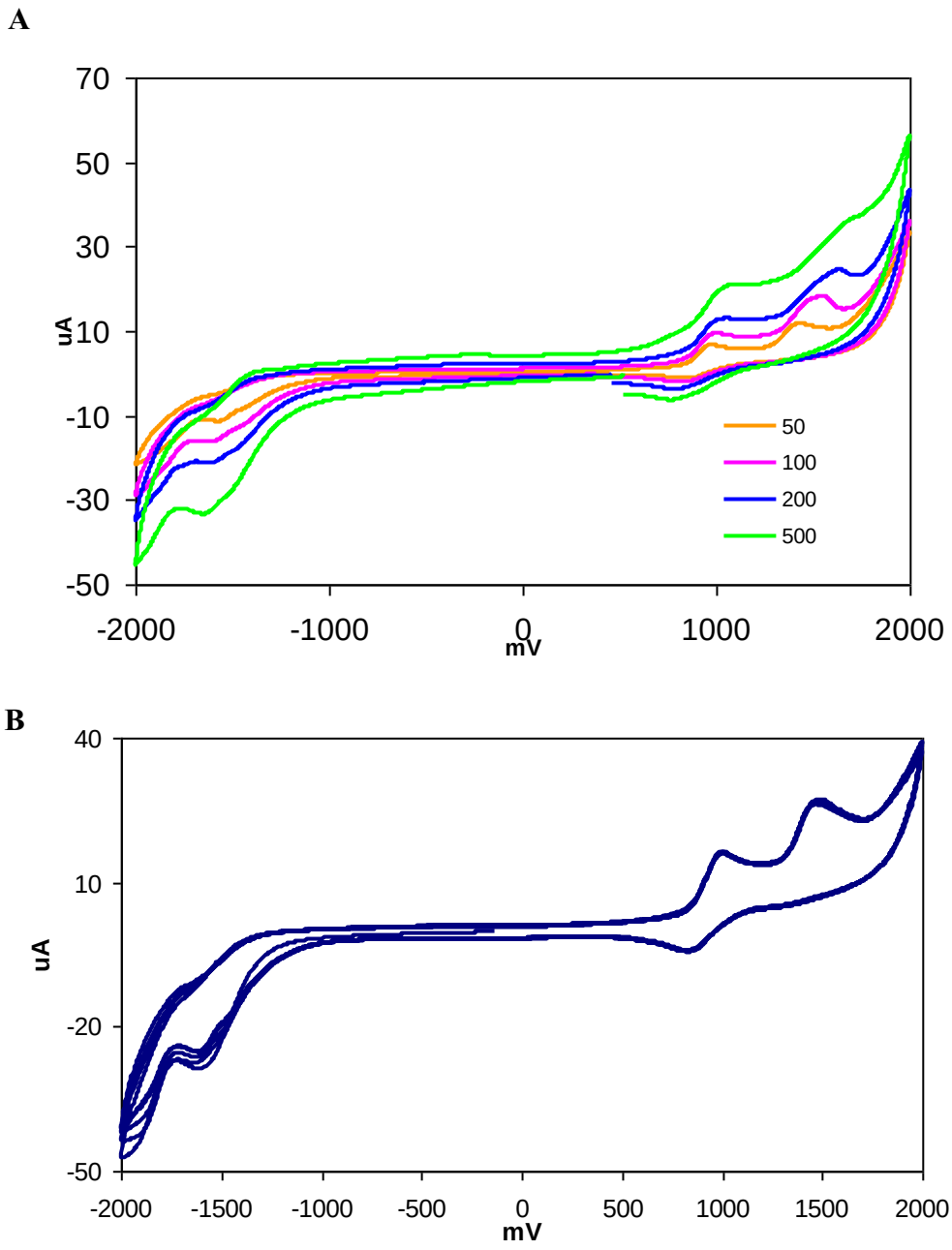

Figure 4.9 Cyclic voltammetry of **(A)** 1 mM (TPP)Zr(OAc)$_2$ solution in dichloromethane containing 0.1 M Bu_4NPF_6 as the supporting electrolyte at different scan rates ranging from 50-500 mV/s. **(B)** After 9 cycles scanned at 100 mV/s compound remains unchanged.

CV curves for both $(Pc)Hf(OAc)_2$ and $(Pc)Zr(OAc)_2$ at negative potential range show one quasi-reversible process, while in the positive potential range, one reversible and one irreversible oxidation process (Figure 4.10(A), 4.11(A)). The quasi-reversible reduction represents formation of Pc radical anion in the range of - 0.873 V HfPc and - 0.890 V vs NHE. The reversible oxidation is due to formation of radical cation in the range 0.769 V for HfPc and 0.780 V for ZrPc vs NHE. Scanning the solution for nine cycles showed us the phthalocyanine complxes are very stable and do not undergo any chemical change throughout the experiment (Figure 4.10(B), 4.11(B)).

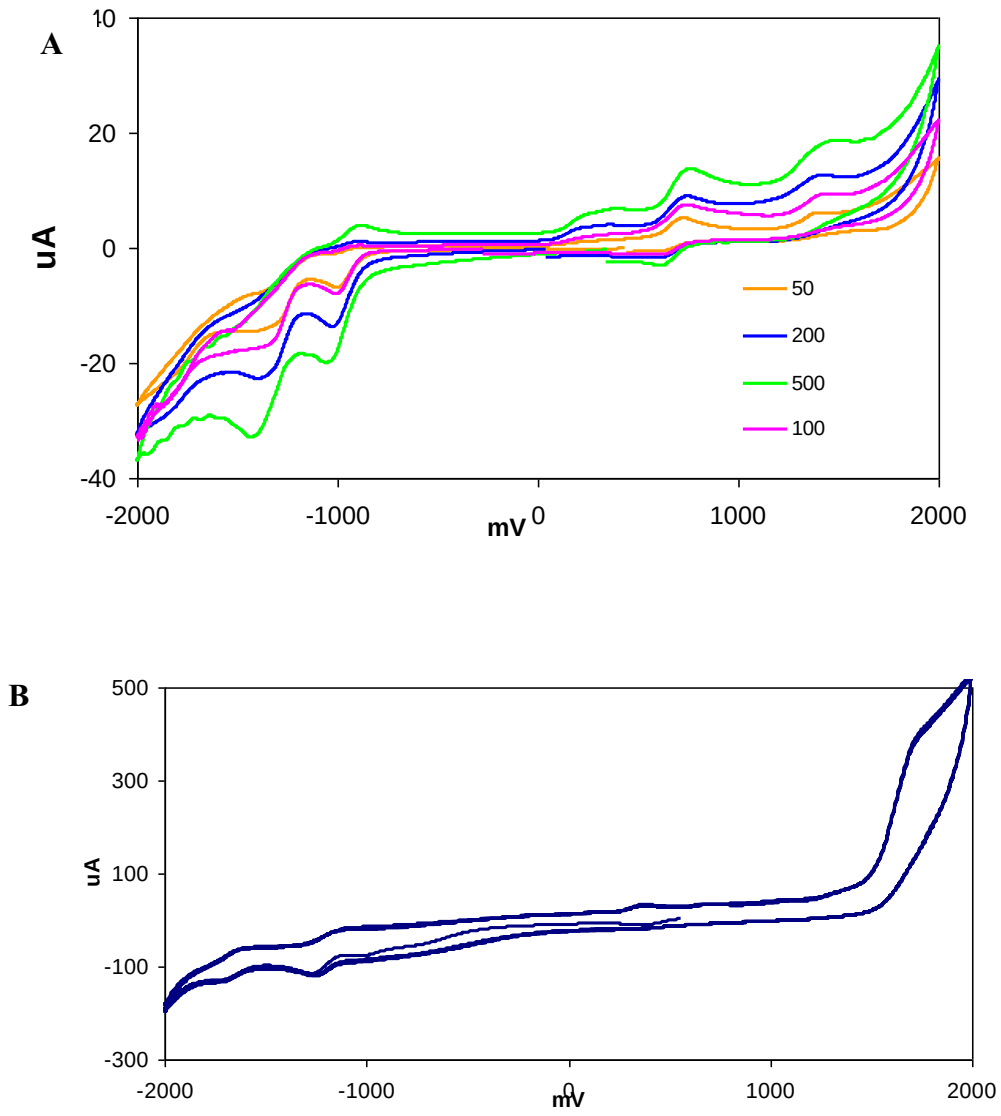

Figure 4.10 Cyclic voltammetry of **(A)** 1 mM (Pc)Hf(OAc)$_2$ solution in dichloromethane containing 0.1M Bu_4NPF_6 as the supporting electrolyte at different scan rates ranging from 50-500mV/s. **(B)** After 9 cycles scanned at 100 mV/s compound remains unaltered.

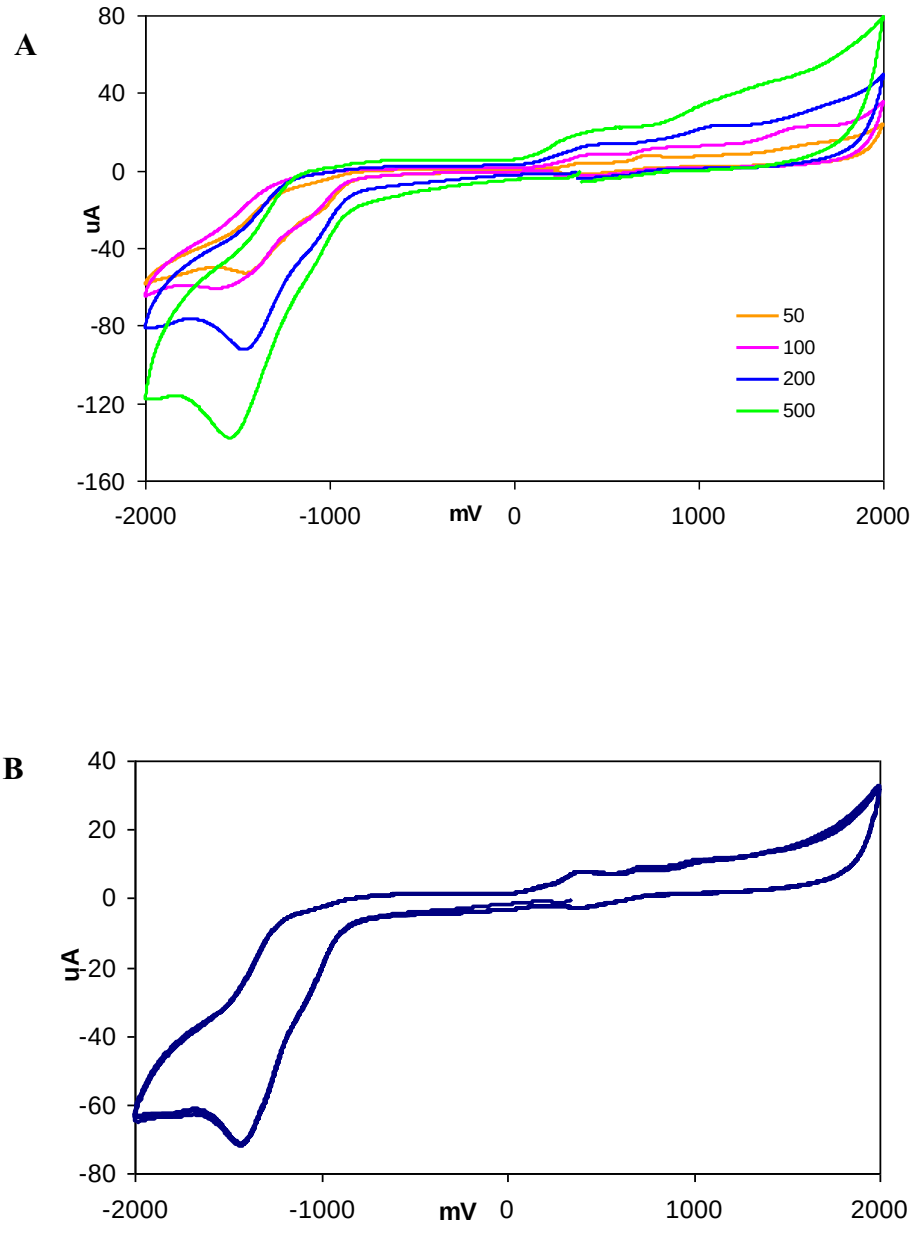

Figure 4.11 Cyclic voltammetry of **(A)** 1 mM $(Pc)Zr(OAc)_2$ solution in dichloromethane containing 0.1 M Bu_4NPF_6 as the supporting electrolyte at different scan rates ranging from 50-500 mV/s. **(B)** After 9 cycles scanned at 100 mV/s compound remains unaltered.

When bound to TiO_2 nanoparticles, we analyzed only the oxidation wave window for all four compounds since TiO_2 electrode itself has a large peak in the negative potential range (Figure A4.8). Generally, the stability of the sensitizer is dominated by the reversibility of the first oxidation wave after the electron is injected into conduction band (CB) of TiO_2. In our system, we observe only the anodic peak current in the first oxidation wave, as an irreversible process, which also diminishes after applying a potential to the electrochemical cell after the second cycle (Figure A4.9). Since the cathodic peak current of the first oxidation potentials in the cyclic voltammograms of analyzed dye solutions at concentrations > 1 mM scanned at 200 mV/s is quasi-reversible, we can assume that the concentration of our dye on TiO_2 surface is not sufficient enough for the cathodic current to be clearly defined. The electrochemical voltage applied to the system can also induce removal of the dye from metal oxide surface. These kinds of systems should be tested with square wave voltammetry or using capillary electrodes that are much more sensitive and lower surface concentrations could be measured.

Energy level calculations for dye-sensitized solar cells

For efficient injection of electrons from the dye excited state to the conduction band of the semiconductor, the LUMO of the dye molecule should lie 0.2-0.3 eV above conduction band (oxidation potential should be more negative than semiconductor CB potential, -0.5 V vs NHE). On the other hand, the HOMO of the dye should have more positive electrochemical potential than the redox mediator (regeneration system 0.4 V vs NHE), so that the oxidized form of the dye after can be easily recovered by reduction by the electrolyte.[2,25] Thus, the HOMO-LUMO gap of the dye should correspond to the band gap of semiconductor so that electron injection to the semiconductor oxide within solar cell can proceed efficiently. Titanium dioxide is a wide band semiconductor and the value of the gap is 3.2 eV. When calculating the HOMO-LUMO gap of the sensitizer, we refer to LUMO as the oxidation potential of excited state $E_{ox}^*(S^*/S^+)$ and HOMO as the ground state oxidation potential. The oxidation potential of excited state $E_{ox}^*(S^*/S^+)$ can be calculated from the ground state oxidation potential and the excitation energy according to equation 4.3:

$$E_{ox}^*(S^*/S^+)=E_{1/2}(S/S^+) - E_{0\text{-}0}/F \qquad \text{(eq. 4.3)}$$

where, $E_{ox}^*(S^*/S^+)$ is the oxidation potential of the excited state (V); $E_{1/2}(S/S^+)$ is the ground state oxidation potential (V); $E_{0\text{-}0}$ is the excitation energy (eV); F = 96485 Q* mol^{-1} , Faraday constant. [27-28] S*= excited state of the dye; S= ground state of the dye; S^+= oxidized form of the dye.

The value of the oxidation potential of the ground state is acquired from cyclic voltammetry data, while excitation energy $E_{0\text{-}0}$ is estimated by the convention from the intersection of the normalized emission and absorption spectra of the dye (Figure A4.10). In table 4.3 below we present the values of the oxidation potentials measured from cyclic voltammetry of all four compounds referenced against the normal hydrogen electrode (NHE) scale. We also summarize calculated values for excited state oxidation potentials. The electrochemical reversibility noted in the last column represents slow electron transfer in these systems, which is not unusual for non-aqueous solutions. Finally, the energy level diagram of our solar device is shown in Figure 4.12. We can say that for all four metalated dyes, electron injection is energetically favorable relative to the conduction band of TiO_2 semiconductor (-0.5 V) and also favorable relative to I_3^-/I^- electrolyte that serves to regenerate the dye. The discrepancies between the dye and electrolyte has the greatest negative influence on low open circuit voltage (Voc) in dye-sensitized solar cell (DSSC). The regeneration of the dye with redox pair is a two electron process and has large driving force 600 mV for most of the Ru dyes and approximately the same for our porphyrin dyes. The phthalocyanine dyes have an advantage since the ground state oxidation potential lies less positive vs NHE making the mismatch with the I_3^-/I^- redox pair smaller, ~ 370 mV.

Table 4.3 Excitation energy (eV), ground and excited state oxidation potentials(V) of dyes.

vs NHE	$E_{1/2}$(V)	$E_{0\text{-}0}$(eV)	Eox*(V)	ΔEp(V)
$(TPP)Zr(OAc)_2$	1.017	2.28 λ=545nm	-1.26	268
$(TPP)Hf(OAc)_2$	1.012	2.28 λ=545nm	-1.26	265
$(Pc)Hf(OAc)_2$	0.769	1.79 λ=690nm	-1.02	152
$(Pc)Zr(OAc)_2$	0.780	1.79 λ=690nm	-1.01	175

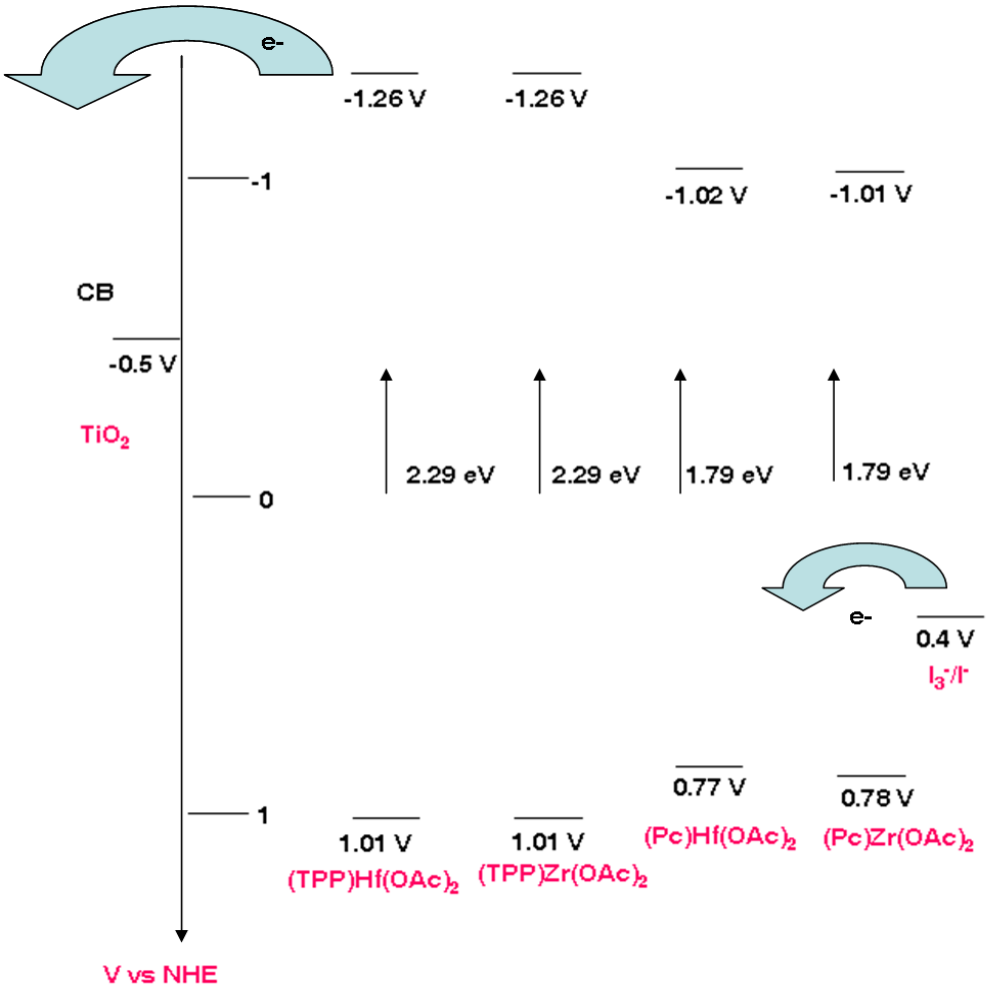

Figure 4.12 Energy level diagram of the device components, in this case the four metallodyes, representing energetically favorable processes within a typical DSSC device. Values in V referenced versus NHE.

4.3.3 Solar cell devices

Dye-sensitized solar cell

Dye-sensitized solar cells (DSSC) have been extensively studied since they have great potential to become one of the cheapest photovoltaic devices.[25] They are particularly attractive because of the simple design and fabrication methods, reduced material and manufacturing costs compared to commercial Si based solar cells, and large demonstration installations already on display around the world. Since the initial development of DSSC in the late 1990s in the Grätzel laboratory, a substantial amount of research has been devoted to improve individual components and optimize the performance of DSSC but the greatest conversion efficiency remains ~11 %.

The various components in DSSC determine the performance of the dye. In DSSC a wide-band gap semiconductor such as TiO_2, ZnO, SnO_2 or other metal oxide is sensitized with a dye molecule that absorb solar light. Nanocrystalline/nanostructured materials are of greatest interest at present. To date, the best hole transporting material (HTM) in these systems is a liquid electrolyte containing I^-/I_3^-. When visible light is absorbed by the dye, an electron from either the singlet or triplet excited state is injected into the conduction band of TiO_2 with charge injection rates ranging from hundreds of femtoseconds to tens of picoseconds. The oxidized dye is regenerated by the redox mediator. The negative charge is collected on a photoanode such as indium-tin-oxide (ITO) (Figure 4.13).The main issues with deployment of DSSC include: long term instability, the properites of the electrolyte, photobleaching, and the expense of the best dyes, all of which contain ruthenium. Manufacturing scalability can also be an issue, e.g. the efficiency rapidly drops from 10.4% for a 1 cm^2 cell to 6.3% for 26.5 cm^2 cell.[27,29]

Quasi-solid and solid hole transporting material (HTM) to replace the I^-/I_3^- typically have efficiencies of ca. 5%.[30]

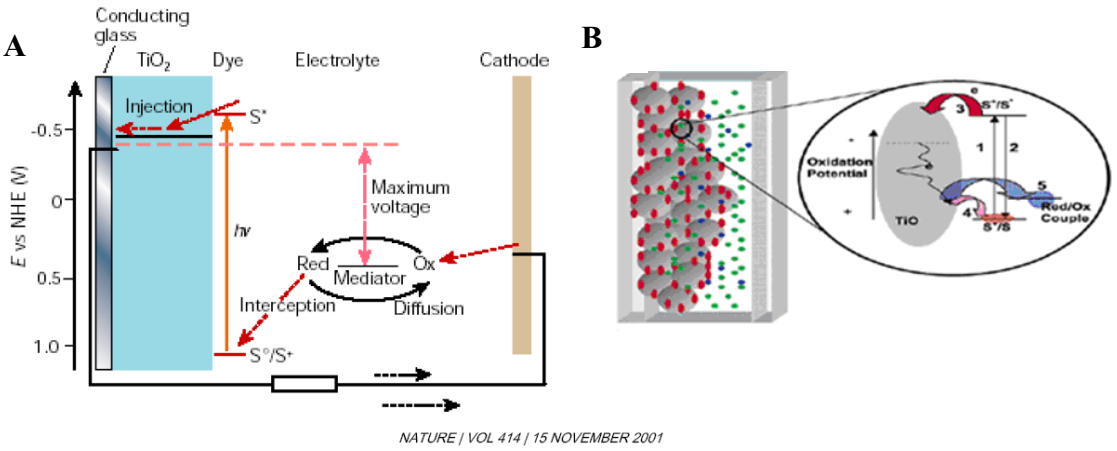

Figure 4.13 (A) Operation principle of DSSC. **(B)** Processes occurring in DSSC: 1) Sensitizer excitation; 2) Sensitizer deactivation ($10^3 - 10^{10}$ s^{-1}); 3) e-injection (10^{12} s^{-1}); 4) Recapture of e-cond. band by oxidized dye; 5) Recapture of e-in conduction band by oxidized form of electrolyte.[2] Adopted from reference (2).

Optimal properties of the sensitizer include: (1) strong absorbance over most of the solar spectrum, including the near IR; (2) a firm anchor to the semiconductor surface; (3) high quantum efficiency of electron injection to conduction band of the metal oxide; (4) facile regeneration by the redox couple; (5) the dye should be stable in operation for over 20 years. In terms of highest conversion efficiency and long term stability, the best performing dyes so far are ruthenium and osmium based polypyridyl complexes.[31] The high cost of these metals are the main drawback of these dyes. Those costs will only increase if the cells are deployed world wide. Other dyes have been investigated extensively in attempt to find cheaper alternatives. In addition to the properties outlined

above, Por chromophores have attracted much attention since these molecules are key to photosynthesis. To date, synthetic organic dyes and natural organic dyes yield lower efficiency DSSC and other devices, but only a relative few potential commercially viable derivatives have so far been investigated.

Organic photovoltaic (polymer) solar cell

Organic solar cells have been investigated since 1986 when Tang discovered that two organic materials (CuPc and perylene) form an interface where excitons can be easily separated and that only those molecules close to the interface were generating free charge carriers. Tang's solar cell eventually reached 1 % efficiency. Nowadays the attainable conversion efficiency of organic devices is around 5 % and the lifetime 1000 h under continuous illumination.[32] In general, organic cells are acceptor–donor type device where after photon absorption, excitons (electron- hole bound pair) are formed and diffuse to the interface of two materials. The exciton is a neutral pair and does not carry current. At the heterojunction, excitons must be separated into free electrons and holes that then travel toward the different contacts producing electrical power (Figure 4.14).[3] The appropriate match of energy levels (HOMO-LUMO) of organic materials and wave functions of contacts is required for producing photocurrent in the system. Generally, bilayer devices are limited by the short diffusion length of the exciton that forms in the donor (D) layer, which needs to diffuse to the acceptor (A) layer before recombining. Thus, recombination, rather than charge transport properties, is the main limiting factor of device efficiency for this geometry.

Semiconducting p-and n- type polymers (polythiophenes, polyphenylvinylidene, C_{60} derivative, PCBM) and small organic molecules such as phthalocyanines, fullerenes, perylenes are the most commonly used organic materials. In polymer solar cells the free carriers have higher mobility which grants them an advantage in terms of conversion efficiency versus cells constructed from small molecules. Also, properties and processing of polymer films are much better understood, which makes the control of morphology and conditions for fabrication more approachable. In terms of fabrication, materials can be solution processed or materials can be deposited by thermal vacuum evaporation. The key issues remain unresolved; the dyes must have stronger absorption throughout the spectral range, polymers of donor type have good hole mobility, and the acceptor materials have to be developed with higher electron mobility.

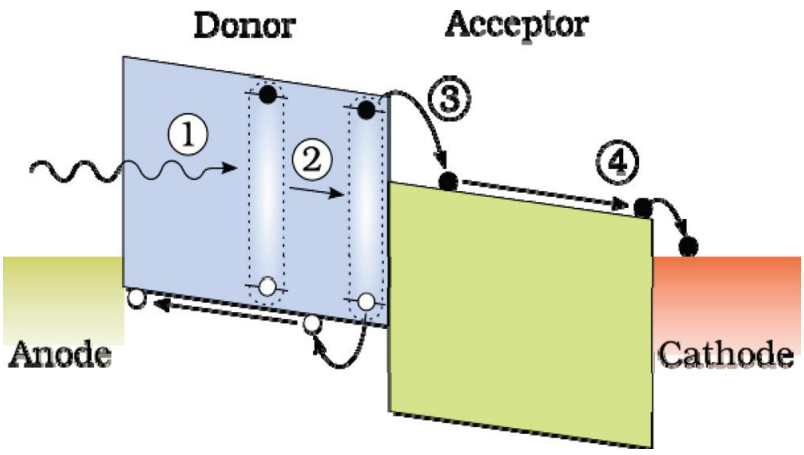

Figure 4.14 Schematic representation of organic solar cell with donor-acceptor interface and processes occurring with in cell : 1) absorption of photon to create an exciton, (2) diffusion of an exciton toward the donor-acceptor interface, (3) charge transfer of an exciton into an electron in the acceptor and hole in the donor, and (4) collection of charges at the contacts.[3-4] Adopted from reference (3).

Performance of the solar cell

The total conversion efficiency of the photovoltaic solar cell in air mass, AM1.5 sun (a standardized solar energy), can be calculated by the equation 4.4 and 4.5:

$$\eta_{global} = V_{oc} J_{sc} FF / P \qquad \text{(eq. 4.4)}$$

$$FF=(V_{mp}J_{mp})/V_{oc}J_{sc} \qquad \text{(eq. 4.5)}$$

where, V_{oc} open circuit voltage, I_{sc} short circuit current and FF fill factor. The fill factor is defined as the ratio of the maximum power (V_{mp} x I_{mp}) divided by the product of short-circuit current (Jsc) and open-circuit voltage (Voc) (eq. 4.5) and represents how the maximum power rectangle fits into J-V curve shown in Figure 4.15. The theoretical

maximum fill factor is 1 but in reality is held under 0.83 for reasons defined by diode equation.[1]

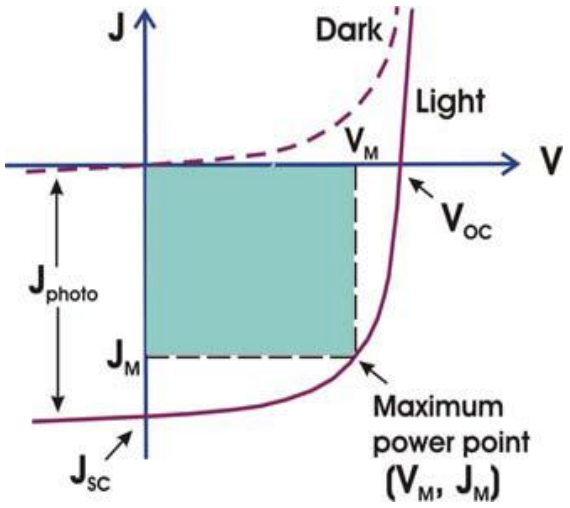

Figure 4.15 Current- voltage characteristics of solar cell device. No current flows at the Voc (open circuit voltage), and no voltage is applied at Jsc (short circuit voltage). When Jsc=Jm and Vm=Voc, FF should have maximum value 1.

Characterization and performance of our solar cell devices

The on-going research in Brookhaven National Laboratory at the Center for Functional Nanomaterials (CFN) is based on fabrication of polymer organic photovoltaic devices. The architecture of the devices they usually create is shown in Figure 4.16, where the "active layer" can be, for example, poly(3-hexylthiophene) (P3HT), p-type/ phenyl-C_{61}-butyric acid methyl ester (PCBM), n-type semiconductors.

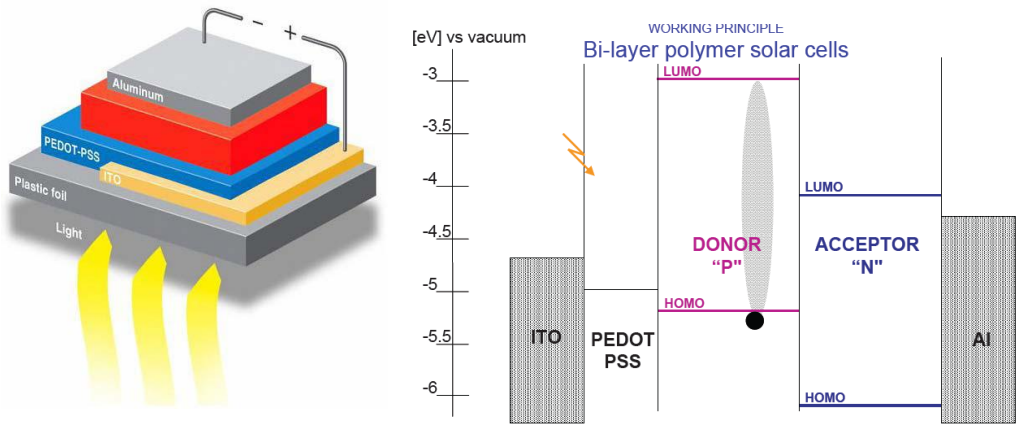

Figure 4.16 A typical organic photovoltaic cell. The active layer (red) can be a bilayer or a bulk heterojunction containing a polymer and C_{60}. [1]

Using the already established device architecture at the CFN, we constructed two different types of solar devices. The first one, Figure 4.17 was constructed from an ITO electrode (photoanode) which was coated with layer of n-type semiconductor titanium oxide (Ti metal deposited from e-beam vacuum evaporation in clean room facility and then oxidized in furnace at 500-600 ^{0}C).[33] The p-type semiconductor used was P3HT spin cast most at 2 krpm. The back electrode was 40-70 nm thick thermally deposited Au

metal contact. Detailed fabrication is explained in experimental section. Note that the dye is adsorbed onto the TiO_2 layer in these devices in contrast to absorbing the dyes on the nanoparticles of TiO_2 first. Optimization of devices was done by varying the thickness of e- beam deposited Ti layer (30 nm and 60 nm), the speed (rpm) of spin coating for P3HT polymer, concentration of the dye solution for sensitization, and deposition method of the dye (spin casting or dipping of the electrode in the solution overnight).

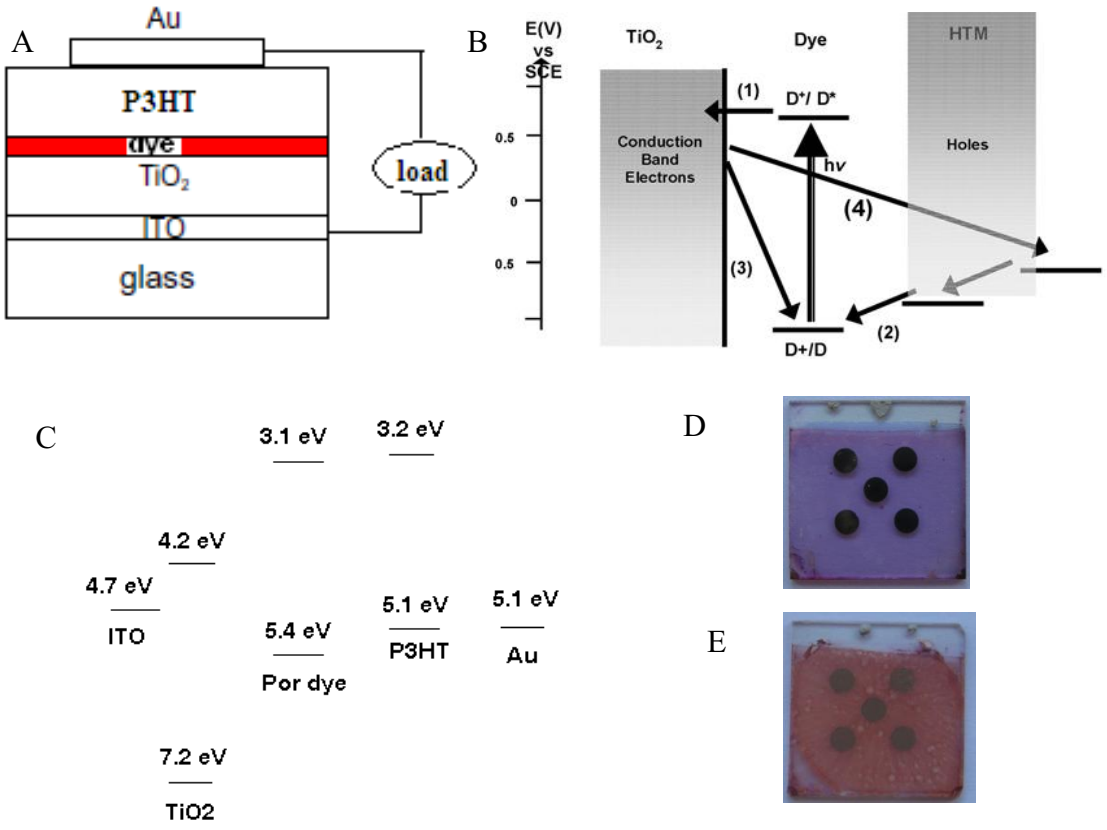

Figure 4.17 (A) Schematic representation of architecture of tested devices. **(B)** Energy diagram and processes occurring within solar device; **(C)** Relative energy levels of device components using (TPP)M(OAc)$_2$ as dye ;**(D)** Image of real tested device of type I architecture; **(E)** Image of real tested device showing irregularity in sensitized film, type II architecture.

In summary, we experienced a lot of difficulties with shorting in the cells. We believe that the holes were often trapped by the ITO electrode because the titanium layer was not uniform or compact enough. We studied the cells with SEM and AFM to confirm morphology and degree of homogeneity of deposited layers. For both thicknesses (30 nm and 60 nm) it seemed as though the layers were quite homogeneous with very few cracks observed (Figure A4.11). There are a variety of processing issues that we have not addressed that may result in poorly made and poorly performing devices (see below).

The data we finally obtained do not show significant values for conversion efficiency of the cell but still indicate the importance of the organic molecules as sensitizers in these systems. The device utilizing 60 nm thick TiO_2 semiconductor with $(TPP)Zr(OAc)_2$ dye showed improvements when compared to the device without the dye (control device). The best performing device gave 0.03 % efficiency while the same device without the dye performs ~ 10 x less with 0.004 % efficiency (Figure 4.18).

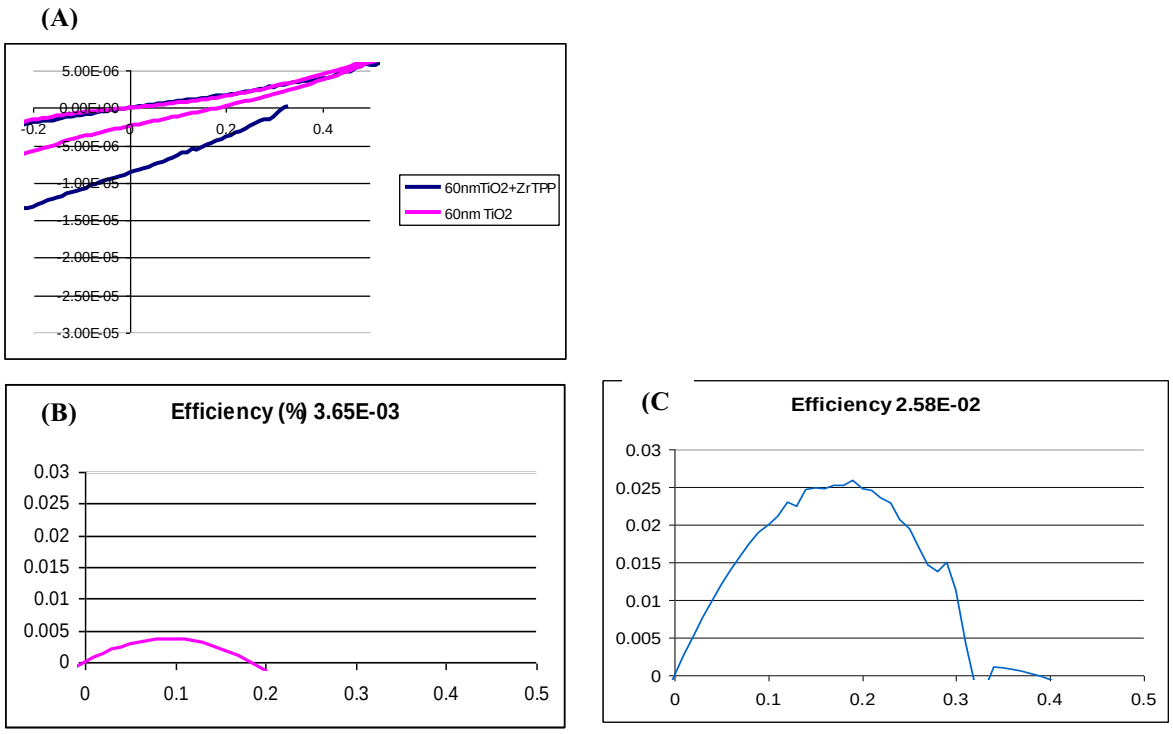

Figure 4.18 Efficiency of PV cell: **(A)** IV curve of in dark and light; 60 nm layer TiO_2 without dye (pink) and sensitized with $Zr(TPP)OAc_2$ (blue); **(B)** calculated 0.004 % efficiency for 60 nm layer TiO_2 without dye and **(C)** calculated 0.03 % efficiency for 60 nm layer TiO_2 sensitized with $Zr(TPP)OAc_2$ dye**.**

There are likely a few different reasons for the poor performance of these devices. The thickness of the Ti layer was not sufficient to cover the ITO photoanode and prevent recombination of positive charge. We also assume that the phase of titanium oxide we obtain by oxidizing Ti metal in air at 600 ^{0}C is anatase. The phase transition from anatase to rutile occurs at 700-1000 ^{0}C.[27] It is known that anatase phase performs much better in transporting electrons.[4,27] However, we never performed any experiment to determine crystal structure of our titanium oxide films. Moreover, the surface coverage of the oxide with the dye is low since these dyes tend to bind to the defect sites.

The nanocrystaline TiO_2 semiconductor (approx. < 10 μm thick) in DSSC performs much better because of increased surface area where more molecules of dye can be attached[25] to the oxide surface. In our second attempt, we decided to test performance of a device where n-type semiconductor is made from a paste of 25 nm Degussa TiO_2 anatase nanoparticles either spin cast on top of conductive electrode ITO or screen printed, and then sintered at 450 ^{0}C for the better interconnection of nanoparticals. Therefore, our second type of the device architecture should in principle be a solid state DSSC, Figure 4.17(B), 4.17(E) using a conducting polymer as the hole transporting material (HTM) instead of a liquid electrolyte. Research in the area of solid state DSSC has advanced to the forefront of science in past years but no DSSC withing this design reached more than 5 % efficiency.[34-38] The fabrication of our solar cell device is in detail described in experimental section (4.3).

In both types of our systems when dyes absorb light, excited electrons get injected into TiO_2 semiconductor while holes travel through the layer of polymer to reach the gold back electrode. Energy levels in Figure 4.17(C) show that electron and hole transport is energetically favored considering relative energies of different components in the device. In this figure we present only values from HOMO and LUMO of metalloporphyrin dyes that were determined from cyclic voltammetry experiments described in previous section. The relative values for metallophthalocyanine dyes are summarized in table in previous section and can easily be incorporated into the energy diagram.

Again, throughout many experiments we faced the problem of short-circuiting our system. We tried to resolve this problem by adding a blocking layer between the ITO and the semiconductor (the same compact 60 nm thick Ti deposited by e-beam vacuum

evaporation and oxidized in air) so that holes could be kept away from electrons in ITO. There has been many reports in literature on different methods how to prepare compact TiO_2 layers that would prevent recombination.[34-35,38]

The photoanode made in this way appeared to be very irregular Figure 4.17(E). Low efficiency could also have been caused by the polymer not penetrating into the pores of TiO_2 well enough thereby failing to regenerate the oxidized dye. Overall, the efficiencies of the second type of device were even lower and the experimental data is therefore excluded.

The main goal in designing and testing solar cells devices was not just to find a dye which performs with high conversion efficiency but also to prove that the new mode of binding of metalloporphyrinoids to the oxide semiconductor is beneficial.

Dye-sensitized solar cell

Dyes, $(TPP)Zr(OAc)_2$ and $(Pc)Zr(OAc)_2$ were further tested in Grätzel type DSSC. Procedure for fabrication of solar cell device is well established and known from the literature.[35] The complete cell was composed of fluorine tin coated glass (FTO) electrode with 8.0-8.5 μm thick TiO_2 (paste containing nanocrystalline anatase 20 nm particles) layer coated with 0.3 mM solution of dye dissolved in CH_2Cl_2 overnight. The electrolyte used was 0.6 M 1- butyl-3-methyl imidazolium iodide (BMII), 0.03 M I_2, 0.10 M guanidinium thiocyanate and 0.5 M 4-tertbutylpyridine in a mixture of acetonitrile and valeronitrile (volume ratio, 85:15). The counter electrode was made from a drop of H_2PtCl_6 solution in ethanol. The cell was sealed with Surlyn spacer. Figure 4.19 represents the standard configuration of Grätzel type DSSC.

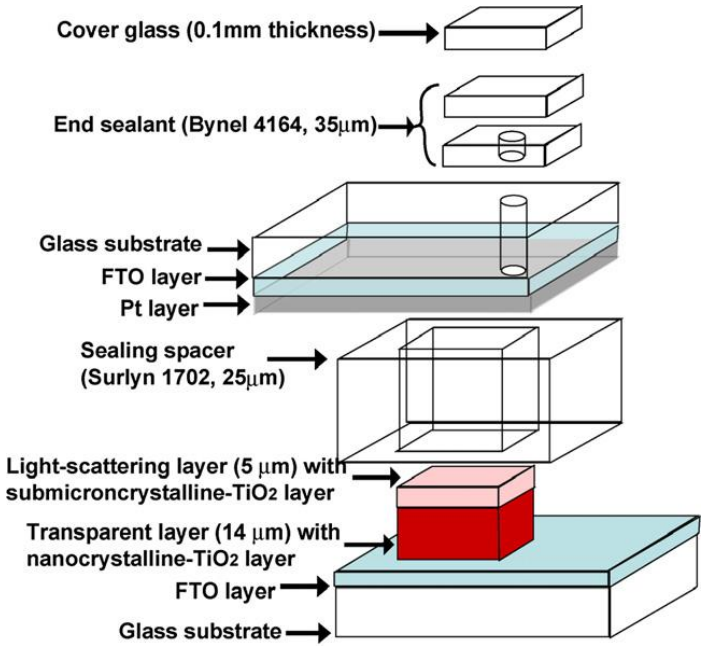

Figure 4.19 Assemblage of dye-sensitized solar cell. Taken from reference (36).

The results we obtained are summarized in table 4.4 and characteristic I-V curves are presented in Figure 4.20. We found that the device operates better than previously described polymer based organic solar cell but still much worse than DSSC with best performing N 719 Ruthenium dye, which under the same conditions shows an efficiency of 6.41% (data not shown here).The cell performance increases slightly after few days since the device relaxes and the 4-tertbutylpyridine from electrolyte penetrates deeper into pores of TiO_2, preventing the FTO from holes.

Table 4.4 Photovoltaic parameters of DSSC sensitized with $(TPP)Zr(OAc)_2$

Time	Voc (V)	Jsc(mA/cm^2)	FF (%)	η (%)
1 day	0.389	0.55	70.3	0.152
3 days	0.40	0.55	86.4	0.184

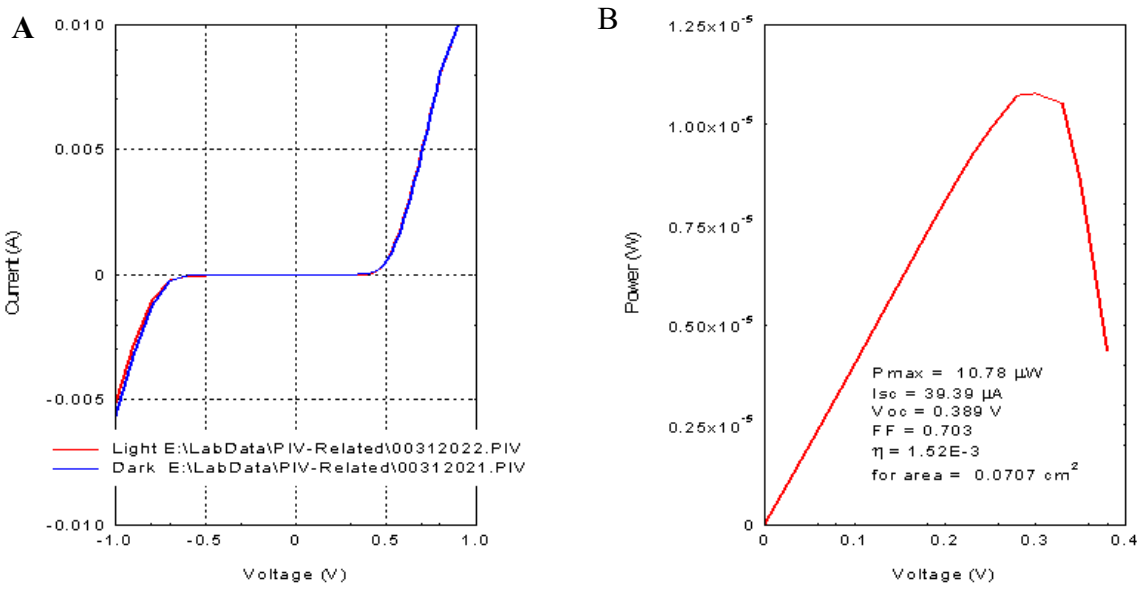

Figure 4.20 (A) Current- voltage characteristics of $(TPP)Zr(OAc)_2$ sensitized solar cell before (blue) and after (red) illumination with simulated 1.5 AM at intensity of $100mW/cm^2$. **(B)** Power- voltage characteristics.

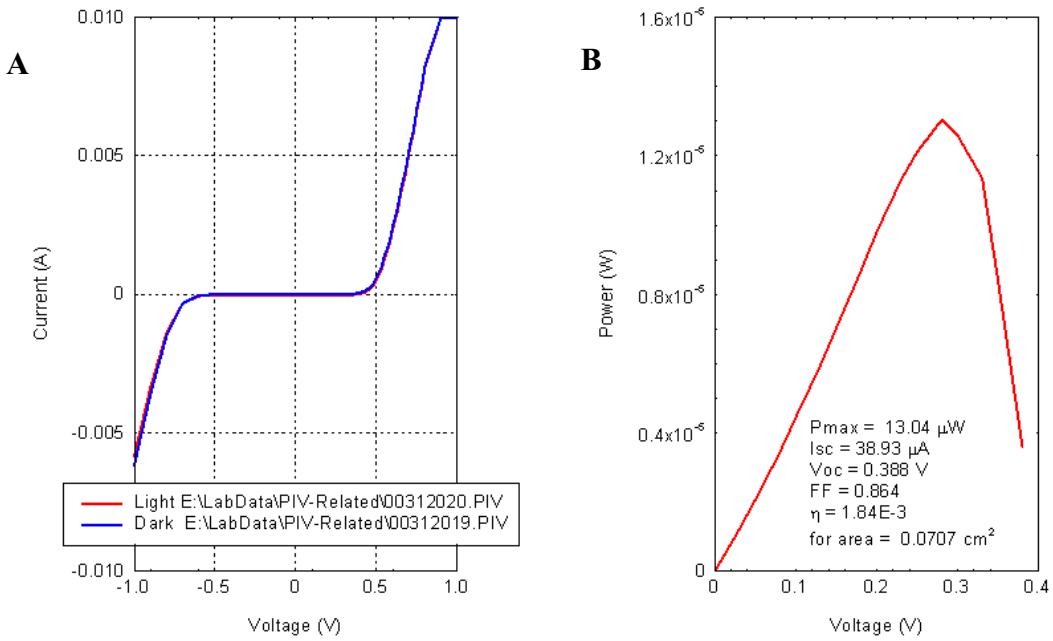

Figure 4.21 (A) Current- voltage characteristics of (TPP)Zr(OAc)$_2$ sensitized solar cell before (blue) and after (red) illumination with simulated 1.5 AM at intensity of 100mW/cm^2. **(B)** Power- voltage characteristics. After 3 days of assemblage.

4.4 EXPERIMENTAL PROCEDURE

Instrumentation and Reagents

Toluene, dichloromethane, pyridine, acetonitrile, were purchased from Sigma Aldrich. Solvents were distilled using standard procedures. ITO coated glass slides were purchased from Aldrich, and the glass cover slips were purchased from Fisher. Titanium(IV) oxide (TiO_2), nanopowder, 99.7%, anatase, tetra(n-butyl) ammonium hexafluorophosphate (Bu_4NPF_6), ferrocene, $AgNO_3$ were purchased from Sigma Aldrich. All UV-visible spectra were taken in 1 cm quartz or glass cuvettes in toluene. Emission spectra of solution phase were taken using right angle mode, while solid samples were tested using front face mode. A Cary 3-Bio UV-visible spectrophotometer, a Spex Tau-3

fluorescence spectrophotometer were used. The atomic force microscope used was a Veeco Multimode SPM. A home-built ozone cleaner was used. Cyclic voltammetry measurements were performed with a BAS CV-50W electrochemical analyzer.

The hafnium and zirconium porphyrinate starting materials, $(TPP)Hf(OAc)_2$ $(TPP)Zr(OAc)_2$, $(Pc)Hf(OAc)_2$, $(Pc)Zr(OAc)_2$ and the corresponding derivatives with two Cl^-, SO_4^{-2} and HPO_4^{-2} were already synthesized in our lab according to literature methods.[43-45] Control molecules TPP, ZnTPP, Pc, ZnPc were purchased from Frontier Scientific.

Binding of Hf(Por)/(Pc) and Zr(Por)/(Pc) to glass, ITO, and TiO_2 surfaces

All glass and ITO substrates were cleaned in an ozone cleaner (20 min) or by a piranha solution (3:1 NH_4OH/H_2O_2 for 30 min) followed by rinsing with copious amounts of water just prior to using. A drop of ca. 4 μM solution of the $(TPP)Hf(OAc)_2$ or $(TPP)Zr(OAc)_2$ in dry toluene was placed on the substrate and allowed to dry in air. Alternatively, the substrate was dipped in a ca. 0.4 mM solution for 1h. After drying, all substrates were washed with toluene to remove any unbound materials.

For TiO_2, 0.8 mg of $(TPP)Hf(OAc)_2$ or $(TPP)Zr(OAc)_2$ is dissolved in 2 mL of distilled toluene and ca. 30 mg titanium(IV) oxide nanopowder, 99.7% antase with average size 5 nm (Aldrich) was added to the solution. After sonicating for 5 min, and the slurry was stirred for over night. The supernatant was still colored indicating that the solution was saturated with the dye. The slurry was then centrifuged for 5 min to separate the coated particles, which are a pink color due to attachment of $Hf(TPP)^{2+}$ or $Zr(TPP)^{2+}$ on TiO_2. Similar treatment of the TiO_2 particles with Zn(TPP) and TPP in control

experiments resulted in most of the porphyrin remaining in solution. The solution was decanted, the coated particles were rinsed with toluene 2-3 times to remove unbound materials, and left to dry in air.

Preparation of samples for Cyclic Voltammetry

A three electrode, one compartment electrochemical cell was used. The reference electrode was Ag/Ag^+ with (0.01 M $AgNO_3$/0.1 M Bu_4NPF_6/CH_3CN); auxiliary electrode was Pt and working electrode was ITO coated glass slide (0.5 cm x 2.5 cm); supporting electrolyte used was 0.1 M Bu_4NPF_6/CH_2Cl_2. All redox potentials were referenced against ferrocene (Fc^+/Fc) internal standard. The electrolyte solution was degassed with nitrogen prior to measurements. Peaks potentials were measured at different scan rates. Values presented in table 4.2 and 4.3 were measured at 200 mV/s. The ITO slides were cleaned by a piranha solution (3:1 NH_4OH/H_2O_2 for 30 min) followed by rinsing with copious amounts of water just prior to using. The concentration of solution in CH_2Cl_2 in all experiments was > 1 mM. When measuring the redox potential of TiO_2 nanoparticles coated with dye, the working electrode was prepared as follows: 6 g commercial Degussa 25 nanopowder TiO_2 were dispersed in 10 mL acetic acid (pH=3-4) with few drops of Triton –X. The particles were ground into paste and then stirred for a minimum 3h. A few drops of TiO_2 paste was spread over the ITO slide and sintered at 450 ^{0}C for 45 min. Still warm (80 ^{0}C) ITO slide was was dipped into 0.5 mM solution of dye overnight. The samples were rinsed with solvent and dried again before using in electrochemical cell.

Fabrication of organic polymer solar device

Type I architecture: By e-beam vacuum deposition 30 nm or 60 nm Ti metal film was deposited on an ITO slide (1cm x 1cm). The flat layer was then oxidized into titanium dioxide in a furnace at 500-600 ^{0}C. Different concentrations of dye in toluene solution were spin cast onto the semiconductor or the electrode with the semiconductor layer was immersed in a dye solution overnight. P3HT was spin cast at 2 krpm on top of the dye. Back contact electrode was 40-70 nm thick Au metal.

Type II architecture: a compact layer of titanium oxide 60 nm was prepared on ITO slide as mentioned above, afterwards a paste of TiO_2 nanoparticles (prepared as explained previously) was either spin-cast or screen spread/printed on ITO slide with compact layer. The sample was sintered at 450 ^{0}C for 30 min in air. When cooled to 80 ^{0}C, the electrode was immersed in 0.5 mM solution of the dye in toluene and left inside overnight. When sensitization was over, the electrode was rinsed with solvent, toluene and dried in air before the layer of polymer polythiophene (P3HT) was spin-cast on top at a speed of 2 krpm. P3HT used was dissolved in chlorobenzene at a concentration of 1 % by weight. As the back electrode, 70 nm Au was thermally evaporated through a mask (active device area: 3.14 mm^2) (Figure 4.20).[36] Some devices were tested without a nanocrystaline porous layer of titanium oxide. Control devices were prepared without the dye. PV parameters of fabricated devices were measured from device current-voltage (I-V) characteristics under simulated solar illumination. A custom-modified probe station equipped with Agilent 4156C precision semiconductor parameter analyzer was used to characterize dark and illuminated I-V characteristics. Oriel 9600 150 W solar simulator

with an AM1.5G filter were used for solar illumination with 100 mW/cm^2 (1 SUN) condition (calibrated by Oriel 70268 thermopile detector).

Figure 4.22 Image of five masked solar devices and Oriel 9600 150 W solar simulator with an AM1.5G filter used for photovoltaic measurements.

Fabrication of dye-sensitized solar cell

The procedure for fabrication of dye-sensitized solar cell (Grätzel type) is well established in the literature,[35] and the same procedure was used in our experiments.

4.5 CONCLUSIONS

New concepts in the design and function of organic dyes as sensitizers for solar energy harvesting are needed. Simple porphyrinoid dyes offer cost effective synthesis and long-term stability but devices still perform with much lower efficiency than best performing Ru- bipyridil sensitizers. Compared to most Ru based complexes, Por and Pc absorb 10 times more light, but since these have narrower absorption bands, combinations of Por and Pc will be needed to cover the solar spectrum. These combinations however, will allow much thinner active layers, e.g. with DSSC potentially reducing the typically 10 μm thick semiconducting layer of dye-coated TiO_2 nanoparticles to 1 μm; thereby decreasing losses during charge transport through this layer and reducing costs.[39] We are developing an alternative way to couple dyes to oxide surfaces using hafnium and zirconium metalloporphyrins and metallophthalocyanins. The synthesized ternary complexes of porphyrin and/or phthalocyanine with Keggin POM, $PW_{11}O_{39}^{-7}$ suggested that one way to self-organize porphyrinoids onto oxide surfaces is to use porphyrinoids coordinated to oxophilic group IV metals Hf and Zr. The 3-4 open metal coordination sites of $Hf(Por)^{2+}$/$Zr(Por)^{2+}$ and $Hf(Pc)^{2+}$/$Zr(Pc)^{2+}$are bound primarily to surface defect sites by displacement of the auxiliary acetate ligands. Degree of orbital mixing of metal ion and porphyrin frontier orbitals depends on specific ions used. For example, first row metals have small mixing, for higher rows the mixing is significantly greater, such as in cerium porphyrin complexes.[40-42] Thus, in bigger metals Hf, Zr the chromophore orbitals are strongly coupled with the metal ion orbitals, and the metal ion is

simultaneously bound to the oxide surface, charge injection is facilitated via both the metal ion and the proximity of the dye to the surface. This new mode of absorption of the sensitizer to surface plays very important role in trapping and injecting electrons in the conduction band of oxide material. On the other hand, the low surface coverage compared to dyes anchored to TiO_2 via carboxylic groups significantly influence efficiency of the device.

Appendix

A

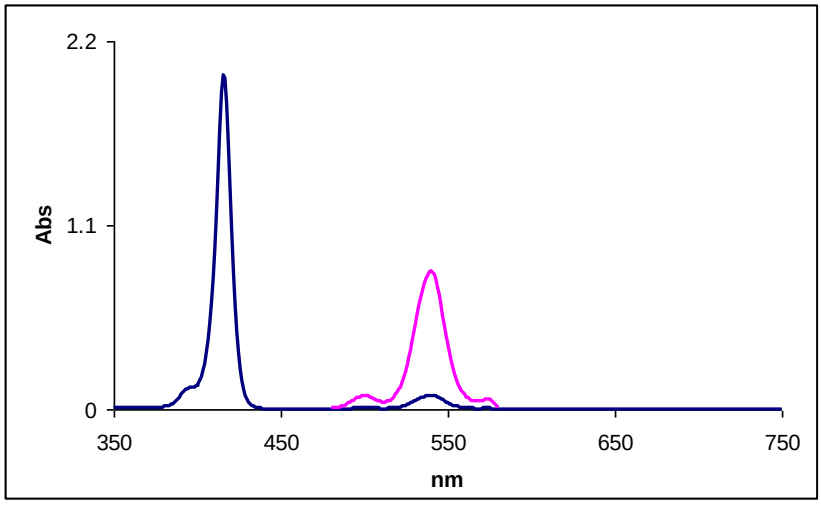

B

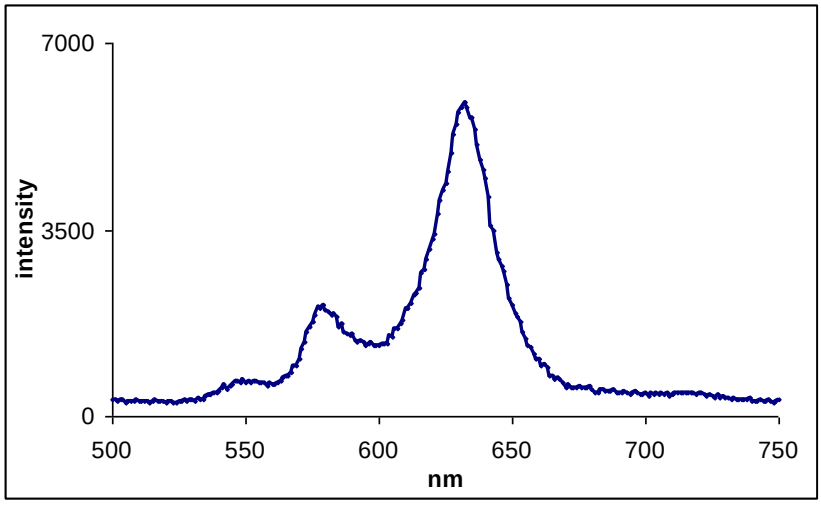

Figure A4.1 UV-Vis spectrum of **(A)** (TPP)Hf(OAc)$_2$ in distilled toluene in a 1 cm glass cuvette. Soret band at 416 nm and Q- bands at 540 nm. Emission spectra of solution **(B)** (TPP)Hf(OAc)$_2$ in distilled toluene, excited at the Soret maximum 416 nm exhibits three bands at 550 nm, 580 nm and the strongest at 633 nm.

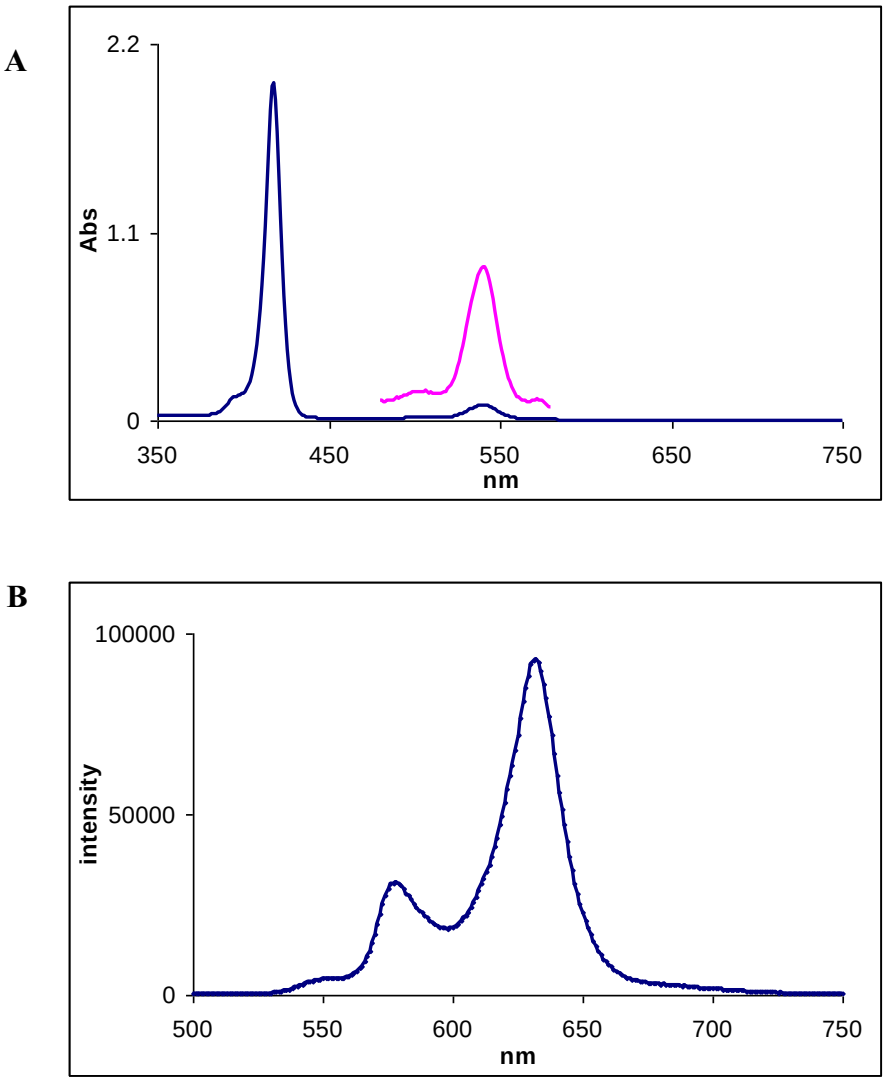

Figure A4.2 UV-Vis spectrum of **(A)** $(TPP)Zr(OAc)_2$ in distilled toluene in a 1 cm glass cuvette. Soret band at 418 nm respectively Q- bands at 540 nm. Emission spectra of solution **(B)** $(TPP)Zr(OAc)_2$ in distilled toluene, excited at the Soret maximum 418 nm exhibits 3 bands at 550 nm, 580 nm and the strongest at 633 nm. Note that the Zr complex luminescence more than Hf complex.

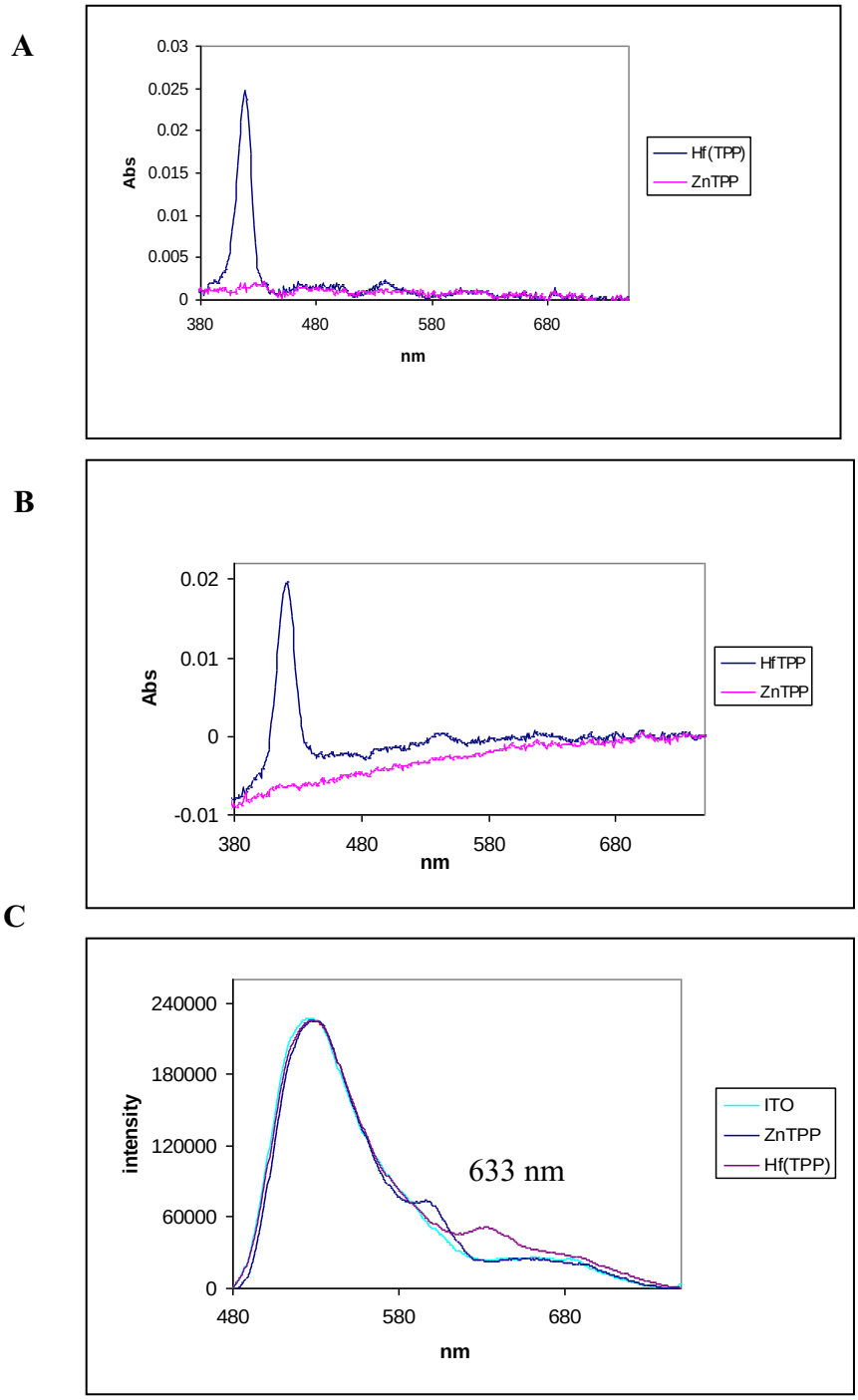

Figure A4.3 (A) UV-Vis spectrum of ca. 4 μM solution of (TPP)Hf(OAc)$_2$ dropcast on pirahna cleaned glass substrate; (**B)** dropcast on an ozone cleaned ITO substrate; Soret band red shifts ca. 4 nm; **(C)** emission spectra on an ozone cleaned ITO. Note that the absorption and emission peaks on the surface correspond to the bands observed in the absorption and emission spectra in solution. The large backgrounds are due to the ITO surface and scattered light. ZnTPP as control.

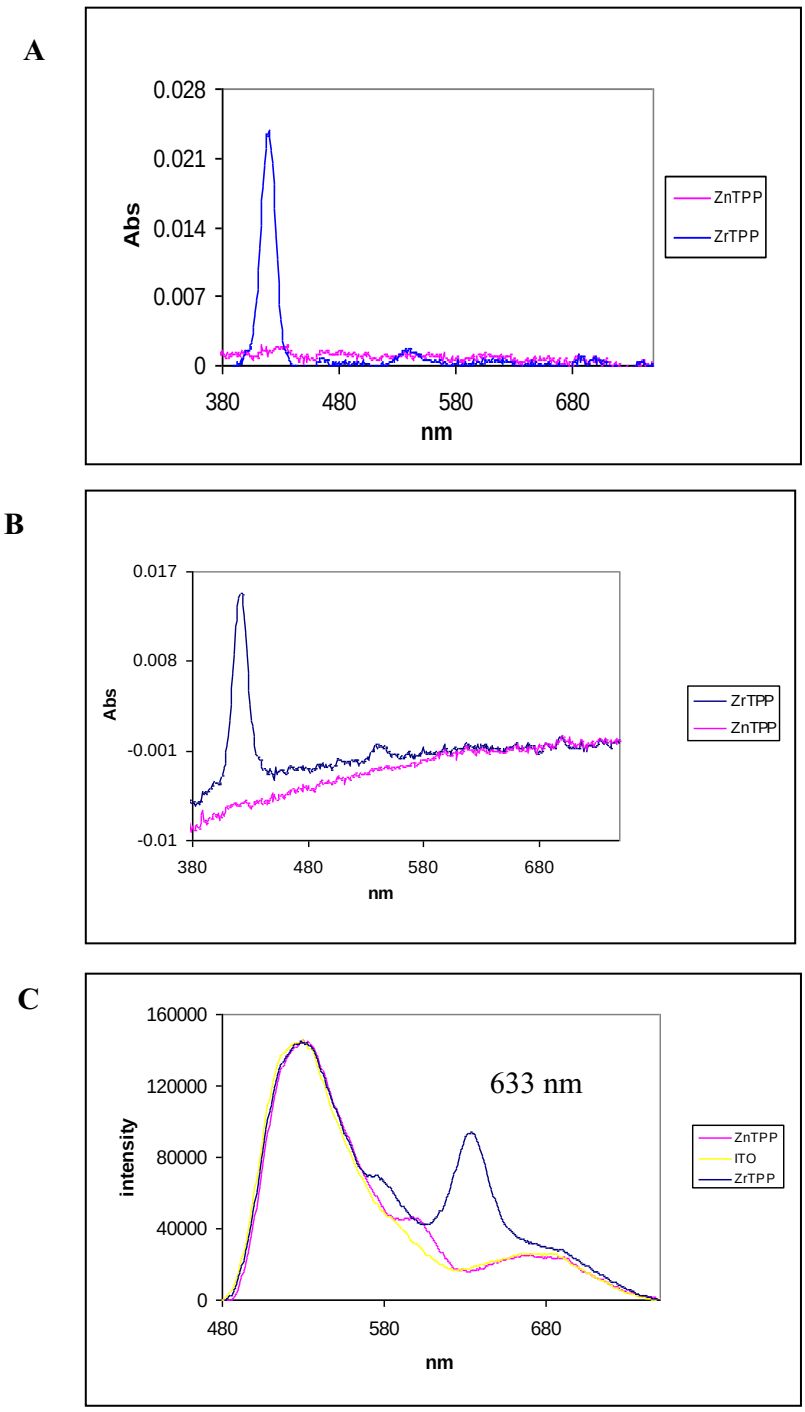

Figure A4.4 (A) UV-Vis spectrum of ca.10 μM (TPP)Zr(OAc)$_2$ solution dropcast on pirahna cleaned glass substrate; (**B)** dropcast on an ozone cleaned ITO substrate; Soret band red shifts ca. 4 nm; **(C)** emission spectra on ozone cleaned ITO. Note that the absorption and emission peaks on the surface correspond to the bands observed in the absorption and emission spectra in solution. The large backgrounds are due to the ITO surface and scattered light. ZnTPP used for control.

A

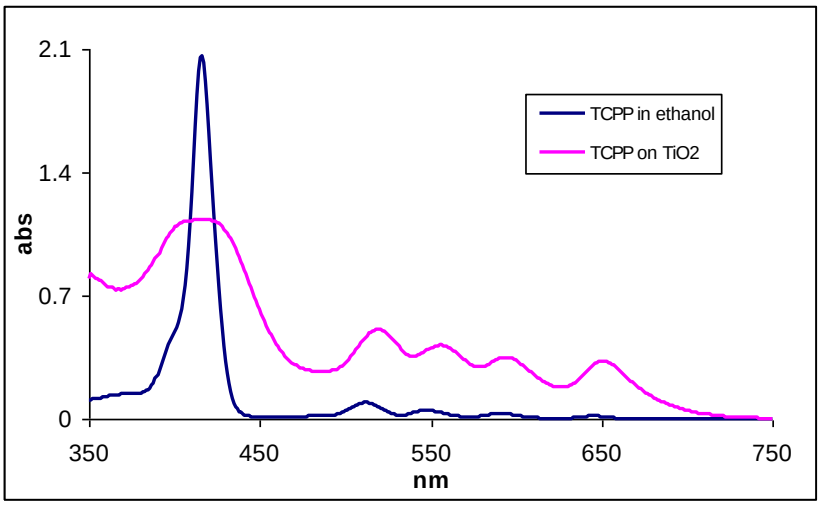

B

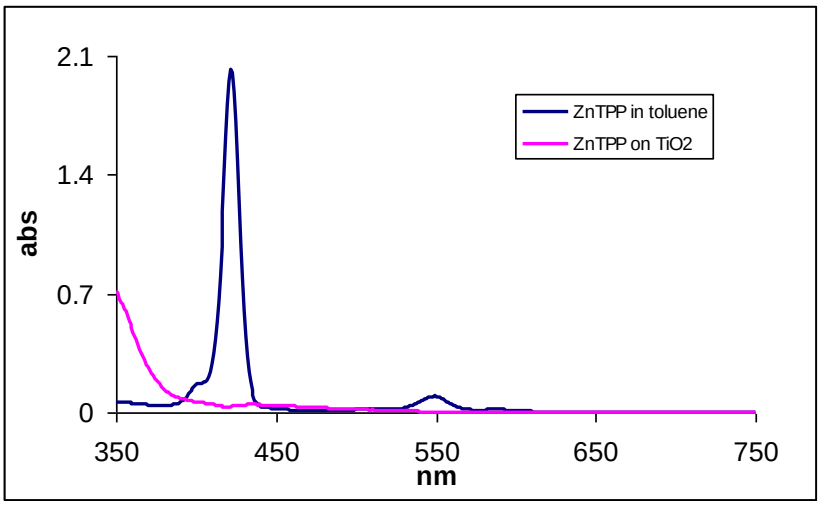

Figure A4.5 (A) UV-visible spectra of the starting TCPP in toluene (pink), reflectance spectrum of a ca. 1 mm film of TiO_2 nanopartiles coated with TCPP (blue), **(B)** UV-visible spectra of the starting Zn(TPP) in toluene (pink), reflectance spectrum of a ca. 1 mm film of TiO_2 nanopartiles coated with Zn(TPP) (blue).

A

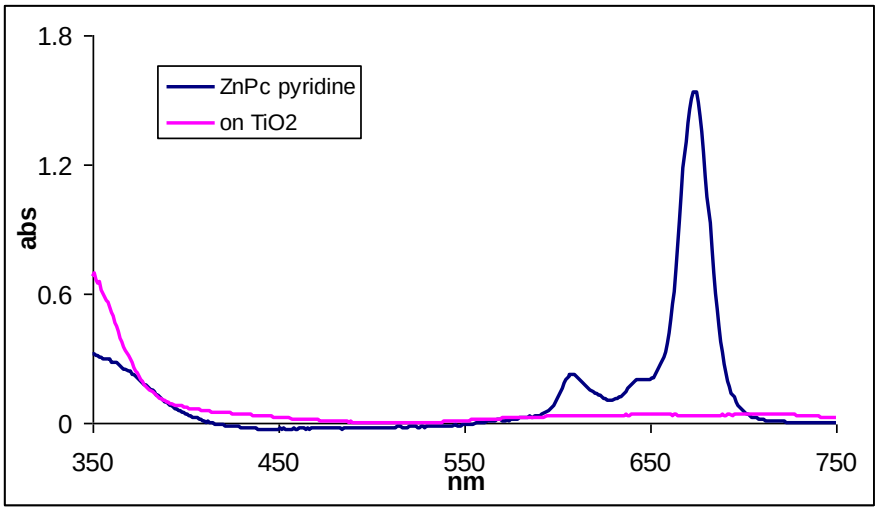

B

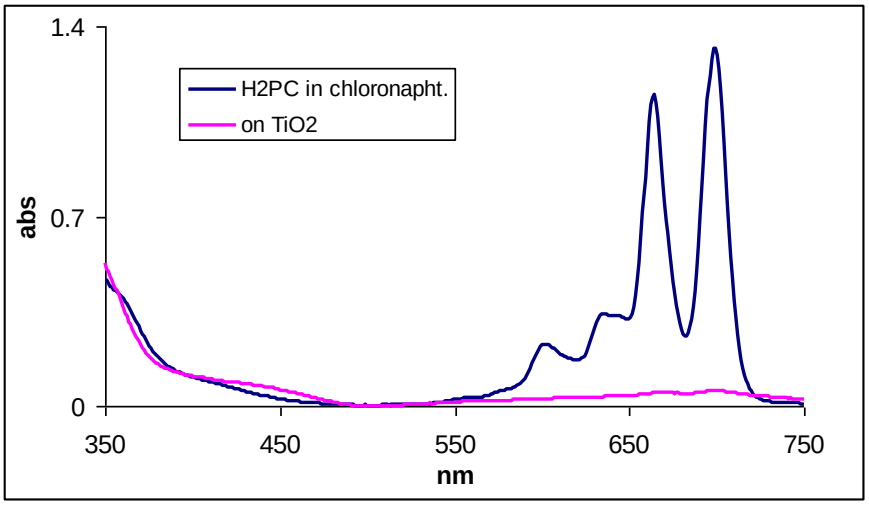

Figure A4.6 (A)UV-visible spectra of the starting ZnPc in pyridine (blue), reflectance spectrum of a ca. 1 mm film of TiO_2 nanopartiles coated with ZnPc (pink), **(B)** UV-visible spectra of the starting H_2Pc in 1-chloronaphtalene (blue), reflectance spectrum of a ca. 1 mm film of TiO_2 nanoparticles coated with H_2Pc (pink). Note that both compounds wash off after rinsing with the solvent.

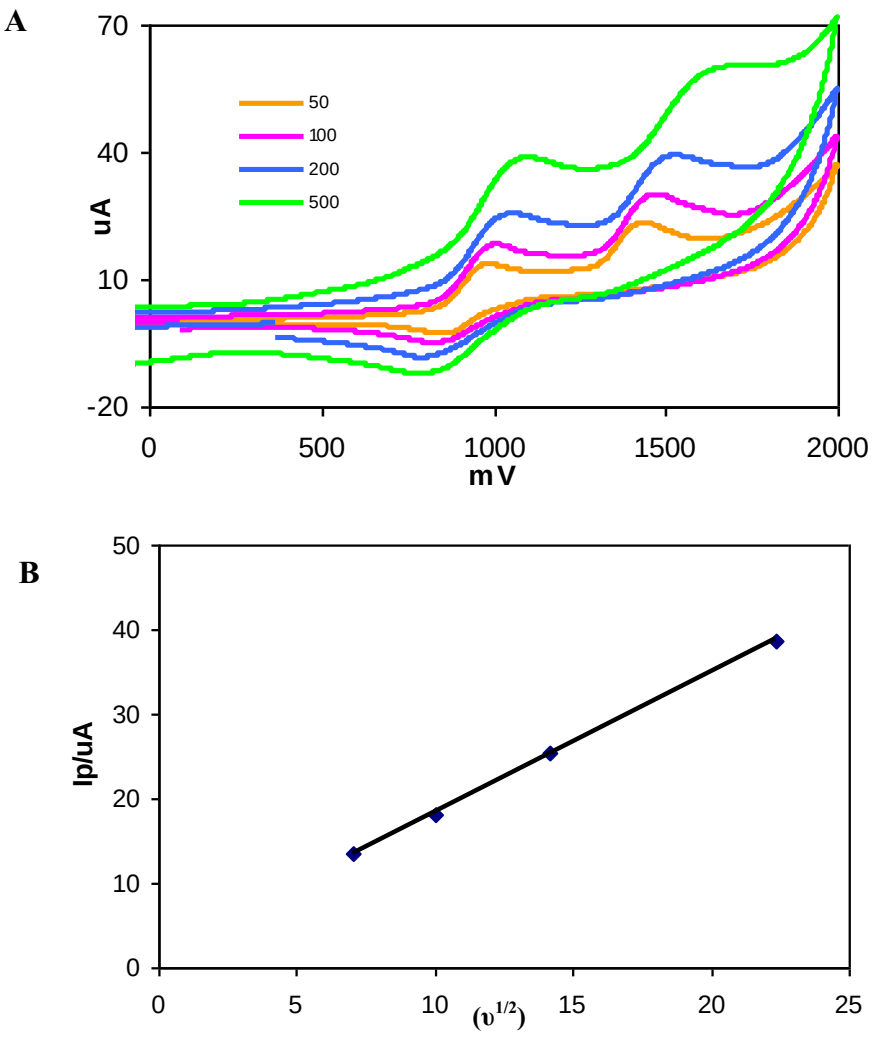

Figure A4.7 (A) Cyclic voltammetry of the oxidation potential window of 1 mM (TPP)Zr(OAc)$_2$ solution in dichloromethane containing 0.1 M Bu_4NPF_6 as the supporting electrolyte at different scan rates ranging from 50-500 mV/s. **(B)** The anodic peak current versus square root of the scan rate ($\upsilon^{1/2}$).

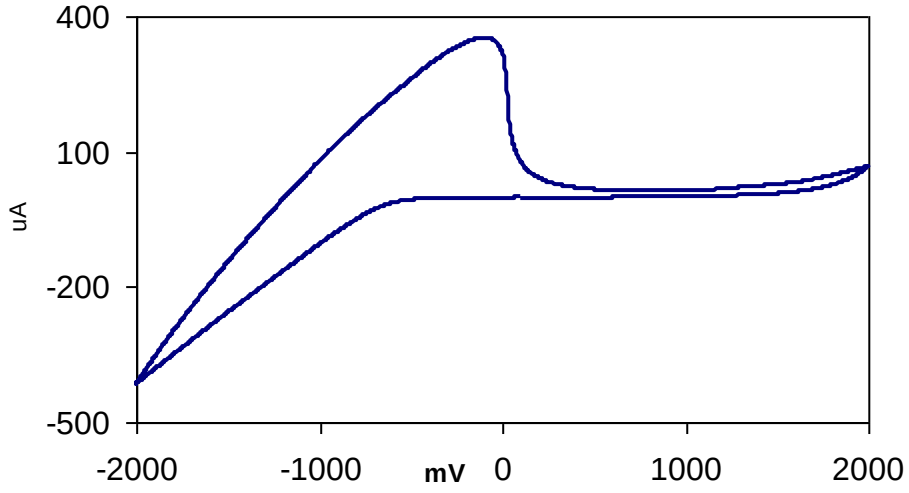

Figure A4.8 Cyclic voltammograph of an electrode made from 25 nm TiO_2 nanoparticles deposited on ITO represents interference in region of negative potentials. Only the positive potentials region could be used as a blank for our studies.

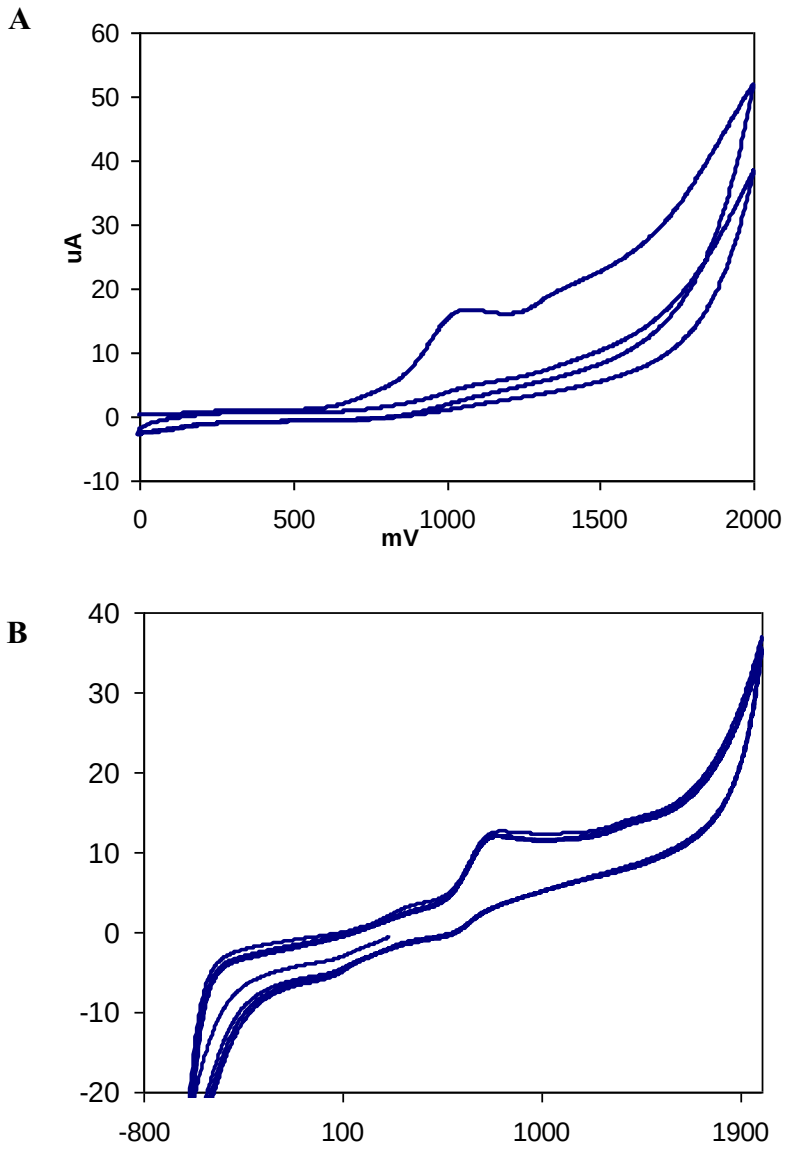

Figure A4.9 Cyclic voltammetry of 1 mM **(A)** (TPP)Hf(OAc)$_2$ **(B)** (Pc)Hf(OAc)$_2$ deposited on TiO_2 electrode in dichloromethane containing 0.1 M Bu_4NPF_6 as the supporting electrolyte at 200mV/s. After the 2nd cycle the HfPor wave is not observed on the TiO_2 electrode but the Hf Pc still remains on TiO_2 electrode

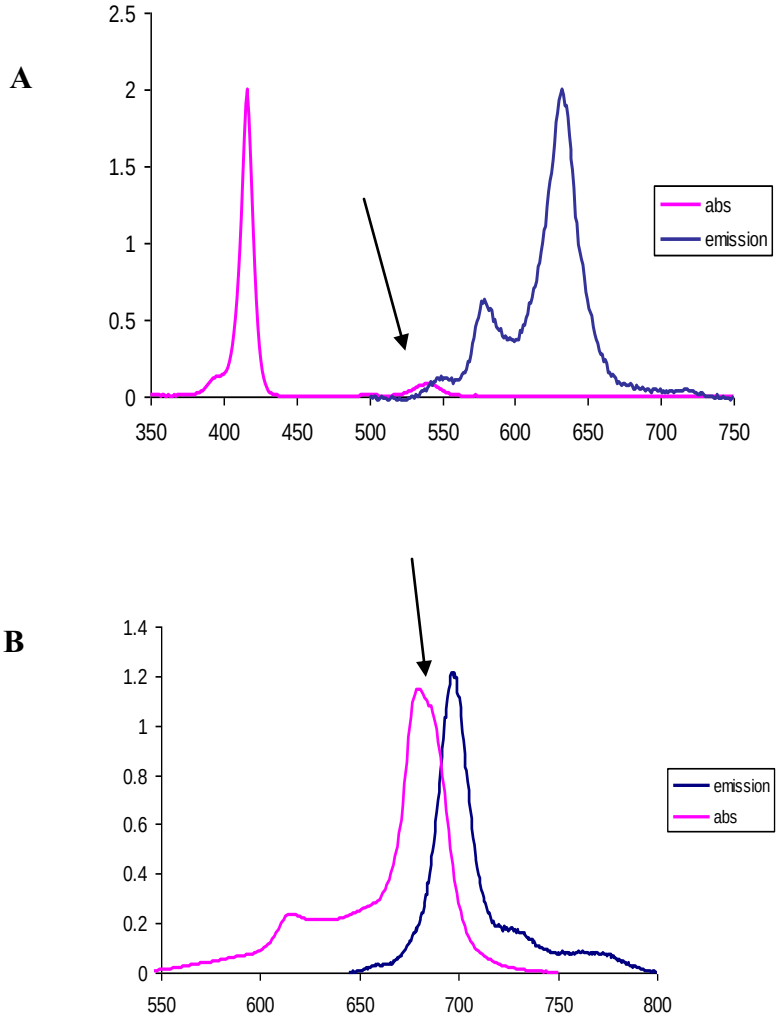

Figure A4.10 The excitation energy $E_{0\text{-}0}$ (eV) is estimated from the intersection of normalized emission and absorption spectra of the dye: **(A)** $(TPP)Hf(OAc)_2$ and **(B)** $(Pc)Hf(OAc)_2$. Similar spectra are observed for the Zr complexes.

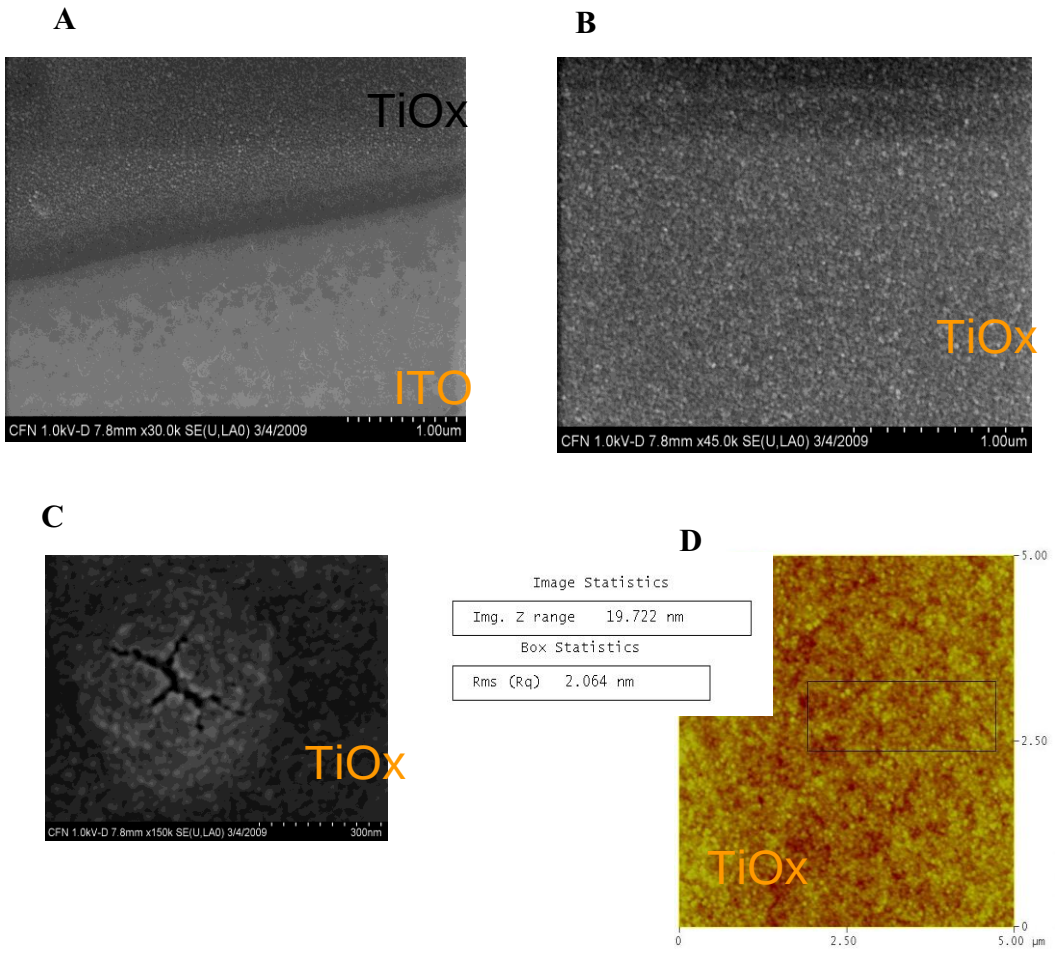

Figure A4.11 E-beam deposited 60 nm Ti layer after oxidation in a furnace at 500-600 ^{0}C. **(A)** SEM image of border layers of ITO and TiOx ; **(B)** 60 nm thick TiOx; **(C)** Crack in the deposited layer of TiOx; **(D)** Tapping mode AFM image of 60 nm compact layer with rms roughness of 2.06 nm

References

(1) http://www.sc.doe.gov/bes/reports/files/SEU_rpt.pdf., 2005.

(2) Grätzel, M. Journal of Photochemistry and Photobiology A: Chemistry 2004, 164, 3.

(3) Heremans, P.; Cheyns, D.; Rand, B. P. S. Accounts of Chemical Research 2009, 42, 1740.

(4) Gratzel, M. Inorg. Chem. 2005, 44, 6841.

(5) Katsoulis, D. E. Chem. Rev. 1998, 98, 359.

(6) Falber, A.; Burton-Pye, B. P.; Radivojevic, I.; Todaro, L.; Saleh, R.; Francesconi, L.; Drain, C. M. Eur.J.Inorg.Chem. 2009, 2459.

(7) Drain, C. M.; Smeureanu, G.; Batteas, J.; Patel, S. In Dekker Encyclopedia of Nanoscience and Nanotechnology; Schwartz, J. A., Contescu, C. I., Putyera, K., Eds.; Marcel Dekker, Inc.: New York, 2004; Vol. 5.

(8) Barlow, D. E.; Scudiero, L.; Hipps, K. W. Langmuir 2004, 20, 4413.

(9) Otsuki, J.; Kawaguchi, S.; Yamakawa, T.; Asakawa, M.; Miyake, K. Langmuir 2006, 22, 5708.

(10) Nazeeruddin, M. K.; Hunphry-Baker, R.; Officer, D. L.; Campbell, W. M.; Burrell, A. K.; Graetzel, M. Langmuir 2004, 20, 6514.

(11) Stromberg, J. R.; Marton, A.; Kee, H. L.; Kirmaier, C.; Diers, J. R.; Muthiah, C.; Taniguchi, M.; Lindsey, J. S.; Bocian, D. F.; Meyer, G. J.; Holten, D. J. Phys. Chem. C 2007, 111, 15464.

(12) Chan, Y.-H.; Schuckman, A. E.; Perez, L. M.; Vinodu, M.; Drain, C. M.; Batteas, J. D. J. Phys. Chem. C 2008, 112, 6110.

(13) Tanaka, M.; Hayashi, S.; Eu, S.; Umeyama, T.; Matano, Y.; Imahori, H. Chem. Commun. 2007, 2069.

(14) Rochford, J.; Galoppini, E. Langmuir 2008, 24, 5366.

(15) Imahori, H.; Norieda, H.; Nishimura, Y.; Yamazaki, I.; Higuchi, K.; Kato, N.; Motohiro, T.; Yamada, H.; Tamaki, K.; Arimura, M.; Sakata, Y. J. Phys. Chem. B 2000, 104, 1253.

(16) Lee, D.-C.; Morales, G. M.; Lee, Y.; Yu, L. Chem. Comm. 2006, 101.

(17) Batteas, J.; Helt, J.; Xu, C.; Weldon, M. ANTEC 2001 Proceedings: Materials 2001, 2, 1951.

(18) Hagfeldt, A.; Grätzel, M. Acc. Chem. Res. 2000, 33, 269.

(19) Rochford, J.; Chu, D.; Hagfeldt, A.; Galoppini, E. J. Am. Chem. Soc. 2007, 129, 4655.

(20) Campbell, W. M.; Jolley, K. W.; Wagner, P.; Wagner, K.; Walsh, P. J.; Gordon, K. C.; Schmidt-Mende, L.; Nazeeruddin, M. K.; Wang, Q.; Grαεtzel, M.; Officer, D. L. J. Phys. Chem. C 2007, 111, 11760.

(21) Drain, C. M.; Varotto, A.; Radivojevic, I. Chemical Reviews 2009, 109, 1630.

(22) Gagne, R. R.; Koval, C. A.; Lisensky, G. C. Inorg. Chem. 1980, 19, 2854.

(23) Bard, A. J.; Faulkner, L. R. Electrochemical Methods: Fundamentals and Applications; Second ed.; John Wiley & Sons, INC., 2001.

(24) Kadish, K. M.; Smith, K. M.; Guilard, R. The Porphyrin Handbook:Electron Transfer; Academic Press: San Diego, 2000.

(25) Gratzel, M. Accounts of Chemical Research 2009, 42, 1788.

(26) Qiankun, Z.; Xiaoxia, G. Science in China 1996, 40, 215.

(27) Junghänel, M. Novel aqueous electrolyte films for hole conduction in dye sensitized solar cells and development of an electron transport model; der Freien Universität Berlin: Berlin, 2007.

(28) Kathiravan, A.; Renganathan, R. Journal of Colloid and Interface Science 2009, 331, 401.

(29) Grätzel, M. Journal of Photochemistry and Photobiology C: Photochemistry Reviews 2003, 4, 145.

(30) L., S.-M.; U., B.; Humphry-Baker, R.; Horiuchi, T.; Miura, H.; Ito, S.; Uchida, S.; Grätzel, M. Advanced Materials 2005, 17, 813.

(31) Yu, K.; Chen, J. Nanoscale. Res. Lett. 2009, 1.

(32) Riede, M.; Mueller, T.; Tress, W.; Schueppel, R.; Leo, K. Nanotechnology 2008, 19, 1.

(33) Ting, C.-C.; Chen, S.-Y.; Liu, D.-M. Journal of Applied Physics 2000, 88, 4628.

(34) O'Regan, B.; Lenzmann, F.; Muis, R.; Wienke, J. Chem. Mater. 2002, 14, 5023.

(35) Ito, S.; Murakami, T. N.; Comte, P.; Liska, P.; Grätzel, C.; Nazeeruddin, M. K.; Grätzel, M. Thin Solid Films 2008, 516, 4613.

(36) G nes, S.; Neugebauer, H.; Sariciftci, N. S.; Roither, J.; Kovalenko, M.; Pillwein, G.; Heiss, W. Adv. Funct. Mater. 2006, 16, 1095.

(37) Qiao, Q.; Beck, J.; Lumpkin, R.; Pretko, J.; McLeskey, J. J. T. Solar Energy Materials and Solar Cells 2006, 90, 1034.

(38) Peng, B.; Jungmann, G.; Jäger, C.; Haarer, D.; Schmidt, H.-W.; Thelakkat, M. Coordination Chemistry Reviews 2004, 248, 1479.

(39) Robertson, N. Angew. Chem. Int. Ed. 2006, 45, 2338

(40) Liao, M.-S.; Scheinera, S. J.Chem. Phys. 2002, 117, 205.

(41) M.Gouterman The Porphyrins; Academic Press: New York, 1978.

(42) Donohoe, R. J.; Duchowski, J. K.; Bocian, D. F. Journal of the American Chemical Society 1988, 110, 6119.

(43) Kim, H. J.; Whang, D.; Kim, K.; Do, Y. Inorg. Chem. 1993, 32, 360.

(44) Ryu, S.; Whang, D.; Kim, J.; Yeo, W.; Kim, K. J. Chem. Soc., Dalton Trans. 1993, 205.

(45) Falber, A.; Todaro, L.; Goldberg, I.; Favilla, M. V.; Drain, C. M. Inorg. Chem. 2008, 47, 454.

CHAPTER 5

Photophysical Characterization of Hf(IV) and Zr(IV) Porphyrinato & Phthalocyaninato Diacetate Complexes: Ultrafast Transient Absorbance and Single Photon Counting Fluorescence Measurements

5.1. ABSTRACT

Electron transfer kinetics of the various processes directly dictate the efficiency of DSSC (Figure 5.1). Since we are proposing a new mode of binding dyes to oxide semiconductors, studies on rate of electron injection from the excited state of the dye to conduction band of TiO_2 are essential. However, the goal of this part of the thesis is primarily to understand the photodynamics of our molecules in solution and provide the platform from which future studies of these molecules can arise. Time-resolved optical spectroscopy is the most commonly used technique for study of interfacial electron transfer. In this chapter we will examine photophysical properties of dye excited states using ultrafast femtosecond and nanosecond scale transient absorbance spectroscopy, determine the rate of the various processes occurring within the molecules, and measure both singlet and triplet state lifetimes.

The excited state lifetime of the dye must be long enough for efficient electron injection into the semiconductor in solar cell devices. Since the injection rate is found to be much faster than recombination, or the backwards electron transfer processes, some scientists assume that electron injection reaction is not crucial for the device improvement. They argue that the injection rate must have an appropriate rate constant

(not too fast, not too slow) to be able to compete with the dye decay from excited state, thereby minimizing "kinetic redundancy".[4-5]

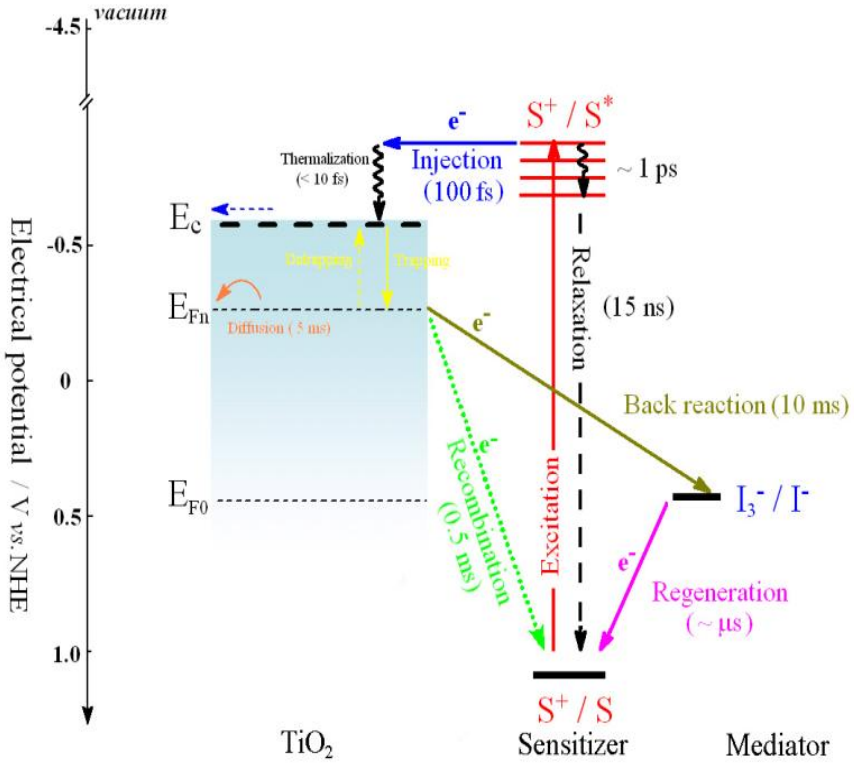

Figure 5.1 Processes and their rate constants occurring within solar cell device during light conversion into electricity. Adopted from reference.[3]

5.2. INTRODUCTION

Porphyrins have a key role in photosynthesis – one of nature's most important reaction schemes. The solar energy in plants is captured with light-harvesting pigments (chlorophylls, carotenoids) that are arranged in highly ordered arrays (photosynthetic antenna complexes) and transferred to the reaction center which then separates the charge across a membrane through a cascade of electron transfer reactions with almost 100% quantum efficiency.[6] The stunning efficiency arises from the precise nanoarchitecture of both components of the photosynthetic apparatus mediated by intermolecular interactions between the chromophores and between the protein scaffolds. Just as importantly, there are a myriad of small, local vibrations and conformational changes that constitute the system dynamics that come from both kT energy and the vibrational energy released as the chromophores traverse from the initially formed excited state to the first excited state.[7-9] The efficiencies of light harvesting and charge separation by artificially synthesized porphyrinic arrays and porphyrinic compounds on surfaces or in a matrix are much less impressive.[10] A fundamental understanding of mechanism of photosynthetic energy and electron transfer reactions are needed to improve the efficiency of man-made dye systems. Porphyrins and phthalocyanines are chlorophyll like pigments and thus are excellent models systems for studying electron transfer dynamics in nature inspired systems. For the same reasons, they are also excellent candidates for other photonics applications, for example as photosensitizers in solar cell devices, sensors, and photodynamic therapy.

5.2.1 Photophysical processes within a molecule

In general, porphyrins have very strong absorption bands around 400-430 nm (Soret or B band) with ε values on the order of 10^5 $M^{-1}cm^{-1}$. Porphyrins also have several Q-bands between 500-650 nm with ε values some 10-20 times less. On the other hand, phthalocyanines[10] have B bands of smaller intensity around 300-400 nm, and Q-bands in the region of 600-800 nm with ε values on the order of 10^5 $M^{-1}cm^{-1}$.

When the chromophores are excited at the B band with visible light predominantly the first excited state (S_1) is populated. Some higher excited states get populated as well, but the deactivation of these states results in very rapid decay to the lowest S_1 state in a few ps. From the S_1 state electrons undergo radiative and non-radiative processes to relax back to the ground state. The emission of photons result from radiative processes called fluorescence ($S_1 \rightarrow S_0$) and phosphorescence ($T_1 \rightarrow S_0$). Internal conversion (IC) back to the ground state is when the excited state energy is lost as heat through collision with solvent molecules and through vibrational/conformational processes. The excited state singlet can decay by intersystem crossing (ISC) to the first triplet excited state (T_1). The spin-allowed optical transitions take place within the singlet manifold. The spin-forbidden intersystem crossing to the triplet manifold is facilitated by spin-orbit coupling, which for free base porphyrinoids can be quite large. The triplet state of porphyrin and phthalocyanine molecules have been extensively used to photosensitize the formation of singlet oxygen by triplet-triplet interactions, so photophysical studies are often performed in deoxygenated solvents. All processes occurring within a molecule after light absorption are represented in a Jablonski diagram (Figure 5.2). Emission spectra of porphyrins are generally observed between wavelengths 600-720 nm while for

phthalocyanines the emission is 680-750 nm. Phosphorescence spectra are harder to detect using standard conditions, and usually appear at much longer wavelengths: 700-800 nm for porphyrins and in the NIR 900-1200 nm for phthalocyanine molecules.

Every photophysical process mentioned above has a characteristic rate constant k (k_{IC} ~ 10^7- 10^{13} s^{-1}; k_{FL} ~ 10^6- 10^{12} s^{-1}; k_{PH} ~ 10^6- 10^{-1} s^{-1}). Overall rate constant for the decay of the singlet excited state is k_s :

$$k_s = k_{ISC} + k_F + k_{IC} \qquad \text{(eq.1)}$$

The total lifetime of singlet excited state is equal to:

$$\tau_s = 1/ k_s \qquad \text{(eq.2)}$$

The fluorescence quantum yield (Φ_F), which represents the ratio of photons absorbed to photons emitted through fluorescence, is another important parameter. The value for Φ_F is between 0 and 1. Quantum yields are usually determined with the comparative method of Williams et al. [11] using a standard sample with known Φ_F value as reference compound (e.g. TPP, ZnTPP or ZnPc):

$$\Phi = \Phi_R \times \frac{Int}{Int_R} \frac{A_R}{A} \frac{n^2}{{n_R}^2} \qquad \text{(eq. 3)}$$

where, A stands for absorbance at the excitation wavelength, n is the refractive index of the solvent, Int is the integral of the area under the fluorescence spectrum peaks. R refers to the reference compound.

The quantum yield of triplet states can be calculated with similar method, but using transient absorbance spectra (singlet depletion method).[12]

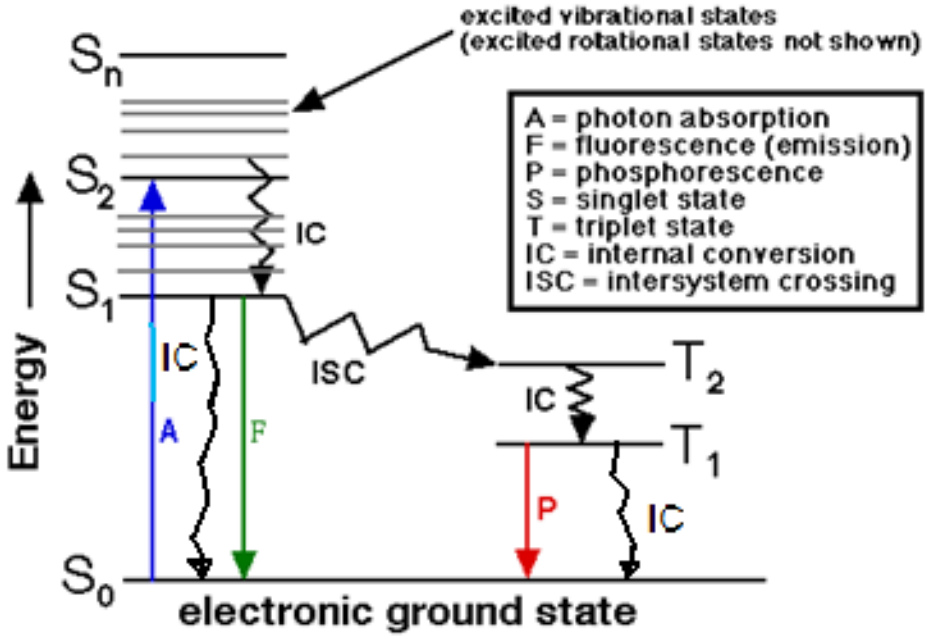

Figure 5.2 Jablonski diagram for photophysical events of organic dyes. Internal conversion are vibrational processes. Adapted from website, reference.[2]

5. 2.2 Characterization methods

Transient Absorbance Spectroscopy

Pump-probe laser spectroscopy is a technique widely used for monitoring fast reactions in photochemistry. The system utilizes a single light source that acts as the source for both pump and probe beams. The sample is irradiated by a pump pulse and monitored by the probe beam after a specified time delay. The short pump pulse has to be shorter than the lifetime of transient species, in other words the laser pulse width must be shorter that the time constant of the reaction. By changing the time between the pump and probe, the kinetics of transient species can be measured. The delay is enabled with the delay line through which the probe travels and is controlled by computer. The probe pulse passes through the sample and both pulses overlap at the detector (Figure 5.3).

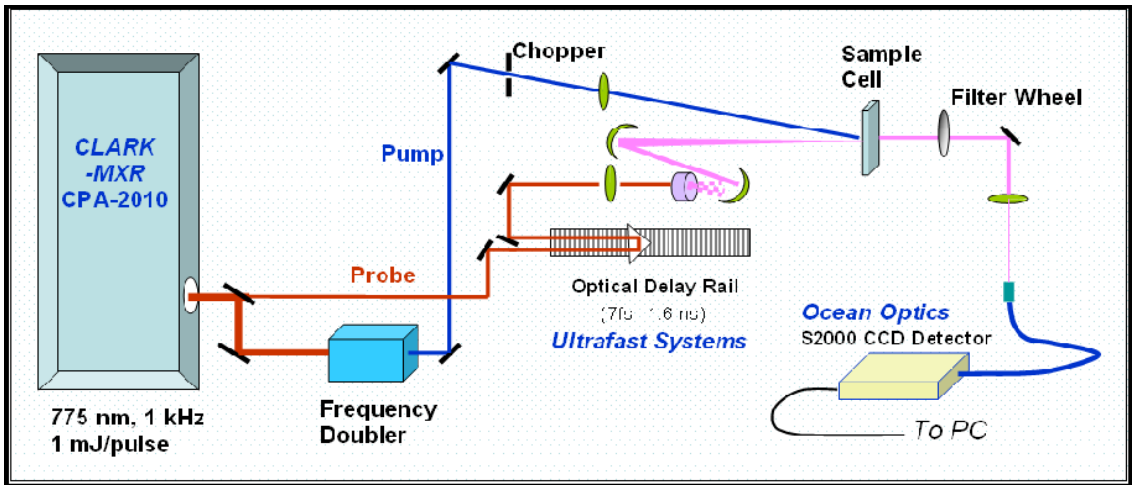

Figure 5.3 Schematic representation of transient absorbance spectrometer. Adopted from website, reference.[1]

Transient absorbance monitors changes in the absorbance (ΔA) between the ground and excited states of the molecule. Those changes can be either positive or negative. Positive change indicates a rise in the population of excited species (singlet and triplet absorption) after irradiating with the pump pulse at the wavelength where the ground state absorption occurs. Negative transient absorbance spectrum indicates disappearance of species present before the pump, and it is seen as state bleaching or stimulated emission. Generally, transient species are short lived.

Change in the sample absorbance is represented as ΔA:

$$\Delta A(t) = -\log [I(t)/I(t<to)] \qquad \text{(eq. 4)}$$

where, I(t<to) is intensity of the probe beam before laser excitation, and I(t) after excitation. The difference in absorbance vs. time at the single wavelength represents kinetic spectrum (time-resolved TA), and when monitored at the certain time at different wavelengths, it represents difference spectrum, TA spectrum (Figure 5.4).

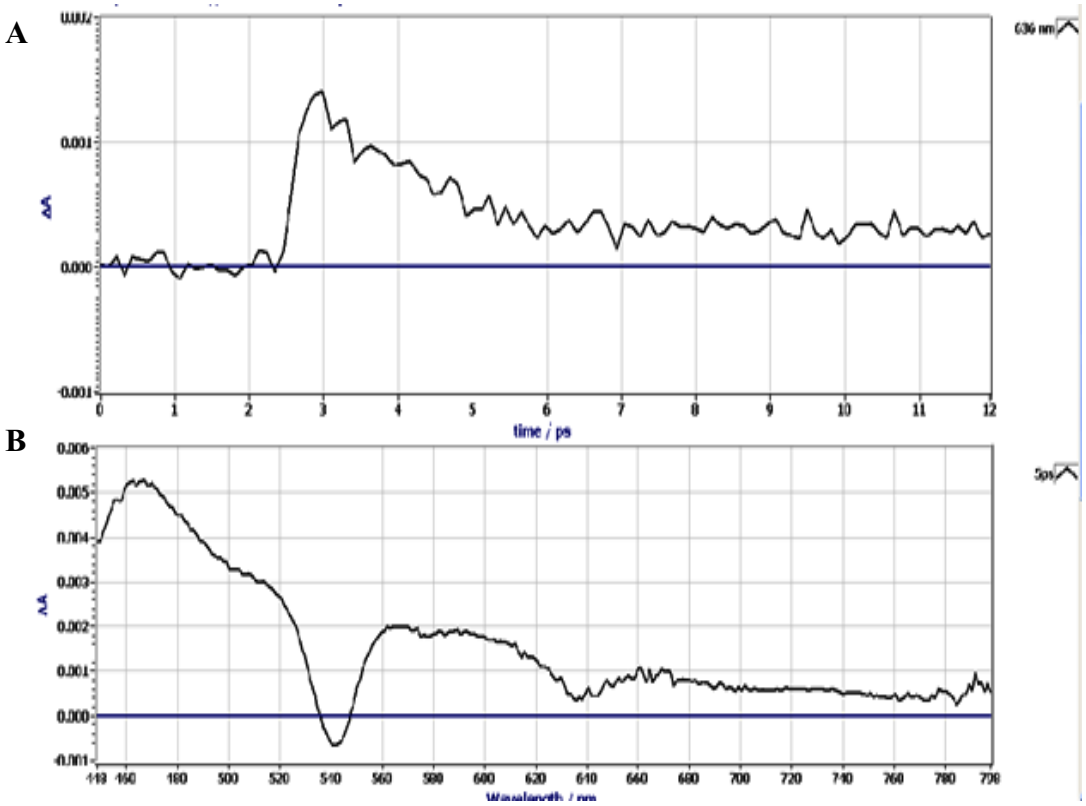

Figure 5.4 An example of (TPP)Hf(OAc)$_2$ spectra in toluene excited at 420 nm.**(A)** Kinetic curve of a time-resolved transient absorbance, probed at 636 nm.**(B)** Difference transient absorbance spectrum.

Time-correlated single photon counting (TCSPC)

The lifetime of fluorescence of the first excited state can be measured using single photon counting. The in principle, the decay in fluorescence can be measured over a wide time range, from a few picoseconds to milliseconds and seconds. In our instrument, the time range is 200 ps to 10 s.

Time resolved up-conversion fluorescence

The molecule is excited with pump light and the fluorescence light is overlapped with the gate beam in a β-BBO crystal. By varying the delay between excitation and gate pulses we can map the temporal behavior of the photoluminescence.[13] The result of mixing the visible luminescence with the NIR gate pulse gives UV photons that we can detect. The instantaneous nature of the nonlinear frequency conversion process gives the time resolution (in the form of the intensity of the UV up-converted signal as a function of delay.

5.3. DISCISSION AND RESULTS

Steady state spectroscopy

The absorption and emission spectra of (TPP)Hf(Ac)$_2$ and (Pc)Hf(Ac)$_2$ in toluene solution are shown in (Figure 5.5). Transitions from ground $S_0 \rightarrow S_2$ state are assigned to Soret or B band, and transitions from $S_0 \rightarrow S_1$ to Q bands (also see the Gouterman 4-orbial theory).[14] The emission spectra is almost a mirror image of the absorption spectra with a Stokes shift of ca. 10 nm indicating that there are small differences between ground and excited state spectra due to vibrational/conformational differences, which are

common for many porphyrins.[15] The Zr(IV) and Hf(IV) complexes of TPP are quite similar, and the Zr(IV) and Hf(IV) complexes of Pc are quite similar – with only ~2 nm differences in the wavelength maxima. In the table 5.1 below, we summarize absorption and emission maxima bands for all four molecules.

Table 5.1 Absorption and fluorescence characteristics of the compounds in toluene

Compound	λ_B^{max}, nm $S_0 \rightarrow S_2$	λ_Q^{max}, nm $S_0 \rightarrow S_1$	λ_{Fl}^{max}, nm $S_1 \rightarrow S_0$
$(TPP)Hf(OAc)_2$	416	539	550, 580, 633
$(TPP)Zr(OAc)_2$	418	540	550, 580, 633
$(Pc)Hf(OAc)_2$	334	614, 684	695,730
$(Pc)Zr(OAc)_2$	336	617, 685	694,726

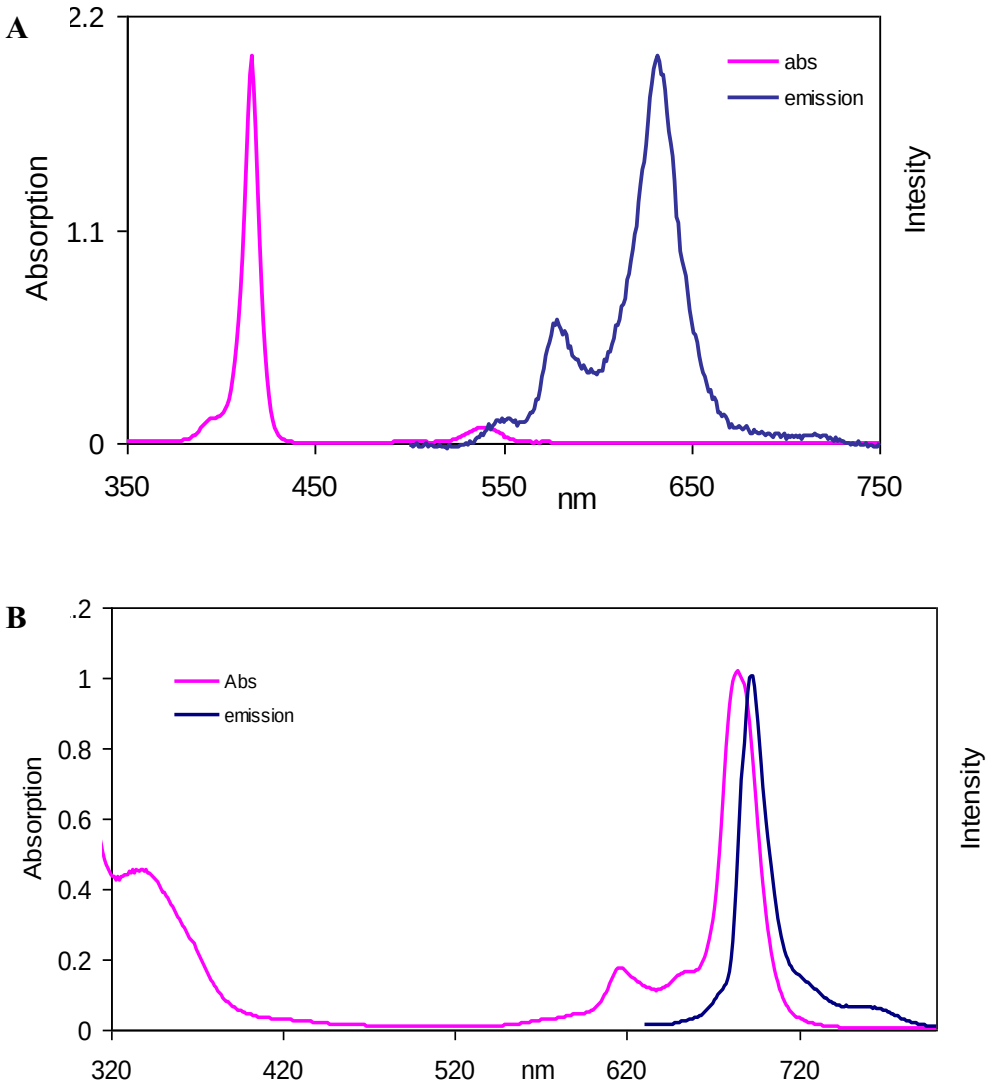

Figure 5.5 Normalized absorption and emission spectra: **(A)** (TPP)Hf(OAc)$_2$ in toluene solution, [4 μM] excited at 416 nm; **(B)** (Pc)Hf(OAc)$_2$ [6 μM] excited at 615 nm. The Stoke shift of ~10 nm is characteristic for both compounds.

Transient absorption measurements (TA)

Porphyrins: $(TPP)Hf(OAc)_2$ and $(TPP)Zr(OAc)_2$

Figure 5.6 represents the characteristic TA spectra of $(TPP)Hf(OAc)_2$ in a toluene solution, excited at 420 nm and probed at 540 nm. The excitation and subsequent relaxation of the B band leads predominately to the population of the lowest singlet excited state (S_1), but higher excited states can be filled as well. For porphyrins in general, excited state absorption of S_2, S_1 and T_1 is characterized by strong bleaching (disappearance of species) in the ground state corresponding to the B band, and weaker bleaching from Q bands. The ultrafast relaxation of the S_2 to S_1 state can be observed as a rise in the magnitude of the S1 bleach at early times. Up to 60 ps we observe no change in TA spectra, nor any shift at the absorption maxima (Figure 5.6). On a femtosecond timescale, conversion of initially formed excited state S_2 to the S_1 state happens very rapidly, in few ps. From TA data we determined that S_2 to S_1 vibrational relaxation process occurs in ~1.5 ps for HfTPP, while ZrTPP the decay to the first excited state occurs in ~1.2 ps. Also, after excitation of S_2 state in PL up-conversion measurements for HfTPP we observed a rise time comparable to the vibrational relaxation to S_1 (Figure 5.8).

Metallotetraphenylporphyrins and tetrabenzoporphyrins can also fluoresce from the S_2 state as well as the S_1 state,[16-17] but the lifetimes are very short and the quantum yields are on the order of 10^{-3}–10^{-4}. For example, fluorescence quantum yields from the S_1 state are 0.11 and 0.033 for TPP and ZnTPP, respectively.[15,18] We did not directly measure fluorescence from higher excited states, but the fast decay and the bleaching of

the Q bands in TA, as well as stimulated emission that we observed, inferred comparable lifetimes of the vibrational relaxation kinetics (Figure 5.8 and 5.9).

The total lifetime of the first excited state involves radiative and nonradiative processes. The lifetime of decay of ~56 ps observed in PL up-conversion measurements of (TPP)Hf(OAc)$_2$ (Figure 5.8) agrees well with the value of ~55 ps extracted from examining the singlet dynamics in transient absorption experiments (Figure 5.7B). The inset in the same figure shows slow ground state recovery must be > 3 ns. Thus we assume that the triplet state is formed via ISC and that this manifold predominates for both Hf and Zr porphyrins. We were able to measure fluorescence lifetime of ZrTPP using a time correlated single photon counting instrument in our laboratory, exciting at 405 nm wavelength, and measuring lifetime at the strongest 633 nm emission band. With and without argon, the lifetimes were very similar τ_{fl} ~0.602 ns in air and τ_{fl} ~0.572 ns in Ar. This lifetime corresponds to decay of S_1 state at stimulated emission peak from TA data, where we observed τ ~587 ps (Figure 5.9).

On the longer nanosecond scale, we observed different time constants when experiments were done when argon was bubbled through the solution versus the same experiment performed in air. In air τ = 672 ns was observed for HfTPP while under an Ar atmosphere, the ground state recovery happens on a microsecond time scale τ_1= 4.8 μs and τ_2= 25 μs (Figure 5.10). When using argon in the experiments, we determined two lifetimes for ZrTPP as well, τ_1~ 2.3 μs and τ_2~ 10.4 μs. Triplet excited state porphyrinoids are known to be very reactive with oxygen since the energy levels of singlet oxygen excited state lie close to the T_1 state of porphyrins. Our data indicates a much longer lived triplet state lifetime in argon; when reactivity with O_2 is decreased.

The ZnTPP S_1 state decays predominantly by intersystem crossing to T_1 and is reported to be 2 ns, compared to 12 ns for free base TPP.[15,18] Heavier atoms such as Hf and Zr enhance ISC, so the T_1 state becomes more efficiently populated due to the greater spin orbit coupling with metal orbitals. From the analyzed data, we observed that for HfTPP complex, intersystem crossing dynamics are much faster compared to ZrTPP due to an even greater influence of the heavy atom effect – which is consistent with previous conclusions.[19-21] Moreover we were able to construct energy level diagram for both HfTPP and ZrTPP acetate complexes, and the singlet dynamics representation is shown in Figure 5.12 and 5.13.

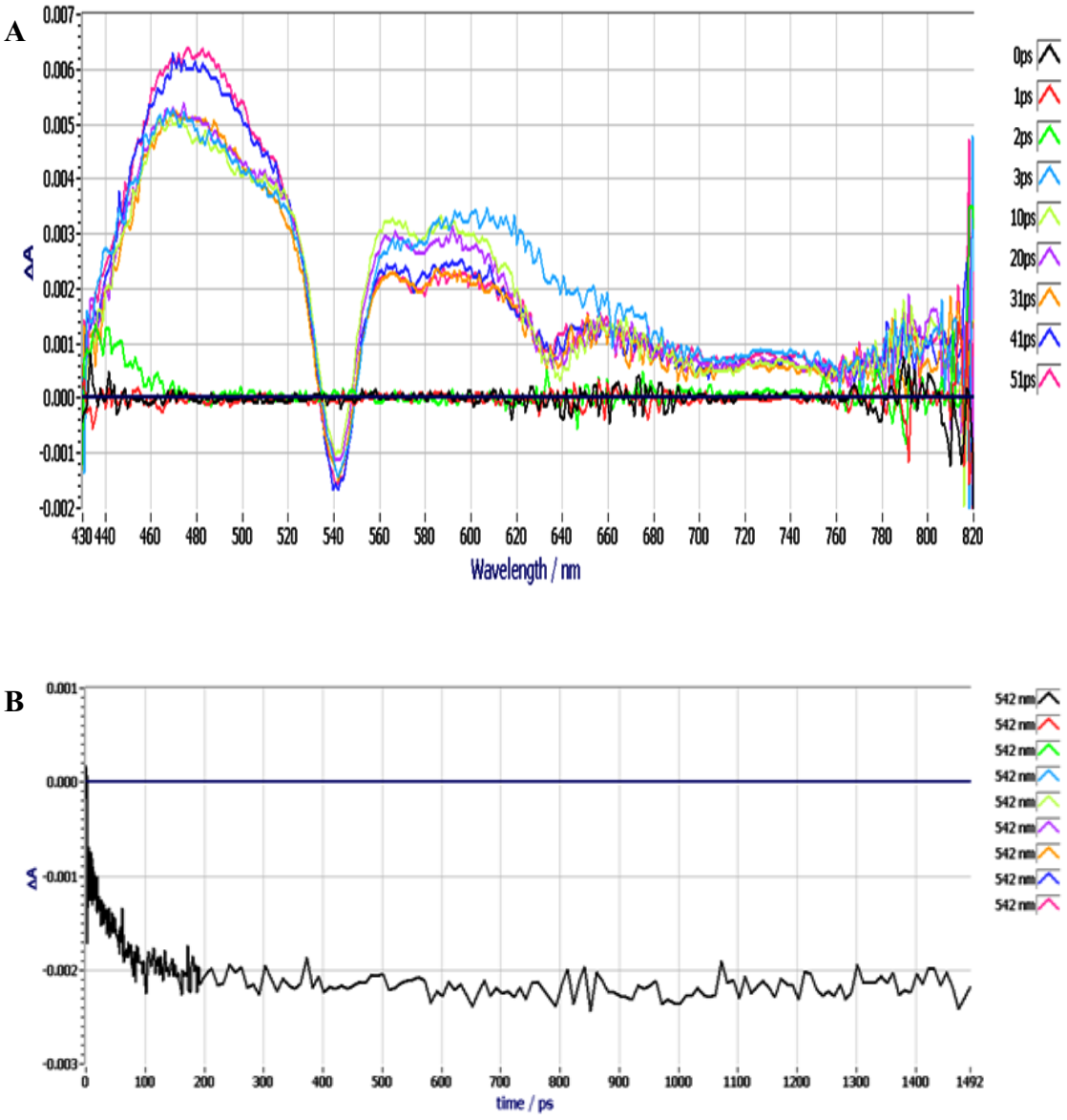

Figure 5.6 (TPP)Hf(OAc)$_2$ in toluene pumped at 420 nm.**(A)**Representative TA spectra at different time from 0 to 51 ps; **(B)** Representative kinetic trace, probed at 542 nm.

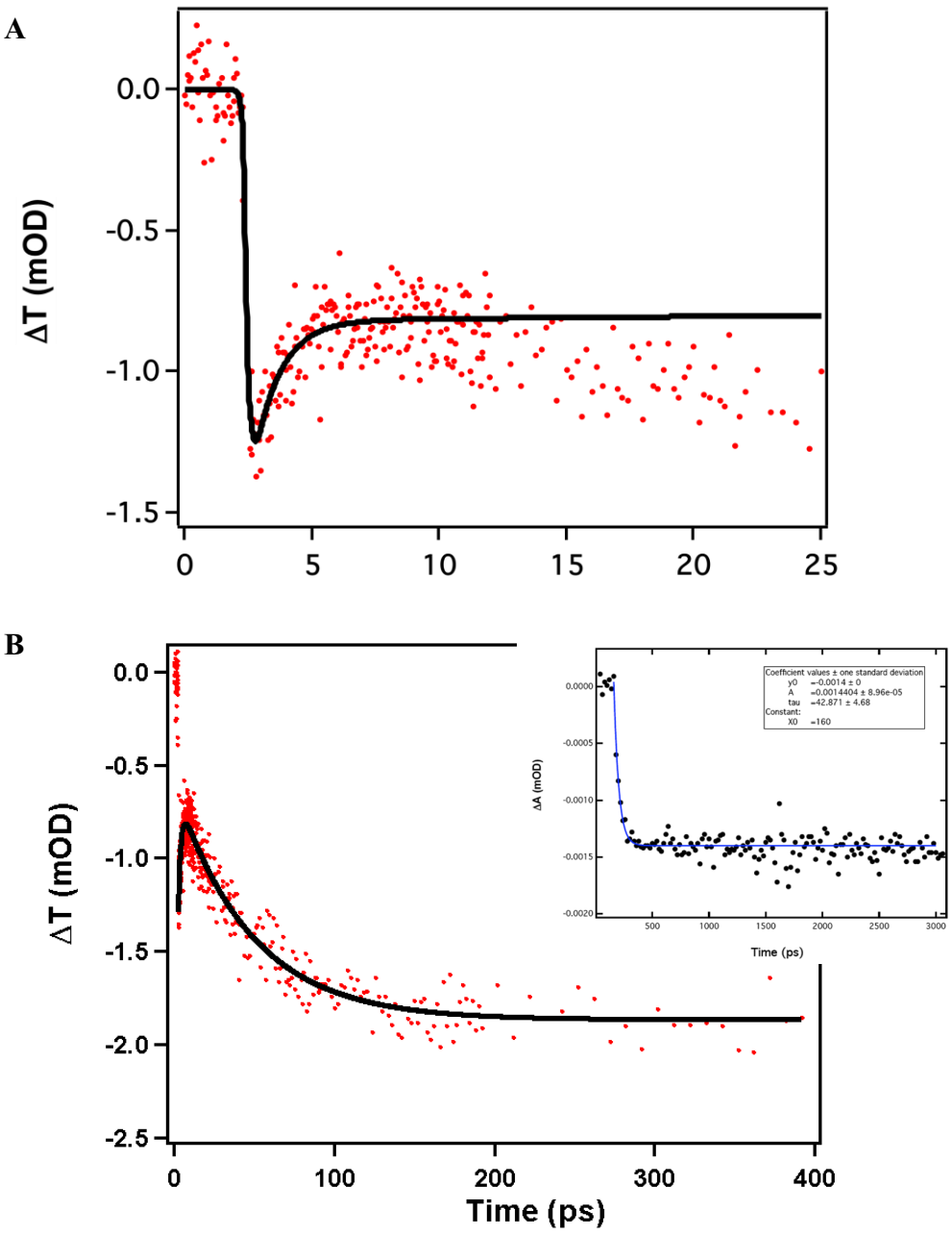

Figure 5.7 Femtosecond transient absorbance of (TPP)Hf(OAc)$_2$. λ_{pump}= 420 nm, λ_{probe}= 540 nm. Solid lines are fits of the experimental data. **(A)** τ= 1.5 ps and **(B)** τ= 55 ps. Inset shows existence if longed lived plateau > 3 ns.

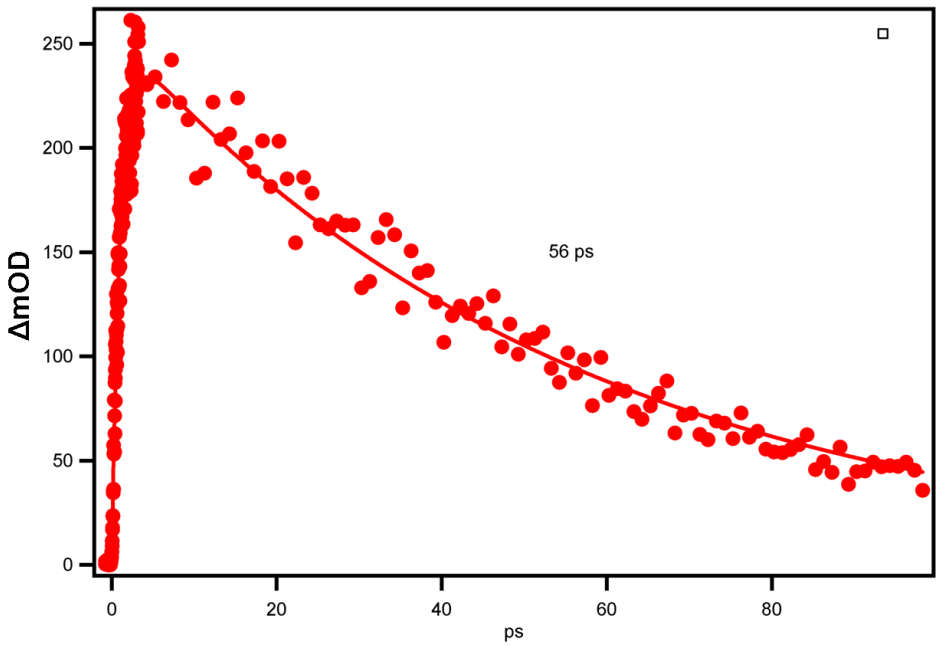

Figure 5.8 Fluorescence up-conversion transients for 420 nm excitation of (TPP)Hf(OAc)$_2$ in toluene. Solid line is the fit of the experimental data. A decay lifetime of τ= 56 ps is found. The fast rise time is comparable to vibrational relaxation to S_1on order of 1 ps.

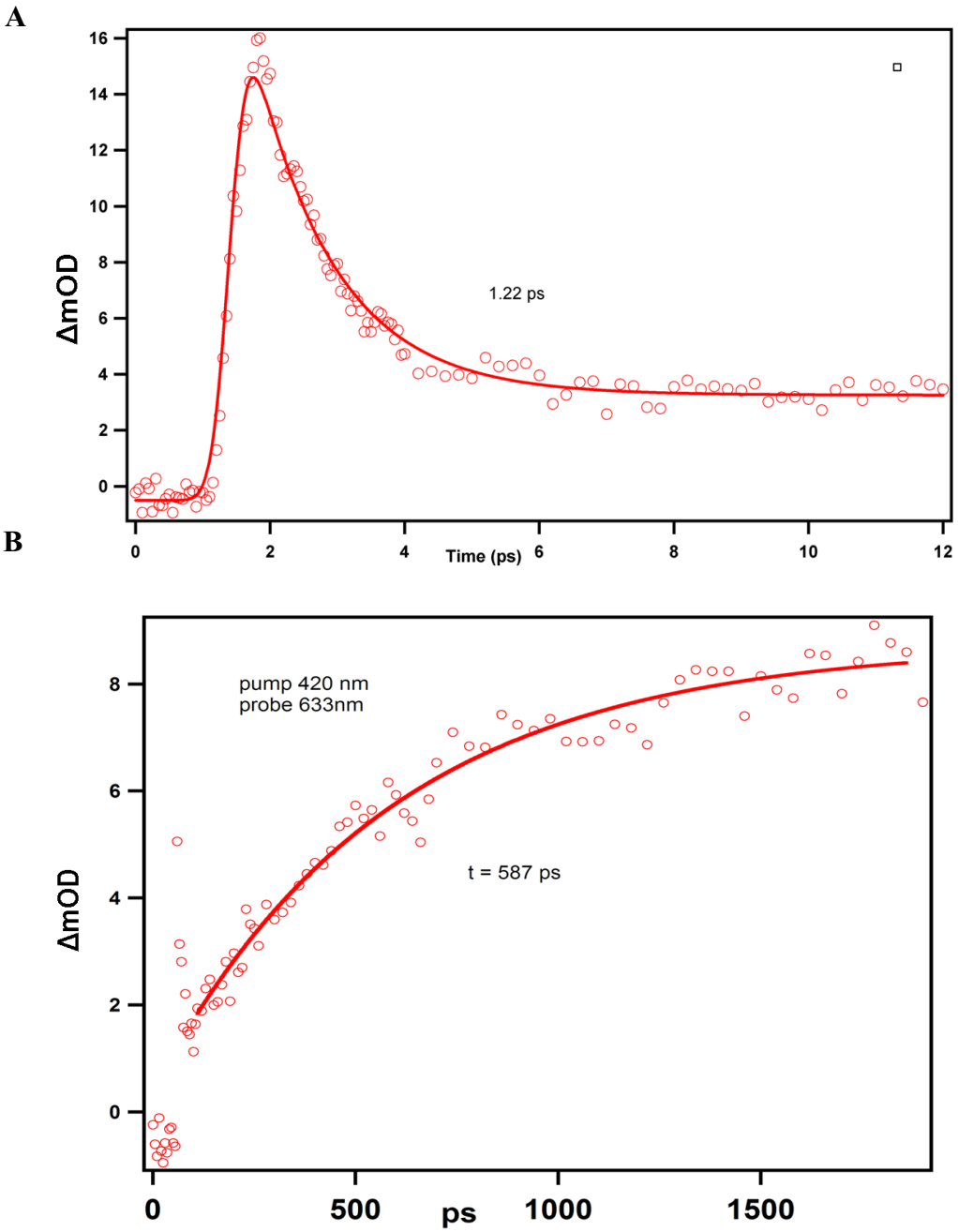

Figure 5.9 Femtosecond transient absorbance of $(TPP)Zr(OAc)_2$. λ_{pump}= 420 nm, λ_{probe}=633 nm. Solid lines are fits of the experimental data for electronic relaxation within S_1. **(A)** τ= 1.2 ps and **(B)** τ= 587 ps .

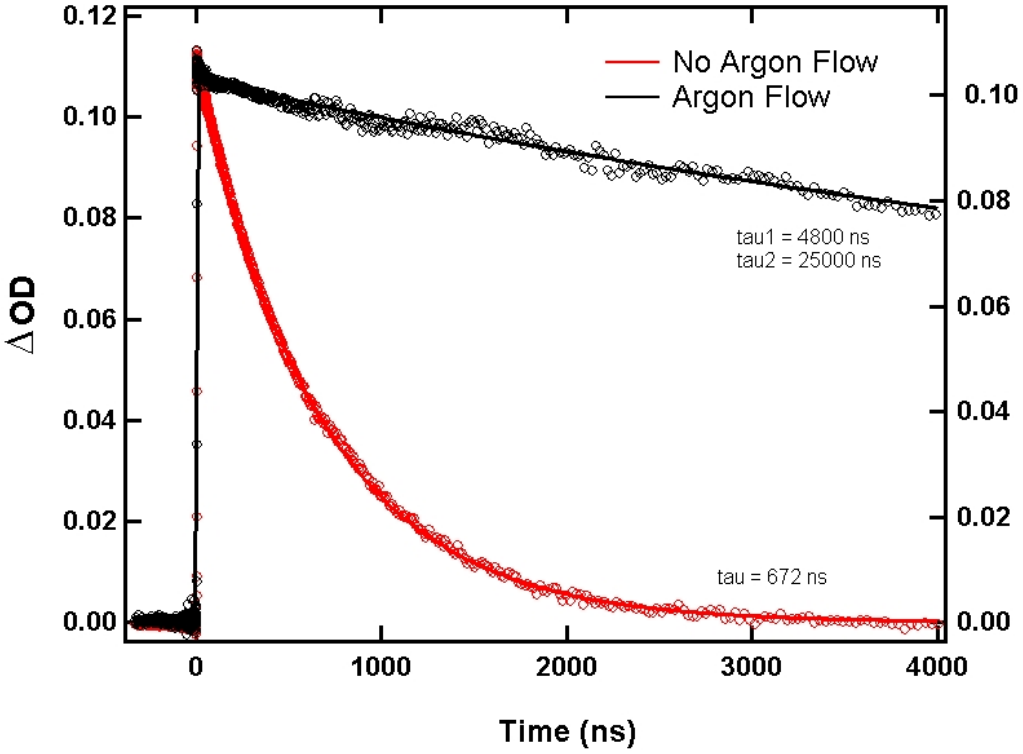

Figure 5.10 Microsecond scale (TPP)Hf(OAc)$_2$ in toluene pump at 420 nm, probe at 460 nm. Decay with argon flowing through the solution is bi-exponential (black fit) with a small faster time constant, and in air the curve is mono-exponential (red fit).

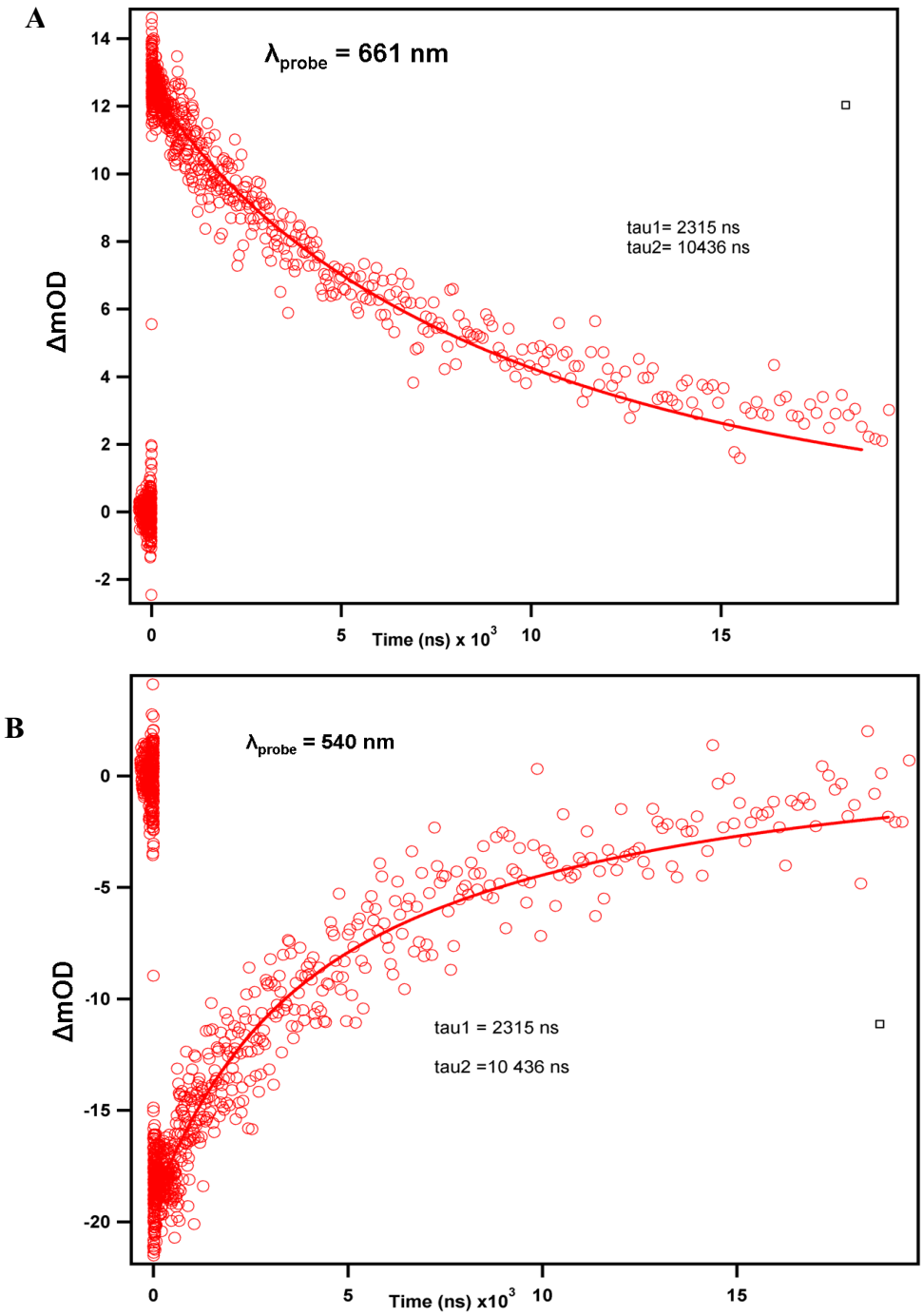

Figure 5.11 Deactivation kinetics of $(TPP)Zr(OAc)_2$ in argon saturated toluene pumped 420 nm. **(A)** When probed at 661 nm, the fit of the curve is bi-exponential with two lifetimes τ_1~ 2315 ns and τ_2~10436 ns. **(B)** When the probe wavelength is 540 nm, similar kinetics are observed, indicating one species.

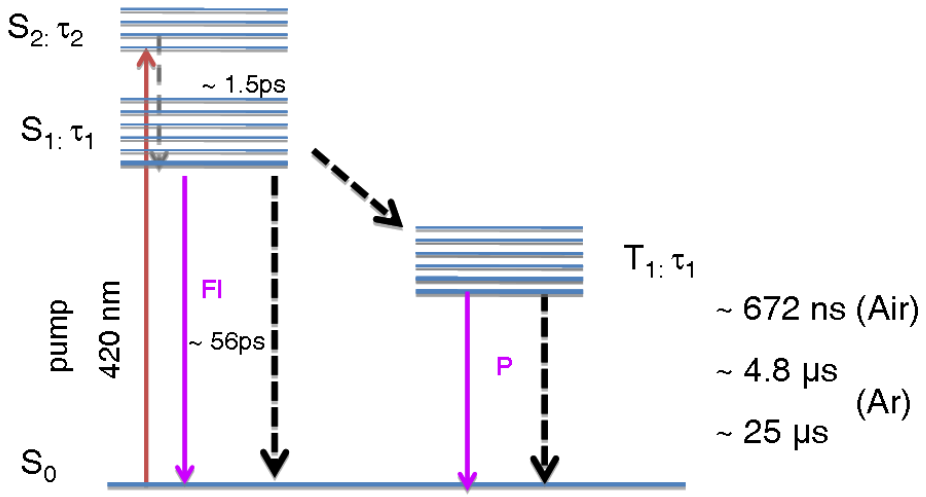

Figure 5.12 Schematic representation of singlet dynamics diagram, (TPP)Hf(OAc)$_2$. The fluorescence time constant is measured from up-conversion experiments. Solid line are for emissive processes and dashed for non-radiative processes.

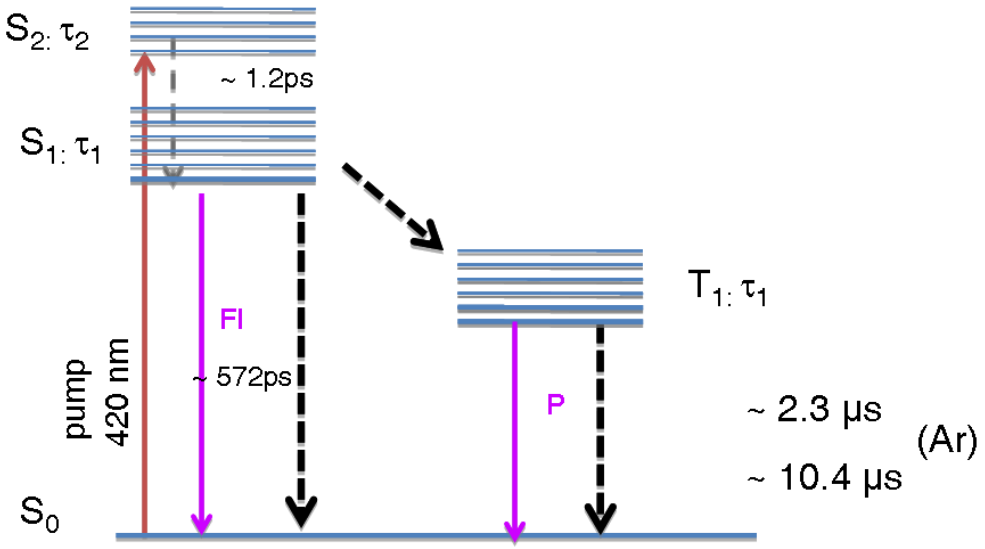

Figure 5.13 Schematic representation of singlet dynamics diagram, (TPP)Zr(OAc)$_2$. The fluorescence time constant is measured from up-conversion experiments. Solid lines are for emissive processes and dashed for non-radiative processes.

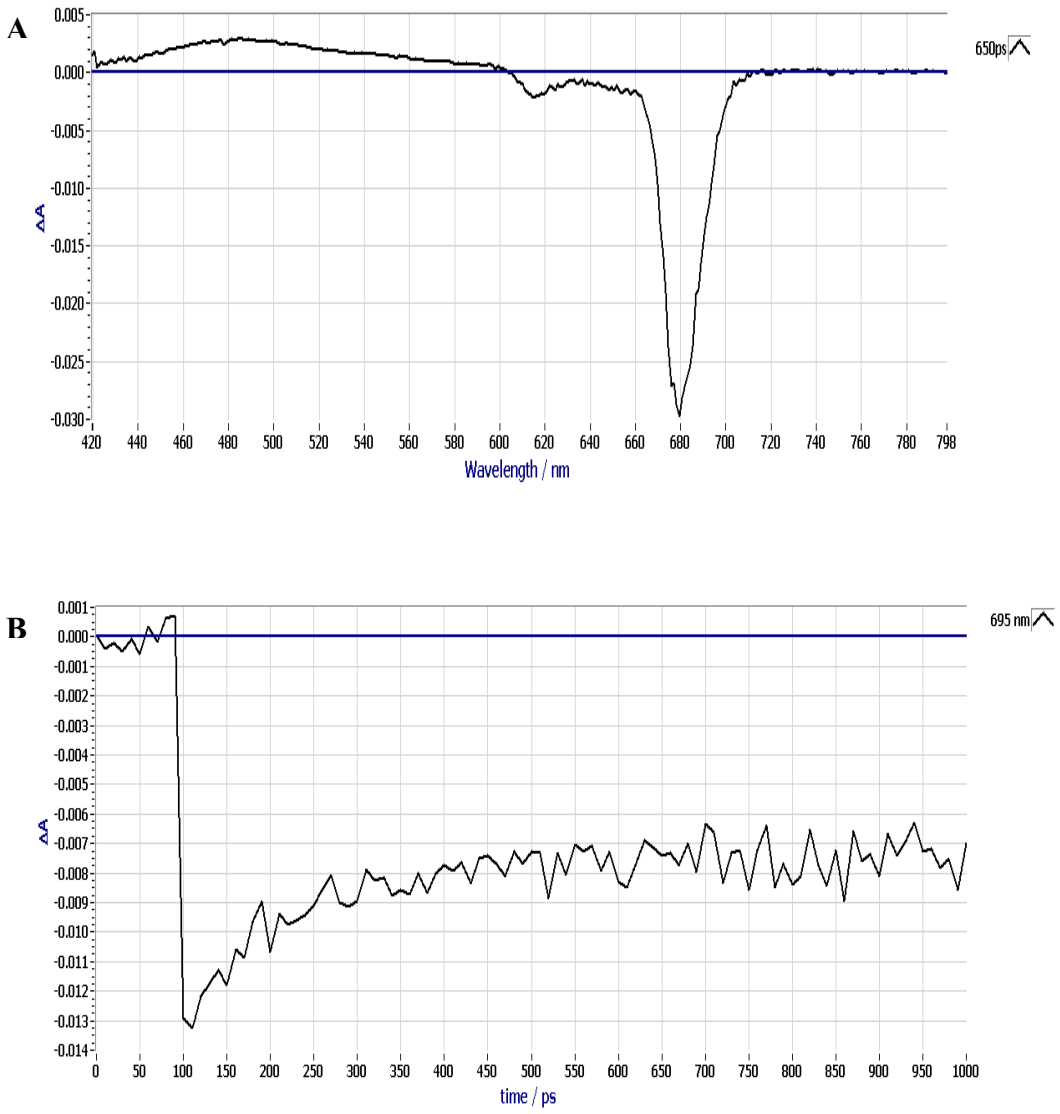

Figure 5.14 (Pc)Hf(OAc)$_2$ in toluene. λ_{pump} = 685 nm; λ_{probe}= 695 nm. **(A)** Representative TA spectra at 650 ps; **(B)** Representative kinetic spectra at 695 nm.

Phthalocyanines: $(Pc)Hf(OAc)_2$ and $(Pc)Zr(OAc)_2$

The timescales attributed to singlet excited states are slower for metallophthalocyanine acetate complexes. The samples were irradiated in the 685 nm (Q band), and singlet excited state dynamics were determined. We also tried pumping in the B band at a wavelength of ~330 nm but experienced difficulties in recording TA spectra because the samples photobleached very quickly giving rise to different transients from sample to sample. The influence of the heavy atom effect was observed with the phthalocyanine compounds as well. Our preliminary interpretation of the femtosecond TA data is that the fluorescence of HfPc complex happens within ~139 ps, but we will have to conduct further studies to make sure this is not IC in the excited state by looking at the fluorescence and/or up-conversion fluorescence. Both the TA and the TCSPC experiments indicate that the ZrPc fluoresces with a time constant of~ 1.0 ns. The fluorescence lifetime measurements were limited due to the instrument response time and could not be detected for $(Pc)Hf(OAc)_2$, but this will be done on up-conversion instrument with smaller resolution in the near future. For ZrPc we found a biexponential curve fitting indicating that ~ 60 % species decay to ground state with lifetime of 1.1 ns, and smaller percentage at τ= 2-3 ns.

Because of their efficient entry into the triplet manifold, phthalocyanines are also quick to react with triplet oxygen, even though the energy of the Pc triplet excited state is much lower, with phosphorescence at wavelengths into the NIR region. HfPc and ZrPc both show different decay constants when in air versus inert atmospheres in toluene. In air, transient absorbance data show identical triplet lifetimes for both compounds > 200 ns (HfPc ~228 ns and ZrPc ~ 223 ns). When experiments were done with Ar bubbled

through the solution, for the triplets HfPc decays with a lifetime of $\tau \sim 2$ μs and ZrPc $\tau \sim 8$ μs. The curve fits of the data in Figure 5.16 and 5.17 are normalized for better comparison of the kinetics in different environments. The energy level diagrams of singlet state dynamics are presented in Figures 5.18 and 5.19.

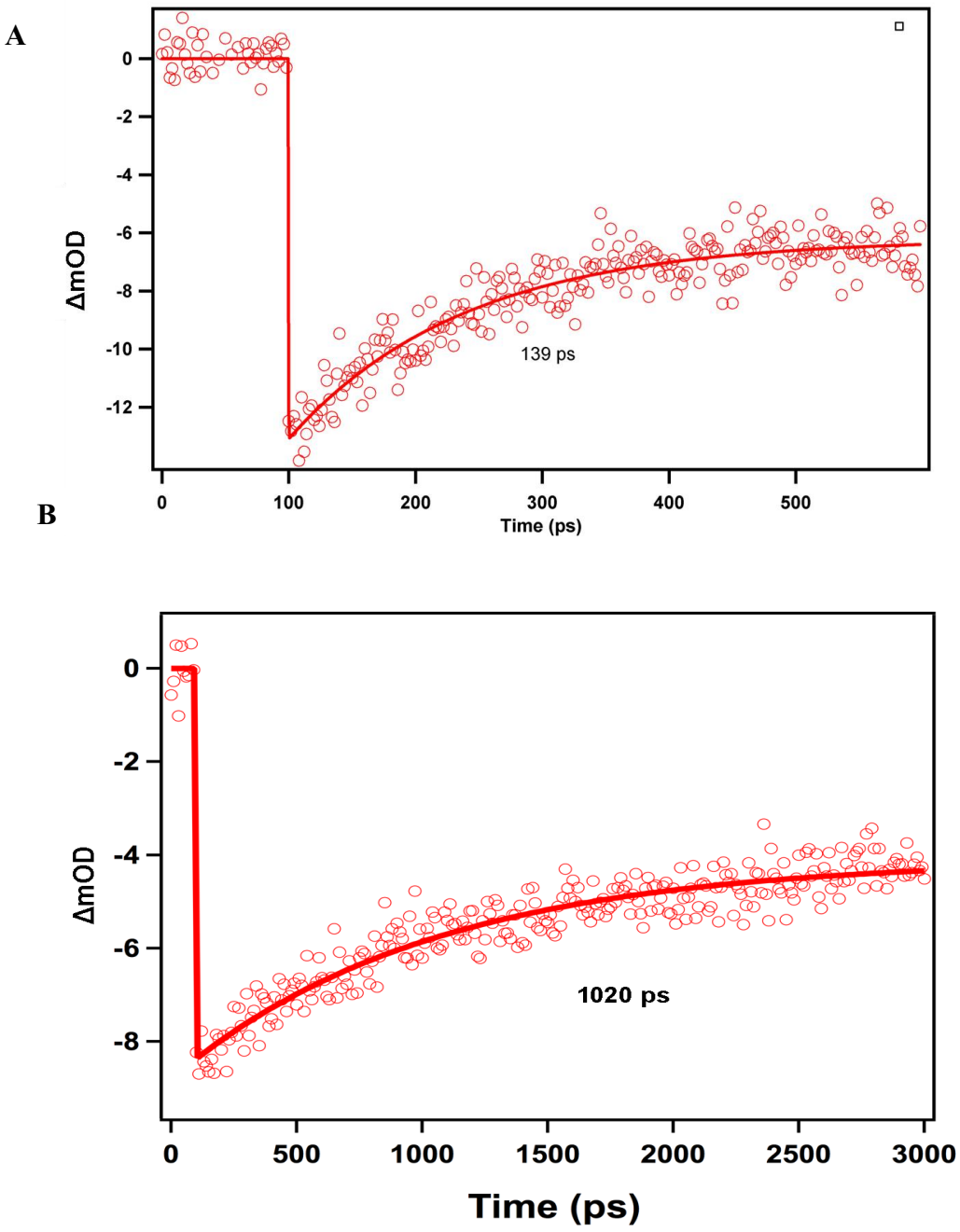

Figure 5.15 Transient absorbance; λ_{pump}= 685 nm, λ_{probe}=695 nm using the fs pump. Solid lines are fits of the experimental data of the singlet excited state decays. **(A)** (Pc)Hf(OAc)$_2$ τ = 138 ps; **(B)** (Pc)Zr(OAc)$_2$ τ = 1020 ps.

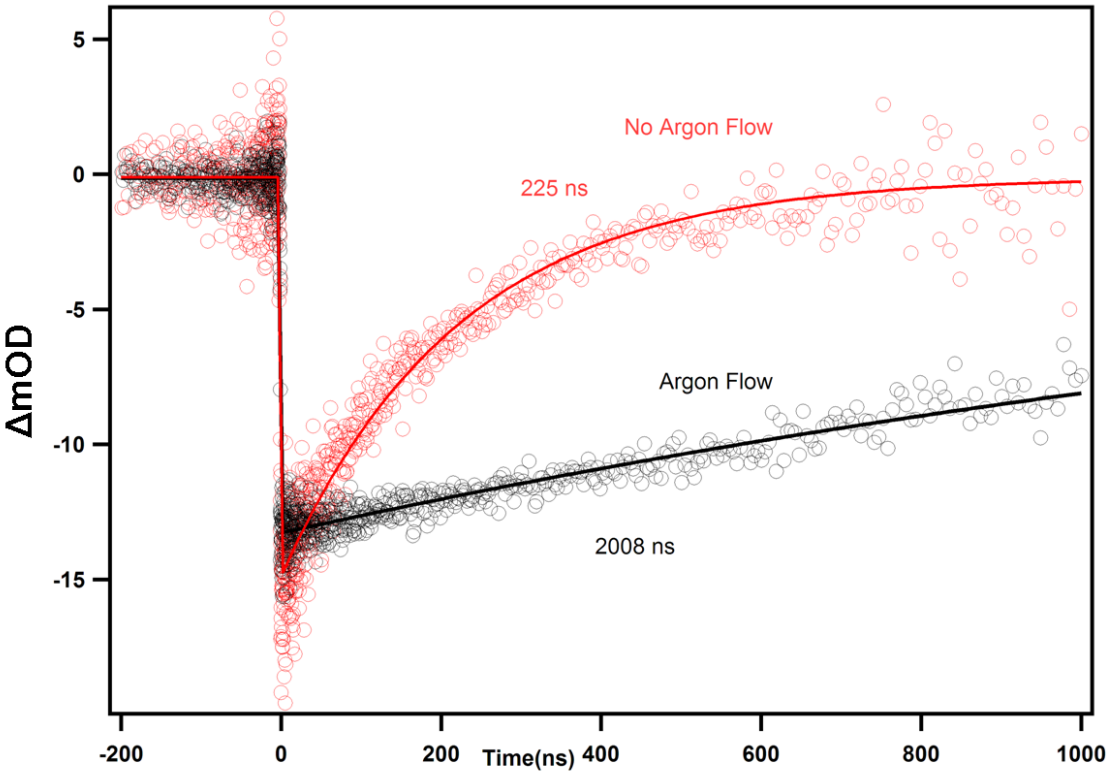

Figure 5.16 (Pc)Hf(OAc)$_2$ in toluene. λ_{pump}=685 nm; λ_{probe}= 695 nm. The different kinetic behavior of the triplet is illustrated by normalizing the fits. In toluene under air τ ~225 ns; In deaerated toluene τ~2.0 μs.

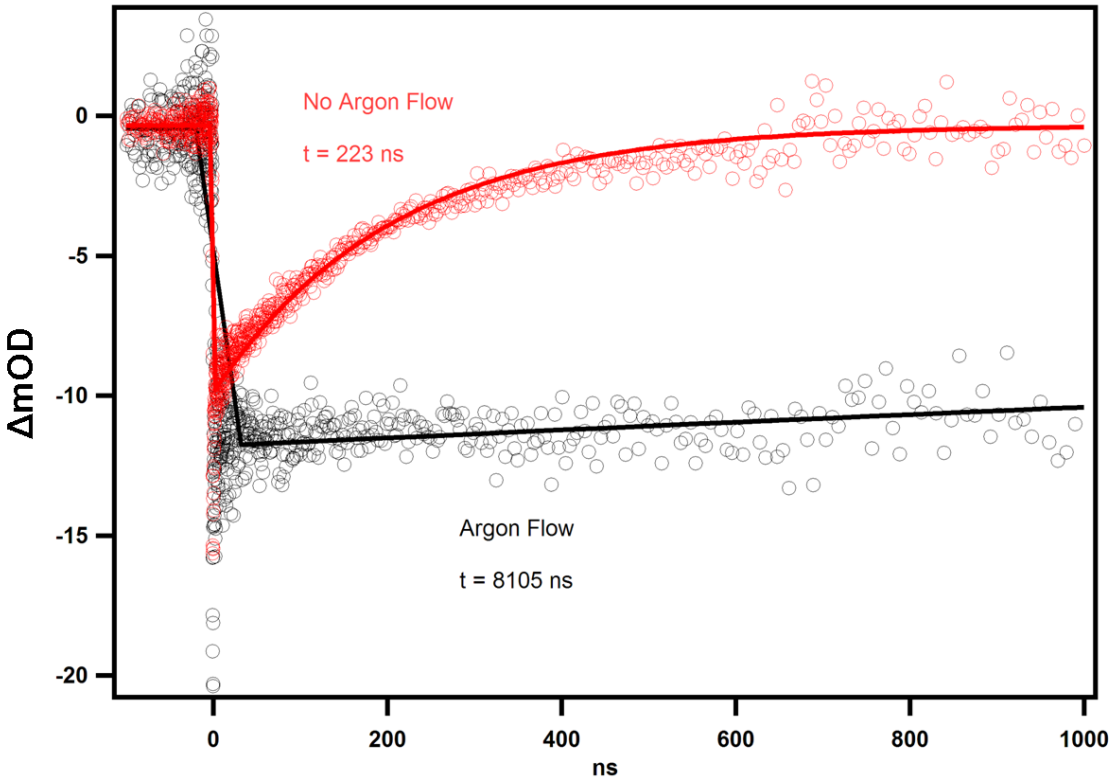

Figure 5.17 (Pc)Zr(OAc)$_2$ in toluene. λ_{pump}=685 nm; λ_{probe}= 695 nm. The different kinetic behavior of the triplet is illustrated by normalizing the fits. In toluene under air τ~223 ns; In deaerated toluene solution τ~8.0 μs.

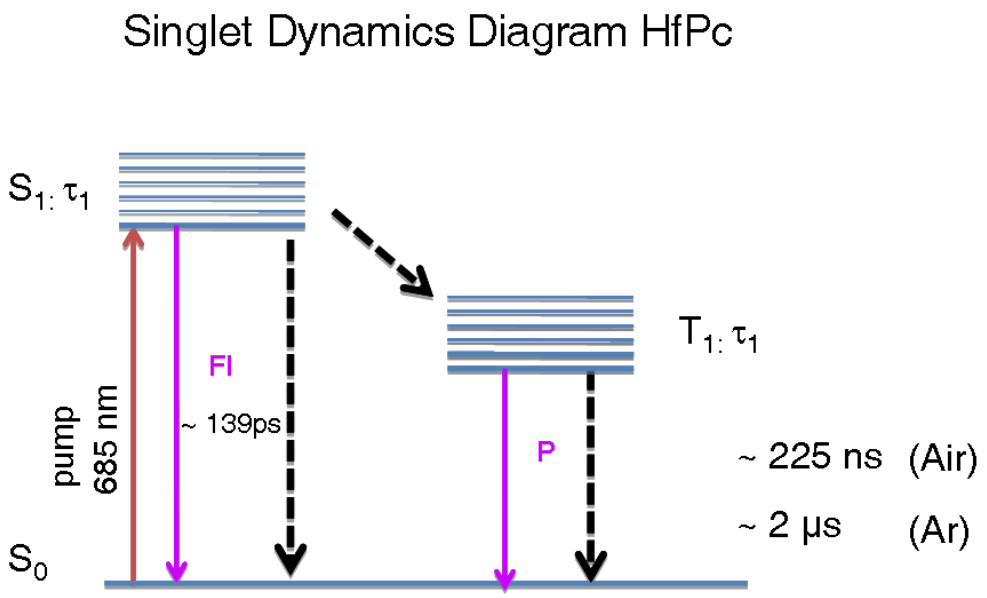

Figure 5.18 Schematic representation of singlet dynamics diagram, (Pc)Hf(OAc)$_2$. The fluorescence time constant is measure from up-conversion experiments. Solid lines are for emissive processes and dashed for non-radiative processes.

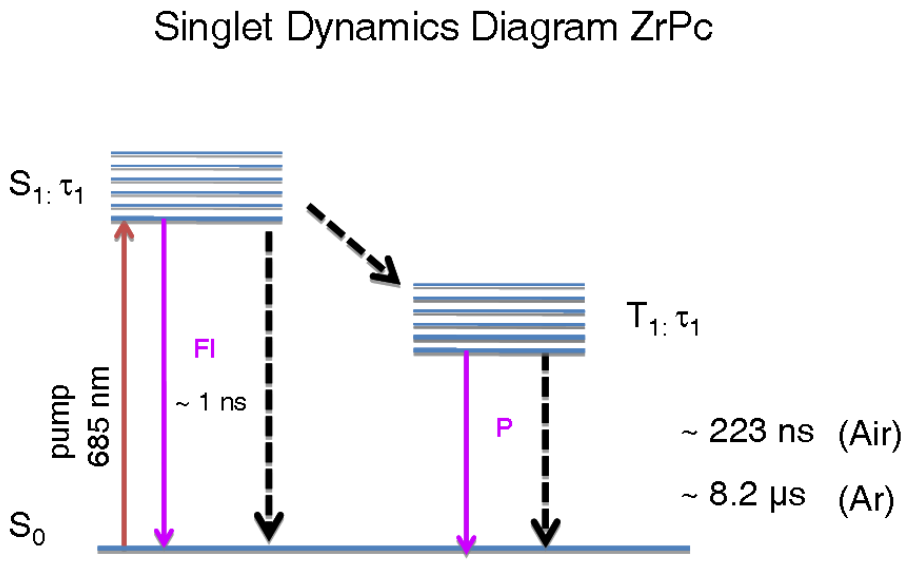

Figure 5.19 Schematic representation of singlet dynamics diagram, $(Pc)Zr(OAc)_2$. The fluorescence time constant is measure from up-conversion experiments. Solid lines are for emissive processes and dashed for non-radiative processes.

Quantum yields

The fluorescence quantum yields (Φ_F) were calculated using comparative method described in section 5.1.1. The samples were in the same medium (toluene for Por and DMSO for Pc), excited at Q bands where O.D was the same for the reference and analyzed compounds (TPP for Pors and ZnPc for Pcs). Φ_F are significantly lower for both Zr and Hf porphyrin and phthaloyanine compounds compared to ZnTPP, TPP and ZnPc attributed to the heavy atom effect that facilitates spin orbit coupling and enhances intersystem crossing to the triplet state. Fluorescence lifetimes and quantum yields are summarized in the table 5.2 below.

Table 5.2 Luminescence data for porphyrines in toluene solution and phthalocyanines in DMSO solution; [a]Ref [15,18], [b]Ref [12]

Compound	Φ_F	$\tau_{F,}$ ns
$(TPP)Hf(OAc)_2$	0.003	0.05
$(TPP)Zr(OAc)_2$	0.02	0.6
$(Pc)Hf(OAc)_2$	0.01	< IRF
$(Pc)Zr(OAc)_2$	0.05	1.1
ZnTPP [a]	0.03	2
TPP [a]	0.11	12
ZnPc [b]	0.20	2-3

Phosphorescence

Generally, many porphyrin solutions at RT emit only fluorescence, while in ridged glasses and/or at low temperatures, 77 K, phosphorescence is also observed. Phosphorescence emission spectra for most porphyrins range from approx. 700-800 nm. ZnTPP has bands with maxima at 770 nm [22] while ZnPc has the a band at 1100 nm.[23] Triplet quantum yields (Φ_{Ph}) for closed shell metalloporphyrins can be > 50% and are beyond the scope of this thesis. We will provide a few examples: ZnTPP Φ_{Ph} = 0.86, TPP Φ_{Ph} = 0.73, MgTPP Φ_{Ph} = 0.47, in toluene matrix at 77 K,[20] and ZnPc Φ_{Ph} = 0.65 in toluene.[12,23] Some palladium and platinum porphyrins have perturbed electronic spectra, and are known to phosphoresce at RT in solution.[19] We only detected phosphorescence for $(TPP)Hf(OAc)_2$ at RT, which is in agreement with already reported data from Knor et al.[19] A small amount of solution was mixed with heavy mineral oil and well degassed of

oxygen. Spectra maximum were observed at 715 nm (Figure 5.20). In the same experiment we were not able to recorded phosphorescence of (TPP)Zr(OAc)$_2$. Knor reported relative phosphorescence quantum yields to be $8x10^{-5}$ relative to ZnTPP standard.

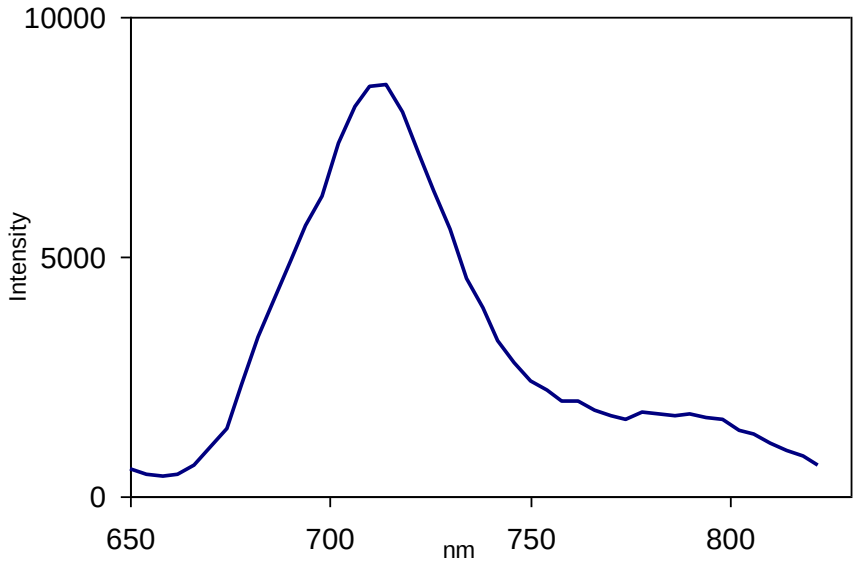

Figure 5.20 Phosphorescence of (TPP)Hf(OAc)$_2$ in toluene at RT in mineral oil with maxima occurring at 715 nm.

5.4 EXPERIMENTAL PROCEDURE

Instrumentation and Reagents

Steady state UV-Visible and fluorescence spectra were taken in 1 cm quartz cuvettes in toluene on a Carey Bio 3 spectrophotometer and on a Horiba Jobin Yvon Fluorog-3 Spectrofluorometer in 1 cm quartz cuvettes in right angle mode. Phosoprescence data were taken with the same instrument, with FL-1040 part. Anhydrous 99.8 % toluene was purchased from Sigma Aldrich and used without further purification. All compounds were synthesized in our laboratory (see prior chapters). Fluorescence quantum yields were measured by the comparative method using TPP and ZnPc as the reference samples. Fluorescence lifetimes were measured on the same TCSPC Fluorog-3 instrument using NanoLed laser 405 nm and 670 nm for excitation of porphyrin and phthalocyanine compounds respectively. Fitting software was provided with the instrument.

Transient absorbance and fluorescence up-conversion measurements were performed in the Brookhaven National Laboratory at the Center for Functional Nanomaterials, Ultrafast Optical Spectroscopy Facility. All measurements were performed at room temperature, with or without argon flow. The optical density used in the pump-probe experiments was < 0.4 in a 2 mm quartz cuvette at 540 nm for porphyrin compounds and < 0.4 at 685 nm for phthalocyanine compounds. The steady state absorption spectra were taken after the measurements to check for sample photobleaching and degradation. Degradation was observed for porphyrin samples which led to more frequent changing of the samples and the use of the argon flow throughout some of the experiments. Broadband transient absorption spectra were recorded using the output

from a 1kHz Ti:Sapphire based amplified laser system. Our molecules were resonantly excited using the tunable output from an optical parametric amplifier (OPA) and the excited state dynamics were probed with femtosecond time resolution using a mechanically delayed white-light pulse produced by focusing a small portion of the amplified fundamental (800 nm) into a sapphire plate. Alternatively, nanosecond transient absorption spectra were recorded by replacing the probe beam with the output of a supercontinuum fiber laser (~ 500 ps pulse width). In this configuration, the relative delay of the pump and probe beams is achieved by fast electronics. Luminescence up-conversion spectra were recorded using the same amplified laser system. In this configuration, the output of the OPA is tuned to an absorption resonance and focused into a sample to induce fluorescence. The emission is collected with parabolic optics and focused into a nonlinear crystal, β-BaB_2O_4, where it is mixed with a femtosecond optical gating pulse. The resulting sum frequency generated signal (SFG) is detected by a photomultiplier tube as a function of the relative delay between the excitation pulse and the gate pulse. Data analysis was done using the Igor Pro software program which allows us to fit the sample kinetics with a convolution of the laser pulse profile and a series of exponential decays.

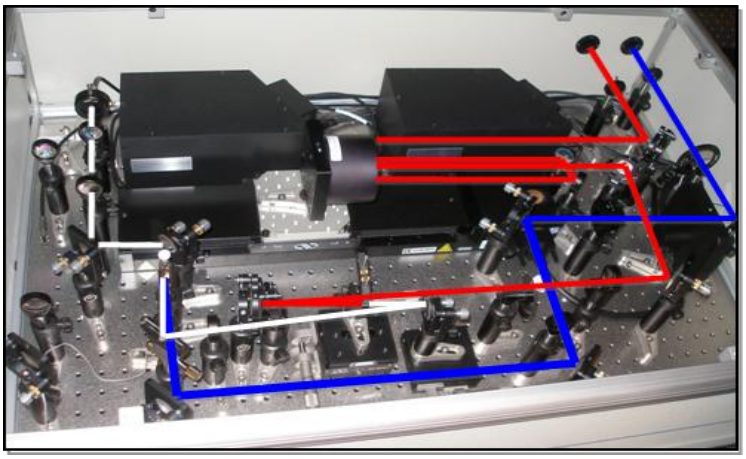

Figure 5.21 Helious Ultrafast System used in Brookhaven National Laboratory .Pump beam shown in blue; probe beam red and white.

5.5 CONCLUSIONS

We described the excited state dynamics of Hf and Zr metalloporphyrins and phthalocyanines with diacetate complexes to balance the (V) charge. Overall, we observed three characteristic excited state processes for (TPP)Hf(OAc)$_2$ and (TPP)Zr(OAc)$_2$: a) conversion of the initially formed excited state to the first excited state in a few ps; b) longer lived S_1 excited state ~ 55 ps and ~600 ps for HfTPP and ZrTPP, respectively; and lastly c) triplet states with lifetimes of more than a few microseconds. The total S_1 lifetime involves both radiative and nonradiative processes, where for both Hf and Zr ISC dominates. The difference observed when measurements were performed with or without argon flow also demonstrated that porphyrinoids may have application as photosensitizers in photodynamic therapy. For both HfTPP and HfPc complexes electron transfer dynamics are much faster when compared to ZrTPP and ZrPc

due to the heavy atom effect. However, the timescale is slower for HfPc and ZrPc. ISC dynamics are also predominating nonradiative processes for metallophthalocyanine molecules.

The interfacial processes within the DSSC depend on the overlap of energy levels of donor (excited state dye) and acceptor (conduction band of TiO_2). Literature reports that in the best performing sensitizer, Ru-bipyridyl dye, electron transfer occurs through anchoring carboxylate group, where π^* orbital and 3d orbital of TiO_2 enable good electronic coupling and fast injection dynamics. In this systems, biphasic behavior is observed with a component of < 100 fs, and a slower one on picosecond and even longer timescale.[3] Thus, the injection of electrons proceeds from either S_1(60 %) or T_1 (40 %) state.[24] For Ru complexes, the energy level of T_1 is low (1-2 eV < S_1) so electron injection is expected to be slower than from S_1 because of the reduced overlap with the acceptor.[24] It is possible that charge transfer in our system follows similar pathway. Thus, the next steps in this work are to define the energy levels of the triplet excited states, to determine the triplet quantum yields, and to determine whether the injection of electrons into conduction band of TiO_2 is possible from these states. Overall we would like to know how well these factors contribute to the performance of a solar cell device.

References

(1) http://www.nd.edu/~pkamat/femto.html.

(2) http://elchem.kaist.ac.kr/vt/chem-ed/quantum/jablonsk.htm.

(3) Zhang, Z. Enhancing the Open-Circuit Voltage of Dye-Sensitized Solar Cells: CoadSorbents and Alternative Redox Couples; École Polytechnique Federale de Lausanne: Lausanne, 2008.

(4) Haque, S. A.; Palomares, E.; Cho, B. M.; Green, A. N. M.; Hirata, N.; Klug, D. R.; Durrant, J. R. J. Am.Chem.Soc. 2005, 127, 3456-3462.

(5) Wenger, B. Effect of electronic and nuclear factors on the dynamics of dye-to-semiconductor electron transfer; École Polytechnique Federale de Lausanne: Lausanne, 2006.

(6) Benniston, A. C.; Harriman, A. Materials Today 2008, 11, 26-34.

(7) Cory, M. G.; Zerner, M. C.; Hu, X.; Schulten, K. J. Phys. Chem. B 1998, 102, 7640-7650.

(8) Hayashi, S.; Tajkhorshid, E.; Kandori, H.; Schulten, K. J. Am. Chem. Soc. 2004, 126, 10516-10517.

(9) Sener, M. K.; Lu, D.; Ritz, T.; Park, S.; Fromme, P.; Schulten, K. J. Phys. Chem. B 2002, 106, 7948-7960.

(10) Drain, C. M.; Varotto, A.; Radivojevic, I. Chem.Rev. 2009, 109, 1630-1658.

(11) Williams, A. T. R.; Winfield, S. A.; Miller, J. N. Analyst 1983, 108, 1067.

(12) Ogunsipe, A.; Chen, J.-Y.; Nyokong, T. New J. Chem. 2004, 28, 822-827.

(13) http://www.chem.ufl.edu/~kleiman/Pages/upconversion.htm.

(14) M.Gouterman The Porphyrins; Academic Press: New York, 1979.

(15) Yu, H.-Z.; Baskin, J. S.; Zewail, A. H. J.Phys.Chem.A 2002, 106, 9845-9854.

(16) Tokumaru, K. J. Porphyrins Phthalocyanines 2001, 5 7 - 86.

(17) Bajema, L.; Gouterman, M.; Rose, C. B. J.Mol.Spec. 1971, 39, 421-431.

(18) Baskin, J. S.; Yu, H.-Z.; Zewail, A. H. J.Phys.Chem.A 2002, 106, 9837-9844.

(19) Knor, G.; Strasser, A. Inorg.Chem.Comm. 2002, 5, 993–995.

(20) Azenha, E. G.; Serra, A. C.; Pineiro, M.; Pereira, M. M.; Seixas de Melo, J.; Arnaut, L. G.; Formosinho, S. J.; Rocha Gonsalves, A. M. d. A. Chem.Phys. 2002, 280, 177-190.

(21) Bilsel, O.; W.Bucher, J.; Hammerschmitt, P.; Rodriguez, J.; Holten, D. Chem.Phys.Lett. 1991, 182, 415-421.

(22) Walters, V. A.; de Paula, J. C.; Jackson, B.; Nutaitis, C.; Hall, K.; Lind, J.; Cardozo, K.; Chandran, K.; Raible, D.; Phillips, C. M. J.Phys.Chem. 1995, 99, 1166-1171.

(23) Savolainen, J.; van der Linden, D.; Dijkhuizen, N.; Herek, J. L. J. Photochem. Photobiol. A–Chem. 2008, 196, 99-105.

(24) Kallioinen, J.; Benko, G.; Sundstrom, V.; Korppi-Tommola, J. E. I.; Yartsev, A. P. J. Phys.Chem. B 2002, 106, 4396-4404.

Bibliography

Chapter 1

(1) Shi, X.; Barkigia, K. M.; Fajer, J.; Drain, C. M. J. Org. Chem. 2001, 66, 6513-6522.

(2) Falber, A.; Todaro, L.; Goldberg, I.; Favilla, M. V.; Drain, C. M. Inor. Chem. 2008, 47, 454-467.

(3) Dolphin, D. The Porphyrins. Physical Chemistry, Part A; Academic Press: New York, 1978; Vol 3.

(4) Smith, K. M. Porphyrins and Metaloporphyrins; Elsevier Amsterdam, 1972.

(5) Suslick, K. S. In The Porphyrin Handbook; Kadish, K. M., Smith, K. M., Guilard, R., Eds.; Academic Press: New York, 2000; Vol. 6

(6) Drain, C. M.; Chen., X. In Encyclopedia of Nanoscience & Nanotechnology; Nalwa, H. S., Ed.; American Scientific Press: New York, 2004; Vol. 9, pp 593-616

(7) Mauzerall, D. C. Clin. Dermatol. 1998, 6, 195–201.

(8) Gouterman, M. In The Porphyrins; Dolphin, D., Ed.; Academic Press: New York, 1978; Vol. 3, p 1-153

(9) Lehn, J.-M. Science 2002, 2400-2403.

(10) Khalil, G. E.; Chang, A.; Gouterman, M.; Callis, J. B.; Dalton, L. R.; Turro, N. J.; Jockusch, S. Rev.Sci. Instrum. 2005, 76, 54101-54101 -54101-54108.

(11) Drain, C. M.; Gentemann, S.; Roberts, J. A.; Nora Y. Nelson; Medforth, C. J.; Jia, S.; Simpson, M. C.; Smith, K. M.; Fajer, J.; Shelnutt, J. A.; Holten, D. J. Am. Chem. Soc. 1998, 120, 3781-3791.

(12) Retsek, J. L.; Drain, C. M.; Kirmaier, C.; Nurco, D. J.; Medforth, C. J.; Smith, K. M.; Sazanovich, I. V.; Chirvony, V. S.; Fajer, J.; Holten., D. J. Am. Chem. Soc. 2003, 125, 9787-9800.

(13) Drain, C. M.; Kirmaier, C.; Medforth, C. J.; Nurco, D. J.; Smith, K. M.; Holten, D. J. Phys. Chem. 1996, 100, 11984-11993.

(14) Retsek, J. L.; Gentemann, S.; Medforth, C. J.; Smith, K. M.; Chirvony, V. S.; Fajer, J.; Holten, D. J. Phys. Chem. B 2000, 104, 6690-6693.

(15) Retsek, J. L.; Medforth, C. J.; Nurco, D. J.; Gentemann, S.; Chirvony, V. S.; Smith, K. M.; Holten, D. J. Phys. Chem. B 2001, 105, 6396-6411.

(16) Drain, C. M.; Christensen, B.; Mauzerall, D. C. Proc. Natl. Acad. Sci. USA 1989, 86, 6959-6962.

(17) Drain, C. M.; Mauzerall, D. Bioelectrochem. Bioenerg. 1990, 24, 263-268.

(18) Drain, C. M.; Mauzerall, D. C. Biophys. J. 1992, 63, 1556-1563.

(19) Drain, C. M.; Lehn, J.-M. Chem. Commun. 1994, 2313-2315 (correction 1995, p2503).

(20) Drain, C. M.; Russel, K. C.; Lehn, J.-M. Chem. Commun. 1996, 337-338.

(21) Drain, C. M.; Nifiatis, F.; Vasenko, A.; Batteas, J. D. Angew. Chem. Int. Ed. 1998, 37, 2344-2347.

(22) Drain, C. M. Proc. Natl. Acad. Sci. USA 2002, 99, 5178-5182.

(23) Drain, C. M.; Batteas, J. D.; Flynn, G. W.; Milic, T.; Chi, N.; Yablon, D. G.; Sommers, H. Proc. Natl. Acad. Sci., USA 2002, 99, 6498-6502.

(24) Drain, C. M.; Smeureanu, G.; Batteas, J.; Patel, S. In Dekker Encyclopedia of Nanoscience and Nanotechnology; Schwartz, J. A., Contescu, C. I., Putyera, K., Eds.; Marcel Dekker, Inc.: New York, 2004; p 3481-3502

(25) Drain, C. M.; Bazzan, G.; Milic, T.; Vinodu, M.; Goeltz, J. C. Isr. J. Chem. 2005, 45, 255–269.

(26) Drain, C. M.; Smeureanu, G.; Patel, S.; Gong, X.; Garno, J.; Arijeloye, J. New J. Chem. 2006, 30, 1834-1843.

(27) Drain, C. M.; Varotto, A.; Radivojevic, I. Chem. Rev. 2009, 109, 1630-1658.

(28) Milic, T. N.; Chi, N.; Yablon, D. G.; Flynn, G. W.; Batteas, J. D.; Drain, C. M. Angew. Chem., Int. Ed. 2002, 41, 2117-2119.

(29) Lehn, J.-M. Supramolecular Chemistry: Concepts and Perspectives; Wiley VCH: Weinheim, 1995.

(30) de Silva, A. P.; Uchiyama, S.; Vance, T. P.; Wannalerse, B. Coord. Chem. Rev. 2007, 251, 1623-1632.

(31) Loeb, S. J. Chem. Soc. Rev. 2007, 36, 226-235.

(32) Hoeben, F. J. M.; Jonkheijm, P.; Meijer, E. W.; Schenning, A. P. H. J. Chem. Rev. 2005, 105, 1491-1546.

(33) Papaefstathiou, G. S.; MacGillivray, L. R. Coord. Chem. Rev. 2003, 246, 169-184.

(34) Alivisatos, A. P.; Barbara, P. F.; Castleman, A. W.; Chang, J.; Dixon, D. A.; Klein, M. L.; McLendon, G. L.; Miller, J. S.; Ratner, M. A.; Rossky, P. J.; Stupp, S. I.; Thompson, M. E. Adv. Mater. 1998, 10, 1297-1336.

(35) Basabe-Desmonts, L.; Reinhoudt, D. N.; Crego-Calama, M. Chem. Soc. Rev. 2007, 36, 993-1017.

(36) Schmittel, M.; Kalsani, V.; Bats, J. W. Inor. Chem. 2005, 44, 4115-4117.

(37) Milic, T.; Garno, J. C.; Batteas, J. D.; Smeureanu, G.; Drain, C. M. Langmuir 2004, 20, 3974-3983.

(38) Drain, C. M.; Milic, T.; Garno, J. C.; Smeureanu, G.; Batteas, J. D. ACS Polymer Reprints 2004, 45, 346-347.

(39) Padmaja, K.; Youngblood, W. J.; Lingyun, W.; Bocian, D. F.; Lindsey, J. S. Inor. Chem. 2006, 45, 5479-5492.

(40) Padmaja, K.; Lingyun, W.; Lindsey, J. S.; Bocian, D. F. J. Org. Chem. 2005, 70, 7972-7978.

(41) Wang, Z.; Zhiyong, L.; Medforth, C. J.; Shelnutt, J. A. J. Am. Chem. Soc. 2007, 129, 2440-2441.

(42) Zhiming, L.; Yasseri, A. A.; Loewe, R. S.; Lysenko, A. B.; Malinovskii, V. L.; Qian, Z.; Surthi, S.; Qiliang, L.; Misra, V.; Lindsey, J. S.; Bocian, D. F. J. Org. Chem. 2004, 69, 5568-5577.

(43) Yasseri, A. A.; Syomin, D.; Loewe, R. S.; Lindsey, J. S.; Zaera, F.; Bocian, D. F. J. Am. Chem. Soc. 2004, 126, 15603-15612.

(44) Qiliang, L.; Surthi, S.; Mathur, G.; Gowda, S.; Qian, Z.; Sorenson, T. A.; Tenent, R. C.; Muthukumaran, K.; Lindsey, J. S.; Misra, V. Appl. Phys. Lett. 2004, 85, 1829-1831.

(45) Muthukumaran, K.; Loewe, R. S.; Ambroise, A.; Tamaru, S. i.; Li, Q.; Mathur, G.; Bocian, D. F.; Misra, V.; Lindsey, J. S. J. Org. Chem. 2004, 69, 1444-1452.

(46) Liu, Z.; Yasseri, A. A.; Loewe, R. S.; Lysenko, A. B.; Malinovskii, V. L.; Zhao, Q.; Surthi, S.; Li, Q.; Misra, V.; Lindsey, J. S.; Bocian, D. F. J. Org. Chem. 2004, 69, 5568-5577.

(47) Patchanita, T.; Lianhe, Y.; Padmaja, K.; Jieying, J.; Bocian, D. F.; Lindsey, J. S. J. Org. Chem. 2006, 71, 1156-1171.

(48) Balakumar, A.; Lysenko, A. B.; Carcel, C.; Malinovskii, V. L.; Gryko, D. T.; Schweikart, K. H.; Loewe, R. S.; Yasseri, A. A.; Liu, Z.; Bocian, D. F.; Lindsey, J. S. J. Org. Chem. 2004, 69, 1435-1443.

(49) Scudiero, L.; Hipps, K. W.; Barlow, D. E. The J.Phys.Chem. B 2003, 107, 2903-2909.

(50) Barlow, D. E.; Scudiero, L.; Hipps, K. W. Langmuir 2004, 20, 4413-4421.

(51) Ogunrinde, A.; Hipps, K. W.; Scudiero, L. Langmuir 2006, 22, 5697-5701.

(52) Wasielewski, M. R. J. Org. Chem. 2006, 71, 5051-5066.

(53) Ahrens, M. J.; R.F.Kelley; Z.E.Dance; M.R.Wasielewski Phys. Chem. Chem. Phys. 2007, 9, 1469-1478.

(54) Balaban, T. S.; Berova, N.; Drain, C. M.; Hauschild, R.; Huan, X.; Kalt, H.; Lebedkin, S.; Lehn, J.-M.; Nifaitis, F.; Pescitelli, G.; Prokhorenko, V. I.; Riedel, G.; Smeureanu, G.; Zeller, J. Chem. Eur. J. 2007, 13, 8411 – 8427.

(55) Kinbara, K.; Aida, T. Chem. Rev.2005, 105, 1377-1400.

(56) Mauzerall, D.; Liu, Y.; Edens, G. J.; Grzymski, J. Photochem. Photobiol. Sci. 2003, 2, 788 - 790.

(57) Salvador, P.; Dannenberg, J. J. J. Phys. Chem. B 2004, 108, 15370-15375.

(58) Wieczorek, R.; Haskamp, L.; Dannenberg, J. J. J. Phys. Chem. A 2004, 108, 6713-6723.

(59) Dannenberg, J. J.; Haskamp, L.; Masunov, A. J. Phys. Chem. A 1999, 103, 7083-7086.

(60) Masunov, A.; Dannenberg, J. J. J. Phys. Chem. B 2000, 104, 806-810.

(61) Asensio, A.; Kobko, N.; Dannenberg, J. J. J. Phys. Chem. A 2003, 107, 6441-6443.

(62) George, S.; Goldberg, I. Cryst. Growth Des. 2006, 6, 755-762.

(63) Fujimoto, K.; Toyoshi, T.; Doi, Y.; Inouye, M. Mater. Sci. Eng. C. 2007, 27, 142.

(64) Drain, C. M.; Fischer, R.; Nolen, E. G.; Lehn, J.-M. Chem. Commun. 1993, 243 - 245.

(65) Lipstman, S.; Muniappan, S.; George, S.; Goldberg, I. CrystEngComm 2006, 8, 601-607.

(66) Shmilovits, M.; Vinodu, M.; Goldberg, I. New J. Chem. 2004, 28, 223-227.

(67) Holten, D.; Bocian, D. F.; Lindsey, J. S. Acc. Chem. Res. 2002, 35, 57-69.

(68) Balaban, T. S.; Linke-Schaetzel, M.; Bhise, A. D.; Vanthuyne, N.; Roussel, C.; Anson, C. E.; Buth, G.; Eichh fer, A.; Foster, K.; Garab, G.; Gliemann, H.; Goddard, R.; Javorfi, T.; Powell, A. K.; R sner, H.; Schimmel, T. Chem. Eur. J. 2005, 11, 2267-2275.

(69) Wei, L.; Syomin, D.; Loewe, R. S.; Lindsey, J. S.; Zaera, F.; Bocian, D. F. J. Phys. Chem. B 2005, 109, 6323-6330.

(70) Koepf, M.; Trabolsi, A.; Elhabiri, M.; Wytko, J. A.; Paul, D.; Albrecht-Gary, A. M.; Weiss, J. Org. Lett. 2005, 7, 1279-1282.

(71) Drain, C. M.; Goldberg, I.; Sylvain, I.; Falber, A. Top.Curr. Chem. 2005, 245, 55-88.

(72) Drain, C. M.; Shi, X.; Milic, T.; Nifiatis, F. Chem. Commun. 2001, 287–288.

(73) Jensen, R. A.; Kelley, R. F.; Lee, S. J.; Wasielewski, M. R.; Hupp, J. T.; Tiede, D. M. Chem. Commun. 2008, 16, 1886–1888.

(74) Falber, A.; Burton-Pye, B. P.; Radivojevic, I.; Todaro, L.; Saleh, R.; Francesconi, L.; Drain, C. M. Eur.J.Inorg.Chem. 2009, 2459-2466.

(75) Chan, Y. H.; Schuckman, A. E.; Perez, L. M.; Vinodu, M.; Drain, C. M.; Batteas, J. D. J. Phys. Chem. C 2008, 112, 6110-6118.

(76) Gong, X.; Milic, T.; Xu, C.; Batteas, J. D.; Drain, C. M. J. Am. Chem. Soc. 2002, 124, 14290-14291.

(77) Liu, Z.; Yasseri, A. A.; Lindsey, J. S.; Bocian, D. F. Science 2003, 302, 1543-1546.

(78) Pasetto, P.; Chen, X.; Drain, C. M.; Franck, R. W. Chem. Commun. 2001, 81–82 (erratum 507).

(79) Kobayashi, N. D. P.; Nakajima, S.-i. D.; Ogata, H. D.; Fukuda, T. D. Chem -A Eur. J. 2004, 10, 6294 - 6312.

(80) Kadish, K.; Smith, K. M.; Guiard, R. The Porphyrin Handbook; Academic Press: New York, 2000,2003.

(81) Varotto, A.; Nam, C.-Y.; Radivojevic, I.; Tom , J. P. C.; Cavaleiro, J. A. S.; Black, C. T.; Drain, C. M. J. Am. Chem. Soc. 2010, 132, 2552-2554.

(82) Leznoff, C. C.; Sosa-Sanchez, J. L. Chem. Commun. 2004, 338 - 339.

(83) Samaroo, D.; Soll, C. E.; Todaro, L. J.; Drain, C. M. Org. Lett. 2006, 8, 4985 - 4988.

(84) Samaroo, D.; Vinodu, M.; Chen, X.; Drain, C. M. J. Combi. Chem 2007, 9, 998-1011.

(85) Campbell, W. M.; Burrell, A. K.; Officer, D. L.; Jolley, K. W. Coor.Chem.Rev. 2004, 248, 1363–1379.

(86) Heremans, P.; Cheyns, D.; Rand, B. P. Acc.Chem. Res. 2009, 42, 1740-1747.

(87) Grätzel, M. Acc.Chem. Res. 2009, 42, 1788-1798.

(88) Yu, K.; Chen, J. Nanoscale. Res. Lett. 2009, 1-10.

(89) Kippelen, B.; Br das, J.-L. Energy Environ. Sci. 2009, 2, 251 - 261.

(90) Mishra, A.; Fischer, M. K. R.; Buerle, P. Angew. Chem. Int. Ed. 2009, 48, 2474 – 2499.

(91) Peet, J.; Heeger, A. J.; Bazan, G. C. Acc.Chem. Res. 2009, 42, 1700-1708.

(92) Potscavage, W. J.; Sharma, A.; Kippelen, B. Acc.Chem.Res. 2009, 42, 1758-1767.

(93) Roncali, J. Acc.Chem.Res. 2009, 42, 1719-1730.

(94) Perez, M. D.; Borek, C.; Forrest, S. R.; Thompson, M. E. J. Am. Chem. Soc. 2009, 131, 9281-9286.

(95) Yang, F.; Forrest, S. R. ACS Nano 2008, 2, 1022-1032.

(96) Grätzel, M. J.Photochem.Photobiol. C: Photochem.Rev. 2003, 4, 145–153.

(97) Kim, S.; Lee, J. K.; Kang, S. O.; Ko, J.; Yum, J. H.; Fantacci, S.; De Angelis, F.; Di Censo, D.; Nazeeruddin, M. K.; Grätzel, M. J. Am. Chem. Soc. 2006, 128, 16701-16707.

(98) J rgen, H. Angew. Chem. Int. Ed. 1984, 23, 831-847.

(99) Bazzan, G.; Smith, W.; Francesconi, L.; Drain, C. M. Langmuir 2007, 24, 3244 - 3249.

(100) Doherty, W. J.; Friedlein, R.; Salaneck, W. R. J. Phys. Chem. C, 2007 2007, 111, 2724–2729.

(101) Wei, L.; Tiznado, H.; Liu, G.; Padmaja, K.; Lindsey, J. S.; Zaera, F.; Bocian, D. F. J. Phys. Chem. B 2005, 109, 23963-23971.

(102) Albinsson, B.; Mårtensson, J. J.Photochem.Photobiol. C: Photochem. Rev. 2008, 9, 138-155.

(103) Honda, S.; Nogami, T.; Ohkita, H.; Benten, H.; Ito, S. ACS Appl. Mater. Interfaces 2009, 1, 804-810.

(104) Drain, C. M.; Hupp, J. T.; Suslick, K. S.; Wasielewski, M. R.; Chen, X. J. Porph. Phthal. 2002, 6, 241-256.

(105) Cheng, K. F.; Thai, N. A.; Teague, L. C.; Grohmann, K.; Drain, C. M. Chem. Commun. 2005, 4678-4680.

(106) Lee, S. J.; Hupp, J. T. Coord. Chem. Rev. 2006, 250, 1710-1723.

(107) Smeureanu, G.; Aggarwal, A.; Soll, C. E.; Arijeloye, J.; Malave, E.; Drain, C. M. Chem. Eur. J. 2009, 15, 12133 - 12140.

(108) Keuren, E. V.; Bone, A.; Ma, C. Langmuir 2008, 24, 6079-6084.

(109) Nitschke, C.; O'Flaherty, S. M.; Kroll, M.; Doyle, J. J.; Blau, W. J. Chem. Phys. Lett. 2004, 383, 555-560.

(110) Berhanu, S.; McLachlan, M. A.; McComb, D. W.; Jones, T. S., San Diego, CA, USA, 2008; p 70521H-70510.

(111) Rangel-Rojo, R.; Matsuda, H.; Kasai, H.; Nakanishi, H. J. Opt. Soc. Am. B 2000, 17, 1376-1382.

Chapter 2

(1) (a) Drain, C. M.; Bazzan, G.; Milic, T.; Vinodu, M.; Goeltz, J. C. Israel J. Chem. 2005, 45, 255–269(b) Doan, S. C.; Shanmugham, S.; Aston, E.; McHale, J. L. J. Am. Chem. Soc. 2005, 127, 5885-5892(c) Drain, C. M.; Batteas, J. D.; Smeureanu, G.; Patel, S. Encyclopedia of Nanoscience and Nanotechnology, ed.J.A.Schwartz, C.I.Contescu and K.Putyera, Marcel Dekker, Inc., New York 2004, 3481-3502.

(2) Milic, T.; Garno, J. C.; Batteas, J. D.; Smeureanu, G.; Drain, C. M. Langmuir 2004, 20, 3974-3983.

(3) (a) Balaban, T. S.; Linke-Schaetzel, M.; Bhise, A. D.; Vanthuyne, N.; Roussel, C.; Anson, C. E.; Buth, G.; Eichh fer, A.; Foster, K.; Garab, G.; Gliemann, H.; Goddard, R.; Javorfi, T.; Powell, A. K.; R sner, H.; Schimmel, T. Chem. Eur. J. 2005, 11, 2267-2275(b) Hameren, R. v.; Sch¨on, P.; Buul, A. M. v.; Hoogboom, J.; Lazarenko, S. V.; Gerritsen, J. W.; Engelkamp, H.; Christianen, P. C. M.; Heus, H. A.; Maan, J. C.; Rasing, T.; Speller, S.; Rowan, A. E.; Elemans, J. A. A. W.; Nolte, R. J. M. Science 2006, 314, 1433-1436(c) Lee, S. J.; Hupp, J. T.; Nguyen, S. T. J. Am. Chem. Soc. 2008, 130, 9632-9633(d) Balaban, Teodor S.; Berova, N.; Drain, Charles M.; Hauschild, R.; Huang, X.; Kalt, H.; Lebedkin, S.; Lehn, J.-M.; Nifiatis, F.; Pescitelli, G.; Prokhorenko, Valentyn I.; Riedel, G.; Smeureanu, G.; Zeller, J. Chem. - A Eur. J. 2007, 13, 8411-8427.

(4) (a) Schwab, A. D.; Smith, D. E.; Bond-Watts, B.; Johnston, D. E.; Hone, J.; Johnson, A. T.; Paula, J. C. d.; Smith, W. F. Nano Lett. 2004, 4, 1261-1265(b) Schwab, A. D.; Smith, D. E.; Rich, C. S.; Young, E. R.; Smith, W. F.; Paula, J. C. d. J. Phys. Chem. B 2003, 107, 11339-11345.

(5) (a) Wang, Z.; Medforth, C. J.; Shelnutt, J. A. J. Am. Chem. Soc. 2004, 126, 15954-15955(b) Wang, Z.; Medforth, C. J.; Shelnutt, J. A. J. Am. Chem. Soc. 2004, 126, 16720-16721(c) Kojima, T.; Harada, R.; Nakanishi, T.; Kaneko, K.; Fukuzumi, S. Chem. Mater. 2007, 19, 51-58.

(6) Li, C.; Ly, J.; Lei, B.; Fan, W.; Zhang, D.; Han, J.; Meyyappan, M.; Thompson, M.; Zhou, C. J. Phys. Chem. B 2004, 108, 9646-9649.

(7) Jeukens, C. c. R. L. P. N.; Lensen, M. C.; Wijnen, F. J. P.; Elemans, J. A. A. W.; Christianen, P. C. M.; Rowan, A. E.; Gerritsen, J. W.; Nolte, R. J. M.; Maan, J. C. Nano Lett. 2004, 4, 1401-1406.

(8) Yuasa, M.; Oyaizu, K.; Yamaguchi, A.; Kuwakado, M. J. Am. Chem. Soc. 2004, 126, 11128-11129.

(9) Medforth, C. J.; Wang, Z.; Martin, K. E.; Song, Y.; Jacobsen, J. L.; Shelnutt, J. A. Chem.Commun. 2009, 7261-7277.

(10) (a) Kobuke, Y. Structure and Bonding 2006, 121, 49-104(b) Kobuke, Y. Eur. J. Inorg. Chem. 2006, 12, 2333-2351.

(11) (a) Jintoku, H.; Sagawa, T.; Takafuji, M.; Ihara, H. Org. Biomol. Chem. 2009, 7, 2430-2434(b) Iavicoli, P.; Simon-Sorbed, M.; Amabilino, D. B. New J. Chem. 2009, 33, 358-365.

(12) Shi, X.; Barkigia, K. M.; Fajer, J.; Drain, C. M. J. Org. Chem. 2001, 66, 6513-6522.

(13) Knor, G. Inorg. Chem. Com. 2001, 4, 160-163.

(14) Hunter, C. A.; Sanders, J. K. M. J. Am. Chem. Soc. 1990, 112, 5525.

(15) Drouet, S.; Paul-Roth, C. O.; Simonneaux, G. Tetrahedron 2009, 65, 2975-2981.

(16) Shi, X. Ph.D. Thesis, City University of New York 2002.

(17) Bazzan, G.; Smith, W.; Francesconi, L. C.; Drain, C. M. Langmuir 2008, 24, 3244-3249.

Chapter 3

(1) Falber, A. Synthesis and Crystallography of Cerium(IV) Bis Porphyrinates and Hafnium(IV) mono Porphyrinates; a Tool Box for Supramolecular Chemistry, Ph.D. Thesis,; City University of New York: New York, 2007.

(2) Hao, J.; Giraudeau, A.; Ping, Z.; Ruhlmann, L. Langmuir 2008, 24, 1600-1603.

(3) Cherian, S.; Wamser, C. C. J. Phys. Chem. B 2000, 104, 3624-3629.

(4) Tachibana, Y.; Haque, S. A.; Mercer, I. P.; Durrant, J. R.; Klug, D. R. J. Phys. Chem. B 2000, 104, 1198-1205.

(5) Drain, C. M.; Bazzan, G.; Milic, T.; Vinodu, M.; Goeltz, J. C. Israel J. Chem. 2005, 45, 255-269.

(6) Drain, C. M.; Chen., X. In Encyclopedia of Nanoscience & Nanotechnology; Nalwa, H. S., Ed.; American Scientific Press: New York, 2004; Vol. 9.

(7) Milic, T. N.; Chi, N.; Yablon, D. G.; Flynn, G. W.; Batteas, J. D.; Drain, C. M. Angew. Chem., Int. Ed. 2002, 41, 2117-2119.

(8) Drain, C. M.; Nifiatis, F.; Vasenko, A.; Batteas, J. D. Angew. Chem. Int. Ed. 1998, 37, 2344-2347.

(9) Dmitrenko, O.; Huang, W.; Polenova, T. E.; Francesconi, L. C.; Wingrave, J. A.; Teplyakov, A. V. J. Phys. Chem. B 2003, 107, 7747-7752.

(10) Toth, J. E.; Anson, F. C. J. Am. Chem. Soc. 1989, 111, 2444-2451.

(11) Keana, J. F. W.; Ogan, M. D. J. Am. Chem. Soc. 1986, 108, 7951-7957.

(12) Keana, J. F. W.; Ogan, M. D.; LU, Y.; Beer, M.; Varkey, J. J. Am. Chem. Soc. 1986, 108, 7957-7963.

(13) Katsoulis, D. E. Chem. Rev. 1998, 98, 359-388.

(14) Long, D. L.; Burkholder, E.; Cronin, L. Chem. Soc. Rev. 2007, 36, 105-121.

(15) Drain, C. M.; Smeureanu, G.; Batteas, J.; Patel, S. In Dekker Encyclopedia of Nanoscience and Nanotechnology; Schwartz, J. A., Contescu, C. I., Putyera, K., Eds.; Marcel Dekker, Inc.: New York, 2004; Vol. 5.

(16) Barlow, D. E.; Scudiero, L.; Hipps, K. W. Langmuir 2004, 20, 4413-4421.

(17) Otsuki, J.; Kawaguchi, S.; Yamakawa, T.; Asakawa, M.; Miyake, K. Langmuir 2006, 22, 5708-5715.

(18) Nazeeruddin, M. K.; Hunphry-Baker, R.; Officer, D. L.; Campbell, W. M.; Burrell, A. K.; Graetzel, M. Langmuir 2004, 20, 6514-6517.

(19) Stromberg, J. R.; Marton, A.; Kee, H. L.; Kirmaier, C.; Diers, J. R.; Muthiah, C.; Taniguchi, M.; Lindsey, J. S.; Bocian, D. F.; Meyer, G. J.; Holten, D. J. Phys. Chem. C 2007, 111, 15464-15478.

(20) Chan, Y.-H.; Schuckman, A. E.; Perez, L. M.; Vinodu, M.; Drain, C. M.; Batteas, J. D. J. Phys. Chem. C 2008, 112, 6110-6118.

(21) Tanaka, M.; Hayashi, S.; Eu, S.; Umeyama, T.; Matano, Y.; Imahori, H. Chem. Commun. 2007, 2069-2071.

(22) Rochford, J.; Chu, D.; Hagfeldt, A.; Galoppini, E. J. Am. Chem. Soc. 2007, 129, 4655-4665.

(23) Varotto, A.; Todaro, L.; Vinodu, M.; Koehne, J.; Liu, G.-y.; Drain, C. M. Chem. Comm. 2008, 4921–4923.

(24) Tong, Lok H.; Wietor, J.-L.; Clegg, W.; Raithby, Paul R.; Pascu, Sofia I.; Sanders, Jeremy K. M. Chem. Eur. J. 2008, 14, 3035-3044.

(25) Marorri, F.; Bonifazi, D.; Gehrig, R.; Gallani, J.-L.; Diederich, F. Israel J. Chem. 2005, 45, 303-319.

(26) Tashiro, K.; Aida, T. Chem. Soc. Rev. 2007, 36, 189-197.

(27) Hasobe, T.; Saito, K.; Kamat, P. V.; Troiani, V.; Qiu, H.; Solladie, N.; Kim, K. S.; Park, J. K.; Kim, D.; D'Souza, F.; Fukuzumi, S. J. Mater. Chem. 2007, 17, 4160–4170.

(28) D'Souza, F.; El-Khouly, M. E.; McCarty, A. L.; Gadde, S.; Karr, P. A.; Zandler, M. E.; Araki, Y.; Ito, O. J. Phys. Chem. B 2005, 109, 10107-10114.

(29) Bazzan, G.; Smith, W.; Francesconi, L. C.; Drain, C. M. Langmuir 2008, 24, 3244-3249.

(30) Santos, I. C. M. S.; Rebelo, S. L. H.; Balula, M. S. S.; Martins, R. R. L.; Pereira, M. M. M. S.; Simoes, M. M. Q.; Neves, M. G. P. M. S.; Cavaleiro, J. A. S.; Cavaleiro, A. M. V. J. Mol. Catal. A: Chem. 2005, 231, 35-45.

(31) Yokoyama, A.; Kojima, T.; Ohkubo, K.; Fukuzumi, S. Chem. Comm. 2007, 3997 – 3999.

(32) Allain, C.; Favette, S.; Chamoreau, L.-M.; Vaissermann, J.; Ruhlmann, L.; Hasenknopf, B. Eur. J. Inorg. Chem. 2008, 2008, 3433-3441.

(33) Hagrman, D.; Hagrman, P. J.; Zubieta, J. Angew. Chem. Int. Ed. 1999, 38, 3165-3168.

(34) Tsuda, A.; Hirahara, E.; Yeong-Sang Kim; Tanaka, H.; Kawai, T.; Aida, T. Angew. Chem. Int. Ed. 2004, 43, 6327 - 6331.

(35) Drain, C. M.; Varotto, A.; Radivojevic, I. Chem. Rev. 2009, 109, 1630-1658.

(36) Babcock, L. M., University of Illinois, 1988.

(37) Kim, H. J.; Jung, S.; Jeon, Y. M.; Whang, D.; Kim, K. Chem. Comm. 1997, 2201-2202.

(38) Falber, A.; Todaro, L.; Goldberg, I.; Favilla, M. V.; Drain, C. M. Inorg. Chem. 2008, 47, 454-467.

(39) Kim, H. J.; Whang, D.; Kim, K.; Do, Y. Inorg. Chem. 1993, 32, 360-362.

(40) Tomachynski, L. A.; Tretyakova, I. N.; Chernii, V. Y.; Volkov, S. V.; Kowalska, M.; Legendziewicz, J.; Gerasymchuk, Y. S.; Radzki, S. Inor.Chim.Acta 2008, 361, 2569-2581

(41) Gerasymchuk, Y. S.; Volkov, S. V.; Chernii, V. Y.; Tomachynski, L. A.; Radzki, S. J. Alloys Compd. 2004, 380, 186–190.

(42) Tretyakova, I. N.; Chernii, V. Y.; Tomachynski, L. A.; Volkov, S. V. Dyes and Pigments 2007, 75, 67-72.

(43) Falber, A.; Burton-Pye, B. P.; Radivojevic, I.; Todaro, L.; Saleh, R.; Francesconi, L.; Drain, C. M. Eur.J.Inorg.Chem. 2009, 2459-2466.

(44) Hagfeldt, A.; Grätzel, M. Acc. Chem. Res. 2000, 33, 269-277.

(45) Nazeeruddin, M. K.; Klein, C.; Liska, P.; Grätzel, M. Coord. Chem. Rev. 2005, 249, 1460-1467.

Chapter 4

(1) http://www.sc.doe.gov/bes/reports/files/SEU_rpt.pdf., 2005.

(2) Grätzel, M. Journal of Photochemistry and Photobiology A: Chemistry 2004, 164, 3.

(3) Heremans, P.; Cheyns, D.; Rand, B. P. S. Accounts of Chemical Research 2009, 42, 1740.

(4) Gratzel, M. Inorg. Chem. 2005, 44, 6841.

(5) Katsoulis, D. E. Chem. Rev. 1998, 98, 359.

(6) Falber, A.; Burton-Pye, B. P.; Radivojevic, I.; Todaro, L.; Saleh, R.; Francesconi, L.; Drain, C. M. Eur.J.Inorg.Chem. 2009, 2459.

(7) Drain, C. M.; Smeureanu, G.; Batteas, J.; Patel, S. In Dekker Encyclopedia of Nanoscience and Nanotechnology; Schwartz, J. A., Contescu, C. I., Putyera, K., Eds.; Marcel Dekker, Inc.: New York, 2004; Vol. 5.

(8) Barlow, D. E.; Scudiero, L.; Hipps, K. W. Langmuir 2004, 20, 4413.

(9) Otsuki, J.; Kawaguchi, S.; Yamakawa, T.; Asakawa, M.; Miyake, K. Langmuir 2006, 22, 5708.

(10) Nazeeruddin, M. K.; Hunphry-Baker, R.; Officer, D. L.; Campbell, W. M.; Burrell, A. K.; Graetzel, M. Langmuir 2004, 20, 6514.

(11) Stromberg, J. R.; Marton, A.; Kee, H. L.; Kirmaier, C.; Diers, J. R.; Muthiah, C.; Taniguchi, M.; Lindsey, J. S.; Bocian, D. F.; Meyer, G. J.; Holten, D. J. Phys. Chem. C 2007, 111, 15464.

(12) Chan, Y.-H.; Schuckman, A. E.; Perez, L. M.; Vinodu, M.; Drain, C. M.; Batteas, J. D. J. Phys. Chem. C 2008, 112, 6110.

(13) Tanaka, M.; Hayashi, S.; Eu, S.; Umeyama, T.; Matano, Y.; Imahori, H. Chem. Commun. 2007, 2069.

(14) Rochford, J.; Galoppini, E. Langmuir 2008, 24, 5366.

(15) Imahori, H.; Norieda, H.; Nishimura, Y.; Yamazaki, I.; Higuchi, K.; Kato, N.; Motohiro, T.; Yamada, H.; Tamaki, K.; Arimura, M.; Sakata, Y. J. Phys. Chem. B 2000, 104, 1253.

(16) Lee, D.-C.; Morales, G. M.; Lee, Y.; Yu, L. Chem. Comm. 2006, 101.

(17) Batteas, J.; Helt, J.; Xu, C.; Weldon, M. ANTEC 2001 Proceedings: Materials 2001, 2, 1951.

(18) Hagfeldt, A.; Grätzel, M. Acc. Chem. Res. 2000, 33, 269.

(19) Rochford, J.; Chu, D.; Hagfeldt, A.; Galoppini, E. J. Am. Chem. Soc. 2007, 129, 4655.

(20) Campbell, W. M.; Jolley, K. W.; Wagner, P.; Wagner, K.; Walsh, P. J.; Gordon, K. C.; Schmidt-Mende, L.; Nazeeruddin, M. K.; Wang, Q.; Grαεtzel, M.; Officer, D. L. J. Phys. Chem. C 2007, 111, 11760.

(21) Drain, C. M.; Varotto, A.; Radivojevic, I. Chemical Reviews 2009, 109, 1630.

(22) Gagne, R. R.; Koval, C. A.; Lisensky, G. C. Inorg. Chem. 1980, 19, 2854.

(23) Bard, A. J.; Faulkner, L. R. Electrochemical Methods: Fundamentals and Applications; Second ed.; John Wiley & Sons, INC., 2001.

(24) Kadish, K. M.; Smith, K. M.; Guilard, R. The Porphyrin Handbook:Electron Transfer; Academic Press: San Diego, 2000.

(25) Gratzel, M. Accounts of Chemical Research 2009, 42, 1788.

(26) Qiankun, Z.; Xiaoxia, G. Science in China 1996, 40, 215.

(27) Junghänel, M. Novel aqueous electrolyte films for hole conduction in dye sensitized solar cells and development of an electron transport model; der Freien Universität Berlin: Berlin, 2007.

(28) Kathiravan, A.; Renganathan, R. Journal of Colloid and Interface Science 2009, 331, 401.

(29) Grätzel, M. Journal of Photochemistry and Photobiology C: Photochemistry Reviews 2003, 4, 145.

(30) L., S.-M.; U., B.; Humphry-Baker, R.; Horiuchi, T.; Miura, H.; Ito, S.; Uchida, S.; Grätzel, M. Advanced Materials 2005, 17, 813.

(31) Yu, K.; Chen, J. Nanoscale. Res. Lett. 2009, 1.

(32) Riede, M.; Mueller, T.; Tress, W.; Schueppel, R.; Leo, K. Nanotechnology 2008, 19, 1.

(33) Ting, C.-C.; Chen, S.-Y.; Liu, D.-M. Journal of Applied Physics 2000, 88, 4628.

(34) O'Regan, B.; Lenzmann, F.; Muis, R.; Wienke, J. Chem. Mater. 2002, 14, 5023.

(35) Ito, S.; Murakami, T. N.; Comte, P.; Liska, P.; Grätzel, C.; Nazeeruddin, M. K.; Grätzel, M. Thin Solid Films 2008, 516, 4613.

(36) G nes, S.; Neugebauer, H.; Sariciftci, N. S.; Roither, J.; Kovalenko, M.; Pillwein, G.; Heiss, W. Adv. Funct. Mater. 2006, 16, 1095.

(37) Qiao, Q.; Beck, J.; Lumpkin, R.; Pretko, J.; McLeskey, J. J. T. Solar Energy Materials and Solar Cells 2006, 90, 1034.

(38) Peng, B.; Jungmann, G.; Jäger, C.; Haarer, D.; Schmidt, H.-W.; Thelakkat, M. Coordination Chemistry Reviews 2004, 248, 1479.

(39) Robertson, N. Angew. Chem. Int. Ed. 2006, 45, 2338

(40) Liao, M.-S.; Scheinera, S. J.Chem. Phys. 2002, 117, 205.

(41) M.Gouterman The Porphyrins; Academic Press: New York, 1978.

(42) Donohoe, R. J.; Duchowski, J. K.; Bocian, D. F. Journal of the American Chemical Society 1988, 110, 6119.

(43) Kim, H. J.; Whang, D.; Kim, K.; Do, Y. Inorg. Chem. 1993, 32, 360.

(44) Ryu, S.; Whang, D.; Kim, J.; Yeo, W.; Kim, K. J. Chem. Soc., Dalton Trans. 1993, 205.

(45) Falber, A.; Todaro, L.; Goldberg, I.; Favilla, M. V.; Drain, C. M. Inorg. Chem. 2008, 47, 454.

Chapter 5

(1) http://www.nd.edu/~pkamat/femto.html.

(2) http://elchem.kaist.ac.kr/vt/chem-ed/quantum/jablonsk.htm.

(3) Zhang, Z. Enhancing the Open-Circuit Voltage of Dye-Sensitized Solar Cells: CoadSorbents and Alternative Redox Couples; École Polytechnique Federale de Lausanne: Lausanne, 2008.

(4) Haque, S. A.; Palomares, E.; Cho, B. M.; Green, A. N. M.; Hirata, N.; Klug, D. R.; Durrant, J. R. J. Am.Chem.Soc. 2005, 127, 3456-3462.

(5) Wenger, B. Effect of electronic and nuclear factors on the dynamics of dye-to-semiconductor electron transfer; École Polytechnique Federale de Lausanne: Lausanne, 2006.

(6) Benniston, A. C.; Harriman, A. Materials Today 2008, 11, 26-34.

(7) Cory, M. G.; Zerner, M. C.; Hu, X.; Schulten, K. J. Phys. Chem. B 1998, 102, 7640-7650.

(8) Hayashi, S.; Tajkhorshid, E.; Kandori, H.; Schulten, K. J. Am. Chem. Soc. 2004, 126, 10516-10517.

(9) Sener, M. K.; Lu, D.; Ritz, T.; Park, S.; Fromme, P.; Schulten, K. J. Phys. Chem. B 2002, 106, 7948-7960.

(10) Drain, C. M.; Varotto, A.; Radivojevic, I. Chem.Rev. 2009, 109, 1630-1658.

(11) Williams, A. T. R.; Winfield, S. A.; Miller, J. N. Analyst 1983, 108, 1067.

(12) Ogunsipe, A.; Chen, J.-Y.; Nyokong, T. New J. Chem. 2004, 28, 822-827.

(13) http://www.chem.ufl.edu/~kleiman/Pages/upconversion.htm.

(14) M.Gouterman The Porphyrins; Academic Press: New York, 1979.

(15) Yu, H.-Z.; Baskin, J. S.; Zewail, A. H. J.Phys.Chem.A 2002, 106, 9845-9854.

(16) Tokumaru, K. J. Porphyrins Phthalocyanines 2001, 5 7 - 86.

(17) Bajema, L.; Gouterman, M.; Rose, C. B. J.Mol.Spec. 1971, 39, 421-431.

(18) Baskin, J. S.; Yu, H.-Z.; Zewail, A. H. J.Phys.Chem.A 2002, 106, 9837-9844.

(19) Knor, G.; Strasser, A. Inorg.Chem.Comm. 2002, 5, 993–995.

(20) Azenha, E. G.; Serra, A. C.; Pineiro, M.; Pereira, M. M.; Seixas de Melo, J.; Arnaut, L. G.; Formosinho, S. J.; Rocha Gonsalves, A. M. d. A. Chem.Phys. 2002, 280, 177-190.

(21) Bilsel, O.; W.Bucher, J.; Hammerschmitt, P.; Rodriguez, J.; Holten, D. Chem.Phys.Lett. 1991, 182, 415-421.

(22) Walters, V. A.; de Paula, J. C.; Jackson, B.; Nutaitis, C.; Hall, K.; Lind, J.; Cardozo, K.; Chandran, K.; Raible, D.; Phillips, C. M. J.Phys.Chem. 1995, 99, 1166-1171.

(23) Savolainen, J.; van der Linden, D.; Dijkhuizen, N.; Herek, J. L. J. Photochem. Photobiol. A–Chem. 2008, 196, 99-105.

(24) Kallioinen, J.; Benko, G.; Sundstrom, V.; Korppi-Tommola, J. E. I.; Yartsev, A. P. J. Phys.Chem. B 2002, 106, 4396-4404.